SEAMLESS DESIGN OF ENERGY MANAGEMENT SYSTEMS

A Dissertation
Presented to
The Academic Faculty

by

Renke Huang

In Partial Fulfillment
Of the Requirements for the Degree
Doctor of Philosophy in the
School of Electrical and Computer Engineering

Georgia Institute of Technology
May 2015

SEAMLESS DESIGN OF ENERGY MANAGEMENT SYSTEMS

Approved by:

Dr. A.P. Meliopoulos, Advisor
School of Electrical and Computer Engineering
Georgia Institute of Technology

Dr. Fumin Zhang,
School of Electrical and Computer Engineering
Georgia Institute of Technology

Dr. Yorai Wardi
School of Electrical and Computer Engineering
Georgia Institute of Technology

Dr. Andy Sun
School of Industrial and Systems Engineering
Georgia Institute of Technology

Dr. David G. Taylor
School of Electrical and Computer Engineering
Georgia Institute of Technology

Date Approved: January 21, 2015

To my father Yiyong Huang, to my mother Qiufen Ren,
and to my friend Changchang Zhu

ACKNOWLEDGEMENTS

The doctoral study at Georgia Tech is a long-distance adventure. This journey would not have been accomplished without the inspiration, encouragement, and help from many people. I would like to express my heartfelt gratitude to all of them at this time.

First of all, I would like to extend my most sincere thanks to my advisor, Dr. A. P. Sakis Meliopoulos. I could not have imagined having a better advisor and mentor during tough times in the Ph.D. pursuit. It is due to his patience, motivation, inspiration, and immense knowledge that I have gained a deeper understanding of engineering and mathematics. His careful guidance on solving problems, writing reports and oral communicating with profession rewards my entire research life. Without his illuminating instruction, consistent encouragement, and confidence in my capability, this thesis work could not be completed in the present form. I am deeply grateful for his guidance and support during my Ph. D. life.

I would also like to extend my sincere gratitude to Dr. Yorai Wardi, Dr. Fumin Zhang, Dr. David G Taylor, and Dr. Andy Sun for serving as my dissertation committee and for their valuable time contribution in reviewing the drafts. Their insightful comments and suggestions have also made considerable contribution the completion of this work.

I am also grateful to Dr. George J. Cokkinides for his valuable support and practical contributions to complete my work. His professional expertise in theory and implementation was always excellent and admirable.

The members of the Power Systems Control and Automation Laboratory (PSCAL) have contributed generously to my personal and research time at Georgia Tech. The people

in the group are friendly and always offer me good advice and collaboration. I would specially thank Dr. Evanglos Farantatos for his unwavering support, insightful suggestions, and kind advice. We cooperated several research projects during our Ph. D researches, and Dr. Evanglos Farantatos generously shared with me his valuable experience and sharp insight with power system analysis experience, practical problem solving, and report and paper writing. I would also like to thank Ye Tao, Zhenyu Tan, Liangyi Sun, Rui Fan, Dongbo Zhao, Yongnam Cho, Sungyun Choi, Yonghee Lee, Xuebei Yu, and Yu Liu for their friendship and support.

I am thankful to all my friends at Georgia Tech. They supported me academically, personally, and especially during difficulties. Among them special thanks go to Jie Tan and his wife Yuting Gu, Chong Han and his wife Yi Wang, and Dr. Chenchi Luo, who have provided encouragement, friendship, and living support throughout my graduate studies.

I am especially thankful to Changchang Zhu, who encouraged me to conquer all the difficulties during my Ph.D, shared with me happiness and pleasure, and comforted me when I had difficulties and problems for both academics and life matters.

Most of all, I owe my loving thanks to my family. My parents' encouragement and support kept me focused and motivated. With their unflagging love, encouragement, and understanding, I eventually reached the final stages of this doctoral degree.

TABLE OF CONTENTS

LIST OF FIGURES

LIST OF TABLES

SUMMARY

As the central nervous system of the power network, the control center – along with its energy management system (EMS), - is a critical component of the power system for the operational reliability. In the last few decades, the advancement of information technologies has greatly enhanced the functionality of the EMS. But the general architecture of collecting and processing all measurement data at a central place has not changed. Also the measurement data acquisition and processing functionalities of the EMS are quite slow. It is clear that this centralized architecture of the EMS will not be able to provide the rapid-response wide-area controls that will be required for the operation and control of the future grid with increasing numbers of renewables and other distributed resources.

Moreover, integrating additional functions into the EMS infrastructure is difficult. Nowadays EMSs are cumbersome in facilitating variations in the system infrastructure or changes in operating objectives. Specifically, EMS uses task-specific models and applications, both of which remain largely incompatible and non-interoperable with each other. To overcome the drawbacks of nowadays EMS, the infrastructure of data acquisition systems, local processing systems, communication systems, and the EMSs should be reorganized into a seamless and distributed system that will (1) provide the information needed at every level of this distributed system, (2) eliminate seams among the various applications by using a unified component model, and (3) autonomously verify models in real time to eliminate human errors and inconsistencies of the data bases.

Towards these goals, the main objectives of this dissertation are (1) to propose an infrastructure of data acquisition systems that provide the necessary information for an automated EMS system enabling autonomous distributed state estimation, model validation, simplified protection, and seamless integration of other EMS applications, (2) to develop an object-oriented, interoperable, and unified component model that can be seamlessly integrated with a variety of applications of the EMS, (3) to develop a distributed dynamic state estimator (DDSE) that can be performed at the substation level based on the proposed data acquisition system and the object-oriented, interoperable, and unified component model, (4) to develop a physically-based synchronous machine model, which is expressed in terms of the actual self and mutual inductances of the synchronous machine windings as a function of rotor position, for the purpose of synchronous machine parameters identification, and (5) to develop a robust and highly efficient algorithm for the optimal power flow (OPF) problem, one of the most important applications of the EMS, based on the validated states and models of the power system provided by the proposed DDSE.

In particular, initially the dissertation proposes a distributed and seamless infrastructure of data acquisition systems that provide the necessary information for an automated and interoperable EMS system. At the lower level (relay level), a dynamic state estimation is performed for each single component in the substation separately. The distributed dynamic state estimation provides the real-time dynamic model of the component as well as the real-time operating conditions. By using GPS synchronized measurements, the real-time model is time tagged with GPS accuracy. Next, the real-time model of substation is autonomously created by combining the real-time models of all the

components in the substation and the interconnecting lines of the same time tag. This process is referred as the substation level state estimation. The substation state model is sent to the control center where the real-time model of the entire system is also autonomously created by combing the real-time model of all substations of the same time tag. The system-wide real-time model is utilized by any EMS application seamlessly.

To guarantee that the system-wide real-time model can be used across all the EMS applications, an object-oriented, unified, and seamless interoperable component model syntax is proposed and referred as the state and control algebraic quadratic companion form (SCAQCF). This can be viewed as an advanced common information model. Applications can directly access and use this model without any filters or interfaces (seamless).

The distributed dynamic state estimator (DDSE) plays an essential role in the proposed modern EMS architecture, since it provides both the real-time states and model of the power system. The DDSE is performed for each single component in the substation by utilizing only local measurements available from PMUs, relays, and FDRs in the substation, thus avoiding all issues associated with transmission of data and associated time latencies. This approach enables very fast DDSE update rate. Two formulations of the proposed DDSE are presented. The first one, referred to as DDSE-Q, is used to capture with high fidelity the electro-mechanical dynamics of the system. The second one, referred to as DDSE-T, is used to capture both electro-mechanical and electro-magnetic transients. The approach utilizes the SCAQCF model of the components, in order to implement the DDSE algorithm in an object-oriented manner and improve the convergence of the algorithm.

Modeling accuracy and fidelity are fundamental in this DDSE approach. For many power system components, high-fidelity models exist. For some new components such as

inverter-interfaced power components, the modeling accuracy may not be as high as that of other components. In both cases the DDSE can be utilized to fine tune the models and/or determine the parameters of the model with greater accuracy. The basic approach is to expand the dynamic state estimator to include some key parameters as unknown states to be estimated. Therefore the proposed modern EMS architecture can also provide better models with field-validated parameters compared with traditional approaches.

The field-validated real-time model of the system with the SCAQCF syntax can be seamlessly integrated with a variety of other applications of the EMS. One of the important applications of the EMS, the optimization of grid operation conditions, is discussed in the dissertation. The optimization of grid operation conditions can be formulated as an optimal power flow (OPF) problem with different objective functions and constraints. The dissertation discusses the autonomous formulation of the OPF problem and its solution methodology by simply integrating the object-oriented SCAQCF component model. The solution methodology is robust and highly efficient with the help of the object-oriented SCAQCF component model. Robustness means the algorithm can provide a solution for any system and high efficiency means a fast convergence speed compared with traditional methods.

CHAPTER 1 INTRODUCTION

1.1 Problem Statement

As the central nervous system of the power network, the control center - along with its energy management system (EMS), - is a critical component of the power system operational reliability. In the last few decades, the advancement of information technologies has greatly enhanced the functionality of the EMS. But the general architecture of collecting and processing all measurement data at a central place has not changed. It is clear that this centralized architecture of the EMS will not be able to handle the increasing volume of measurements and the rapid-response wide-area controls that will be required for the operation and control of the future grid.

State estimation (SE) is a fundamental function of any EMS on which all other optimization, regulation, and security functions are based. The function of SE is to process a set of redundant measurements to obtain the best estimate of the current state of a power system. In particular, SE is performed in a centralized manner based on asynchronous measurements that are collected in the control center where the SE is performed every few minutes [1]-[2]. Steady-state system models are used, while measurements of various electrical quantities (such as voltage and current magnitudes, active and reactive power flows) are available via a supervisory control and data acquisition (SCADA) system with a communication frequency of every two to ten seconds. The complexity, large dimensionality, and geographic separation of the modern power system impose significant biases on the formulation and execution of SE [3]. In addition, present state estimators provide only the real-time state of the system (bus voltage values) versus the real-time

model of all the components of the power system. Moreover, the need of electric power utilities to improve their service, and the need to accommodate new developments in a smart grid with penetration of smart sensors and distributed generation (DG), require much higher time resolution and more precise time-synchronization for the SE to deal with emerging monitoring, control, and protection needs.

The introduction and continuously growing installation of the phasor measurement units (PMUs) that provide highly accurate synchronized measurements 30-120 times per second at the substation level have opened up the possibility for a faster, more efficient, and more accurate SE in real time. Biases in existing state estimators can be eliminated by using the PMU measurements in combination with highly accurate, three-phase, and asymmetric power system models. In addition, they allow for the implementation of SE in a distributed and decentralized architecture that eliminates the biases resulting from a centralized architecture.

The power system states, computed with the SE, are combined with the component models in the EMS database to execute EMS applications. The objective of these applications is to make the power system operate securely and reliably. However, integrating additional functions into this kind of EMS is difficult [4]. According to [5], EMSs fail to offer the scalability, functionality, and operational capabilities required for managing the large number of distributed and demand-side resources in the power system. Moreover, present day EMSs are cumbersome in facilitating variations in the system infrastructure or changes in operating objectives. In other words, each EMS uses task-specific and piece-meal models and applications, both of which remain largely incompatible and non-interoperable, and is designed to be applied only on the

corresponding systems for which it was originally designed. The objective of introducing the common information model (CIM) is to facilitate the integration of applications. Yet, because of lack of commensurate changes in the EMS architecture, the benefits of the CIM are not fully realized. An important issue is that the present system is dependent upon largely manual verification of the data bases. To overcome the drawbacks of nowadays EMS, the infrastructure of data acquisition systems, local processing systems, communication systems, and the EMSs should be reorganized into a distributed system that will (1) provide the information needed at every level of this distributed system, (2) eliminate seams among the various applications by using a unified component model, and (3) autonomously verify models in real time to eliminate human errors and inconsistencies of the data bases. Advances in high-performance computation, modern software architectures, innovative common models, and unified application propositions, have the potential to make the EMS a seamless integration platform for various applications, which has a unified component model data base to support massive data and provides much more powerful computation and analytics capabilities.

1.2 Research Objectives

The dissertation objectives are (1) to propose an infrastructure of data acquisition systems that provide the necessary information for an automated EMS system enabling autonomous distributed state estimation, model validation, simplified protection, and seamless integration of other EMS applications, (2) to develop an object-oriented, interoperable, and unified component model that can be seamlessly integrated with a variety of applications of the EMS, (3) to develop a distributed dynamic state estimator

(DDSE) that can be performed at the substation level based on the proposed data acquisition system and the object-oriented, interoperable, and unified component model, (4) to develop a physically-based synchronous machine model, which is expressed in terms of the actual self and mutual inductances of the synchronous machine windings as a function of rotor position, for the purpose of synchronous machine parameters identification, and (5) to develop a robust and highly efficient algorithm for the optimal power flow (OPF) problem, one of the most important applications of the EMS, based on the validated states and models of the power system provided by the proposed DDSE.

In particular, initially the dissertation proposes a distributed and seamless infrastructure of data acquisition systems that provide the necessary information for an automated and interoperable EMS system. At the lower level (relay level), a dynamic state estimation is performed for each single component in the substation separately. The distributed dynamic state estimation provides the real-time dynamic model of the component as well as the real-time operating conditions. By using GPS synchronized measurements, the real-time model is time tagged with GPS accuracy. Next, the real-time model of substation is autonomously created by combining the real-time models of all the components in the substation and the interconnecting lines of the same time tag. This process is referred as the substation level state estimation. The substation state model is send to the control center where the real-time model of the entire system is also autonomously created by combing the real-time model of all substations of the same time tag. The system-wide real-time model is utilized by any EMS application seamlessly.

To guarantee that the system-wide real-time model can be used across all the EMS applications and across all relevant temporal and spatial scales, an object-oriented, unified,

and seamless interoperable component model syntax is proposed and referred as the state and control algebraic quadratic companion form (SCAQCF). This can be viewed as an advanced common information model. Applications can directly access and use this model without any filters or interfaces (seamless).

The distributed dynamic state estimator (DDSE) plays an essential role in the proposed modern EMS architecture. The DDSE is performed for each single component in the substation by utilizing only local measurements available from PMUs, relays, and FDRs in the substation only, thus avoiding all issues associated with transmission of data and associated time latencies. This approach enables very fast DDSE update rate. Two formulations of the proposed DDSE are presented. The first one, referred as DDSE-Q, is used to capture with high fidelity the electro-mechanical dynamics of the system. The second one, referred as DDSE-T, is used to capture both electro-mechanical and electro-magnetic transients. The approach utilizes the SCAQCF model of the components, in order to implement the DDSE algorithm in an object-oriented manner and improve the convergence of the algorithm. Moreover, the SCAQCF model is a three-phase, asymmetric, and breaker oriented power system model in order to account for system imbalances, asymmetries, and topology changes. The object-oriented formulation of the DDSE is emphasized which is one of the key characteristics in the implementation of the DDSE towards its very fast execution rates.

Modeling accuracy and fidelity is fundamental in this DDSE approach. For many power system components, high-fidelity models exist. For some new components such as inverter-interfaced power components, the modeling accuracy may not be as high as that of other components. In both cases the DDSE can be utilized to fine tune the models and/or

determine the parameters of the model with greater accuracy. The basic approach is to expand the dynamic state estimator to include some key parameters as unknown states to be estimated. Therefore the proposed modern EMS architecture can also provide better models with field-validated parameters compared with traditional approaches. The dissertation provides an example of this kind of model parameters identification for a synchronous machine.

The field-validated real-time model of the system with the SCAQCF syntax can be seamlessly integrated with a variety of other applications of the EMS. One of the important applications of the EMS, the optimization of grid operation conditions, is discussed in the dissertation. The optimization of grid operation conditions can be formulated as an OPF problem with different objective functions and constraints. The dissertation discusses the autonomous formulation of the OPF problem and its solution methodology by simply integrating the object-oriented SCAQCF component model. The solution methodology is robust and highly efficient with the help of the object-oriented SCAQCF component model. Robustness means the algorithm can provide a solution for any system. The algorithm starts from an infeasible optimal state and moves to the feasible region while maintaining optimality. System feasibility is maintained by introducing artificial mismatch current sources at each bus. At each iteration, the mismatches reduce while the optimization method ensures the solution is optimal at each iteration. If the feasible solution is found, it is optimal; otherwise, the algorithm returns a suboptimal point, providing the best choice to solve system infeasibility by a set of remedial actions. High efficiency means a fast convergence speed. First, the algorithm models the OPF as a quadratic problem for fast convergence. Second, the algorithm reduces the size of the original optimization problem

by two approaches: (1) identifying the active constraints and only adding the active constraint set to the optimization problem; (2) eliminating all the power flow equality constraints of the original optimization problem during the linearization procedure, since the linearization uses the co-state method and the power flow equations are implicitly included in the linearization.

1.3 Thesis Outline

The outline of the remaining parts of this dissertation is as follows.

In Chapter 2, background information is provided on the origin of the topic along with presently available technologies that are being used. In addition, a thorough literature survey is presented that summarizes related research work efforts. In particular, this chapter starts with a summary of the current architecture, technologies, functionalities, and limitations of the EMS. The presently utilized technology for state estimation along with its biases and limitations are presented. Synchrophasor technology and how it can be utilized for the development of advanced state estimators is also presented. A literature review on the state-of-the-art algorithms utilized for optimal power flow problem follows. Finally, the parameters identification technology for a synchronous machine is summarized.

Chapter 3 presents a distributed and seamless infrastructure of data acquisition systems that provide the necessary information for an automated and interoperable EMS system, which spans from the protective relay in the substation to the control center.

Chapter 4 presents the general and detailed methodology for the derivation of an object-oriented, interoperable, and unified model for the component in the power system. The model is named as the state and control algebraic quadratic companion form

(SCAQCF). Examples for how to derive the SCAQCF model from the original differential and algebraic equations of the component are also given.

Chapter 5 presents in detail the mathematical formulation and the solution methodology of the developed distributed dynamic state estimator (DDSE). More specifically, two DDSE formulations (DDSE-Q and DDSE-T) are presented in details. The mathematical model and the categorization of the DDSE measurements are also presented. The DDSE solution algorithm and performance evaluation, along with bad data detection, identification, and rejection methodology follow. Finally, demonstration results for the DDSE are presented.

Chapter 6 presents that the DDSE can be utilized to fine tune the models and/or determine the parameters of the model with great accuracy. The basic approach is to expand the DDSE to include some key parameters as unknown states. The mathematical formulation of the synchronous machine physical parameters identification problem is described in this chapter, to illustrate the procedure of expanding the DDSE to include some key parameters as unknown states. Demonstration results of the synchronous machine physical parameters identification are also presented in this chapter.

Chapter 7 presents the autonomous formulation of the OPF problem and its solution methodology, to illustrate that the real-time models extracted from the DDSE can be seamlessly integrated with a variety of other applications of EMS. The proposed solution algorithm for the OPF problem is robust and highly efficient. Demonstration results of the proposed OPF solution algorithm are also given in this chapter.

Finally, Chapter 8 summarizes the research work and outlines the results and contributions of this dissertation.

There are also three appendices in this dissertation. In Appendix A, the quadratic integration method is summarized. Appendix B describes the SCAQCF models of the generator used in the OPF problem. Finally Appendices C describes the SCAQCF models of the transformer used in the OPF problem.

CHAPTER 2 LITERATURE REVIEW

2.1 Overview

This chapter provides the background information of existing technologies related to the proposed research along with a literature review of the research efforts on these topics. Section 2.2 starts with a summary of the current architecture, technologies, functionalities, and limitations of the EMS. Section 2.3 summarizes the currently utilized technology in state estimation and explores its biases and limitations. Section 2.4 provides a literature review on the state-of-the-art algorithms utilized for optimal power flow problem. Section 2.5 summarizes the parameters identification technology for a synchronous machine.

2.2 The Evolution of the EMS

An energy management system (EMS) monitors and manages flows in the high-voltage transmission network. Early control centers were hardwired analog systems with meters and switches. Thumbwheels were used to change operating set points in the field. Modern-day EMS functions were initially developed in the 1970s with the advent of digital computers. The fast processing capabilities of computers were exploited to efficiently solve large and complex mathematical problems. Over the past several decades, these EMS functions have continually evolved.

EMS applications have evolved in line with the following business and operational objectives [5]:

(1) Real-time monitoring of network conditions: the first EMS application implemented was the SCADA system. SE runs about every 10 to 30 seconds and uses SCADA measurements with a network model to calculate a “best guess” of system

conditions across the entire network, especially for network nodes not measured by SCADA. SE has become a critical must-run EMS function, since it forms the foundation for subsequent network analytics and also provides a coherent grid-wide view of conditions. SE lets the operator visually monitor grid conditions from a central location and take manual action, if warranted.

(2) Optimizing grid operating conditions: optimization applications use the model coming from SE to achieve desired operational objectives, such as dispatching generators to minimize total system-wide generation cost, minimizing transmission losses, flattening the grid voltage profile, and recommending corrective and preventive control actions. These optimization applications are usually formulated as different kinds of optimal power flow (OPF) problems.

(3) Maintaining system frequency: the objective of load frequency control (LFC) is to automatically maintain system frequency as load changes by automatically modifying generation to meet demands. When it was introduced in the early 1960s, LFC was a pioneering "smart grid" EMS automation application.

(4) Performing what-if studies: contingency analysis (CA) uses the model coming from SE to carry out a series of "what-if" studies by simulating the effects of potential user-defined contingencies. A contingency is an unplanned loss of key grid components. CA assesses the potential over-loads or problems that could consequently happen. Operators usually have a dedicated display screen to show these results, as a heads-up to warn them of what may be lurking ahead.

(5) Assessing grid stability: recently, operators have been pushing the grid to operate closer to its dynamic voltage and transient stability limits. This is due in part to deregulated

electricity markets aiming to maximize utilization of all available transmission capacity. Therefore, stability limits need to be updated in real time, a requirement that has led to the implementation of advanced dynamic simulation applications simulating grid dynamic behavior in the face of disturbances. These stability applications also use SE and are computationally very intensive.

Traditionally, the SCADA measurements are sent to the EMS every two to ten seconds [5]. This was considered sufficient since EMS was primarily designed for tracking normal and alert states. The desire of electric power utilities to improve their service, and the need to accommodate new developments in a smart grid with penetration of smart sensors and distributed generation (DG), lead to the need of much higher time resolution and precise time-synchronization for the SE to deal with emerging monitoring, control, and protection needs, which cannot be achieved by the traditional SCADA system in today's EMS.

In the meantime, the current approach to EMS applications has developed over the last several decades in a piecemeal fashion where the various applications run separately using their own models and formats. Although these tools have been improved, the applications are still built upon the core technology and software architectures of decades ago, developed individually for their own unique purposes, often with legacy code implementing old algorithms, and designed for sequential computing hardware. Most existing applications have their various components tightly coupled and non-separable. The internal code is not structured and often very old. In addition, external data interfaces are unwieldy, the user interface is weak, and there is usually no centralized engine to house the numerical methods used in the application. Updating or extending such software is very

tedious. It is often easier to create new software completely. Achieving interoperability for such applications is extremely cumbersome if not impossible.

These limitations of today's EMSs need to be overcome by the state-of-the-art analytical tools that can support modernization of the electricity industry. New models and tools are required to handle emerging needs driven by increasing model size, renewable penetration, PMU-based wide-area monitoring and control, and the need to share models, analyses, and results across a wide spectrum of organizations. Current and future computing requirements necessitate an integrated approach built upon state-of-the-art algorithms, hardware, and modern methods for data management across a shared environment for the EMS.

2.3 Conventional and PMU-Based State Estimation

Control and operation of electric power systems is based on the ability to determine the system's state in real time. A reliable and accurate real-time model of a power system is of paramount importance to its effective control and operation. Historically, the importance of this issue was recognized immediately after the 1965 blackout. Power system state estimation (SE) was introduced in the late 60s to achieve this objective [6]-[8] and has traditionally been treated as a static state estimation problem. It is based on a centralized approach that makes use of a steady-state system model and measurements of various electrical quantities (voltage and current magnitudes, active and reactive power flows) available via a SCADA system [1]-[2]. All the measurements are sent from local remote terminal units (RTUs) to a central control center monitoring the entire system under control. The resulting real-time model of the system is of key importance to the system

monitoring and control. In fact, all the additional applications that may run in an EMS of a power system control center, like contingency analysis, unit commitment, and economic dispatch, use the results of state estimation as their input and perform their analysis based on these results. Therefore, state estimation is currently the cornerstone of EMS real-time applications.

The complexity, as well as geographic spread and separation of an electric power system, has imposed significant restrictions on the implementation of power system state estimation. Measurements originating from multiple different locations (substations) have to travel significant distances to the EMS. Therefore, communication issues and latencies become important problems [9]. Furthermore, if measurements are not accurately time-stamped in a unified way, dependent upon the measurement location and thus not synchronized, they can introduce significant biases in the estimation, and may even be practically useless in a dynamic estimation framework. The current centralized state estimation is also characterized by biases which arise from system asymmetries (not taken into account in current system-modeling technologies), imbalanced operation, and instrumentation errors [3], [10]. Additional disadvantages of centralized state estimation are (a) long execution time needed for the state estimation as a result of the large number of data as well as the size and complexity of the model, (b) bad data detection and identification becoming more complex and less sharp, and (c) excessive communication requirements, since all SCADA data must be sent to a central location.

A promising technology that can revolutionize state estimation is the phasor measurement unit (PMU) [11]-[17]. PMUs provide synchronized measurements where synchronization is achieved via a GPS (Global Positioning System) clock that provides the

synchronizing signal with a potential accuracy of 1 μsec. This time precision is translated into a precision of 0.02 degrees of the U.S. power frequency (60 Hz). Therefore, the technology provides a means to measure the phase angles with a precision of 0.02 degrees. This means that measurements taken, or phasors computed via a time reference, at one location, are globally valid. This kind of synchronized measurement eliminates problems originating from the wide geographic separation of the components of a power system. The first use of the technology is described in [11]. The harmonic state estimator, when applied additionally to the fundamental estimator, is only a linear state estimator as described in [11]. The system was placed in operation in the time period 1993 to 1998.

Recent major power system outages such as the 2003 U.S.-Canada blackout demonstrated the need for more efficient methods of monitoring the state of power systems. The advantages from the integration of synchronized measurements into an existing nonlinear estimator have been addressed in several publications [20]-[21]. Moreover, state estimators that utilize only the PMU measurements and as a result turn out to be linear estimators, have also been proposed [22]-[23]. Another advantage is that the introduction of PMUs has made it possible to measure both magnitude and phase of electrical quantities locally, and to distribute the state estimation procedure. Therefore, the PMU technology opens up the possibility of developing distributed state estimation approaches, which has been an active research topic for the past few years [24]-[29]. Inclusion of the dynamic behavior of the system into the state estimation algorithm results in a dynamic state estimator (DSE). DSE has been introduced, to some basic level, for power system applications in the past [34]-[36]. However, it has not been widely spread, let alone implemented, as a result of the fact that implementation of such concepts could not be

possible without the phasor measurement units with GPS-synchronization and a distributed state estimation architecture. The majority of the related publications are based on simplified power system dynamic models. They utilize Kalman-filter algorithms for the estimation procedure [36]-[38] and consequently are practically unsuitable for large-scale and real-time implementations. Research attempts have also been made for DSE by using computational intelligence techniques such as artificial neural networks [39].

2.4 The Formulation and Algorithm Classification of the OPF Problem

This section presents a brief literature survey on the state of the art of the formulation and algorithm for the optimal power flow (OPF) methodologies.

The optimization applications in an EMS use the model from SE to achieve desired operational objectives. These optimization applications are usually formulated as different kinds of OPF problems with a certain objective function and several operation constraints of the power system. The typical objective of an OPF problem can be minimizing total system-wide generation cost [41]-[44], minimizing transmission losses, or flattening the grid voltage profile [45]-[46]. The constraints of an OPF problem usually include limitations of voltage magnitude at each bus, limitations of active/reactive power of generators, limitations of tap-ratio of controllable transformers, and limitations of capacity of transmission lines. However, these constraints cannot ensure safe operation of power systems when contingencies occur. Therefore, the OPF problem is extended to the security constrained optimal power flow (SCOPF) problem to ensure that the power system operates in its safety region when contingencies occur [47]-[49]. As a result of the complexity of the power system, the OPF problem is nonlinear, non-convex, and large

scale, and these features of the OPF problem increase the difficulty of solving itself in a fast and efficient way and getting a global optimal point.

The OPF problem has been researched for over 40 years. Since Carpentier [50] defined the OPF problem in 1962, many algorithms have been designed to solve the basic OPF problem and its derivative problems. Current OPF algorithms can be classified into the following categories: sequential algorithms [51]-[56], nonlinear programming [57]-[65], and intelligential search methods [66]-[68].

Sequential algorithms usually use linear programming (LP) as the tool to improve the solution in each iteration. Since Danzig proposed the simplex algorithm in 1947, LP has become a very important optimization tool. In the early years, Danzig and Wolfe's algorithm [69] and revised simplex algorithm [70] are the pioneering linear optimization methods for OPF. The cost function and constraints are both linearized and solved by simplex algorithm or primal-dual algorithm. Brian Stott and Eric Hobson designed an iterative LP-based algorithm with piecewise linear objective functions for a power system [52]. The selection of a penalty function is a very popular topic in sequential algorithms. A well-designed penalty function can guarantee moving from infeasibility to feasibility, and as the values of the penalty items reduce, the state of the system gets close to the feasible region [55]. These sequential algorithms still have some shortcomings, especially when the dimension of the problem is large, the difference between the linearized problem and original problem prevents these sequential algorithms from getting a solution in a fast and efficient way.

For the nonlinear programming algorithms, the original nonlinear OPF problem is usually transformed into an unconstrained problem (Kuhn-Tucker condition equations) by

Lagrangian function, Powell method [49], [42], sequential unconstrained minimization technique (SUMT) [43], and interior-point method (IPM) [59]. After the transformation, the transformed problem can be solved by gradient method [72], Newton-Raphson method [73], and Fletcher-Powell method [41]-[42]. IPM and Newton-Raphson methods are the most widely used among these methods for their high efficiency. In the early 1990's, IPM was introduced to solve OPF problems with different objective functions such as minimization operation cost [71], optimal reactive dispatch [74], and maximum load-ability [75]. IPM has several versions, such as prime-dual algorithm [59], predictor-corrector algorithm [57], and multiple centrality corrections (MCC) algorithm [76]. Prime-dual algorithm performs linear search within the feasible region. Predictor-corrector algorithm is a famous IPM revision reported in [57]. In each iteration, the algorithm first estimates the potential variable changes, and then adjusts the estimation according to the values of the nonlinear terms. MCC algorithm also needs a correction step but focuses on enlarging the step length of current iteration, improving the centrality of the next iteration, and increasing the speed at which a feasible solution is reached. Newton method has been proved to be the most efficient method in solving unconstrained optimization problems. However, Newton method may zigzag in some specific conditions [77], especially when approaching the optimal point. Nonlinear programming algorithms require feasible solution as a start point, and the model of the algorithms includes all constraints, which leads to a limitation of the robustness and efficiency.

The intelligent search method blooming in recent years has become a very important technology for searching the global or near global optimal solution. The OPF problem is tested by a variety of different intelligent search methods such as genetic algorithm (GA)

[68], evolution algorithm (EA) [66], and particle swarm optimizer (PSO) [79]-[83]. However, intelligent search methods are first-order methods and they are totally inefficient for large-scale OPF problems.

2.5 Parameters Identification of the Synchronous Machine

Knowledge of the operational parameters of synchronous machines is vital for reliable stability studies and "post mortem" analyses. Having accurate models of dynamic elements (including synchronous machines and other power plant controllers) is very important for optimal decision making, planning, and efficient operation of the power grid.

Parameters of generators may differ from those in the utility's database due to aging processes, magnetic saturation, or changes of temperature during machine operation. As a matter of fact, many utilities around the world still use machine model parameters calculated during generator commissioning, leading to substantial differences between the actual and simulated dynamic behavior.

Traditional methods had been developed under the guidance of IEEE Standards and some National Electrical Standards from many countries to measure the parameters [93]. However, all of these methods are conducted under off-line conditions. Different methods have also been developed in recent years to estimate the parameters of synchronous machines from online measurements [94-98]. Zhengming et al. [94] propose a parameter estimator that uses the rotor angle as measurement and performs a linearization of the machine equations. The work presented in [95-97] introduces a nonlinear parameter estimator, where a Kalman-filter-based estimator is proposed [95-96] while [97] is using a nonlinear least squares algorithm. Paper [98] applies the unscented Kalman filter for the

nonlinear estimation of synchronous machine parameters by applying online operation data. However, most of the online parameters identification methodologies use measurements from the normal operation conditions of the synchronous machine and they can only estimate the magnetizing reactance of the generator and cannot identify the transient and sub-transient parameters. Another disadvantage for these methodologies is that the estimation accuracy of the parameters are heavily dependent on whether the measurement of the rotor angle of the generator is available. If the rotor angle measurement is not available, all these methods need to have a pre-estimation procedure for the rotor angle. The estimation of the rotor angle proposed in these methods is accurate only for round rotor generators while the accuracy is reduced for salient pole machines under the assumption that the d and q axis reactance are unknown.

Furthermore, most of these studies mentioned above are mainly conducted based on the models of the synchronous machine derived from the conventional Park's transformation and the d-q-o frame of reference. In spite of its simple structure, d-q-o models are not capable of simulating unbalanced and rectifier type loading conditions. Also, as a result of simplifying assumptions associated with these models, it is difficult to include the higher order harmonics, which exist in the real machines. A more accurate approach to this problem is to simulate the synchronous generators with physically existing parameters, that is, the actual self and mutual inductances of the generator windings as a function of the rotor position. By this way, various loading conditions such as sudden application and removal of balanced and unbalanced loads, rectifier loads, and symmetrical and asymmetrical faults can be easily investigated.

2.6 Summary

This chapter presents an overall description and related work on the research topics of this dissertation. In particular, Section 2.2 gives a summary of the current architecture, technologies, functionalities, and limitations of the energy management system. Section 2.3 summarizes the present practices on state estimation and its limitations. The synchrophasor technology is also introduced and it is discussed how it can contribute to the reformulation of state estimation and the elimination of its biases. Section 2.4 provides a literature review of the methods that have been used and proposed for optimal power flow problem. The advantages and disadvantages of each method are discussed. Finally, in Section 2.5, the present state-of-the-art technology on generator parameters identification is summarized.

CHAPTER 3 THE OVERALL OPPROACH

3.1 Overview

In this chapter, a distributed and seamless infrastructure of data acquisition systems that provide the necessary information for an automated and interoperable EMS system, which spans from the protective relay in the substation to the control center, is proposed.

At the lower level (relay level), a dynamic state estimation is performed for each single component (protection zone) in the substation separately. The distributed dynamic state estimation provides the real-time dynamic model of the component as well as the real-time operating conditions. By using GPS synchronized measurements, the real-time model is time tagged with GPS accuracy. Next, the real-time model of substation is autonomously created by combining the real-time models of all the components in the substation and the interconnecting lines of the same time tag. This process is referred as the substation level state estimation. The substation state model is send to the control center where the real-time model of the entire system is also autonomously created by combing the real-time model of all substations of the same time tag. The system-wide real-time model is utilized by any EMS application seamlessly. If an EMS application generates a command for a specific component, this command is sent to the component through the same communication structure. Section 3.2 gives the detailed description of the proposed infrastructure.

3.2 The Proposed Infrastructure

The overall proposed structure is shown in Figure 3.1 [99-100]. The system starts from the relays, PMUs, and digital fault records (DFRs) that monitor power apparatus and collect the measurements at the apparatus level in a substation. The relays and PMUs performs the distributed dynamic state estimation (DDSE) to filter the streaming data and extract the real-time model of each power apparatus, as well as the states, in the substation. The relays and PMUs indicated here are referred as universal monitoring protection and control unit (UMPCU) [99-100], since a number of new functions have been added. Note that there are two categories of measurement data, time-domain sinusoidal waveforms and frequency-domain phasors. The time-domain sinusoidal waveform is directly sampled by the relays and DFRs. A typical sampling rate is 4,000 times per second. The frequency-domain phasor of the electrical quantities is a complex number with a magnitude and a phase angle, which is computed by the PMUs based on the time-domain waveform, and this kind of phasor data has a typical sampling rate of 30 to 120 times per second. The DDSE can be categorized as Quasi-dynamic DDSE (DDSE-Q) or full time domain DDSE (DDSE-T) depending on the type of measurements the data acquisition system provides, i.e. time-domain waveforms or frequency-domain phasors. The details of this DDSE methodology are described in Chapter 5.

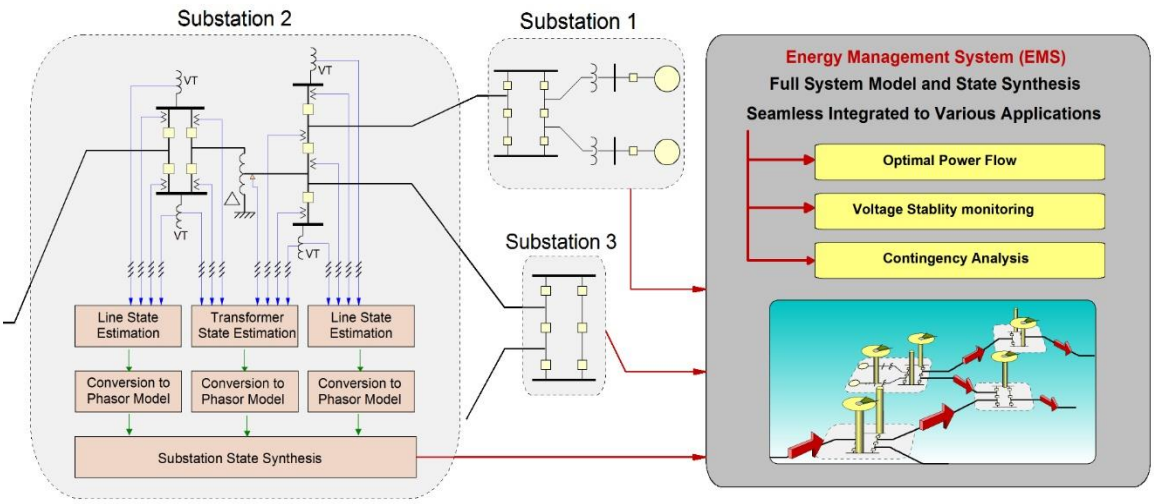

Figure 3.1. Overall approach of the proposed data acquisition system. [99-100]

If the input measurement data for the DDSE are time-domain waveforms, the estimated states coming out from the DDSE will also be time-domain waveforms, and the estimation results of the DDSE over a period of one cycle will be used to compute the states of the component in the "phasor domain", as shown in the block "conversion to phasor model" in Figure 3.1. A simplified example for the conversion of time-domain model to phasor-domain model is shown in Figure 3.2. This example handles with a very simple pi-equivalent model of a transmission line. As Figure 3.2 illustrates, the results of the DDSE over a period of one cycle are in the time domain. Specifically, the points on wave data are available for each variable of the component. This data is converted into the phasor-domain (frequency domain) by applying Fourier transform on the time-domain data over a user specified time interval, for example one cycle. Because the frequency of the system may vary in real time, the Fourier transform must estimate the frequency first and then perform the Fourier analysis over the actual time of one cycle. Otherwise issues of spectral leakage may appear. The end result of these computations is the zone model of the component in

phasor (frequency) domain, as indicated by Figure 3.2 [99]. Note also that at the time domain, the transmission line model is represented by a set of differential equations describing the voltage and current relationship for the inductance and capacitors of the transmission line. While at the phasor domain, the transmission line model is represented just by its admittance matrix. On the other hand, if the streaming data fed into the DDSE are already phasors, the output states of the DDSE will also be phasors, and there will be no need for extraction of the states in the "phasor domain".

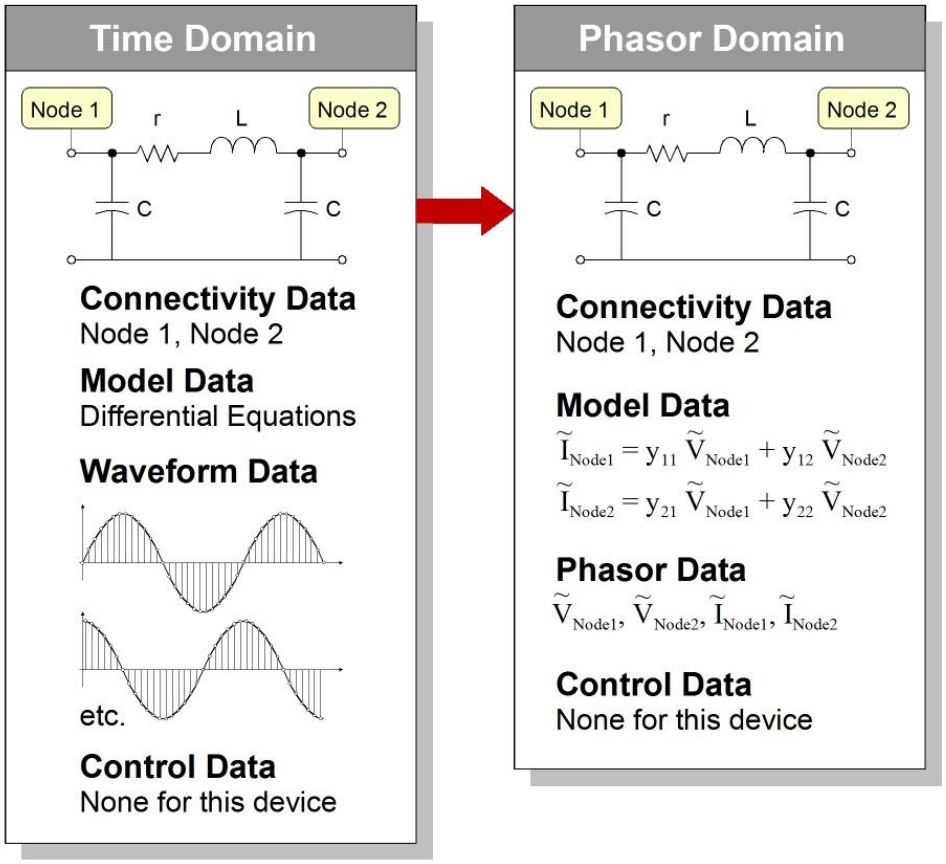

Figure 3.2. Conversion from time-domain to phasor-domain [99].

As a summary, the outputs of the DDSE are the real-time models and accurate operating conditions of the components at the substation level with GPS-synchronous time-stamp, which consist of (1) autonomously defined state and control variables, (2) an object-oriented, unified, and interoperable model of the component (described in section 4.2), and (3) connectivity information. Subsequently, this information is used to synthesize the substation state estimate. This process is quite simple: the state estimates of each component are aligned by the time stamp. The zone models of a specific time stamp are collected to form the substation state estimate. In the dissertation, a time interval of one cycle is used and therefore the substation state estimate is updated once per cycle. Note that the synthesis of the substation state does not require additional computations since the component models are all in UTC time (due to the GPS synchronized measurements) and therefore they can be simply merged to provide the substation model.

Subsequently, the substation state estimate (in frequency domain) is transmitted to the control center at a rate of 60 times per second, and in the control center, synthesis of system-wide states and model can be done. Figure 3.3 illustrates how the EMS synthesizes the system-wide model from substation state estimates [99]. The connectivity data of each component is used to compose the topology of the substation and then the entire system. Based on the topology, state estimates that have the same GPS time-stamp from each component are immediately combined to obtain the system-wide state estimate. Note that the synthesis of the system-wide state at the control center does not require additional computations since the component models are all in UTC time (as a result of the GPS-synchronized measurements) and therefore they can be simply merged.

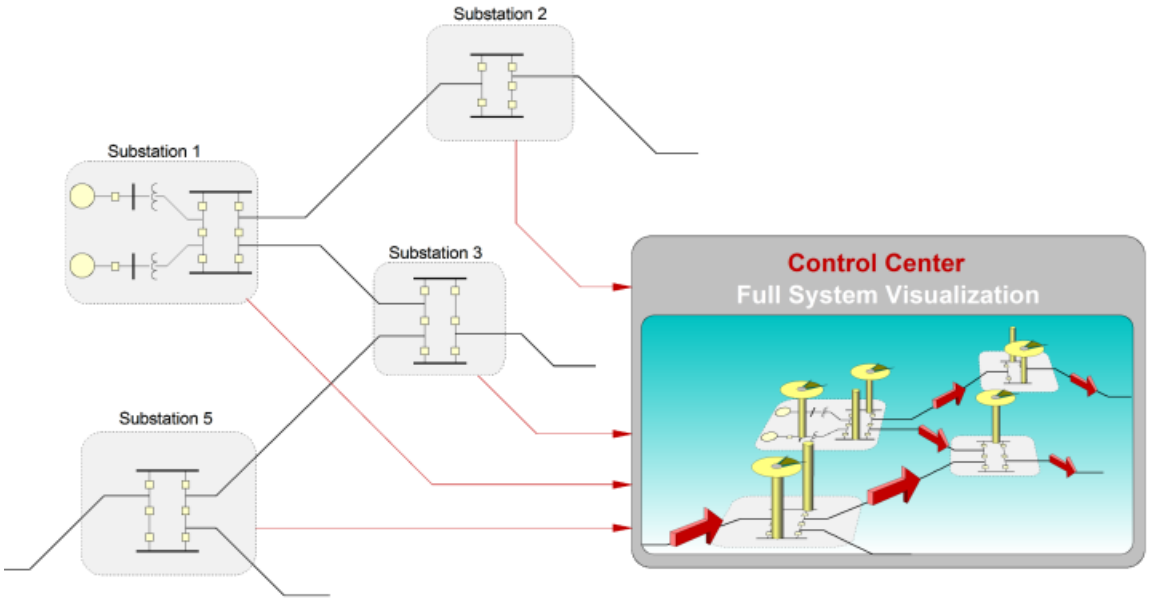

Figure 3.3. Synthesis of the system wide real-time model [99].

It should be stressed that the functional specifications of the UMPCU can be met by current top-of-the-line numerical protective relays. Specifically, the computational power of these relays is adequate to perform the analytics of the UMPCU, i.e. the state estimation for each component and the extraction of the real-time model of the component by appropriate programming. The UMPCUs are also able to receive commands from the control center and apply them to control power apparatus just as present relays are able to do.

It is emphasized that the proposed approach facilitates efficient communications. Specifically, each substation sends to the EMS only its real-time model which comprises a very small number of data. When connectivity changes (for example during breaker operation), connectivity data are transmitted by exception. Similarly if model changes occur (for example a tap change in a transformer), the new model will be transmitted by exception. The result is that while the instrumentation may be collecting data at rates of

thousands of data points per second, after the state estimation and conversion of data, the frequency-domain states (phasors) are only a few tens of data points per second. Only the frequency-domain component states are transmitted to the EMS. In a typical two kV level substation with 23 relays, and each relay has an average sampling rate of 2400 samples per second, the compression rate of sampled data to substation state is 352,800:28. The compression rate of phasor data to substation state is 294:28 (translated to real states, i.e. a phasor provides two states, real and imaginary).

Modeling accuracy and fidelity are fundamental in this approach. For many power system components, high-fidelity models exist. For some new components such as inverter-interfaced power components, the modeling accuracy may not be as high as that of other components. In both cases the DDSE can be utilized to fine tune the models and/or determine the parameters of the model with greater accuracy. The basic approach is to expand the dynamic state estimator to include some key parameters as unknown states. This is a procedure of parameters identification and model validation. Therefore the proposed overall approach can also provide better models with field-validated parameters compared with traditional approaches. Chapter 6 provides detailed discussions about the parameters identification and model validation.

The proposed approach provides the possibility that a high-fidelity model can be used as the main depository of the component model (protective relay level). This data base of high-fidelity component models can provide appropriate models for other EMS applications, which achieves a seamless integration with these applications. For example, for EMS applications such as optimization of the system operation conditions, a positive-sequence model can be computed from the high-fidelity model and sent to the EMS data

base. To guarantee that the high-fidelity model can be used across other EMS applications and across all relevant temporal and spatial scales, an object-oriented, unified, and seamless interoperable component model syntax is proposed and referred to as the state and control algebraic quadratic companion form (SCAQCF). This can be viewed as an advanced common information model. Applications can directly access and use this model without any filters or interfaces (seamless). The procedure for the automatic computation of the SCAQCF model is described in Chapter 4.

The advantage of the above autonomous model synthesis is that protective relays are ubiquitous, which means that the entire power system could be covered with the validated SCAQCF models provided by the DDSE in real time (perpetual model validation). And this approach enables an automated extraction of the validated real-time model of the system, with all necessary information and operating conditions for all the controllable and non-controllable devices. Since the validated high-fidelity real-time model is in an object-oriented SCAQCF syntax with seamless integration of other EMS applications, it is especially useful in cases where more and more renewable energy sources, such as wind and photovoltaic generation, characterized by high volatility and low prediction accuracy, are integrated into existing power systems. Any new resource (component) added to the system will be automatically accounted for in the EMS applications as long as its model is presented in the SCAQCF syntax.

3.3 Summary

A distributed and seamless infrastructure of data acquisition systems that provide the necessary information for an automated and interoperable EMS system is proposed in this

chapter. The advantages of the proposed modern EMS architecture include: (1) efficient communications (60 times per second) are guaranteed, since only the substation state (in phasor-domain) is transmitted to the control center while connectivity and model changes are transmitted by exception; (2) DDSE is performed at a fast executive rate, compared with the traditional state estimation with a centralized architecture; (3) synthesis of the system states does not require additional computation; (4) SCAQCF provides an object-oriented, unified, and interoperable model syntax for the components, enabling seamless integration of all EMS applications; (5) DDSE can be utilized to fine tune the models and/or determine the parameters of the model with greater accuracy; (6) the relay can be used as the main depository of the high-fidelity component model – this model is transmitted to all user including the EMS at the control center.

CHAPTER 4 THE STATE AND CONTROL ALGEBRAIC QUADRATIC COMPANION FORM

4.1 Overview

In this chapter, an object-oriented, interoperable, and unified state and control algebraic quadratic companion form (SCAQCF) for the component model in the power system is proposed and the methodology for obtaining this SCAQCF model is presented. The proposed SCAQCF model can be seamlessly integrated with various EMS applications such as SE and OPF. In this chapter, only a dynamic model of a device is discussed since a static model can be treated just as a specific case of the dynamic model without the dynamic equations.

Section 4.2 gives the general and detailed methodology for the derivation of the SCAQCF model of a component from the original model of the component, which is described by a set of dynamic and algebraic equations. To illustrate the implementation of this methodology, section 4.3 and section 4.4 give examples of the derivation of the SCAQCF model for the synchronous machine in the time domain and the phasor domain respectively.

4.2 The Derivation of the SCAQCF Model

In this section, an object-oriented, interoperable, and unified SCAQCF model is proposed and the methodology for obtaining this SCAQCF model is presented. The proposed SCAQCF model can be seamlessly integrated with various EMS applications such as DDSE and OPF. In this section, only a dynamic model of a device is discussed

since a static model can be treated just as a specific case of a dynamic model without the dynamic equations.

In general, the dynamic model of a device is described by a set of differential and algebraic equations (DAE), which express the dynamics of the system as follows:

$$\begin{aligned} \frac{dx(t)}{dt} &= f(x(t), y(t), t), \\ 0 &= g(x(t), y(t), t), \end{aligned} \tag{4.1}$$

where x and y are the dynamic and algebraic states of the system respectively. Given the set of DAE, a quadratization procedure is applied. This can be achieved without any approximations by introducing additional state variables and defining algebraic equations. Upon the quadratization procedure the model can be cast in the following form:

$$\begin{aligned} \frac{dx(t)}{dt} &= A_1 x(t) + A_2 y(t) + A_3 z(t) + C, \\ 0 &= E_1 x(t) + E_2 y(t) + E_3 z(t) + \begin{bmatrix} \left[x(t), y(t), z(t)\right] F_1 \left[x(t), y(t), z(t)\right]^T \\ \vdots \\ \left[x(t), y(t), z(t)\right] F_n \left[x(t), y(t), z(t)\right]^T \end{bmatrix} + D, \end{aligned} \tag{4.2}$$

where $z(t)$ are additional algebraic (internal) states introduced for the quadratization of the model. To bring the model in the SCAQCF form, the variables are categorized into through variables, external state variables, internal state variables, and control variables. The model equation set (4.2) is rearranged such that external equations connecting the through variables to the state variables and control variables are given first, followed by internal equations that are either differential or algebraic equations of order no more than two.

$$
\begin{aligned}
&A_1 \cdot \frac{di(t)}{dt} + A_2 \cdot i(t) = B_1 \cdot v(t) + B_2 \cdot x(t) + B_3 \cdot y(t) + B_4 \cdot u(t), \\
&0 = \frac{dx(t)}{dt} + C_1 v(t) + C_2 x(t) + C_3 y(t) + C_3 u(t), \\
&0 = E_1 v(t) + E_2 x(t) + E_3 y(t) + E_4 u(t) + \begin{bmatrix} [v(t), x(t), y(t), u(t)] F_1 [v(t), x(t), y(t), u(t)]^T \\ \vdots \\ [v(t), x(t), y(t), u(t)] F_n [v(t), x(t), y(t), u(t)]^T \end{bmatrix} + D,
\end{aligned}
\tag{4.3}
$$

where $i(t)$ represents the through variables of the device model, $v(t)$ represents the external states of the device model, $x(t)$ represents the internal dynamic states of the device model, $y(t)$ represents the internal algebraic states of the device model, and $u(t)$ represents the control variables of the device model.

Given the model described by equation set (4.3), the next step is to integrate the dynamical system. In this proposal, the quadratic-integration method that outperforms trapezoidal integration is used. The reason for this selection is its improved accuracy and ability to eliminate numerical oscillations that are often introduced by the trapezoidal-integration method [84]-[85]. The quadratic-integration method is described in Appendix A in details.

The dynamic functions are assumed to vary quadratically within the integration step [t-h, t]. This assumption is illustrated in Figure 4.1 [84]. Note that the three points $x(t-h)$, x_m and $x(t)$ fully define the quadratic function in the interval [t-h, t]. The general integration results over time intervals [t-h, t_m] and [t-h, t] are listed as follows:

$$
\begin{aligned}
&\int_{t-h}^{t_m} x(\tau) d\tau = \frac{5h}{24} x(t-h) + \frac{h}{3} x_m - \frac{h}{24} x(t), \\
&\int_{t-h}^{t} x(\tau) d\tau = \frac{h}{6} x(t-h) + \frac{2h}{3} x_m + \frac{h}{6} x(t).
\end{aligned}
\tag{4.4}
$$

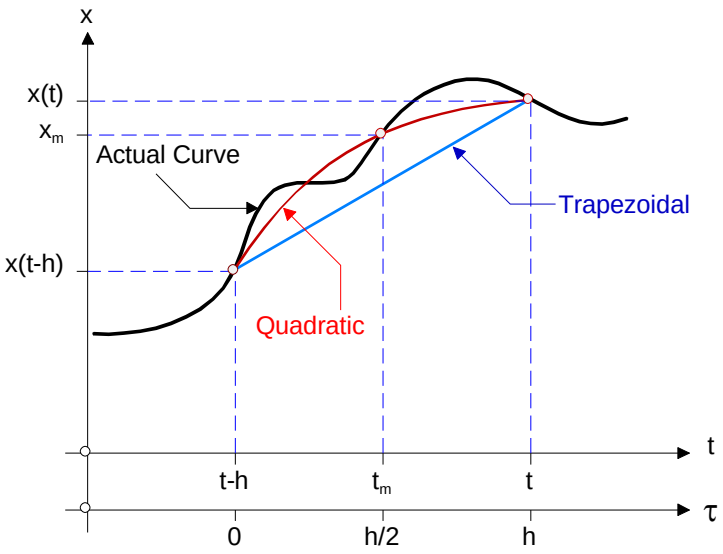

Figure 4.1. Illustration of the quadratic-integration method [84].

Quadratic integration is used to integrate the dynamic model of the device. The result is the following algebraic form:

$$
\begin{aligned}
&A_1\cdot(i(t)-i(t-h))+A_2\cdot(\frac{h}{6}\cdot i(t)+\frac{2h}{3}\cdot i(t_m)+\frac{h}{6}\cdot i(t-h))=B_1\cdot(\frac{h}{6}\cdot v(t)+\frac{2h}{3}\cdot v(t_m)+\frac{h}{6}\cdot v(t-h))\\
&\qquad +B_2\cdot(\frac{h}{6}\cdot x(t)+\frac{2h}{3}\cdot x(t_m)+\frac{h}{6}\cdot x(t-h))+B_3\cdot(\frac{h}{6}\cdot y(t)+\frac{2h}{3}\cdot y(t_m)+\frac{h}{6}\cdot y(t-h)),\\
&A_1\cdot(i(t_m)-i(t-h))+A_2\cdot(-\frac{h}{24}\cdot i(t)+\frac{h}{3}\cdot i(t_m)+\frac{5h}{24}\cdot i(t-h))=B_1\cdot(-\frac{h}{24}\cdot v(t)+\frac{h}{3}\cdot v(t_m)+\frac{5h}{24}\cdot v(t-h))\\
&\qquad +B_2\cdot(-\frac{h}{24}\cdot x(t)+\frac{h}{3}\cdot x(t_m)+\frac{5h}{24}\cdot x(t-h))+B_3\cdot(-\frac{h}{24}\cdot y(t)+\frac{h}{3}\cdot y(t_m)+\frac{5h}{24}\cdot y(t-h)),\\
&0=x(t)-x(t-h)+C_1\cdot(\frac{h}{6}\cdot v(t)+\frac{2h}{3}\cdot v(t_m)+\frac{h}{6}\cdot v(t-h))\\
&\quad +C_2\cdot(\frac{h}{6}\cdot x(t)+\frac{2h}{3}\cdot x(t_m)+\frac{h}{6}\cdot x(t-h))+C_3\cdot(\frac{h}{6}\cdot y(t)+\frac{2h}{3}\cdot y(t_m)+\frac{h}{6}\cdot y(t-h)),\\
&0=x(t_m)-x(t-h)+C_1\cdot(-\frac{h}{24}\cdot v(t)+\frac{h}{3}\cdot v(t_m)+\frac{5h}{24}\cdot v(t-h))\\
&\quad +C_2\cdot(-\frac{h}{24}\cdot x(t)+\frac{h}{3}\cdot x(t_m)+\frac{5h}{24}\cdot x(t-h))+C_3\cdot(-\frac{h}{24}\cdot y(t)+\frac{h}{3}\cdot y(t_m)+\frac{5h}{24}\cdot y(t-h)),\\
&0=E_1v(t)+E_2x(t)+E_3y(t)+E_4u(t)+\begin{bmatrix}[v(t),x(t),y(t),u(t)]F_1[v(t),x(t),y(t),u(t)]^T\\ \vdots\\ [v(t),x(t),y(t),u(t)]F_n[v(t),x(t),y(t),u(t)]^T\end{bmatrix}+D,\\
&0=E_1v(t_m)+E_2x(t_m)+E_3y(t_m)+E_4u(t_m)+\begin{bmatrix}[v(t_m),x(t_m),y(t_m),u(t_m)]F_1[v(t_m),x(t_m),y(t_m),u(t_m)]^T\\ \vdots\\ [v(t_m),x(t_m),y(t_m),u(t_m)]F_n[v(t_m),x(t_m),y(t_m),u(t_m)]^T\end{bmatrix}+D,
\end{aligned}
\tag{4.5}
$$

where subscripts t and t_m denote the time point t and the middle time point between t and t-h.

Upon manipulations on the equation set (4.5) and by defining $\mathbf{x}(t) = \begin{bmatrix} v(t) & x(t) & y(t) \end{bmatrix}$ as the states of the device (dynamic and algebraic), the integrated SCAQCF device model can be cast in the following form:

$$\begin{Bmatrix} I(\mathbf{x},\mathbf{u}) \\ \vdots \\ 0 \\ \vdots \end{Bmatrix} = Y_{eqx}\mathbf{x} + \begin{Bmatrix} \vdots \\ \mathbf{x}^T F_{eqx}^i \mathbf{x} \\ \vdots \end{Bmatrix} + Y_{equ}\mathbf{u} + \begin{Bmatrix} \vdots \\ \mathbf{u}^T F_{equ}^i \mathbf{u} \\ \vdots \end{Bmatrix} + \begin{Bmatrix} \vdots \\ \mathbf{x}^T F_{eqxu}^i \mathbf{u} \\ \vdots \end{Bmatrix} - B_{eq}, \tag{4.6}$$

$$B_{eq} = -N_{eqx}\mathbf{x}(t-h) - N_{equ}\mathbf{u}(t-h) - M_{eq}I(t-h) - K_{eq},$$

where $I(\mathbf{x},\mathbf{u})$ represents the through variables of the device model, $I = [I(t), I(t_m)]$, $\mathbf{x}$ represents the external and internal state variables of the device model, $\mathbf{x} = [\mathbf{x}(t), \mathbf{x}(t_m)]$, $\mathbf{u}$ represents the control variables of the device model, Y_{eqx} represents the matrix defining the linear part for state variables, F_{eqx} represents the matrices defining the quadratic part for state variables, Y_{equ} represents the matrix defining the linear part for control variables, F_{equ} represents the matrices defining the quadratic part for control variables, F_{eqxu} represents the matrices defining the quadratic part for the product of state and control variables, B_{eq} is the history dependent vector of the device model, N_{eqx} is the matrix defining the integration of last step state variables, M_{eq} is the matrix defining the integration of last step through variables, and K_{eq} is the constant vector of the device model.

Detailed examples of the formulation of the SCAQCF model for the synchronous machine in time-domain and phasor-domain are given in the following two sections.

4.3 The SCAQCF Model for a Synchronous Machine in Time Domain

This section presents the SCAQCF for the energy conversion model of a synchronous machine that includes two damper windings. First the compact model is presented and then the SCAQCF model is presented by applying model quadratization and quadratic integration.

4.3.1 Synchronous Machine in Time Domain - Compact Form

Figure 4.2 illustrates the diagram of the synchronous machine energy conversion model with two damper windings.

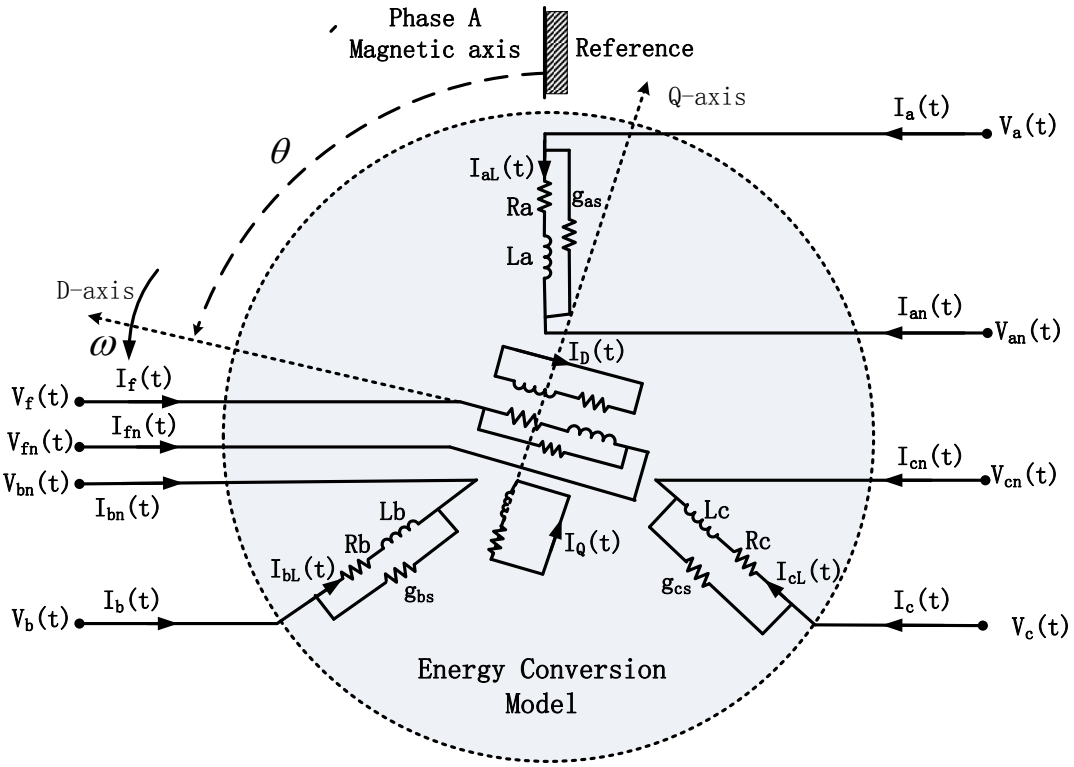

Figure 4.2. Synchronous machine model-two damper windings.

The windings model can be formulated in compact form as follows:

$$i_{abc}(t) = i_{aL\ bL\ cL}(t) + g_{as,bs,cs} \cdot (v_{abc}(t) - v_{an\ bn\ cn}(t)), \tag{4.7}$$

$$i_{an\ bn\ cn}(t) = -i_{aL\ bL\ cL}(t) + g_{as,bs,cs} \cdot (v_{an\ bn\ cn}(t) - v_{abc}(t)), \tag{4.8}$$

$$i_f(t) = i_{fL}(t) + g_{fs} \cdot (v_f(t) - v_{fn}(t)), \tag{4.9}$$

$$i_{fn}(t) = -i_{fL}(t) + g_{fs} \cdot (v_{fn}(t) - v_f(t)), \tag{4.10}$$

$$T_m(t) = J \frac{d\omega_m(t)}{dt} - T_e(t) - T_{wf}(t), \tag{4.11}$$

$$0 = v_{abc}(t) - v_{an\ bn\ cn}(t) - R_{abc} i_{aL\ bL\ cL}(t) + e_{abc}(t), \tag{4.12}$$

$$0 = v_f(t) - R_f i_{fL}(t) - e_f(t) - v_{fn}(t), \tag{4.13}$$

$$0 = R_{DQ} i_{DQ}(t) + e_{DQ}(t), \tag{4.14}$$

$$0 = \frac{d\theta_m(t)}{dt} - \omega_m(t), \tag{4.15}$$

$$0 = \theta(t) - \frac{p}{2}\theta_m(t), \tag{4.16}$$

$$0 = \omega(t) - \frac{p}{2}\omega_m(t), \tag{4.17}$$

$$0 = \theta(t) - \delta(t) - \frac{\pi}{2}, \tag{4.18}$$

$$0 = T_{wf}(t) + \left(D_{fw} + D'_{fw} \cdot \omega_m(t) + D''_{fw} \cdot \omega_m(t)^2\right), \tag{4.19}$$

$$0 = P_{em}(t) - e_{abc}(t)^T i_{aL\ bL\ cL}(t), \tag{4.20}$$

$$0 = T_e - \frac{1}{\sqrt{3}} \cdot n_p \cdot \begin{pmatrix} i_{aL}(t)\lambda_b(t) - i_{aL}(t)\lambda_c(t) + i_{bL}(t)\lambda_c(t) \\ -i_{bL}(t)\lambda_a(t) + i_{cL}(t)\lambda_a(t) - i_{cL}(t)\lambda_b(t) \end{pmatrix}, \tag{4.21}$$

$$0 = \frac{d\lambda_{abc}(t)}{dt} - e_{abc}(t), \tag{4.22}$$

$$0 = \frac{d\lambda_{fDQ}(t)}{dt} - e_{fDQ}(t), \tag{4.23}$$

$$\begin{bmatrix} \lambda_{abc}(t) \\ \lambda_{fDQ}(t) \end{bmatrix} = \begin{bmatrix} L_{ss}(\theta(t)) & L_{sr}(\theta(t)) \\ L_{rs}(\theta(t)) & L_{rr} \end{bmatrix} \begin{bmatrix} -i_{aL\ bL\ cL}(t) \\ i_{fL\ DQ}(t) \end{bmatrix}, \tag{4.24}$$

where $i_{abc}(t)$, $i_{an\ bn\ cn}(t)$, $i_f(t)$ and $i_{fn}(t)$ are vectors of the terminal currents flowing through the windings of phases A, B, C, or the field winding f respectively. $i_{aL\ bL\ cL}(t)$, $i_{fL\ DQ}(t)$ are vectors of the current flowing through the inductance of phases A, B, C, or the field winding f, or the damper windings D and Q respectively. $v_{abc}(t)$, $v_{an\ bn\ cn}(t)$, $v_f(t)$ and $v_{fn}(t)$ are vectors of the terminal voltages of the windings of phases A, B, C, or the field winding f respectively. $e_{abc}(t), e_{fDQ}(t)$ are vectors of phases A, B, C, field winding f, and D and Q-damper internal EMFs respectively. $\lambda_{abc}(t), \lambda_{fDQ}(t)$ are vectors of phases A, B, C, field winding f, and D and Q-damper flux linkages respectively. $L_{ss}(\theta(t))$, $L_{sr}(\theta(t))$, $L_{rs}(\theta(t))$ and $L_{rr}(\theta(t))$ are matrices of the self and mutual inductances of the machine stator and rotor windings.

Detailed description of the above inductances is as follows,

Stator Self-Inductances

Stator self-inductances, L_{aa}, L_{bb} and L_{cc}, in general depend on rotor position. An approximate expression of this dependence is

$$L_{aa}(t) = L_s + L_m \cos\left(2\theta(t)\right), \tag{4.25}$$

$$L_{bb}(t) = L_s + L_m \cos\left(2\theta(t) - {}^{4\pi}\!/_{3}\right), \tag{4.26}$$

$$L_{cc}(t) = L_s + L_m \cos\left(2\theta(t) + {}^{4\pi}\!/_{3}\right), \tag{4.27}$$

where L_s is the self-inductance due to space-fundamental air-gap flux and the armature leakage flux; the additional component that varies with 2θ is due to the rotor saliency.

Rotor Self-Inductances

Rotor self-inductances, L_{ff}, L_{DD}, and L_{QQ}, are approximately constants and can be symbolized with

$$L_{ff} = L_f, \qquad L_{DD} = L_D, \qquad L_{QQ} = L_Q. \tag{4.28}$$

Stator Mutual Inductances

Stator mutual inductances, L_{ab}, L_{bc}, and L_{ca}, are negative. They are functions of the rotor position $\theta(t)$. Approximate expressions for these functions are

$$L_{ab}(t) = L_{ba}(t) = -M_S - L_m \cos 2\left(\theta(t) + \pi/6\right) = -M_S - L_m \cos\left(2\theta(t) + \pi/3\right), \tag{4.29}$$

$$L_{bc}(t) = L_{cb}(t) = -M_S - L_m \cos 2\left(\theta(t) - \pi/2\right) = -M_S - L_m \cos\left(2\theta(t) - \pi\right), \tag{4.30}$$

$$L_{ca}(t) = L_{ac}(t) = -M_S - L_m \cos 2\left(\theta(t) - 7\pi/6\right) = -M_S - L_m \cos\left(2\theta(t) - \pi/3\right). \tag{4.31}$$

Rotor Mutual Inductances

Rotor mutual inductances, L_{fD}, L_{DQ}, and L_{Qf}, are constants and independent of $\theta(t)$, because the rotor windings are stationary with one another.

$$L_{fD} = L_{Df} = M_R, \qquad L_{DQ} = L_{QD} = 0 \;\; L_{Qf} = L_{fQ} = 0. \tag{4.32}$$

Mutual Inductances between Stator and rotor

Mutual inductances between stator's windings and rotor's windings, L_{af}, L_{bf}, and L_{cf}, are dependent upon the rotor position $\theta(t)$ as follows:

$$L_{af}(t) = L_{fa}(t) = M_F \cos\theta(t), \tag{4.33}$$

$$L_{bf}(t) = L_{fb}(t) = M_F \cos\left(\theta(t) - 2\pi/3\right), \tag{4.34}$$

$$L_{cf}(t) = L_{fc}(t) = M_F \cos\left(\theta(t) - 4\pi/3\right) = M_F \cos\left(\theta(t) + 2\pi/3\right). \tag{4.35}$$

Similarly,

$$L_{aD}(t) = L_{Da}(t) = M_D \cos\theta(t), \tag{4.36}$$

$$L_{bD}(t) = L_{Db}(t) = M_D \cos\left(\theta(t) - 2\pi/3\right), \tag{4.37}$$

$$L_{cD}(t) = L_{Dc}(t) = M_D \cos\left(\theta(t) - 4\pi/3\right) = M_D \cos\left(\theta(t) + 2\pi/3\right). \tag{4.38}$$

The damper winding Q is orthogonal to the D winding. According to our definition of rotor d-axis and q-axis, we have:

$$L_{aQ}(t) = L_{Qa}(t) = M_Q \cos\left(\theta(t) - \pi/2\right) = M_Q \sin\theta(t), \tag{4.39}$$

$$L_{bQ}(t) = L_{Qb}(t) = M_Q \cos\left(\theta(t) - \pi/2 - 2\pi/3\right) = M_Q \sin\left(\theta(t) - 2\pi/3\right), \tag{4.40}$$

$$L_{cQ}(t) = L_{Qc}(t) = M_Q \sin(\theta(t) - 4\pi/3) = M_Q \sin(\theta(t) + 2\pi/3). \tag{4.41}$$

4.3.2 Synchronous Machine in Time Domain - Quadratized Form

The self and mutual inductances of the machine stator and rotor windings are dependent on the position of the rotor, which is time-varying, thus these inductances are also time-dependent. For example, phase A self-inductance is found to be:

$$L_{aa}(t) = L_s + L_m \cos\left(2\theta(t)\right) = L_s + L_m(\cos^2\left(\theta(t)\right) - \sin^2\left(\theta(t)\right)). \tag{4.42}$$

By introducing $c(t) = \cos\left(\theta(t)\right)$ and $s(t) = \sin\left(\theta(t)\right)$ as new state variables, the equation becomes quadratic in terms of the new variables:

$$L_{aa}(t) = L_s + L_m\left(c(t)^2 - s(t)^2\right). \tag{4.43}$$

With the above introduced variables, the flux equation terms are quadratized. Illustrative examples are shown below:

$$L_{bb}(t)i_{bL}(t)=\left(L_s+L_m\cos\left(2\theta(t)-4\pi/3\right)\right)i_{bL}(t)=L_s i_{bL}(t)-\frac{1}{2}L_m c_2(t)i_{bL}(t)-\frac{\sqrt{3}}{2}L_m s_2(t)i_{bL}(t), \quad (4.44)$$

$$L_{ab}(t)i_{bL}(t)=\left(-M_s-L_m\cos\left(2\theta(t)+\pi/3\right)\right)i_{bL}(t)=-M_s i_{bL}(t)-\frac{1}{2}L_m c_2(t)i_{bL}(t)+\frac{\sqrt{3}}{2}L_m s_2(t)i_{bL}(t), \quad (4.45)$$

$$L_{bD}(t)i_{bL}(t)=M_D\cos\left(\theta(t)-2\pi/3\right)i_{bL}(t)=-\frac{1}{2}M_D c(t)i_{bL}(t)+\frac{\sqrt{3}}{2}M_D s(t)i_{bL}(t). \quad (4.46)$$

Following this methodology the quadratized model of the synchronous machine is formulated as follows:

$$i_{abc}(t)=i_{aL\ bL\ cL}(t)+g_{as,bs,cs}\cdot(v_{abc}(t)-v_{an\ bn\ cn}(t)), \quad (4.47)$$

$$i_{an\ bn\ cn}(t)=-i_{aL\ bL\ cL}(t)+g_{as,bs,cs}\cdot(v_{an\ bn\ cn}(t)-v_{abc}(t)), \quad (4.48)$$

$$i_f(t)=i_{fL}(t)+g_{fs}\cdot(v_f(t)-v_{fn}(t)), \quad (4.49)$$

$$i_{fn}(t)=-i_{fL}(t)+g_{fs}\cdot(v_{fn}(t)-v_f(t)), \quad (4.50)$$

$$T_m(t)=T_{acc}-T_e(t)-T_{wf}(t), \quad (4.51)$$

$$0=v_{abc}(t)-v_{an\ bn\ cn}(t)-R_{abc}i_{aL\ bL\ cL}(t)+e_{abc}(t), \quad (4.52)$$

$$0=v_f(t)-R_f i_{fL}(t)-e_f(t)-v_{fn}(t), \quad (4.53)$$

$$0=R_{DQ}i_{DQ}(t)+e_{DQ}(t), \quad (4.54)$$

$$0=\theta(t)-\frac{p}{2}\theta_m(t), \quad (4.55)$$

$$0=\omega(t)-\frac{p}{2}\omega_m(t), \quad (4.56)$$

$$0=\theta(t)-\delta(t)-\frac{\pi}{2}, \quad (4.57)$$

$$0 = \frac{d\theta_m(t)}{dt} - \omega_m(t), \tag{4.58}$$

$$0 = \frac{d\lambda_{abc}(t)}{dt} - e_{abc}(t), \tag{4.59}$$

$$0 = \frac{d\lambda_{fDQ}(t)}{dt} - e_{fDQ}(t), \tag{4.60}$$

$$0 = \frac{d\omega_m(t)}{dt} - \frac{1}{J}T_{acc}(t), \tag{4.61}$$

$$0 = \frac{dc(t)}{dt} - y_1(t), \tag{4.62}$$

$$0 = \frac{ds(t)}{dt} - y_2(t), \tag{4.63}$$

$$0 = T_{wf}(t) + \left(D_{fw} + D'_{fw} \cdot \omega_m(t) + D''_{fw} \cdot \omega_m(t)^2\right), \tag{4.64}$$

$$0 = P_{em}(t) - e_{abc}(t)^T i_{aL\ bL\ cL}(t), \tag{4.65}$$

$$0 = T_e - \frac{1}{\sqrt{3}} \cdot n_p \cdot \begin{pmatrix} i_{aL}(t)\lambda_b(t) - i_{aL}(t)\lambda_c(t) + i_{bL}(t)\lambda_c(t) \\ -i_{bL}(t)\lambda_a(t) + i_{cL}(t)\lambda_a(t) - i_{cL}(t)\lambda_b(t) \end{pmatrix}, \tag{4.66}$$

$$0 = y_1(t) + s(t) \cdot \omega(t), \tag{4.67}$$

$$0 = y_2(t) - c(t) \cdot \omega(t), \tag{4.68}$$

$$0 = c_2(t) - c^2(t) + s^2(t), \tag{4.69}$$

$$0 = s_2(t) - 2c(t)s(t), \tag{4.70}$$

$$\begin{bmatrix} \lambda_{abc}(t) \\ \lambda_{fDQ}(t) \end{bmatrix} = \left(A \cdot c(t) + B \cdot s(t) + C \cdot c_2(t) + D \cdot s_2(t) + E\right) \cdot \begin{bmatrix} -i_{aL\ bL\ cL}(t) \\ i_{fL\ DQ}(t) \end{bmatrix}, \tag{4.71}$$

where the following definitions hold:

$$c(t) = \cos\left(\theta(t)\right),$$

$$s(t) = \sin\left(\theta(t)\right),$$

$$c_2(t) = \cos(2 \cdot \theta(t)),$$

$$s_2(t) = \sin(2 \cdot \theta(t)).$$

And A, B, C, D, and E are constant matrices defined as follows:

$$A = \begin{bmatrix} 0 & 0 & 0 & M_F & M_D & 0 \\ 0 & 0 & 0 & -\frac{1}{2}M_F & -\frac{1}{2}M_D & -\frac{\sqrt{3}}{2}M_Q \\ 0 & 0 & 0 & -\frac{1}{2}M_F & -\frac{1}{2}M_D & \frac{\sqrt{3}}{2}M_Q \\ M_F & -\frac{1}{2}M_F & -\frac{1}{2}M_F & 0 & 0 & 0 \\ M_D & -\frac{1}{2}M_D & -\frac{1}{2}M_D & 0 & 0 & 0 \\ 0 & -\frac{\sqrt{3}}{2}M_Q & \frac{\sqrt{3}}{2}M_Q & 0 & 0 & 0 \end{bmatrix},$$

$$B = \begin{bmatrix} 0 & 0 & 0 & 0 & 0 & M_Q \\ 0 & 0 & 0 & \frac{\sqrt{3}}{2}M_F & \frac{\sqrt{3}}{2}M_D & -\frac{1}{2}M_Q \\ 0 & 0 & 0 & -\frac{\sqrt{3}}{2}M_F & -\frac{\sqrt{3}}{2}M_D & -\frac{1}{2}M_Q \\ 0 & \frac{\sqrt{3}}{2}M_F & -\frac{\sqrt{3}}{2}M_F & 0 & 0 & 0 \\ 0 & \frac{\sqrt{3}}{2}M_D & -\frac{\sqrt{3}}{2}M_D & 0 & 0 & 0 \\ M_Q & -\frac{1}{2}M_Q & -\frac{1}{2}M_Q & 0 & 0 & 0 \end{bmatrix},$$

$$C = \begin{bmatrix} L_m & -\frac{1}{2}L_m & -\frac{1}{2}L_m & 0 & 0 & 0 \\ -\frac{1}{2}L_m & -\frac{1}{2}L_m & L_m & 0 & 0 & 0 \\ -\frac{1}{2}L_m & L_m & -\frac{1}{2}L_m & 0 & 0 & 0 \\ 0 & 0 & 0 & 0 & 0 & 0 \\ 0 & 0 & 0 & 0 & 0 & 0 \\ 0 & 0 & 0 & 0 & 0 & 0 \end{bmatrix},$$

$$D = \begin{bmatrix} 0 & \frac{\sqrt{3}}{2}L_m & -\frac{\sqrt{3}}{2}L_m & 0 & 0 & 0 \\ \frac{\sqrt{3}}{2}L_m & -\frac{\sqrt{3}}{2}L_m & 0 & 0 & 0 & 0 \\ -\frac{\sqrt{3}}{2}L_m & 0 & \frac{\sqrt{3}}{2}L_m & 0 & 0 & 0 \\ 0 & 0 & 0 & 0 & 0 & 0 \\ 0 & 0 & 0 & 0 & 0 & 0 \\ 0 & 0 & 0 & 0 & 0 & 0 \end{bmatrix},$$

$$E = \begin{bmatrix} L_s & -M_s & -M_s & 0 & 0 & 0 \\ -M_s & L_s & -M_s & 0 & 0 & 0 \\ -M_s & -M_s & L_s & 0 & 0 & 0 \\ 0 & 0 & 0 & L_f & M_R & 0 \\ 0 & 0 & 0 & M_R & L_D & 0 \\ 0 & 0 & 0 & 0 & 0 & L_Q \end{bmatrix}.$$

The definition of the external state, internal state, and through variables are listed in Table 4.1 to Table 4.3, respectively.

Table 4.1. External states of the synchronous machine.

Index	Variable	Description
0	$v_a(t)$	terminal voltage of stator phase A (kV)
1	$v_b(t)$	terminal voltage of stator phase B (kV)
2	$v_c(t)$	terminal voltage of stator phase C (kV)
3	$v_{an}(t)$	terminal voltage of stator phase AN (kV)
4	$v_{bn}(t)$	terminal voltage of stator phase BN (kV)
5	$v_{cn}(t)$	terminal voltage of stator phase CN (kV)
6	$v_f(t)$	terminal voltage of rotor field winding (kV)
7	$v_{fn}(t)$	terminal voltage of rotor field winding neutral (kV)
8	$\omega_m(t)$	machine mechanical shaft speed (rad/s)

Table 4.2. Internal states of the synchronous machine.

Index	Variable	Description
9	$i_{aL}(t)$	current through the inductance of stator phase A (kA)
10	$i_{bL}(t)$	current through the inductance of stator phase B (kA)
11	$i_{cL}(t)$	current through the inductance of stator phase C (kA)
12	$i_{fL}(t)$	current through the inductance of field winding (kA)
13	$i_D(t)$	current through rotor d-axis damper-winding (kA)
14	$i_Q(t)$	current through rotor q-axis damper-winding (kA)
15	$\theta_m(t)$	rotor angular position w.r.t. a stationary reference axis (rad)
16	$\theta(t)$	electrical rotor position angle (rad)
17	$\omega(t)$	machine electrical shaft speed (rad/s)
18	$\delta(t)$	machine power angle (rad)
19	$T_{fw}(t)$	friction and windage torque (MNm)
20	$P_{em}(t)$	internal electrical power (MW)
21	$T_e(t)$	machine electrical torque (MNm)
22	$e_a(t)$	stator winding internal EMF, phase A (kV)
23	$e_b(t)$	stator winding internal EMF, phase B (kV)
24	$e_c(t)$	stator winding internal EMF, phase C (kV)
25	$e_f(t)$	field winding internal EMF (kV)

26	$e_D(t)$	D-damper winding internal EMF (kV)
27	$e_Q(t)$	Q-damper winding internal EMF (kV)
28	$\lambda_a(t)$	flux linkage through stator winding of phase A (kWb)
29	$\lambda_b(t)$	flux linkage through stator winding of phase B (kWb)
30	$\lambda_c(t)$	flux linkage through stator winding of phase C (kWb)
31	$\lambda_f(t)$	flux linkage through rotor field winding (kWb)
32	$\lambda_D(t)$	flux linkage through rotor d-axis damper-winding (kWb)
33	$\lambda_Q(t)$	flux linkage through rotor q-axis damper-winding (kWb)
34	$T_{acc}(t)$	machine accelerating torque (MNm)
35	$c(t)$	cos($\theta(t)$) [state 16]
36	$s(t)$	sin($\theta(t)$) [state 16]
37	$y_1(t)$	internal variable y1 (rad/s)
38	$y_2(t)$	internal variable y2 (rad/s)
39	$c_2(t)$	cos($2\theta(t)$) [state 16]
40	$s_2(t)$	sin($2\theta(t)$) [state 16]

Table 4.3. Through variables of the synchronous machine.

Index	Variable	Description
0	$i_a(t)$	current through stator winding of phase a
1	$i_b(t)$	current through stator winding of phase b
2	$i_c(t)$	current through stator winding of phase c
3	$i_{an}(t)$	current through stator winding of phase an
4	$i_{bn}(t)$	current through stator winding of phase bn
5	$i_{cn}(t)$	current through stator winding of phase cn
6	$i_f(t)$	current through rotor field winding
7	$i_{fn}(t)$	current through rotor field winding (neutral side)
8	$T_m(t)$	mechanical torque applied on the machine shaft (MNm)

4.3.3 Synchronous Machine in Time Domain - SCAQCF

We use quadratic integration method to integrate the differential equations, and for the algebra equations, we just change the time variable at time t and tm, the equations come out to be as follows:

$$i_{abc}(t) = i_{aL\ bL\ cL}(t) + g_{as,bs,cs} \cdot (v_{abc}(t) - v_{an\ bn\ cn}(t)), \tag{4.72}$$

$$i_{an\ bn\ cn}(t) = -i_{aL\ bL\ cL}(t) + g_{as,bs,cs} \cdot (v_{an\ bn\ cn}(t) - v_{abc}(t)), \tag{4.73}$$

$$i_f(t) = i_{fL}(t) + g_{fs} \cdot (v_f(t) - v_{fn}(t)), \tag{4.74}$$

$$i_{fn}(t) = -i_{fL}(t) + g_{fs} \cdot (v_{fn}(t) - v_f(t)), \tag{4.75}$$

$$T_m(t) = T_{acc} - T_e(t) - T_{wf}(t), \tag{4.76}$$

$$0 = v_{abc}(t) - v_{an\ bn\ cn}(t) - R_{abc} i_{aL\ bL\ cL}(t) + e_{abc}(t), \tag{4.77}$$

$$0 = v_f(t) - R_f i_{fL}(t) - e_f(t) - v_{fn}(t), \tag{4.78}$$

$$0 = R_{DQ} i_{DQ}(t) + e_{DQ}(t), \tag{4.79}$$

$$0 = \theta(t) - \frac{p}{2}\theta_m(t), \tag{4.80}$$

$$0 = \omega(t) - \frac{p}{2}\omega_m(t), \tag{4.81}$$

$$0 = \theta(t) - \delta(t) - \frac{\pi}{2}, \tag{4.82}$$

$$0 = \frac{h}{6}\omega_m(t) + \frac{2h}{3}\omega_m(t_m) - \theta_m(t) + \left(\frac{h}{6}\omega_m(t-h) + \theta_m(t-h)\right), \tag{4.83}$$

$$0 = \frac{h}{6}e_{abc}(t) + \frac{2h}{3}e_{abc}(t_m) - \lambda_{abc}(t) + \left(\frac{h}{6}e_{abc}(t-h) + \lambda_{abc}(t-h)\right), \tag{4.84}$$

$$0 = \frac{h}{6}e_{fDQ}(t) + \frac{2h}{3}e_{fDQ}(t_m) - \lambda_{fDQ}(t) + \left(\frac{h}{6}e_{fDQ}(t-h) + \lambda_{fDQ}(t-h)\right), \tag{4.85}$$

$$0 = \frac{h}{6 \cdot J} T_{acc}(t) + \frac{2h}{3 \cdot J} T_{acc}(t_m) - \omega_m(t) + \left(\frac{h}{6 \cdot J} T_{acc}(t-h) + \omega_m(t-h) \right), \tag{4.86}$$

$$0 = \frac{h}{6} y_1(t) + \frac{2h}{3} y_1(t_m) - c(t) + \left(\frac{h}{6} y_1(t-h) + c(t-h) \right), \tag{4.87}$$

$$0 = \frac{h}{6} y_2(t) + \frac{2h}{3} y_2(t_m) - s(t) + \left(\frac{h}{6} y_2(t-h) + s(t-h) \right), \tag{4.88}$$

$$0 = T_{wf}(t) + \left(D_{fw} + D'_{fw} \cdot \omega_m(t) + D''_{fw} \cdot \omega_m(t)^2 \right), \tag{4.89}$$

$$0 = P_{em}(t) - e_{abc}(t)^T i_{aL\ bL\ cL}(t), \tag{4.90}$$

$$0 = T_e - \frac{1}{\sqrt{3}} \cdot n_p \cdot \begin{pmatrix} i_{aL}(t) \lambda_b(t) - i_{aL}(t) \lambda_c(t) + i_{bL}(t) \lambda_c(t) \\ -i_{bL}(t) \lambda_a(t) + i_{cL}(t) \lambda_a(t) - i_{cL}(t) \lambda_b(t) \end{pmatrix}, \tag{4.91}$$

$$0 = y_1(t) + s(t) \cdot \omega(t), \tag{4.92}$$

$$0 = y_2(t) - c(t) \cdot \omega(t), \tag{4.93}$$

$$0 = c_2(t) - c^2(t) + s^2(t), \tag{4.94}$$

$$0 = s_2(t) - 2c(t)s(t), \tag{4.95}$$

$$\begin{bmatrix} \lambda_{abc}(t) \\ \lambda_{fDQ}(t) \end{bmatrix} = \left(A \cdot c(t) + B \cdot s(t) + C \cdot c_2(t) + D \cdot s_2(t) + E \right) \cdot \begin{bmatrix} -i_{aL\ bL\ cL}(t) \\ i_{fL\ DQ}(t) \end{bmatrix}. \tag{4.96}$$

$$i_{abc}(t_m) = i_{aL\ bL\ cL}(t_m) + g_{as,bs,cs} \cdot (v_{abc}(t_m) - v_{an\ bn\ cn}(t_m)), \tag{4.97}$$

$$i_{an\ bn\ cn}(t_m) = -i_{aL\ bL\ cL}(t_m) + g_{as,bs,cs} \cdot (v_{an\ bn\ cn}(t_m) - v_{abc}(t_m)), \tag{4.98}$$

$$i_f(t_m) = i_{fL}(t_m) + g_{fs} \cdot (v_f(t_m) - v_{fn}(t_m)), \tag{4.99}$$

$$i_{fn}(t_m) = -i_{fL}(t_m) + g_{fs} \cdot (v_{fn}(t_m) - v_f(t_m)), \tag{4.100}$$

$$T_m(t_m) = T_{acc}(t_m) - T_e(t_m) - T_{wf}(t_m), \tag{4.101}$$

$$0 = v_{abc}(t_m) - v_{an\ bn\ cn}(t_m) - R_{abc} i_{aL\ bL\ cL}(t_m) + e_{abc}(t_m), \tag{4.102}$$

$$0 = v_f(t_m) - R_f i_{fL}(t_m) - e_f(t_m) - v_{fn}(t_m), \tag{4.103}$$

$$0 = R_{DQ} i_{DQ}(t_m) + e_{DQ}(t_m), \tag{4.104}$$

$$0 = \theta(t_m) - \frac{p}{2}\theta_m(t_m), \tag{4.105}$$

$$0 = \omega(t_m) - \frac{p}{2}\omega_m(t_m), \tag{4.106}$$

$$0 = \theta(t_m) - \delta(t_m) - \frac{\pi}{2}, \tag{4.107}$$

$$0 = -\frac{h}{24}\omega_m(t) + \frac{h}{3}\omega_m(t_m) - \theta_m(t_m) + \left(\frac{5h}{24}\omega_m(t-h) + \theta_m(t-h)\right), \tag{4.108}$$

$$0 = -\frac{h}{24}e_{abc}(t) + \frac{h}{3}e_{abc}(t_m) - \lambda_{abc}(t_m) + \left(\frac{5h}{24}e_{abc}(t-h) + \lambda_{abc}(t-h)\right), \tag{4.109}$$

$$0 = -\frac{h}{24}e_{fDQ}(t) + \frac{h}{3}e_{fDQ}(t_m) - \lambda_{fDQ}(t_m) + \left(\frac{5h}{24}e_{fDQ}(t-h) + \lambda_{fDQ}(t-h)\right), \tag{4.110}$$

$$0 = -\frac{h}{24\cdot J}T_{acc}(t) + \frac{h}{3\cdot J}T_{acc}(t_m) - \omega_m(t_m) + \left(\frac{5h}{24\cdot J}T_{acc}(t-h) + \omega_m(t-h)\right), \tag{4.111}$$

$$0 = -\frac{h}{24}y_1(t) + \frac{h}{3}y_1(t_m) - c(t_m) + \left(\frac{5h}{24}y_1(t-h) + c(t-h)\right), \tag{4.112}$$

$$0 = -\frac{h}{24}y_2(t) + \frac{h}{3}y_2(t_m) - s(t_m) + \left(\frac{5h}{24}y_2(t-h) + s(t-h)\right), \tag{4.113}$$

$$0 = T_{wf}(t_m) + \left(D_{fw} + D'_{fw}\cdot\omega_m(t_m) + D''_{fw}\cdot\omega_m(t_m)^2\right), \tag{4.114}$$

$$\mathbf{0} = \boldsymbol{P}_{em}(t_m) - \boldsymbol{e}_{abc}(t_m)^T \boldsymbol{i}_{aL\ bL\ cL}(t_m), \tag{4.115}$$

$$0 = T_e(t_m) - \frac{1}{\sqrt{3}}\cdot n_p \cdot \begin{pmatrix} i_{aL}(t_m)\lambda_b(t_m) - i_{aL}(t_m)\lambda_c(t_m) + i_{bL}(t_m)\lambda_c(t_m) \\ -i_{bL}(t_m)\lambda_a(t_m) + i_{cL}(t_m)\lambda_a(t_m) - i_{cL}(t_m)\lambda_b(t_m) \end{pmatrix}, \tag{4.116}$$

$$0 = y_1(t_m) + s(t_m) \cdot \omega(t_m), \tag{4.117}$$

$$0 = y_2(t_m) - c(t_m) \cdot \omega(t_m), \tag{4.118}$$

$$0 = c_2(t_m) - c^2(t_m) + s^2(t_m), \tag{4.119}$$

$$0 = s_2(t_m) - 2c(t_m)s(t_m), \tag{4.120}$$

$$\begin{bmatrix} \lambda_{abc}(t_m) \\ \lambda_{fDQ}(t_m) \end{bmatrix} = \left(A \cdot c(t_m) + B \cdot s(t_m) + C \cdot c_2(t_m) + D \cdot s_2(t_m) + E \right) \cdot \begin{bmatrix} -i_{aL\ bL\ cL}(t_m) \\ i_{fL\ DQ}(t_m) \end{bmatrix}. \tag{4.121}$$

We could also re-organize the equations to the matrix form of the SCAQCF as following, where $I(t)$ is the vector containing all the through variables and $X(t)$ is the vector containing all the states (including the external states and the internal states).

$$A_1 \cdot \begin{bmatrix} I(t) \\ I(t_m) \end{bmatrix} = \begin{bmatrix} B_1 & B_2 \\ B_3 & B_4 \end{bmatrix} \cdot \begin{bmatrix} X(t) \\ X(t_m) \end{bmatrix} - N \cdot X(t-h), \tag{4.122}$$

$$0 = T_{wf}(t) + \left(D_{fw} + D'_{fw} \cdot \omega_m(t) + D''_{fw} \cdot \omega_m(t)^2 \right), \tag{4.123}$$

$$0 = P_{em}(t) - e_{abc}(t)^T i_{aL\ bL\ cL}(t), \tag{4.124}$$

$$0 = T_e - \frac{1}{\sqrt{3}} \cdot n_p \cdot \begin{pmatrix} i_{aL}(t)\lambda_b(t) - i_{aL}(t)\lambda_c(t) + i_{bL}(t)\lambda_c(t) \\ -i_{bL}(t)\lambda_a(t) + i_{cL}(t)\lambda_a(t) - i_{cL}(t)\lambda_b(t) \end{pmatrix}, \tag{4.125}$$

$$0 = y_1(t) + s(t) \cdot \omega(t), \tag{4.126}$$

$$0 = y_2(t) - c(t) \cdot \omega(t), \tag{4.127}$$

$$0 = c_2(t) - c^2(t) + s^2(t), \tag{4.128}$$

$$0 = s_2(t) - 2c(t)s(t), \tag{4.129}$$

$$\begin{bmatrix} \lambda_{abc}(t) \\ \lambda_{fDQ}(t) \end{bmatrix} = \left(A \cdot c(t) + B \cdot s(t) + C \cdot c_2(t) + D \cdot s_2(t) + E \right) \cdot \begin{bmatrix} -i_{aL\ bL\ cL}(t) \\ i_{fL\ DQ}(t) \end{bmatrix}, \tag{4.130}$$

where

$$A_1 = \begin{bmatrix} A_{11} & 0_{28\times28} \\ 0_{28\times28} & A_{22} \end{bmatrix},$$

$$A_{11} = A_{22} = \begin{bmatrix} I_{9\times9} & 0_{9\times19} \\ 0_{19\times9} & 0_{28\times28} \end{bmatrix},$$

$$B_1 = \begin{bmatrix} B_{1\_11} & B_{1\_12} \\ B_{1\_21} & B_{1\_22} \end{bmatrix},$$

$$B_{1_11} = \begin{bmatrix}
g_{as} & 0 & 0 & -g_{as} & 0 & 0 & 0 & 0 & 0 & 1 & 0 & 0 & 0 & 0 & 0 & 0 & 0 & 0 & 0 & 0 & 0 & 0 \\
0 & g_{bs} & 0 & 0 & -g_{bs} & 0 & 0 & 0 & 0 & 0 & 1 & 0 & 0 & 0 & 0 & 0 & 0 & 0 & 0 & 0 & 0 & 0 \\
0 & 0 & g_{cs} & 0 & 0 & -g_{cs} & 0 & 0 & 0 & 0 & 0 & 1 & 0 & 0 & 0 & 0 & 0 & 0 & 0 & 0 & 0 & 0 \\
-g_{as} & 0 & 0 & g_{as} & 0 & 0 & 0 & 0 & 0 & -1 & 0 & 0 & 0 & 0 & 0 & 0 & 0 & 0 & 0 & 0 & 0 & 0 \\
0 & -g_{bs} & 0 & 0 & g_{bs} & 0 & 0 & 0 & 0 & 0 & -1 & 0 & 0 & 0 & 0 & 0 & 0 & 0 & 0 & 0 & 0 & 0 \\
0 & 0 & -g_{cs} & 0 & 0 & g_{cs} & 0 & 0 & 0 & 0 & 0 & -1 & 0 & 0 & 0 & 0 & 0 & 0 & 0 & 0 & 0 & 0 \\
0 & 0 & 0 & 0 & 0 & 0 & g_{fs} & -g_{fs} & 0 & 0 & 0 & 0 & 1 & 0 & 0 & 0 & 0 & 0 & 0 & 0 & 0 & 0 \\
0 & 0 & 0 & 0 & 0 & 0 & -g_{fs} & g_{fs} & 0 & 0 & 0 & 0 & -1 & 0 & 0 & 0 & 0 & 0 & 0 & 0 & 0 & 0 \\
0 & 0 & 0 & 0 & 0 & 0 & 0 & 0 & 0 & 0 & 0 & 0 & 0 & 0 & 0 & 0 & 0 & 0 & 0 & -1 & 0 & -1 \\
1 & 0 & 0 & -1 & 0 & 0 & 0 & 0 & 0 & -R_a & 0 & 0 & 0 & 0 & 0 & 0 & 0 & 0 & 0 & 0 & 0 & 0 \\
0 & 1 & 0 & 0 & -1 & 0 & 0 & 0 & 0 & 0 & -R_b & 0 & 0 & 0 & 0 & 0 & 0 & 0 & 0 & 0 & 0 & 0 \\
0 & 0 & 1 & 0 & 0 & -1 & 0 & 0 & 0 & 0 & 0 & -R_c & 0 & 0 & 0 & 0 & 0 & 0 & 0 & 0 & 0 & 0 \\
0 & 0 & 0 & 0 & 0 & 0 & 1 & -1 & 0 & 0 & 0 & 0 & -R_f & 0 & 0 & 0 & 0 & 0 & 0 & 0 & 0 & 0 \\
0 & 0 & 0 & 0 & 0 & 0 & 0 & 0 & 0 & 0 & 0 & 0 & 0 & R_D & 0 & 0 & 0 & 0 & 0 & 0 & 0 & 0 \\
0 & 0 & 0 & 0 & 0 & 0 & 0 & 0 & 0 & 0 & 0 & 0 & 0 & 0 & R_Q & 0 & 0 & 0 & 0 & 0 & 0 & 0 \\
0 & 0 & 0 & 0 & 0 & 0 & 0 & 0 & 0 & 0 & 0 & 0 & 0 & 0 & 0 & -\frac{P}{2} & 1 & 0 & 0 & 0 & 0 & 0 \\
0 & 0 & 0 & 0 & 0 & 0 & 0 & 0 & -\frac{P}{2} & 0 & 0 & 0 & 0 & 0 & 0 & 0 & 0 & 1 & 0 & 0 & 0 & 0 \\
0 & 0 & 0 & 0 & 0 & 0 & 0 & 0 & 0 & 0 & 0 & 0 & 0 & 0 & 0 & 0 & 1 & 0 & -1 & 0 & 0 & 0
\end{bmatrix}_{18\times22},$$

$$B_{1_12} = \begin{bmatrix}
0 & 0 & 0 & 0 & 0 & 0 & 0 & 0 & 0 & 0 & 0 & 0 & 0 & 0 & 0 & 0 & 0 & 0 & 0 \\
0 & 0 & 0 & 0 & 0 & 0 & 0 & 0 & 0 & 0 & 0 & 0 & 0 & 0 & 0 & 0 & 0 & 0 & 0 \\
0 & 0 & 0 & 0 & 0 & 0 & 0 & 0 & 0 & 0 & 0 & 0 & 0 & 0 & 0 & 0 & 0 & 0 & 0 \\
0 & 0 & 0 & 0 & 0 & 0 & 0 & 0 & 0 & 0 & 0 & 0 & 0 & 0 & 0 & 0 & 0 & 0 & 0 \\
0 & 0 & 0 & 0 & 0 & 0 & 0 & 0 & 0 & 0 & 0 & 0 & 0 & 0 & 0 & 0 & 0 & 0 & 0 \\
0 & 0 & 0 & 0 & 0 & 0 & 0 & 0 & 0 & 0 & 0 & 0 & 0 & 0 & 0 & 0 & 0 & 0 & 0 \\
0 & 0 & 0 & 0 & 0 & 0 & 0 & 0 & 0 & 0 & 0 & 0 & 0 & 0 & 0 & 0 & 0 & 0 & 0 \\
0 & 0 & 0 & 0 & 0 & 0 & 0 & 0 & 0 & 0 & 0 & 0 & 0 & 0 & 0 & 0 & 0 & 0 & 0 \\
0 & 0 & 0 & 0 & 0 & 0 & 0 & 0 & 0 & 0 & 0 & 0 & 1 & 0 & 0 & 0 & 0 & 0 & 0 \\
-1 & 0 & 0 & 0 & 0 & 0 & 0 & 0 & 0 & 0 & 0 & 0 & 0 & 0 & 0 & 0 & 0 & 0 & 0 \\
0 & -1 & 0 & 0 & 0 & 0 & 0 & 0 & 0 & 0 & 0 & 0 & 0 & 0 & 0 & 0 & 0 & 0 & 0 \\
0 & 0 & -1 & 0 & 0 & 0 & 0 & 0 & 0 & 0 & 0 & 0 & 0 & 0 & 0 & 0 & 0 & 0 & 0 \\
0 & 0 & 0 & -1 & 0 & 0 & 0 & 0 & 0 & 0 & 0 & 0 & 0 & 0 & 0 & 0 & 0 & 0 & 0 \\
0 & 0 & 0 & 0 & -1 & 0 & 0 & 0 & 0 & 0 & 0 & 0 & 0 & 0 & 0 & 0 & 0 & 0 & 0 \\
0 & 0 & 0 & 0 & 0 & -1 & 0 & 0 & 0 & 0 & 0 & 0 & 0 & 0 & 0 & 0 & 0 & 0 & 0 \\
0 & 0 & 0 & 0 & 0 & 0 & 0 & 0 & 0 & 0 & 0 & 0 & 0 & 0 & 0 & 0 & 0 & 0 & 0 \\
0 & 0 & 0 & 0 & 0 & 0 & 0 & 0 & 0 & 0 & 0 & 0 & 0 & 0 & 0 & 0 & 0 & 0 & 0 \\
0 & 0 & 0 & 0 & 0 & 0 & 0 & 0 & 0 & 0 & 0 & 0 & 0 & 0 & 0 & 0 & 0 & 0 & 0
\end{bmatrix}_{18\times19},$$

$$
B_{1\_21} = \begin{bmatrix}
0 & 0 & 0 & 0 & 0 & 0 & 0 & 0 & \frac{h}{6} & 0 & 0 & 0 & 0 & 0 & 0 & -1 & 0 & 0 & 0 & 0 & 0 & 0 \\
0 & 0 & 0 & 0 & 0 & 0 & 0 & 0 & 0 & 0 & 0 & 0 & 0 & 0 & 0 & 0 & 0 & 0 & 0 & 0 & 0 & 0 \\
0 & 0 & 0 & 0 & 0 & 0 & 0 & 0 & 0 & 0 & 0 & 0 & 0 & 0 & 0 & 0 & 0 & 0 & 0 & 0 & 0 & 0 \\
0 & 0 & 0 & 0 & 0 & 0 & 0 & 0 & 0 & 0 & 0 & 0 & 0 & 0 & 0 & 0 & 0 & 0 & 0 & 0 & 0 & 0 \\
0 & 0 & 0 & 0 & 0 & 0 & 0 & 0 & 0 & 0 & 0 & 0 & 0 & 0 & 0 & 0 & 0 & 0 & 0 & 0 & 0 & 0 \\
0 & 0 & 0 & 0 & 0 & 0 & 0 & 0 & 0 & 0 & 0 & 0 & 0 & 0 & 0 & 0 & 0 & 0 & 0 & 0 & 0 & 0 \\
0 & 0 & 0 & 0 & 0 & 0 & 0 & 0 & 0 & 0 & 0 & 0 & 0 & 0 & 0 & 0 & 0 & 0 & 0 & 0 & 0 & 0 \\
0 & 0 & 0 & 0 & 0 & 0 & 0 & 0 & -1 & 0 & 0 & 0 & 0 & 0 & 0 & 0 & 0 & 0 & 0 & 0 & 0 & 0 \\
0 & 0 & 0 & 0 & 0 & 0 & 0 & 0 & 0 & 0 & 0 & 0 & 0 & 0 & 0 & 0 & 0 & 0 & 0 & 0 & 0 & 0 \\
0 & 0 & 0 & 0 & 0 & 0 & 0 & 0 & 0 & 0 & 0 & 0 & 0 & 0 & 0 & 0 & 0 & 0 & 0 & 0 & 0 & 0
\end{bmatrix}_{10\times 22},
$$

$$
B_{1\_22} = \begin{bmatrix}
0 & 0 & 0 & 0 & 0 & 0 & 0 & 0 & 0 & 0 & 0 & 0 & 0 & 0 & 0 & 0 & 0 & 0 & 0 \\
\frac{h}{6} & 0 & 0 & 0 & 0 & 0 & -1 & 0 & 0 & 0 & 0 & 0 & 0 & 0 & 0 & 0 & 0 & 0 & 0 \\
0 & \frac{h}{6} & 0 & 0 & 0 & 0 & 0 & -1 & 0 & 0 & 0 & 0 & 0 & 0 & 0 & 0 & 0 & 0 & 0 \\
0 & 0 & \frac{h}{6} & 0 & 0 & 0 & 0 & 0 & -1 & 0 & 0 & 0 & 0 & 0 & 0 & 0 & 0 & 0 & 0 \\
0 & 0 & 0 & \frac{h}{6} & 0 & 0 & 0 & 0 & 0 & -1 & 0 & 0 & 0 & 0 & 0 & 0 & 0 & 0 & 0 \\
0 & 0 & 0 & 0 & \frac{h}{6} & 0 & 0 & 0 & 0 & 0 & -1 & 0 & 0 & 0 & 0 & 0 & 0 & 0 & 0 \\
0 & 0 & 0 & 0 & 0 & \frac{h}{6} & 0 & 0 & 0 & 0 & 0 & -1 & 0 & 0 & 0 & 0 & 0 & 0 & 0 \\
0 & 0 & 0 & 0 & 0 & 0 & 0 & 0 & 0 & 0 & 0 & 0 & \frac{h}{6}\cdot\frac{1}{J} & 0 & 0 & 0 & 0 & 0 & 0 \\
0 & 0 & 0 & 0 & 0 & 0 & 0 & 0 & 0 & 0 & 0 & 0 & 0 & -1 & 0 & \frac{h}{6} & 0 & 0 & 0 \\
0 & 0 & 0 & 0 & 0 & 0 & 0 & 0 & 0 & 0 & 0 & 0 & 0 & 0 & -1 & 0 & \frac{h}{6} & 0 & 0
\end{bmatrix}_{10\times 19},
$$

$$
B_2 = \begin{bmatrix} 0_{18\times 22} & 0_{18\times 19} \\ B_{2\_21} & B_{2\_22} \end{bmatrix},
$$

$$B_{2\_21}=\begin{bmatrix} 0&0&0&0&0&0&0&0&\frac{2h}{3}&0&0&0&0&0&0&0&0&0&0&0&0&0\\ 0&0&0&0&0&0&0&0&0&0&0&0&0&0&0&0&0&0&0&0&0&0\\ 0&0&0&0&0&0&0&0&0&0&0&0&0&0&0&0&0&0&0&0&0&0\\ 0&0&0&0&0&0&0&0&0&0&0&0&0&0&0&0&0&0&0&0&0&0\\ 0&0&0&0&0&0&0&0&0&0&0&0&0&0&0&0&0&0&0&0&0&0\\ 0&0&0&0&0&0&0&0&0&0&0&0&0&0&0&0&0&0&0&0&0&0\\ 0&0&0&0&0&0&0&0&0&0&0&0&0&0&0&0&0&0&0&0&0&0\\ 0&0&0&0&0&0&0&0&0&0&0&0&0&0&0&0&0&0&0&0&0&0\\ 0&0&0&0&0&0&0&0&0&0&0&0&0&0&0&0&0&0&0&0&0&0\\ 0&0&0&0&0&0&0&0&0&0&0&0&0&0&0&0&0&0&0&0&0&0 \end{bmatrix}_{10\times 22},$$

$$B_{2\_22}=\begin{bmatrix} 0&0&0&0&0&0&0&0&0&0&0&0&0&0&0&0&0&0&0\\ \frac{2h}{3}&0&0&0&0&0&0&0&0&0&0&0&0&0&0&0&0&0&0\\ 0&\frac{2h}{3}&0&0&0&0&0&0&0&0&0&0&0&0&0&0&0&0&0\\ 0&0&\frac{2h}{3}&0&0&0&0&0&0&0&0&0&0&0&0&0&0&0&0\\ 0&0&0&\frac{2h}{3}&0&0&0&0&0&0&0&0&0&0&0&0&0&0&0\\ 0&0&0&0&\frac{2h}{3}&0&0&0&0&0&0&0&0&0&0&0&0&0&0\\ 0&0&0&0&0&\frac{2h}{3}&0&0&0&0&0&0&0&0&0&0&0&0&0\\ 0&0&0&0&0&0&0&0&0&0&0&0&\frac{2h}{3}\cdot\frac{1}{J}&0&0&0&0&0&0\\ 0&0&0&0&0&0&0&0&0&0&0&0&0&0&0&\frac{2h}{3}&0&0&0\\ 0&0&0&0&0&0&0&0&0&0&0&0&0&0&0&0&\frac{2h}{3}&0&0 \end{bmatrix}_{10\times 19},$$

$$B_3=\begin{bmatrix} 0_{18\times 22} & 0_{18\times 19}\\ B_{3\_21} & B_{3\_22} \end{bmatrix},$$

$$B_{3\_21}=\begin{bmatrix} 0&0&0&0&0&0&0&0&-\frac{h}{24}&0&0&0&0&0&0&0&0&0&0&0&0&0\\ 0&0&0&0&0&0&0&0&0&0&0&0&0&0&0&0&0&0&0&0&0&0\\ 0&0&0&0&0&0&0&0&0&0&0&0&0&0&0&0&0&0&0&0&0&0\\ 0&0&0&0&0&0&0&0&0&0&0&0&0&0&0&0&0&0&0&0&0&0\\ 0&0&0&0&0&0&0&0&0&0&0&0&0&0&0&0&0&0&0&0&0&0\\ 0&0&0&0&0&0&0&0&0&0&0&0&0&0&0&0&0&0&0&0&0&0\\ 0&0&0&0&0&0&0&0&0&0&0&0&0&0&0&0&0&0&0&0&0&0\\ 0&0&0&0&0&0&0&0&0&0&0&0&0&0&0&0&0&0&0&0&0&0\\ 0&0&0&0&0&0&0&0&0&0&0&0&0&0&0&0&0&0&0&0&0&0\\ 0&0&0&0&0&0&0&0&0&0&0&0&0&0&0&0&0&0&0&0&0&0 \end{bmatrix}_{10\times 22},$$

$$B_{3\_22}=\begin{bmatrix} 0&0&0&0&0&0&0&0&0&0&0&0&0&0&0&0&0&0&0\\ -\frac{h}{24}&0&0&0&0&0&0&0&0&0&0&0&0&0&0&0&0&0&0\\ 0&-\frac{h}{24}&0&0&0&0&0&0&0&0&0&0&0&0&0&0&0&0&0\\ 0&0&-\frac{h}{24}&0&0&0&0&0&0&0&0&0&0&0&0&0&0&0&0\\ 0&0&0&-\frac{h}{24}&0&0&0&0&0&0&0&0&0&0&0&0&0&0&0\\ 0&0&0&0&-\frac{h}{24}&0&0&0&0&0&0&0&0&0&0&0&0&0&0\\ 0&0&0&0&0&-\frac{h}{24}&0&0&0&0&0&0&0&0&0&0&0&0&0\\ 0&0&0&0&0&0&0&0&0&0&0&0&-\frac{h}{24}\cdot\frac{1}{J}&0&0&0&0&0&0\\ 0&0&0&0&0&0&0&0&0&0&0&0&0&0&0&-\frac{h}{24}&0&0&0\\ 0&0&0&0&0&0&0&0&0&0&0&0&0&0&0&0&-\frac{h}{24}&0&0 \end{bmatrix}_{10\times 19},$$

$$B_4=\begin{bmatrix} B_{4\_11} & B_{4\_12}\\ B_{4\_21} & B_{4\_22} \end{bmatrix},$$

$$
B_{4\_11} = \begin{bmatrix}
g_{as} & 0 & 0 & -g_{as} & 0 & 0 & 0 & 0 & 0 & 1 & 0 & 0 & 0 & 0 & 0 & 0 & 0 & 0 & 0 & 0 & 0 & 0 \\
0 & g_{bs} & 0 & 0 & -g_{bs} & 0 & 0 & 0 & 0 & 0 & 1 & 0 & 0 & 0 & 0 & 0 & 0 & 0 & 0 & 0 & 0 & 0 \\
0 & 0 & g_{cs} & 0 & 0 & -g_{cs} & 0 & 0 & 0 & 0 & 0 & 1 & 0 & 0 & 0 & 0 & 0 & 0 & 0 & 0 & 0 & 0 \\
-g_{as} & 0 & 0 & g_{as} & 0 & 0 & 0 & 0 & 0 & -1 & 0 & 0 & 0 & 0 & 0 & 0 & 0 & 0 & 0 & 0 & 0 & 0 \\
0 & -g_{bs} & 0 & 0 & g_{bs} & 0 & 0 & 0 & 0 & 0 & -1 & 0 & 0 & 0 & 0 & 0 & 0 & 0 & 0 & 0 & 0 & 0 \\
0 & 0 & -g_{cs} & 0 & 0 & g_{cs} & 0 & 0 & 0 & 0 & 0 & -1 & 0 & 0 & 0 & 0 & 0 & 0 & 0 & 0 & 0 & 0 \\
0 & 0 & 0 & 0 & 0 & 0 & g_{fs} & -g_{fs} & 0 & 0 & 0 & 0 & 1 & 0 & 0 & 0 & 0 & 0 & 0 & 0 & 0 & 0 \\
0 & 0 & 0 & 0 & 0 & 0 & -g_{fs} & g_{fs} & 0 & 0 & 0 & 0 & -1 & 0 & 0 & 0 & 0 & 0 & 0 & 0 & 0 & 0 \\
0 & 0 & 0 & 0 & 0 & 0 & 0 & 0 & 0 & 0 & 0 & 0 & 0 & 0 & 0 & 0 & 0 & 0 & 0 & -1 & 0 & -1 \\
1 & 0 & 0 & -1 & 0 & 0 & 0 & 0 & 0 & -R_a & 0 & 0 & 0 & 0 & 0 & 0 & 0 & 0 & 0 & 0 & 0 & 0 \\
0 & 1 & 0 & 0 & -1 & 0 & 0 & 0 & 0 & 0 & -R_b & 0 & 0 & 0 & 0 & 0 & 0 & 0 & 0 & 0 & 0 & 0 \\
0 & 0 & 1 & 0 & 0 & -1 & 0 & 0 & 0 & 0 & 0 & -R_c & 0 & 0 & 0 & 0 & 0 & 0 & 0 & 0 & 0 & 0 \\
0 & 0 & 0 & 0 & 0 & 0 & 1 & -1 & 0 & 0 & 0 & 0 & -R_f & 0 & 0 & 0 & 0 & 0 & 0 & 0 & 0 & 0 \\
0 & 0 & 0 & 0 & 0 & 0 & 0 & 0 & 0 & 0 & 0 & 0 & 0 & R_D & 0 & 0 & 0 & 0 & 0 & 0 & 0 & 0 \\
0 & 0 & 0 & 0 & 0 & 0 & 0 & 0 & 0 & 0 & 0 & 0 & 0 & 0 & R_Q & 0 & 0 & 0 & 0 & 0 & 0 & 0 \\
0 & 0 & 0 & 0 & 0 & 0 & 0 & 0 & 0 & 0 & 0 & 0 & 0 & 0 & 0 & -\frac{P}{2} & 1 & 0 & 0 & 0 & 0 & 0 \\
0 & 0 & 0 & 0 & 0 & 0 & 0 & 0 & -\frac{P}{2} & 0 & 0 & 0 & 0 & 0 & 0 & 0 & 0 & 1 & 0 & 0 & 0 & 0 \\
0 & 0 & 0 & 0 & 0 & 0 & 0 & 0 & 0 & 0 & 0 & 0 & 0 & 0 & 0 & 0 & 1 & 0 & -1 & 0 & 0 & 0
\end{bmatrix}_{18\times 22},
$$

$$
B_{4\_12} = \begin{bmatrix}
0 & 0 & 0 & 0 & 0 & 0 & 0 & 0 & 0 & 0 & 0 & 0 & 0 & 0 & 0 & 0 & 0 & 0 & 0 \\
0 & 0 & 0 & 0 & 0 & 0 & 0 & 0 & 0 & 0 & 0 & 0 & 0 & 0 & 0 & 0 & 0 & 0 & 0 \\
0 & 0 & 0 & 0 & 0 & 0 & 0 & 0 & 0 & 0 & 0 & 0 & 0 & 0 & 0 & 0 & 0 & 0 & 0 \\
0 & 0 & 0 & 0 & 0 & 0 & 0 & 0 & 0 & 0 & 0 & 0 & 0 & 0 & 0 & 0 & 0 & 0 & 0 \\
0 & 0 & 0 & 0 & 0 & 0 & 0 & 0 & 0 & 0 & 0 & 0 & 0 & 0 & 0 & 0 & 0 & 0 & 0 \\
0 & 0 & 0 & 0 & 0 & 0 & 0 & 0 & 0 & 0 & 0 & 0 & 0 & 0 & 0 & 0 & 0 & 0 & 0 \\
0 & 0 & 0 & 0 & 0 & 0 & 0 & 0 & 0 & 0 & 0 & 0 & 0 & 0 & 0 & 0 & 0 & 0 & 0 \\
0 & 0 & 0 & 0 & 0 & 0 & 0 & 0 & 0 & 0 & 0 & 0 & 0 & 0 & 0 & 0 & 0 & 0 & 0 \\
0 & 0 & 0 & 0 & 0 & 0 & 0 & 0 & 0 & 0 & 0 & 0 & 1 & 0 & 0 & 0 & 0 & 0 & 0 \\
-1 & 0 & 0 & 0 & 0 & 0 & 0 & 0 & 0 & 0 & 0 & 0 & 0 & 0 & 0 & 0 & 0 & 0 & 0 \\
0 & -1 & 0 & 0 & 0 & 0 & 0 & 0 & 0 & 0 & 0 & 0 & 0 & 0 & 0 & 0 & 0 & 0 & 0 \\
0 & 0 & -1 & 0 & 0 & 0 & 0 & 0 & 0 & 0 & 0 & 0 & 0 & 0 & 0 & 0 & 0 & 0 & 0 \\
0 & 0 & 0 & -1 & 0 & 0 & 0 & 0 & 0 & 0 & 0 & 0 & 0 & 0 & 0 & 0 & 0 & 0 & 0 \\
0 & 0 & 0 & 0 & -1 & 0 & 0 & 0 & 0 & 0 & 0 & 0 & 0 & 0 & 0 & 0 & 0 & 0 & 0 \\
0 & 0 & 0 & 0 & 0 & -1 & 0 & 0 & 0 & 0 & 0 & 0 & 0 & 0 & 0 & 0 & 0 & 0 & 0 \\
0 & 0 & 0 & 0 & 0 & 0 & 0 & 0 & 0 & 0 & 0 & 0 & 0 & 0 & 0 & 0 & 0 & 0 & 0 \\
0 & 0 & 0 & 0 & 0 & 0 & 0 & 0 & 0 & 0 & 0 & 0 & 0 & 0 & 0 & 0 & 0 & 0 & 0 \\
0 & 0 & 0 & 0 & 0 & 0 & 0 & 0 & 0 & 0 & 0 & 0 & 0 & 0 & 0 & 0 & 0 & 0 & 0
\end{bmatrix}_{18\times 19},
$$

$$B_{4_21}=\begin{bmatrix}
0&0&0&0&0&0&0&0&\frac{h}{3}&0&0&0&0&0&0&-1&0&0&0&0&0&0\\
0&0&0&0&0&0&0&0&0&0&0&0&0&0&0&0&0&0&0&0&0&0\\
0&0&0&0&0&0&0&0&0&0&0&0&0&0&0&0&0&0&0&0&0&0\\
0&0&0&0&0&0&0&0&0&0&0&0&0&0&0&0&0&0&0&0&0&0\\
0&0&0&0&0&0&0&0&0&0&0&0&0&0&0&0&0&0&0&0&0&0\\
0&0&0&0&0&0&0&0&0&0&0&0&0&0&0&0&0&0&0&0&0&0\\
0&0&0&0&0&0&0&0&0&0&0&0&0&0&0&0&0&0&0&0&0&0\\
0&0&0&0&0&0&0&0&-1&0&0&0&0&0&0&0&0&0&0&0&0&0\\
0&0&0&0&0&0&0&0&0&0&0&0&0&0&0&0&0&0&0&0&0&0\\
0&0&0&0&0&0&0&0&0&0&0&0&0&0&0&0&0&0&0&0&0&0
\end{bmatrix}_{10\times 22},$$

$$B_{4_22}=\begin{bmatrix}
0&0&0&0&0&0&0&0&0&0&0&0&0&0&0&0&0&0&0\\
\frac{h}{3}&0&0&0&0&0&-1&0&0&0&0&0&0&0&0&0&0&0&0\\
0&\frac{h}{3}&0&0&0&0&0&-1&0&0&0&0&0&0&0&0&0&0&0\\
0&0&\frac{h}{3}&0&0&0&0&0&-1&0&0&0&0&0&0&0&0&0&0\\
0&0&0&\frac{h}{3}&0&0&0&0&0&-1&0&0&0&0&0&0&0&0&0\\
0&0&0&0&\frac{h}{3}&0&0&0&0&0&-1&0&0&0&0&0&0&0&0\\
0&0&0&0&0&\frac{h}{3}&0&0&0&0&0&-1&0&0&0&0&0&0&0\\
0&0&0&0&0&0&0&0&0&0&0&0&\frac{h}{3}\cdot\frac{1}{J}&0&0&0&0&0&0\\
0&0&0&0&0&0&0&0&0&0&0&0&0&-1&0&\frac{h}{3}&0&0&0\\
0&0&0&0&0&0&0&0&0&0&0&0&0&0&-1&0&\frac{h}{3}&0&0
\end{bmatrix}_{10\times 19},$$

$$N=\begin{bmatrix}
0_{18\times 41}\\
N_{21}\quad N_{22}\\
0_{18\times 41}\\
N_{41}\quad N_{42}
\end{bmatrix},$$

$$N_{21}=\begin{bmatrix}
0&0&0&0&0&0&0&0&-\frac{h}{6}&0&0&0&0&0&0&1&0&0&0&0&0&0\\
0&0&0&0&0&0&0&0&0&0&0&0&0&0&0&0&0&0&0&0&0&0\\
0&0&0&0&0&0&0&0&0&0&0&0&0&0&0&0&0&0&0&0&0&0\\
0&0&0&0&0&0&0&0&0&0&0&0&0&0&0&0&0&0&0&0&0&0\\
0&0&0&0&0&0&0&0&0&0&0&0&0&0&0&0&0&0&0&0&0&0\\
0&0&0&0&0&0&0&0&0&0&0&0&0&0&0&0&0&0&0&0&0&0\\
0&0&0&0&0&0&0&0&0&0&0&0&0&0&0&0&0&0&0&0&0&0\\
0&0&0&0&0&0&0&0&-1&0&0&0&0&0&0&0&0&0&0&0&0&0\\
0&0&0&0&0&0&0&0&0&0&0&0&0&0&0&0&0&0&0&0&0&0\\
0&0&0&0&0&0&0&0&0&0&0&0&0&0&0&0&0&0&0&0&0&0
\end{bmatrix}_{10\times 22},$$

$$N_{22}=\begin{bmatrix}
0&0&0&0&0&0&0&0&0&0&0&0&0&0&0&0&0&0&0\\
-\frac{h}{6}&0&0&0&0&0&-1&0&0&0&0&0&0&0&0&0&0&0&0\\
0&-\frac{h}{6}&0&0&0&0&0&-1&0&0&0&0&0&0&0&0&0&0&0\\
0&0&-\frac{h}{6}&0&0&0&0&0&-1&0&0&0&0&0&0&0&0&0&0\\
0&0&0&-\frac{h}{6}&0&0&0&0&0&-1&0&0&0&0&0&0&0&0&0\\
0&0&0&0&-\frac{h}{6}&0&0&0&0&0&-1&0&0&0&0&0&0&0&0\\
0&0&0&0&0&-\frac{h}{6}&0&0&0&0&0&-1&0&0&0&0&0&0&0\\
0&0&0&0&0&0&0&0&0&0&0&0&-\frac{h}{6}\cdot\frac{1}{J}&0&0&0&0&0&0\\
0&0&0&0&0&0&0&0&0&0&0&0&0&-1&0&-\frac{h}{6}&0&0&0\\
0&0&0&0&0&0&0&0&0&0&0&0&0&0&-1&0&-\frac{h}{6}&0&0
\end{bmatrix}_{10\times 19},$$

$$N_{41}=\begin{bmatrix}
0&0&0&0&0&0&0&0&-\frac{5h}{24}&0&0&0&0&0&0&1&0&0&0&0&0&0\\
0&0&0&0&0&0&0&0&0&0&0&0&0&0&0&0&0&0&0&0&0&0\\
0&0&0&0&0&0&0&0&0&0&0&0&0&0&0&0&0&0&0&0&0&0\\
0&0&0&0&0&0&0&0&0&0&0&0&0&0&0&0&0&0&0&0&0&0\\
0&0&0&0&0&0&0&0&0&0&0&0&0&0&0&0&0&0&0&0&0&0\\
0&0&0&0&0&0&0&0&0&0&0&0&0&0&0&0&0&0&0&0&0&0\\
0&0&0&0&0&0&0&0&0&0&0&0&0&0&0&0&0&0&0&0&0&0\\
0&0&0&0&0&0&0&0&-1&0&0&0&0&0&0&0&0&0&0&0&0&0\\
0&0&0&0&0&0&0&0&0&0&0&0&0&0&0&0&0&0&0&0&0&0\\
0&0&0&0&0&0&0&0&0&0&0&0&0&0&0&0&0&0&0&0&0&0
\end{bmatrix}_{10\times 22},$$

$$N_{22} = \begin{bmatrix}
0 & 0 & 0 & 0 & 0 & 0 & 0 & 0 & 0 & 0 & 0 & 0 & 0 & 0 & 0 & 0 & 0 & 0 & 0 \\
-\frac{5h}{24} & 0 & 0 & 0 & 0 & 0 & -1 & 0 & 0 & 0 & 0 & 0 & 0 & 0 & 0 & 0 & 0 & 0 & 0 \\
0 & -\frac{5h}{24} & 0 & 0 & 0 & 0 & 0 & -1 & 0 & 0 & 0 & 0 & 0 & 0 & 0 & 0 & 0 & 0 & 0 \\
0 & 0 & -\frac{5h}{24} & 0 & 0 & 0 & 0 & 0 & -1 & 0 & 0 & 0 & 0 & 0 & 0 & 0 & 0 & 0 & 0 \\
0 & 0 & 0 & -\frac{5h}{24} & 0 & 0 & 0 & 0 & 0 & -1 & 0 & 0 & 0 & 0 & 0 & 0 & 0 & 0 & 0 \\
0 & 0 & 0 & 0 & -\frac{5h}{24} & 0 & 0 & 0 & 0 & 0 & -1 & 0 & 0 & 0 & 0 & 0 & 0 & 0 & 0 \\
0 & 0 & 0 & 0 & 0 & -\frac{5h}{24} & 0 & 0 & 0 & 0 & 0 & -1 & 0 & 0 & 0 & 0 & 0 & 0 & 0 \\
0 & 0 & 0 & 0 & 0 & 0 & 0 & 0 & 0 & 0 & 0 & 0 & -\frac{5h}{24}\cdot\frac{1}{J} & 0 & 0 & 0 & 0 & 0 & 0 \\
0 & 0 & 0 & 0 & 0 & 0 & 0 & 0 & 0 & 0 & 0 & 0 & 0 & -1 & 0 & -\frac{5h}{24} & 0 & 0 & 0 \\
0 & 0 & 0 & 0 & 0 & 0 & 0 & 0 & 0 & 0 & 0 & 0 & 0 & 0 & -1 & 0 & -\frac{5h}{24} & 0 & 0
\end{bmatrix}_{10\times 19}.$$

4.4 The SCAQCF Model for a Synchronous Machine in Phasor Domain

Figure 4.3 shows a phasor diagram of the two-axis synchronous machine model. Note that the positive flow direction of the current I_a is defined to be out of the generator terminals.

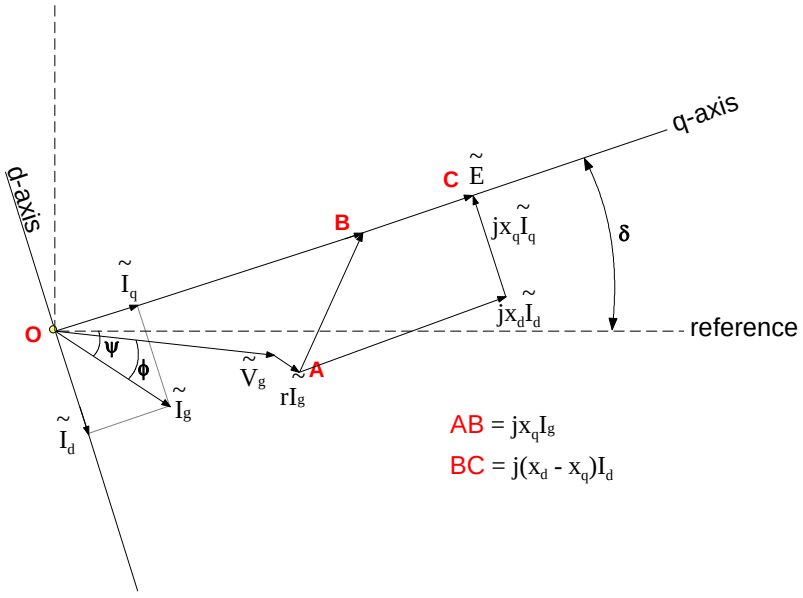

Figure 4.3. Two-axis synchronous machine phasor diagram.

Since the quasi-transient model of the two-axis synchronous machine only considers the mechanical dynamics, the electrical dynamics in the field winding is neglected, and the magnitude of the internal exciter voltage E is derived directly from the field current as:

$$I_f = \frac{\sqrt{2} \cdot |E|}{\omega M_F}. \tag{4.131}$$

Also since the electrical dynamics in the field winding is neglected, the current of the field will be treated as a DC current and the relationship between the field winding current and voltage are as follows:

$$V_f = r_f I_f. \tag{4.132}$$

For the mechanical dynamics, here we first define the angle of rotor position (d-axis) $\theta(t)$ and the rotor angular velocity $\omega(t)$. We define the rotor angle as

$$\delta(t) = \theta(t) - \omega_0 t - \frac{\pi}{2}, \tag{4.133}$$

where $\delta(t) + \frac{\pi}{2}$ is the angle difference between the rotor (d-axis), rotating at speed $\omega(t)$, and a synchronously rotating reference frame at speed ω_0.

$$\frac{d\delta(t)}{dt} = \frac{d\theta(t)}{dt} - \omega_0 = \omega(t) - \omega_0 = \frac{p}{2}\omega_m(t) - \omega_0, \tag{4.134}$$

and

$$\frac{d^2\delta(t)}{dt^2} = \frac{d^2\theta(t)}{dt^2} = \frac{d\omega(t)}{dt} = \frac{p}{2}\frac{d\omega_m(t)}{dt}, \tag{4.135}$$

where

$\tilde{I}_g$: armature current (positive direction is into the generator),

r : armature resistance,

x_d : direct-axis synchronous reactance,

x_q : quadrature-axis synchronous reactance.

4.4.1 Synchronous Machine in Phasor Domain - Compact Form

The compact form equations for the quasi-dynamic model of the synchronous machine are

$$\tilde{I}_a = \tilde{I}_1 + \tilde{I}_2 + \tilde{I}_0, \tag{4.136}$$

$$\tilde{I}_b = \left(-\frac{1}{2} - j\frac{\sqrt{3}}{2}\right)\tilde{I}_1 + \left(-\frac{1}{2} + j\frac{\sqrt{3}}{2}\right)\tilde{I}_2 + \tilde{I}_0, \tag{4.137}$$

$$\tilde{I}_c = \left(-\frac{1}{2} + j\frac{\sqrt{3}}{2}\right)\tilde{I}_1 + \left(-\frac{1}{2} - j\frac{\sqrt{3}}{2}\right)\tilde{I}_2 + \tilde{I}_0, \tag{4.138}$$

$$\tilde{I}_{an} = -\tilde{I}_1 - \tilde{I}_2 - \tilde{I}_0, \tag{4.139}$$

$$\tilde{I}_{bn} = -\left(-\frac{1}{2} - j\frac{\sqrt{3}}{2}\right)\tilde{I}_1 - \left(-\frac{1}{2} + j\frac{\sqrt{3}}{2}\right)\tilde{I}_2 - \tilde{I}_0, \tag{4.140}$$

$$\tilde{I}_{cn} = -\left(-\frac{1}{2} + j\frac{\sqrt{3}}{2}\right)\tilde{I}_1 - \left(-\frac{1}{2} - j\frac{\sqrt{3}}{2}\right)\tilde{I}_2 - \tilde{I}_0, \tag{4.141}$$

$$I_{f1} = \frac{1}{r_f}\left(V_{f1} - V_{f2}\right), \tag{4.142}$$

$$I_{f2} = -\frac{1}{r_f}\left(V_{f1} - V_{f2}\right), \tag{4.143}$$

$$T_m(t) = J \cdot \frac{d\omega_m(t)}{dt} - T_e(t), \tag{4.144}$$

$$0 = \tilde{V}_a - \tilde{V}_{an} - \tilde{V}_1 - \tilde{V}_2 - \tilde{V}_0, \tag{4.145}$$

$$0 = \tilde{V}_b - \tilde{V}_{bn} - \left(-\frac{1}{2} - j\frac{\sqrt{3}}{2}\right)\tilde{V}_1 - \left(-\frac{1}{2} + j\frac{\sqrt{3}}{2}\right)\tilde{V}_2 - \tilde{V}_0, \tag{4.146}$$

$$0 = \tilde{V}_c - \tilde{V}_{cn} - \left(-\frac{1}{2} + j\frac{\sqrt{3}}{2}\right)\tilde{V}_1 - \left(-\frac{1}{2} - j\frac{\sqrt{3}}{2}\right)\tilde{V}_2 - \tilde{V}_0, \tag{4.147}$$

$$0 = \tilde{E} - \tilde{V}_1 + r\left(\tilde{I}_d + \tilde{I}_q\right) + jx_d\tilde{I}_d + jx_q\tilde{I}_q, \tag{4.148}$$

$$0 = \tilde{V}_2 - \tilde{I}_2 \cdot \left(r + \frac{1}{2}j(x_d + x_q)\right), \tag{4.149}$$

$$0 = \tilde{V}_0 - \tilde{I}_0 \cdot \left(r + jx_0\right), \tag{4.150}$$

$$0 = \tilde{I}_1 - \tilde{I}_d - \tilde{I}_q, \tag{4.151}$$

$$0 = \frac{1}{r_f}\left(V_{f1} - V_{f2}\right) - \frac{\sqrt{2}\cdot\left|\tilde{E}\right|}{\omega M_F}, \tag{4.152}$$

$$0 = angle(\tilde{E}) - \delta(t), \tag{4.153}$$

$$0 = P_e(t) - \mathrm{Re}\left\{3\cdot E_r\left(I_{dr} + I_{qr}\right) + 3\cdot E_i\left(I_{di} + I_{qi}\right)\right\}, \tag{4.154}$$

$$0 = T_e(t) - \frac{P_e(t)}{\omega_m \cdot \frac{p}{2}}, \tag{4.155}$$

$$0 = \mathrm{Re}\{\tilde{E}\tilde{I}_d^*\}, \tag{4.156}$$

$$0 = \mathrm{Im}\{\tilde{E}\tilde{I}_q^*\}, \tag{4.157}$$

$$\frac{d\delta(t)}{dt} = \frac{p}{2}\omega_m(t) - \omega_0. \tag{4.158}$$

The external states and internal states of the model is defined as follows:

$$X_{external} = \left[\tilde{V}_a \quad \tilde{V}_b \quad \tilde{V}_c \quad \tilde{V}_{an} \quad \tilde{V}_{bn} \quad \tilde{V}_{cn} \quad \tilde{V}_{f1} \quad \tilde{V}_{f2} \quad \omega_m\right],$$
$$X_{internal} = \left[\tilde{V}_1 \quad \tilde{V}_2 \quad \tilde{V}_0 \quad \tilde{I}_1 \quad \tilde{I}_2 \quad \tilde{I}_0 \quad \tilde{E} \quad \tilde{I}_d \quad \tilde{I}_q \quad P_e \quad T_e \quad \delta\right].$$

4.4.2 Synchronous Machine in Phasor Domain - Quadratized Form

After introduce new variables to quadratize the model, we have the quadratic model for the quasi-transient synchronous machine below. The states of the model are defined as follows:

$$X^T = \begin{bmatrix} y^T & x^T \end{bmatrix}$$
$$y = \begin{bmatrix} y_{external} & y_{internal} \end{bmatrix},$$
$$y_{external} = \begin{bmatrix} \tilde{V}_a & \tilde{V}_b & \tilde{V}_c & \tilde{V}_{an} & \tilde{V}_{bn} & \tilde{V}_{cn} & \tilde{V}_{f1} & \tilde{V}_{f2} & \omega_m & \omega_{m\_pseudo} \end{bmatrix},$$
$$y_{internal} = \begin{bmatrix} \tilde{V}_1 & \tilde{V}_2 & \tilde{V}_0 & \tilde{I}_1 & \tilde{I}_2 & \tilde{I}_0 & \tilde{E} & \tilde{I}_d & \tilde{I}_q & z_1 & z_2 & y_1 & y_2 & T_e & E_{abs} \end{bmatrix},$$
$$x^T = \begin{bmatrix} \delta(t) & al(t) & s(t) & c(t) \end{bmatrix}.$$

Here a pseudo external state ω_{m_pseudo} is introduced to keep the external nodes as complex numbers.

The quadratic equations of the model are defined as follows:

$$I_{ar} = I_{1r} + I_{2r} + I_{0r}, \tag{4.159}$$

$$I_{ai} = I_{1i} + I_{2i} + I_{0i}, \tag{4.160}$$

$$I_{br} = -\frac{1}{2} I_{1r} + \frac{\sqrt{3}}{2} I_{1i} - \frac{1}{2} I_{2r} - \frac{\sqrt{3}}{2} I_{2i} + I_{0r}, \tag{4.161}$$

$$I_{bi} = -\frac{\sqrt{3}}{2} I_{1r} - \frac{1}{2} I_{1i} + \frac{\sqrt{3}}{2} I_{2r} - \frac{1}{2} I_{2i} + I_{0i}, \tag{4.162}$$

$$I_{cr} = -\frac{1}{2} I_{1r} - \frac{\sqrt{3}}{2} I_{1i} - \frac{1}{2} I_{2r} + \frac{\sqrt{3}}{2} I_{2i} + I_{0r}, \tag{4.163}$$

$$I_{ci} = \frac{\sqrt{3}}{2} I_{1r} - \frac{1}{2} I_{1i} - \frac{\sqrt{3}}{2} I_{2r} - \frac{1}{2} I_{2i} + I_{0i}, \tag{4.164}$$

$$I_{anr} = -I_{1r} - I_{2r} - I_{0r}\,, \tag{4.165}$$

$$I_{ani} = -I_{1i} - I_{2i} - I_{0i}\,, \tag{4.166}$$

$$I_{bnr} = \frac{1}{2} I_{1r} - \frac{\sqrt{3}}{2} I_{1i} + \frac{1}{2} I_{2r} + \frac{\sqrt{3}}{2} I_{2i} - I_{0r}\,, \tag{4.167}$$

$$I_{bni} = \frac{\sqrt{3}}{2} I_{1r} + \frac{1}{2} I_{1i} - \frac{\sqrt{3}}{2} I_{2r} + \frac{1}{2} I_{2i} - I_{0i}\,, \tag{4.168}$$

$$I_{cnr} = \frac{1}{2} I_{1r} + \frac{\sqrt{3}}{2} I_{1i} + \frac{1}{2} I_{2r} - \frac{\sqrt{3}}{2} I_{2i} - I_{0r}\,, \tag{4.169}$$

$$I_{cni} = -\frac{\sqrt{3}}{2} I_{1r} + \frac{1}{2} I_{1i} + \frac{\sqrt{3}}{2} I_{2r} + \frac{1}{2} I_{2i} - I_{0i}\,, \tag{4.170}$$

$$I_{f1r} = \frac{1}{R_f}\left(V_{f1r} - V_{f2r}\right), \tag{4.171}$$

$$I_{f1i} = \frac{1}{R_f}\left(V_{f1i} - V_{f2i}\right), \tag{4.172}$$

$$I_{f2r} = -\frac{1}{R_f}\left(V_{f1r} - V_{f2r}\right), \tag{4.173}$$

$$I_{f2i} = -\frac{1}{R_f}\left(V_{f1i} - V_{f2i}\right), \tag{4.174}$$

$$T_m(t) = J \cdot al(t) - T_e\left(t\right), \tag{4.175}$$

$$0 = \omega_{m\_pseudo}\,, \tag{4.176}$$

$$0 = V_{ar} - V_{anr} - V_{1r} - V_{2r} - V_{0r}\,, \tag{4.177}$$

$$0 = V_{ai} - V_{ani} - V_{1i} - V_{2i} - V_{0i}\,, \tag{4.178}$$

$$0 = V_{br} - V_{bnr} + \frac{1}{2} V_{1r} - \frac{\sqrt{3}}{2} V_{1i} + \frac{1}{2} V_{2r} + \frac{\sqrt{3}}{2} V_{2i} - V_{0r}\,, \tag{4.179}$$

$$0 = V_{bi} - V_{bni} + \frac{\sqrt{3}}{2} V_{1r} + \frac{1}{2} V_{1i} - \frac{\sqrt{3}}{2} V_{2r} + \frac{1}{2} V_{2i} - V_{0i}\,, \tag{4.180}$$

$$0 = V_{cr} - V_{cnr} + \frac{1}{2} V_{1r} + \frac{\sqrt{3}}{2} V_{1i} + \frac{1}{2} V_{2r} - \frac{\sqrt{3}}{2} V_{2i} - V_{0r}\,, \tag{4.181}$$

$$0 = V_{ci} - V_{cni} - \frac{\sqrt{3}}{2} V_{1r} + \frac{1}{2} V_{1i} + \frac{\sqrt{3}}{2} V_{2r} + \frac{1}{2} V_{2i} - V_{0i}\,, \tag{4.182}$$

$$0 = E_r - V_{1r} + rI_{dr} + rI_{qr} - x_d I_{di} - x_q I_{qi}\,, \tag{4.183}$$

$$0 = E_i - V_{1i} + rI_{di} + rI_{qi} + x_d I_{dr} + x_q I_{qr}\,, \tag{4.184}$$

$$0 = V_{2r} - rI_{2r} + x_2 I_{2i}\,, \tag{4.185}$$

$$0 = V_{2i} - rI_{2i} - x_2 I_{2r}\,, \tag{4.186}$$

$$0 = V_{0r} - rI_{0r} + x_0 I_{0i}\,, \tag{4.187}$$

$$0 = V_{0i} - rI_{0i} - x_0 I_{0r}\,, \tag{4.188}$$

$$0 = E_r s(t) - E_i c(t)\,, \tag{4.189}$$

$$0 = E_r^2 + E_i^2 - E_{abs}^2\,, \tag{4.190}$$

$$0 = I_{1r} - I_{dr} - I_{qr}\,, \tag{4.191}$$

$$0 = I_{1i} - I_{di} - I_{qi}\,, \tag{4.192}$$

$$0 = E_r I_{dr} + E_i I_{di}\ , \tag{4.193}$$

$$0 = E_i I_{qr} - E_r I_{qi}\ , \tag{4.194}$$

$$0 = z_1 \cdot \omega_m(t) - E_r\ , \tag{4.195}$$

$$0 = z_2 \cdot \omega_m(t) - E_i\,, \tag{4.196}$$

$$0 = y_1(t) + \frac{p}{2} s(t) \cdot \omega_m(t) - \omega_0 \cdot s(t)\,, \tag{4.197}$$

$$0 = y_2(t) - \frac{p}{2} c(t) \cdot \omega_m(t) + \omega_0 \cdot c(t), \tag{4.198}$$

$$0 = T_e(t) - 3 \cdot \left[z_1 \left(I_{dr} + I_{qr} \right) + z_2 \left(I_{di} + I_{qi} \right) \right], \tag{4.199}$$

$$0 = \frac{1}{R_f} \left(V_{f1r} - V_{f2r} \right) - \frac{\sqrt{2}}{\omega \cdot M_f} \cdot E_{abs}, \tag{4.200}$$

$$\frac{d\delta(t)}{dt} = \frac{p}{2} \omega_m(t) - \omega_0 \ , \tag{4.201}$$

$$\frac{d\omega_m(t)}{dt} = al(t) \ , \tag{4.202}$$

$$\frac{dc(t)}{dt} = y_1(t) \ , \tag{4.203}$$

$$\frac{ds(t)}{dt} = y_2(t), \tag{4.204}$$

4.4.3 Synchronous Machine in Phasor Domain - SCAQCF

We use quadratic integration method to integrate the differential equations from (4.201) to (4.204), and for the algebra equations from (4.159) to (4.200), we just change the time variable at time t and tm. Here we just listed the integration equations for equations from (4.201) to (4.204) as follows:

$$0 = \frac{h}{6} \frac{p}{2} \omega_m(t) + \frac{2h}{3} \frac{p}{2} \omega_m(t_m) - \delta(t) + \left(\frac{h}{6} \frac{p}{2} \omega_m(t-h) + \delta(t-h) \right), \tag{4.205}$$

$$0 = \frac{h}{6} al(t) + \frac{2h}{3} al(t_m) - \omega_m(t) + \left(\frac{h}{6} al(t-h) + \omega_m(t-h) \right), \tag{4.206}$$

$$0 = \frac{h}{6} y_1(t) + \frac{2h}{3} y_1(t_m) - c(t) + \left(\frac{h}{6} y_1(t-h) + c(t-h) \right), \tag{4.207}$$

$$0 = -\frac{h}{24}\frac{p}{2}\omega_m(t) + \frac{h}{3}\frac{p}{2}\omega_m(t_m) - \delta(t) + \left(\frac{5h}{24}\frac{p}{2}\omega_m(t-h) + \delta(t-h)\right), \tag{4.208}$$

$$0 = \frac{h}{6}y_2(t) + \frac{2h}{3}y_2(t_m) - s(t) + \left(\frac{h}{6}y_2(t-h) + s(t-h)\right), \tag{4.209}$$

$$0 = -\frac{h}{24}al(t) + \frac{h}{3}al(t_m) - \omega_m(t_m) + \left(\frac{5h}{24}al(t-h) + \omega_m(t-h)\right), \tag{4.210}$$

$$0 = -\frac{h}{24}y_1(t) + \frac{h}{3}y_1(t_m) - c(t_m) + \left(\frac{5h}{24}y_1(t-h) + c(t-h)\right), \tag{4.211}$$

$$0 = -\frac{h}{24}y_2(t) + \frac{h}{3}y_2(t_m) - s(t_m) + \left(\frac{5h}{24}y_2(t-h) + s(t-h)\right). \tag{4.212}$$

4.5 Summary

The mathematical formulation and derivation of the SCAQCF model for power system components are presented in this chapter. Detailed examples for the derivation of the SCAQCF models of the synchronous machine at both time domain and phasor domain have been presented in this chapter to illustrate the procedure of obtaining the SCAQCF model for a component.

CHAPTER 5 PMU-BASED DISTRIBUTED DYNAMIC STATE ESTIMATION

5.1 Overview

A distributed dynamic state estimation (DDSE) method is proposed, which operates at the substation level on a model that consists of the substation and the interconnecting transmission circuits, using only local data (any data collected with IEDs within the substation), to provide a high-fidelity real-time substation model. In particular, the DDSE algorithm utilizes a SCAQCF and instrumentation channel inclusive model of the system, along with the set of measurements from PMUs, relays, DFRs, and smart meters, to perform state estimation, bad data detection and identification, and topology error detection and identification, for the purpose of extracting the real-time dynamic model of the system. The high update-rates performance of DDSE is scalable to any size system since the computations are fully distributed.

Note that there are two kinds of dynamics for the DDSE related with the data acquisition, as a result, the DDSE can be categorized as DDSE-T and DDSE-Q respectively. Section 5.3 and Section 5.4 give detailed discussions about the DDSE-T and DDSE-Q. The object-oriented DDSE measurement model is described in Section 5.5. The different types of measurements used in the DDSE process are explained in detail. The DDSE solution algorithm is given in Section 5.6. Sections 5.7 describes the procedures for evaluating the quality of the results of the state estimator. Sections 5.8 describes the bad data detection, identification, and rejection method in case of existing bad data. The object-oriented implementation algorithm for the DDSE is summarized in Section 5.9. Section 5.10

discusses the specific case of multiple-step DDSE. Finally, demonstration results for the DDSE are given in Section 5.11, 5.12, and 5.13.

5.2 DDSE Introduction

In general, the DDSE extends the concept of static state estimation by including the dynamic states of the power system and the differential equations that describes the dynamics of the power system. Typical dynamic states of the power system can be the generator speed, generator torque angle, or the generator acceleration. The generic dynamic state estimation model is described by a set of differential and algebraic equations (DAEs), which express the dynamics of the system as follows:

$$\begin{aligned} \frac{dx(t)}{dt} &= f(x(t), y(t), t), \\ 0 &= g(x(t), y(t), t), \end{aligned} \tag{5.1}$$

where x and y are the dynamic and algebraic states of the system respectively. Note that equation set (5.1) could be expressed by the standard SCAQCF syntax as described in Section 4.2. The system measurements z are related to the states through the following equations:

$$z = h(x(t), y(t), t) + \eta, \tag{5.2}$$

where η represents the measurement error, which is often described as random variable with Gaussian probability distribution. The measurement error is directly related to the accuracy of the data acquisition system.

The overall approach is illustrated in Figure 5.1 [101]. The set of physical measurements z_a are obtained from PMUs, relays, and other metering devices at the substation level. These values are then compared with the "model" values, which are

obtained from the dynamic model of the power system, i.e., z_m , forming a measurement error e. Additional relations that hold based on the system model (5.1) are also included in the measurement set and are referred to as virtual measurements. Such equations are also of the form (5.2), with a measurement value of 0 and a very small measurement error. A standard least squares estimation is performed, which minimizes the sum of the errors squared and provides the best estimate of the system state. If the dynamic state estimator results are not satisfactory, this might indicate the presence of bad data. Statistical hypothesis methods are used, based on the chi-square criterion to check the presence of bad data. The bad data are identified, based on their normalized residual values, removed from the measurement set and the procedure is repeated. Otherwise, the best estimates of the system states and measurements denoted by $\hat{x}_e$, $\hat{y}_e$ and $\hat{z}_e$ are calculated and can be used as an input for numerous other EMS applications such as stability monitoring.

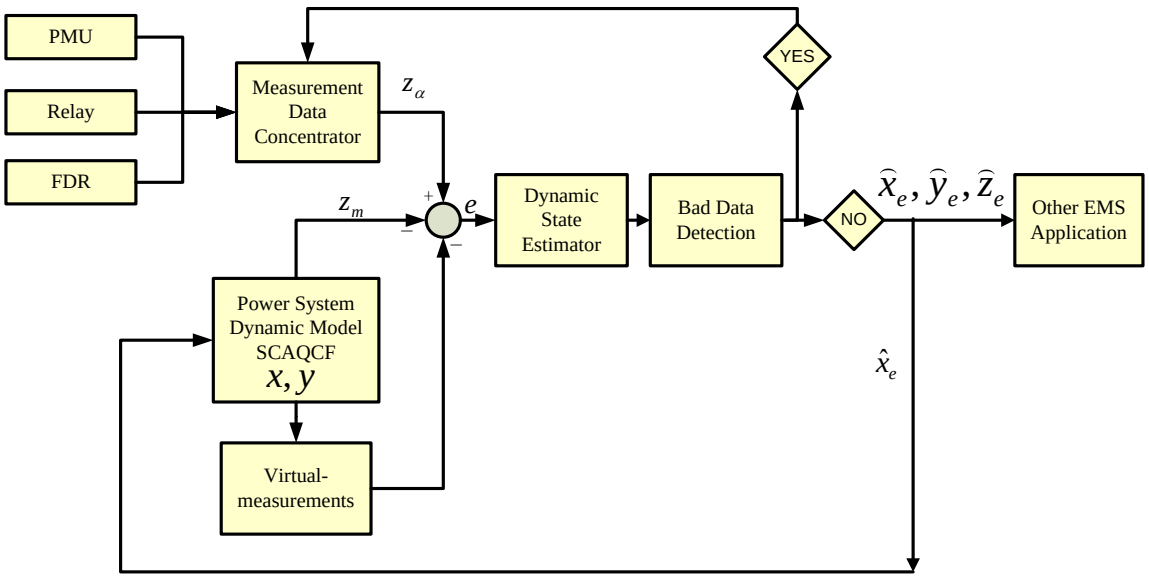

Figure 5.1. Schematic diagram of the DDSE.

The DDSE is implemented in a distributed architecture, at the substation level. This is a novel approach compared to presently available state estimation applications that are based on a centralized architecture and are executed in the control center. The distributed application of the state estimation is enabled by the availability of synchronized measurements that are referenced to the GPS clock signal. As a result, these measurements are globally valid and enable a distributed approach for the implementation of state estimation.

Local (substation) measurements are used to estimate the states of the substation but also the states of the buses at the other ends of the lines/circuits that connect the substation of interest with the neighboring substations. The DDSE uses data from relays, PMUs, meters, and FDRs in the substation only, thus avoiding all issues associated with transmission of data and associated time latencies.

Note that there are two kinds of dynamics for the DDSE related with the data acquisition, as a result, the DDSE can be categorized as DDSE-T and DDSE-Q respectively. If the measurements are phasors from PMUs, the DDSE-Q takes account of the mechanical and electro-mechanical dynamics only while the electrical dynamics are neglected, since the electrical quantities (voltages and currents) are represented in phasor form. DDSE-Q runs at rates comparable to the suggested rates in the synchrophasors standard C37.118. Presently it has been implemented to execute with rate at 60 times per second thus providing the dynamic state of the substation more than 60 times per second. On the other hand, if the measurements are time-domain waveforms sampled from relays and DFRs, the DDSE-T will consider both the mechanical and electrical dynamics of the power system

and is implemented with detailed time-domain system models; that is, actual time-domain waveforms are used to capture not only fast dynamics but also the exact frequency of each waveform. DDSE-T runs at rates comparable to the sampling rates of the relays, that is, 2000 times per second to 8000 times per second. Performing state estimation thousands of times per second is a heavy computation task, and thus the DDSE-T can only be implemented at the scope of a single component of the power system, that is, the DDSE-T is performed for each single component of the power system in a distributed manner. Presently it has been implemented to execute with rate at 2000 times per second thus providing the full dynamic and transient behaviors of a component of the power system.

The advantages of the distributed architecture are numerous. First of all, the state estimation algorithm is implemented using only local measurements to estimate only the states of the substation and of the neighboring buses. As a result the dimensionality of the problem is significantly decreased compared to the dimensionality of a centralized state estimator, as indicated in Table 5.1. This allows for very fast execution times and utilization of very detailed power system models (three-phase static or dynamic models, instrumentation inclusive). The three-phase, instrumentation channel inclusive model for the power system can eliminate the estimation errors from the imbalanced operations and system asymmetric, as well as the measurement errors introduced by the instrumentation channels. In addition, the estimation results are very accurate not only due to the improved modeling but also due to the measurement redundancy inside a substation. Note that in a typical traditional state estimator only few measurements are used per substation. On the contrary, in the approach of this dissertation, it is proposed that all the measurements within the substation should be used. And as Section 3.2 discussed, upon execution of the

distributed state estimation on all substations, the results can be collected at a central location (control center) to synthesize the system-wide operating state of the system.

Table 5.1. State estimation dimensionality.

	Typical Substation	**ISO/Utility**
States	60	40,000
Measurements	1,200	250,000
State Estimation Execution Time	At least 1 execution per cycle	1-3 minutes

5.3 Relay Level DDSE (DDSE–T)

The DDSE-T considers both the mechanical and electrical dynamics of the power system and is implemented with detailed time-domain component models; that is, actual time-domain waveforms are used to capture not only fast dynamics but also the exact frequency of each waveform. The DDSE-T is performed at the relay level for each power system component in a distributed manner, and the inputs of the DDSE-T are the measurements (voltages, currents, and any other measurable quantities) of the component in time-domain waveforms. The states of the DDSE-T are defined as the voltages at the terminals of the component and all the internal states in the SCAQCF model of the component, which describes the full time-domain dynamic behavior of the component. The outputs of the DDSE-T are the real-time models and accurate operating conditions of the

components with GPS-synchronous time-stamp, which consist of (1) autonomously defined state and control variables, (2) an object-oriented, unified, and interoperable model of the component with SCAQCF syntax, and (3) connectivity information.

With the help of the SCAQCF syntax, the measurement model of the DDSE-T for one component can be extracted in the following form:

$$\mathbf{y}(\mathbf{x},\mathbf{u}) = Y_{m,x}\mathbf{x} + \left\{ \begin{array}{c} \vdots \\ \mathbf{x}^T F_{m,x}^i \mathbf{x} \\ \vdots \end{array} \right\} + Y_{m,u}\mathbf{u} + \left\{ \begin{array}{c} \vdots \\ \mathbf{u}^T F_{m,u}^i \mathbf{u} \\ \vdots \end{array} \right\} + \left\{ \begin{array}{c} \vdots \\ \mathbf{x}^T F_{m,xu}^i \mathbf{u} \\ \vdots \end{array} \right\} + C_m + sigma, \quad (5.3)$$

$$C_m = N_{m,x}\mathbf{x}(t-h) + N_{m,u}\mathbf{u}(t-h) + M_m I(t-h) + K_m, \quad (5.4)$$

where $\mathbf{y}(\mathbf{x},\mathbf{u})$ represents measurement variables at both time t and time t_m, $\mathbf{y} = [\mathbf{y}(t), \mathbf{y}(t_m)]$. $\mathbf{x}$ represents external and internal state variables of the measurement model, $\mathbf{x} = [\mathbf{x}(t), \mathbf{x}(t_m)]$. $\mathbf{u}$ represents control variables of the measurement model, i.e. transformer tap, $\mathbf{u} = [\mathbf{u}(t), \mathbf{u}(t_m)]$. Note that all the state variables and control variables are in the time-domain waveform format, represented by real numbers. $Y_{m,x}$ represents matrix defining the linear part for state variables, $F_{m,x}$ represents the matrices defining the quadratic part for state variables, $Y_{m,u}$ represents the matrix defining the linear part for control variables, $F_{m,u}$ represents the matrices defining the quadratic part for control variables, $F_{m,xu}$ represents the matrices defining the quadratic part for the product of state and control variables, C_m represents the history dependent vector of the measurement model, $N_{m,x}$ represents the matrix defining the last integration step state variables part, $N_{m,u}$ represents the matrix defining the last integration step control variables part, M_m: represents the matrix defining

the last integration step through variables part, K_m represents the constant vector of the measurement model, and *sigma* represents the vector defining the standard deviation in metric unit.

The measurement model should be constructed from the device model and the definition of the measurements. The measurements include actual measurements, pseudo measurements, virtual measurements and derived measurements. Section 5.5 gives the detailed explanation for each type of the measurements and how to form the above measurement model from the SCAQCF model of the device in a systematic and object-oriented approach.

Figure 5.2 illustrates the data flow of the DDSE-T [99]. The merging units change the analog signals from CT/PTs to optic signals and the optic signals are transmitted through optic fibers into the process bus in the panel house of the substation. The process bus behaves as a common data concentrator for all the relays in the panel house. Each relay obtains the digital signals of the measurements from the process bus to perform the DDSE-T for the component monitored by the relay. The DDSE-T is performed a few thousand times per second depending on the sampling period of the merging units. For example, if the merging units samples 4000 times per second, the dynamic state estimation is executed 2000 times per second (it performs dynamic state estimation using two successive sampled data). Performing dynamic state estimation 2000 times per second is a heavy computational tasks, and this execution rate is only achievable for estimating the dynamic states of one component, since the model of one component is much smaller than the model of the whole system, and this is why the DDSE-T is performed at the relay level.

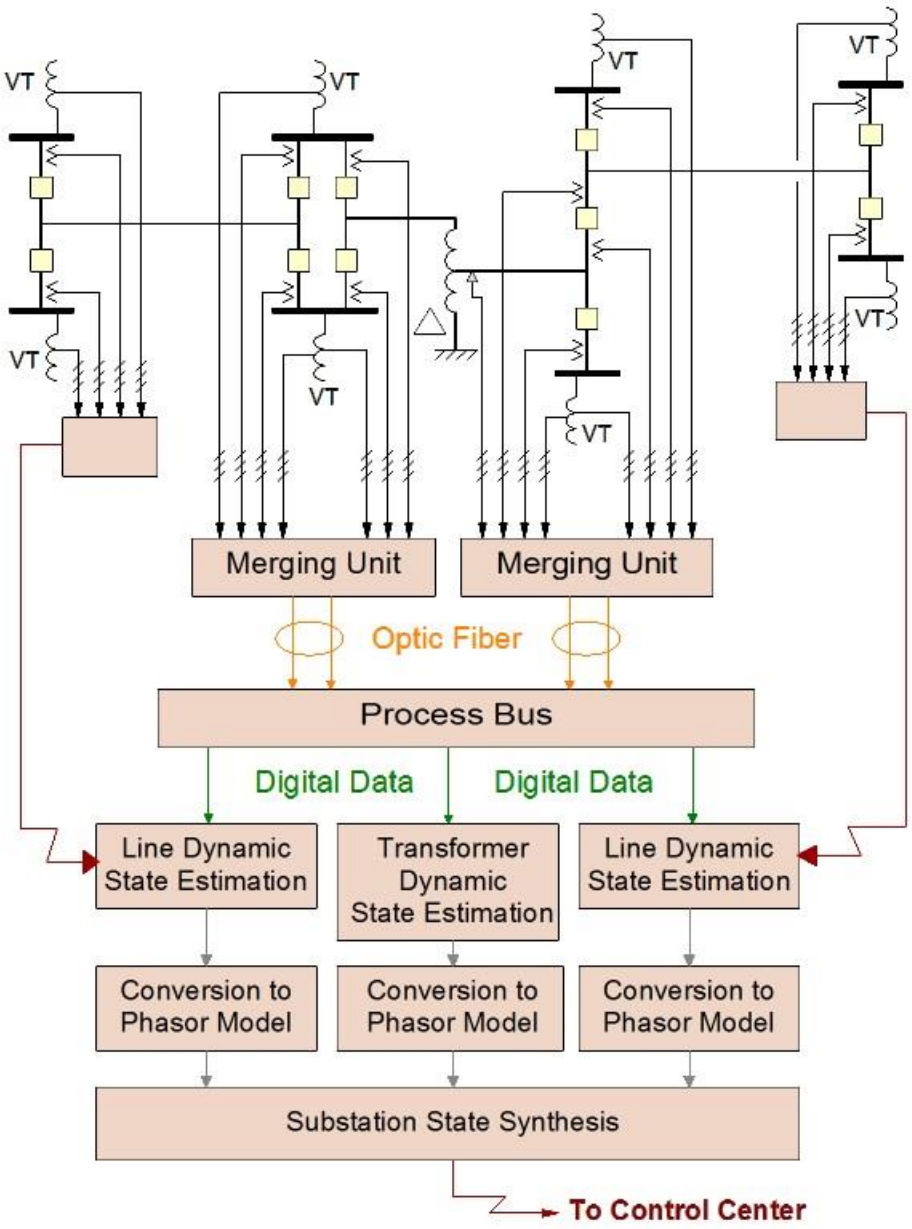

Figure 5.2. Data flow of the DDSE-T [99].

It should be stressed that the functional specifications of the DDSE-T can be met by current top-of-the-line numerical protective relays. Specifically, the computational power of these relays is adequate to perform the DDSE-T and the extraction of the real-time model of the component by appropriate programming. The DDSE-based relays are also able to

receive commands from the control center and apply them to control power apparatus just as present relays are able to do.

5.4 Substation Level DDSE (DDSE–Q)

As discussed in Section 5.3, in the proposed data acquisition infrastructure, ideally, the merging units change the analog signals from CT/PTs to optic signals. The optic signals are transmitted through optic fibers into the process bus in the panel house of the substation, and the process bus behaves as a common data concentrator for all the DDSE-based relays. The DDSE-T is performed at the relay level for each component or protection zone of the substation separately. The time-domain to phasor-domain transformation module in the relay is responsible for the conversion of the component model from the time-domain to the phasor-domain, based on the estimation results of each component. However, in reality, substations are a mixed system, which means old and new technologies both exist in the substation. Many of the analog measurements from CT/PTs do not go through the merging units and the process bus: they may go directly to the PMUs, relays, and FDRs.

In order to accommodate all measurements from different types of measurement devices (PMUs, relays, and FDRs), a substation level DDSE is proposed. The concept of the substation level DDSE is illustrated by Figure 5.3. The substation level DDSE uses data from relays, PMUs and other IEDs in the substation along with a detailed substation model to generate the local state estimate. The substation model is a breaker oriented, instrumentation inclusive, three-phase model presented in the SCAQCF syntax. This approach allows sharp bad data detection and identification. The advantage comes from the fact that at the substation level, there is greater redundancy of data compared with a

typical centralized state estimator based on SCADA data alone, facilitating the detection of bad data and system topology errors. In addition, the state estimation problem is much smaller in size and therefore powerful hypothesis testing methods are applied for both bad data and topology errors identification without substantial deterioration of the computational efficiency, which is not the case in a centralized approach due to enormous number of hypotheses. Moreover, the use of the three-phase and breaker-oriented model facilitates the identification of symmetric and asymmetric topology errors (one pole stuck, etc.) that traditional symmetric state estimators cannot identify.

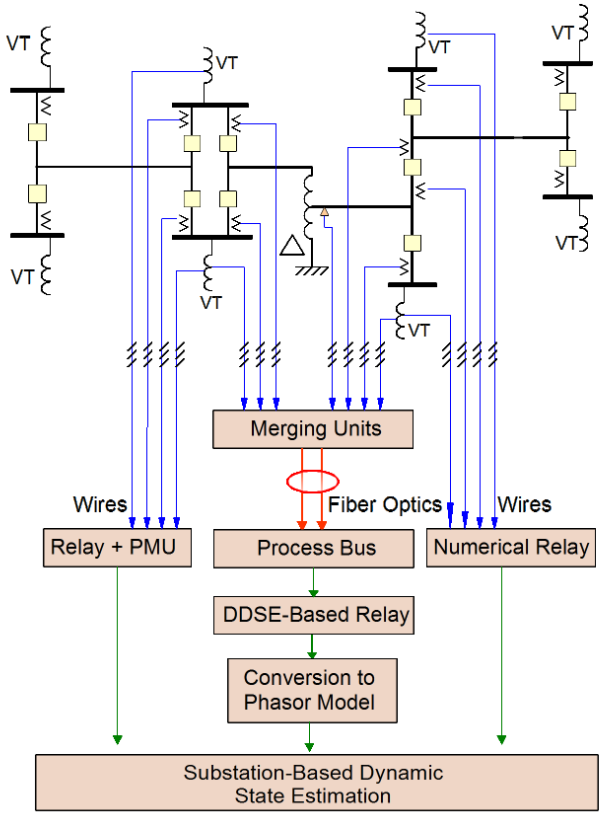

Figure 5.3. Schematic diagram of the substation level DDSE.

Note that compared with the relay level DDSE, which is performed based on the time-domain waveforms and has a typical sampling and execution rate from two to eight kilohertz, the substation level DDSE obtains the measurements form PMUs, which can

only provide the phasor data with a sampling rate of 30 to 120 samples per second. The sampling rate of 30 to 120 samples per second can only capture the electro-mechanical dynamics of the power system, while cannot capture the electrical dynamics that has a typical time duration of milliseconds. Also note that the model of the substation level DDSE contains all the SCAQCF model of the components and all the available measurements in the substation, and a typical substation has 10 to 20 components and hundreds of measurements. As a result, the dimension of the model for the substation level DDSE is much larger than the dimension of the model for the relay level DDSE, typically 40 to 60 times as large as the relay level model. As a conclusion, it is impractical and unnecessary to utilize the full time-domain model for the entire substation and to estimate both the mechanical and electrical dynamics of the components in the substation. Based on the above conclusion, the substation level DDSE takes account of the mechanical and electro-mechanical dynamics only while the electrical dynamics are neglected, and the electrical quantities (voltages and currents) in the substation level DDSE are represented in phasor form. Here we name the substation level DDSE as DDSE-Q, and the suffix Q represents the abbreviation of Quasi-dynamic. Presently it has been implemented to execute with rates at 60 to 120 times per second thus providing the dynamic states of the substation more than 60 times per second.

The state of the DDSE-Q is defined as the collection of the voltage phasors for each phase at each bus of the substation. So for every bus i of the substation the voltage state is defined as

$$\tilde{V}_i = \begin{bmatrix} \tilde{V}_{i,A} & \tilde{V}_{i,B} & \tilde{V}_{i,C} & \tilde{V}_{i,N} \end{bmatrix}^T \quad . \tag{5.5}$$

Note that in a rectangular coordinates formulation there are two states for each phasor voltage, the real and the imaginary part. So the actual states are:

$$V_i = \begin{bmatrix} V_{i,A,R} & V_{i,A,I} & V_{i,B,R} & V_{i,B,I} & V_{i,C,R} & V_{i,C,I} & V_{i,N,R} & V_{i,N,I} \end{bmatrix}^T, \tag{5.6}$$

where subscripts R and I denote real and imaginary part.

The state is extended to include internal states (algebraic or dynamic) of the devices, for example the torque angle and the rotor speed of a generator or the magnetic flux linkage of a transformer. The system state also includes the states of the buses at the other ends of the lines/circuits connected to the substation. The conceptual illustration of the dynamic state estimator and the state definition are shown in Figure 5.4.

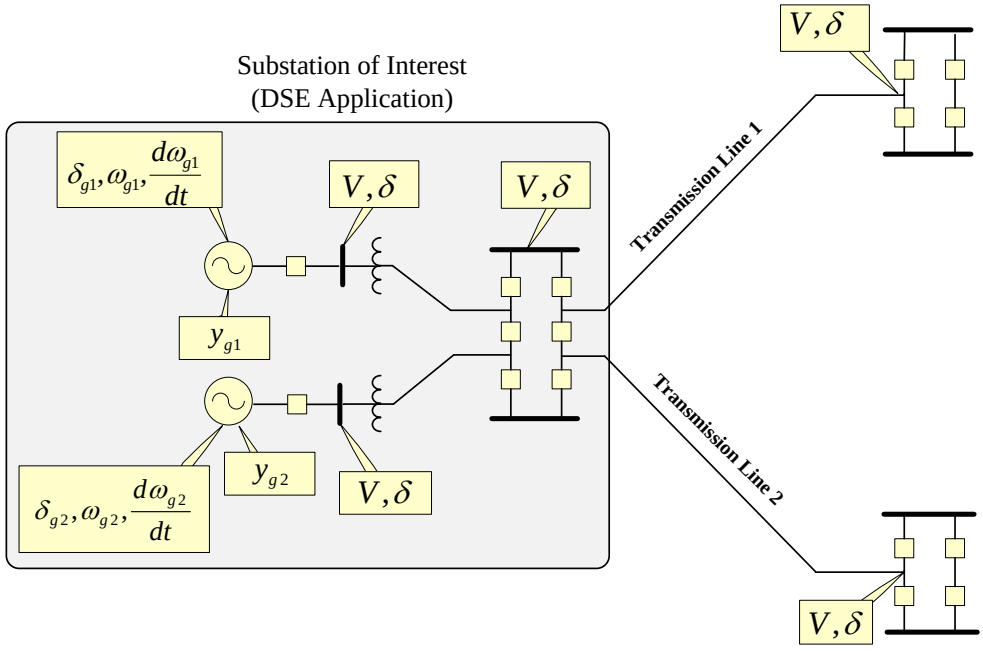

Figure 5.4. Definition of DDSE-Q state.

The data flow for the substation level DDSE is illustrated in Figure 5.5 [31]. As discussed previously in this section, local (substation) measurements are used to estimate not only the states of the substation but also the states of the buses at the other ends of the

lines/circuits that connect the substation of interest with the neighboring substations. The substation level DDSE uses data from relays, PMUs, meters, and FDRs in the substation only, thus avoiding all issues associated with transmission of data and associated time latencies. It runs at rates comparable to the suggested rates in the synchrophasors standard C37.118. Presently it has been implemented to execute with rates at 60 to 120 times per second thus providing the dynamic state of the substation more than 60 times per second.

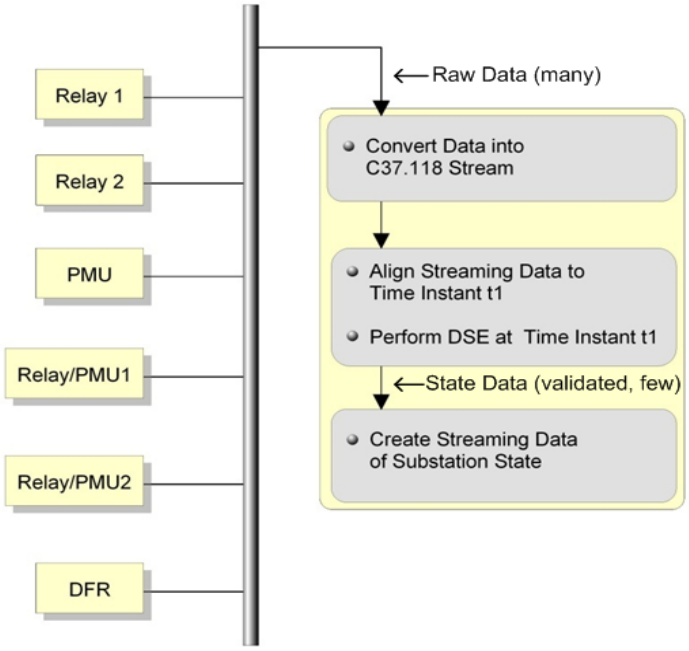

Figure 5.5. Data flow in substation level DDSE [31].

With the help of the SCAQCF syntax, the measurement model of the DDSE-Q at the substation level can be extracted in the following form:

$$\tilde{\mathbf{Y}} = Y_{mx}\tilde{\mathbf{X}} + \begin{Bmatrix} \vdots \\ \tilde{\mathbf{X}}^T F_{mx}^i \tilde{\mathbf{X}} \\ \vdots \end{Bmatrix} + Y_{mu}\tilde{\mathbf{U}} + \begin{Bmatrix} \vdots \\ \tilde{\mathbf{U}}^T F_{mu}^i \tilde{\mathbf{U}} \\ \vdots \end{Bmatrix} + \begin{Bmatrix} \vdots \\ \tilde{\mathbf{X}}^T F_{mxu}^i \tilde{\mathbf{U}} \\ \vdots \end{Bmatrix} + C_m + sigma\ , \qquad (5.7)$$

$$C_m = N_{m,x}\tilde{\mathbf{X}}(t-h) + N_{m,u}\tilde{\mathbf{U}}(t-h) + M_m\tilde{\mathbf{I}}(t-h) + K_m\,, \qquad (5.8)$$

where $\tilde{\mathbf{Y}}$ represents measurement variables at both time t and time t_m, $\tilde{\mathbf{Y}} = [\tilde{\mathbf{Y}}(t), \tilde{\mathbf{Y}}(t_m)]$, $\tilde{\mathbf{X}}$ represents external and internal state variables of the measurement model, $\tilde{\mathbf{X}} = [\tilde{\mathbf{X}}(t), \tilde{\mathbf{X}}(t_m)]$, $\tilde{\mathbf{U}}$ represents control variables of the measurement model, i.e. transformer tap, $\tilde{\mathbf{U}} = [\tilde{\mathbf{U}}(t), \tilde{\mathbf{U}}(t_m)]$, note that all the state variables are in the phasor domain, and represented by complex numbers. $Y_{m,x}$ represents matrix defining the linear part for state variables, $F_{m,x}$ represents the matrices defining the quadratic part for state variables, $Y_{m,u}$ represents the matrix defining the linear part for control variables, $F_{m,u}$ represents the matrices defining the quadratic part for control variables, $F_{m,xu}$ represents the matrices defining the quadratic part for the product of state and control variables, C_m represents the history dependent vector of the measurement model, $N_{m,x}$ represents the matrix defining the last integration step state variables part, $N_{m,u}$ represents the matrix defining the last integration step control variables part, M_m : represents the matrix defining the last integration step through variables part, K_m represents the constant vector of the measurement model, and *sigma* represents the vector defining the standard deviation in metric unit.

The measurement model should be constructed from the device model and the definition of the measurements. The measurements include actual measurements, pseudo measurements, virtual measurements and derived measurements. Section 5.5 gives the detailed explanation for each type of measurements and how to form the above measurement model from the SCAQCF model of the device in a systematic and object-

oriented approach. Section 5.12 gives a detailed example of how the states and the measurement model are defined for a synchronous machine in phasor domain.

5.5 Object-Oriented Measurement Model

The system measurements z are in general related to the states through the following equations:

$$z = h(x(t)) + \eta, \tag{5.9}$$

where η represents the measurement error, which is often described as random variables with Gaussian probability distribution and $x(t)$ is the system state vector. Note that the formula (5.9) is a general expression for the measurements and is suitable for both DDSE-T and DDSE-Q. As a result of the existence of a variety of measurements and models (GPS synchronized, non-synchronized, nonlinear models, etc.), the relationship between the states and the measurements is not necessarily linear. However due to the quadratic modeling with the SCAQCF syntax that is followed in the described formulation, a physical measurement or a virtual-measurement is at most quadratic in terms of the states and will have the following generic formulation:

$$z_k = c_k + \sum_i a_{k,i} \cdot x_i + \sum_{i,j} b_{k,i,j} \cdot x_i \cdot x_j + \eta_k \,, \tag{5.10}$$

where

z_k is the measured value,

c_k is the constant term,

$a_{k,i}$ are the linear coefficients,

$b_{k,i,j}$ are the nonlinear coefficients,

η_k is the error term.

Note that the measurements are related to the states with a degree of at most quadratic. The set of physical measurements z are obtained from PMUs, relays, and other metering devices at the substation level. Additional relations that hold based on the system SCAQCF model are also included in the measurement set and are referred as virtual measurements. Such equations are also of the form (5.10), with a measurement value of 0 and a very small measurement error.

The measurements are classified in seven categories:

(1) Actual Across Measurement:

This type of measurement is a real measurement that can be obtained by available metering devices. It is a direct state measurement so it is not related to a device. Typical measurements that belong in this category are voltage phasor measurements.

(2) Pseudo Across Measurement:

This type of measurement is not a real measurement. The pseudo across measurement is also not related to a device. For example if only the voltage phasor measurement for phase A, is available, the voltage phasor measurements for phase B and C can be added as pseudo across measurements in the estimation algorithm with the same magnitude and a phase difference of +/- 120 accordingly.

(3) Actual Through Measurement:

This type of measurement is a real measurement that can also be obtained by available metering devices. Typical measurements that belong in this category are current phasor measurements or real power measurements. Actual through measurements are related to a

specific device of the system. Thus, for creating the model of an actual through measurement, the device (distribution line, transformer, etc.) that this measurement refers to, has to be known. Then the measurement formula is derived as a function of the states of the device.

As discussed in section 4.2, each device is represented by the SCAQCF syntax. The model of the actual through measurement can be easily derived from the SCAQCF syntax of the corresponding device. For example the model of a synchronized current phasor measurement that is taken from phase k of a device is expressed as

$$i_k^m = \sum_i Y_{eq,i}^k \cdot x_i + \sum_{i,j} F_{eqi,j}^{\ k} \cdot x_i \cdot x_j - b_{eq}^k + \eta_k , \tag{5.11}$$

where

$Y_{eq}^{\ k}$ are the elements of the kth row of the Yeqx matrix of the corresponding device SCAQCF.

$F_{eq}^{\ k}$ are the elements of the kth Feqx matrix that corresponds to the kth equation of the device SCAQCF.

b_{eq}^k is the kth element of the Beq vector of the corresponding device SCAQCF.

(4) Virtual (noiseless) Through Measurement:

This type of measurement is not a real measurement and it is also derived from the SCAQCF of the device. Virtual through measurements are related to the internal equations of the SCAQCF model of the device. Note that as explained in section 4.2, due to the quadratization procedure, additional internal states and equations may be created for a specific model. Inclusion of these measurements in the state estimation procedure, achieves

observability of the internal states of the devices and increases the measurement redundancy.

The models of the virtual through measurements of a device are created upon reading of the first actual through measurement that is related to this device. The measurement value of the virtual through measurement is 0 (noiseless), because it is created from the internal equations of the device SCAQCF. For example the model of a virtual measurement is

$$0 = \sum_{i} Y_{eq,i}^{k} \cdot x_i + \sum_{i,j} F_{eq}{}_{i,j}^{k} \cdot x_i \cdot x_j - b_{eq}^{k} + \eta_k , \tag{5.12}$$

where k is the corresponding row of the virtual measurement to the SCAQCF model of the device.

(5) Pseudo Through Measurement:

This type of measurement is not a real measurement. Typical measurements that belong in this category are derived from the network topology such as Kirchhoff's current law, neutral/shield wire current etc. [28], [30]-[33]. For example, if only the current phasor measurement of phase A is available, the current phasor measurements for phases B and C can be added as pseudo across measurements in the estimation algorithm with the same magnitude and a phase difference of +/- 120 accordingly.

(6) Derived Through Measurement:

A derived measurement is a through measurement (measurement related to a device) that is included in the measurement set and increases the observability and the measurement redundancy of the system. For example, assume a phasor current measurement that is taken at Node1 of a single phase capacitor as is shown in Figure 5.6.

Then a derived current measurement for Node2 with the opposite value compared to the original measurement can be created and used in the estimation, that is

$$i_2(t) = -i_1(t). \tag{5.13}$$

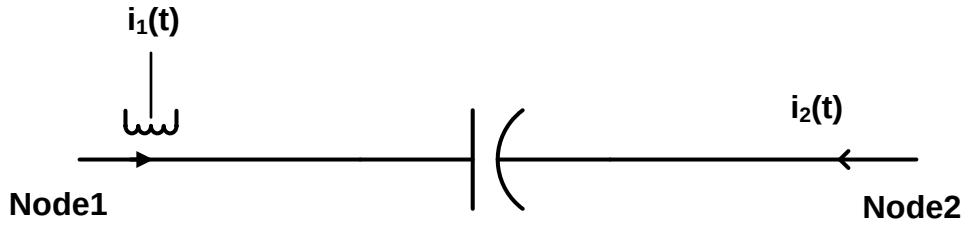

Figure 5.6. Derived measurement on a device.

Another example of a derived measurement is given next. Assume a node where three branches are connected and GPS synchronized current measurements are available for two of the devices, as shown in Figure 5.7. Then a derived measurement can be created for the current in the third device with the value of the measurement being the negative of the sum of the two original measurements that is

$$i_3(t) = -i_1(t) - i_2(t). \tag{5.14}$$

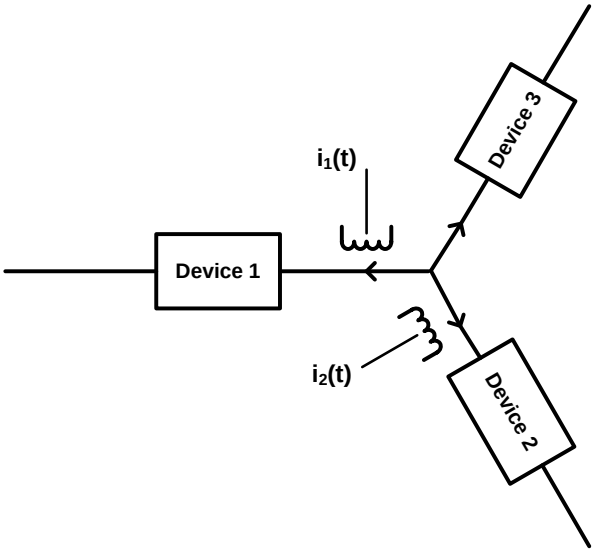

Figure 5.7. Derived measurement on a node.

(7) KCL Virtual Measurement:

Another type of measurement that can be added in the estimation procedure is the KCL virtual measurement. Assume for example the case with the three branches as in Figure 5.7 but with one GPS-synchronized and one non-synchronized measurement. Then a derived measurement cannot be introduced since the value of the current at the third device cannot be computed, however a KCL virtual measurement can be added, with the measurement formula being

$$0 = i_1(t) + i_2(t) + i_3(t). \tag{5.15}$$

Note that the value of the measurement is 0 and there is no error in this measurement since it is derived by a physical law, so a very small standard deviation is given for this measurement.

The block diagram of the algorithm for the inclusion of the derived measurements and the KCL virtual measurements is shown in Figure 5.8. Initially the derived measurements that result from devices that have the same current at a terminal pair are included. Once this is defined for each device (only during initialization), and there is a through measurement in such a node, then a derived measurement is added for the other corresponding node. Then the derived measurements for a node where a measurement is missing from a link are introduced. In particular, for each node, the number of links and the corresponding devices that are connected are defined. If all these devices are modeled and if there is at least one missing measurement then, the number of missing measurements has to be found. If there are more than one missing measurements then a flag is set for this node for introducing a KCL virtual measurement. For the case that only one measurement is missing, if at least one of the available measurements is non-GPS synchronized then the

flag for introducing a KCL virtual measurement is also set. Otherwise, if only one measurement is missing and all the available measurements are GPS synchronized then a derived measurement can be added and there is no need for a KCL virtual measurement to be added for this node. Note that the whole procedure is repeated until there is no added derived measurement after scanning all the devices and all the nodes. Finally, after including all the derived measurements, the KCL virtual measurements are included for the nodes for which the corresponding flag is set.

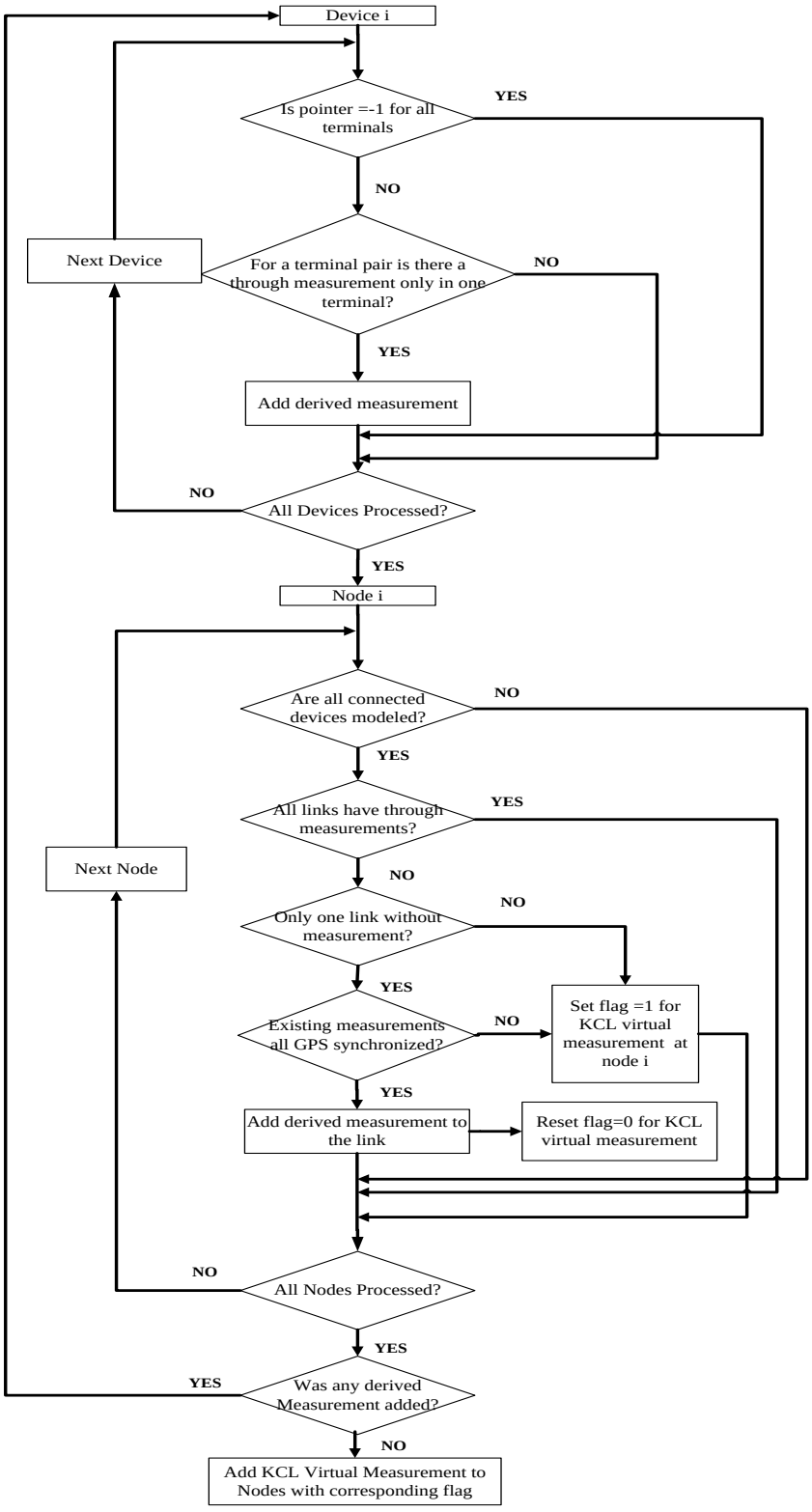

Figure 5.8. Block diagram for derived and KCL measurements.

Another key issue in the proposed formulation of the state estimator is the processing of non-synchronized phasor measurements. If a metering device does not have a GPS clock, the phasor measurements are not synchronized to the global time reference that the GPS clock offers. Data from metering devices that are not GPS synchronized are referenced to the phase A voltage. The "actual" phase angle of the phase A voltage is introduced as an "unknown state" that is estimated by the state estimation as follows:

$$\tilde{A}_{non-synch} = \tilde{A}_{synch} \cdot e^{ja}, \tag{5.16}$$

where $e^{ja} = \cos(\alpha) + j\sin(\alpha) = x_{NS,R} + j \cdot x_{NS,I}$. (5.17)

The introduced "unknown state" is a complex variable with the restriction that its magnitude is 1 and its phase angle is α. As a result the following virtual measurement can also be added:

$$0 = {x_{NS,R}}^2 + {x_{NS,I}}^2 - 1. \tag{5.18}$$

Note that there is one α variable for each non-synchronized metering device.

5.6 DDSE Solution Algorithm

The problem is defined, at each time step, as a static estimation problem. The objective is to estimate the state vector x which in general includes both dynamic and algebraic states. The least squares approach is used and the problem is formulated as follows:

$$Minimize \qquad J(x, y) = \eta^T W \eta, \tag{5.19}$$

where

$$\eta = z - h(x), \tag{5.20}$$

and W is a diagonal matrix, the non-zero entries of which are equal to the inverse of the variance of the measurement errors:

$$W = diag\left[\frac{1}{\sigma_v^2}\right]. \tag{5.21}$$

The best estimate of the system state is obtained from the Gauss-Newton iterative algorithm:

$$\hat{x}^{\nu+1} = \hat{x}^{\nu} - (H^T W H)^{-1} H^T W (h(\hat{x}^{\nu}) - z) \ , \tag{5.22}$$

where $\hat{x}$ refers to the best estimate of the state vector x, and H is the Jacobian matrix of the measurement equations.

The derivation of the information matrix $H^T W H$ and the vector $H^T W (h(\hat{x}^{\nu}) - z)$ from the measurement data is performed using sparcity techniques and a suitable sparse matrix library. In particular, at each time step of the estimation algorithm, the contributions of each measurement to the information matrix $H^T W H$ and the vector $H^T W (h(\hat{x}^{\nu}) - z)$ are computed based on the object-oriented measurement model described in Section 5.5. For example assuming that the ith measurement has the following generic form:

$$z_i = c_i + a_{i1} \cdot x_{i1} + a_{i2} \cdot x_{i2} \cdot x_{i3} + \eta_i \ . \tag{5.23}$$

Then the Jacobian matrix's ith row will be:

$$\begin{bmatrix} 0 & \cdots & a_{i1} & \cdots & a_{i2} \cdot x_{i2} & \cdots & a_{i2} \cdot x_{i3} & \cdots & 0 \end{bmatrix}. \tag{5.24}$$

The contribution of this row to the information matrix is the following:

$$\begin{bmatrix} 0 & \cdots & 0 & \cdots & 0 & \cdots & 0 & \cdots & 0 \\ \vdots & & \vdots & & \vdots & & \vdots & & \vdots \\ 0 & \cdots & w_i a_{i1} a_{i1} & \cdots & w_i a_{i1} a_{i2} x_{i2} & \cdots & w_i a_{i1} a_{i2} \cdot x_{i3} & \cdots & 0 \\ \vdots & & \vdots & & \vdots & & \vdots & & \vdots \\ 0 & \cdots & w_i a_{i1} a_{i2} \cdot x_{i2} & \cdots & w_i \left(a_{i2} \cdot x_{i2}\right)^2 & \cdots & w_i a_{i2}^2 \cdot x_{i2} x_{i3} & \cdots & 0 \\ \vdots & & \vdots & & \vdots & & \vdots & & \vdots \\ 0 & \cdots & w_i a_{i1} a_{i2} \cdot x_{i3} & \cdots & w_i a_{i2}^2 \cdot x_{i2} x_{i3} & \cdots & w_i \left(a_{i2} \cdot x_{i3}\right)^2 & \cdots & 0 \\ \vdots & & \vdots & & \vdots & & \vdots & & \vdots \\ 0 & \cdots & 0 & \cdots & 0 & \cdots & 0 & \cdots & 0 \end{bmatrix}. \tag{5.25}$$

The contribution of the measurement to the vector $H^T W(h(\hat{x}^\nu) - z)$ is the following:

$$\begin{bmatrix} 0 \\ \vdots \\ w_i a_{i1} b_i \\ \vdots \\ w_i a_{i2} \cdot x_{i2} b_i \\ \vdots \\ w_i a_{i2} \cdot x_{i3} b_i \\ \vdots \\ 0 \end{bmatrix}, \quad where \quad b_i = c_i + a_{i1} \cdot x_{i1} + a_{i2} \cdot x_{i2} \cdot x_{i3} - z_i \,. \tag{5.26}$$

Based on the above formulas, the non-zero contributions of each measurement formula are computed and the contributions are inserted to the information matrix $H^T WH$ and the vector $H^T W(h(\hat{x}^\nu) - z)$. Once the reading of all the measurements is completed and their contribution is added to the corresponding matrix and vector, the formation of the information matrix $H^T WH$ and the vector $H^T W(h(\hat{x}^\nu) - z)$ is completed and stored in sparse form using a suitable sparse library.

5.7 State Estimation Performance Metrics

The accuracy of the state estimate and the estimation confidence levels are obtained via a standard, chi-square-based analysis. The normalized residual (or error) for each measurement i is defined as

$$s_i = \frac{\eta_i}{\sigma_i} \ , \tag{5.27}$$

and thus the vector of normalized residuals is

$$s = \sqrt{W} \cdot \eta \ . \tag{5.28}$$

It is assumed that the normalized errors are Gaussian-distributed with standard deviation 1.0 and zero cross-correlation. The variable

$$\chi^2 = s^T s \tag{5.29}$$

is a random variable and it is chi-square distributed with $v = m - n$ degrees of freedom, where m is the total number of measurements, including virtual measurements and pseudo measurements, and n is the number of state variables that are estimated. Defining

$$\zeta = \hat{s}^T \hat{s} \ , \tag{5.30}$$

where the "hat" symbol indicates quantities computed at the estimate $\hat{x}$, the estimation confidence level at each step is given by the probability:

$$\Pr\left[\chi^2 \geq \zeta\right] = 1.0 - \Pr\left[\chi^2 \leq \zeta\right] = 1.0 - \Pr(\zeta, v) \ . \tag{5.31}$$

The chi-square test is utilized to provide the probability that the expected error of the estimated state values will be within a specific range. Because there are many data acquisition devices in any substation with different accuracy, a normalization constant k has been introduced. The variable k is defined as follows: if it is 1.0 then the standard deviation of each measurement is equal to the accuracy of the meter with which this

measurement was obtained. If different than 1.0 then the standard deviation of the measurement error equal the accuracy of the meter times k. The introduction of the variable k allows us to characterize the accuracy of the estimated state with only one variable. This is equivalent of providing the expected error (which equals the variable k times the standard deviation of the measurement error) versus probability (confidence level). Figure 5.9 illustrates the K-factor curve, which is the parameter k versus confidence level.

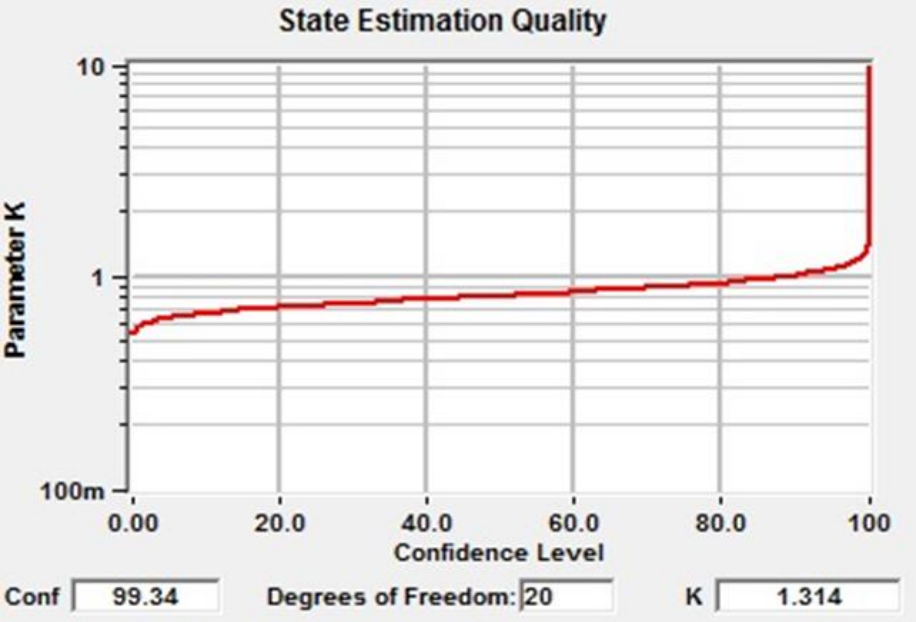

Figure 5.9. State estimation quality - Chi Square test.

For an acceptable confidence level, the accuracy of the solution, at each time step, is computed via the covariance (or information) matrix. The covariance matrix of the state is defined as

$$C_x = E\left[(\hat{x} - \bar{x})(\hat{x} - \bar{x})^T\right], \tag{5.32}$$

where $\bar{x}$ denotes the true state value, and computed as

$$C_x = \left(H^T W H\right)^{-1}. \tag{5.33}$$

Once the information matrix of the solution has been computed, the standard deviation of a component of the solution vector is given by

$$\sigma_{x_i} = \sqrt{C_x(i,i)}\,, \tag{5.34}$$

where $C_x(i,i)$ is the ith diagonal entry of the C_x. The expected value of is

$$E[\hat{x}] = \bar{x}\ . \tag{5.35}$$

The estimates of the measurements are defined as

$$\hat{b} = h(\hat{x}, \hat{y})\,. \tag{5.36}$$

Their expected value is

$$E[\hat{b}] = h(\bar{x}, \bar{y})\,, \tag{5.37}$$

and their covariance matrix

$$Cov(\hat{b}) = H\left(H^T W H\right)^{-1} H^T\ . \tag{5.38}$$

5.8 Bad Data Detection and Identification

Detection of the existence of bad data can be achieved with the chi-square test, i.e. by computing the confidence level. If the system measurement equations are free of bad data, the confidence level will be high. In the presence of one or more bad data, the confidence level will decrease. Figure 5.10 gives an example of the chi-square test which shows a very low confidence level due to the effect of some bad data. Note that the chi-square test does not indicate which datum or data is bad. The identification of the bad data is described next.

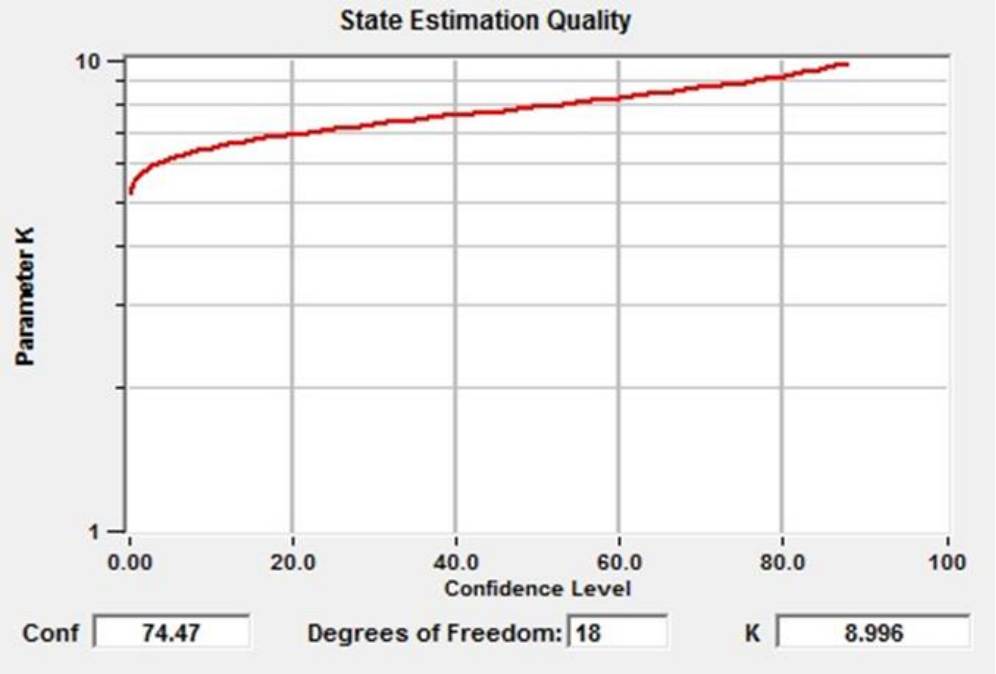

Figure 5.10. Low confidence level due to the effect of bad data.

Bad data can be classified into the following types:

1) Measurement Bad Data, which means that the measurement may contain a significant error comparing with its actual value.

2) Status/Topology Bad Data, which means that the bad data is related with the breaker or switch's open/close status or in other words, the topology of the system.

The methodology of the identification of bad data normally consists of two steps. In the first step, bad data may be identified by inspection or simple consistency rules. This step identifies the obviously bad data and it is very much system dependent. As an example, in power system state estimation, measurements of voltages, power flow, etc., are known to have specific ranges. If a measurement is out of this range, it will be classified as a bad measurement or at least as a measurement suspected of being bad (suspect measurement). In the second step, bad data are identified with statistical analysis of the residuals and/or

its effects on confidence level. This analysis depends on the selected method for the solution of the estimation problem. In the case of least square solution, the possible bad data are identified with their large residuals. However, it is known that it is possible that: (1) a measurement with a large residual may not be always a bad measurement and (2) a bad measurement may have a very small residual (outliers). A rather secure, but computationally demanding, way to identify a bad datum is by means of hypothesis testing. Specifically, assume that a measurement (or a group of measurements) has been identified as suspect (this characterization may be due to a large normalized residual or because of failure to pass a consistency check, etc.). For this purpose, the suspect datum is removed, i.e. the corresponding equation $b_i = h_i(\mathbf{x})$ is removed from measurement equations set and the least square solution is computed again. Subsequently, the confidence level is computed. A drastic improvement in the confidence level indicates that the data under consideration is bad.

5.9 Object-oriented DDSE Algorithm Implementation

This section describes an object-oriented approach for the formulation and execution of the DDSE-T and DDSE-Q. Object orientation requires the introduction of abstraction to the point that models and measurements acquire a general form that can be manipulated and processed with the same algorithms independently of the specific physical quantity that is represented. With the help of the SCAQCF syntax of the device model described in Section 4.2 and the general measurement model described in Section 5.5, object-oriented algorithms are designed both for the relay level DDSE (DDSE-T) and substation level DDSE (DDSE-Q).

5.9.1 Object-oriented Algorithm for DDSE-T

The flow charts of object-oriented DDSE-T for the linear and non-linear case are shown in Figure 5.11 and Figure 5.12, respectively. All the SCAQCF component models are stored in the standard matrices which are introduced in section 4.2. In the initialization step, the program reads all the matrices and calculates the linear part of the Jacobian matrix H. After the initialization, the DDSE-T starts to read the streaming data of the measurements of the component from the process bus. It performs the Chi-square test based on the calculated measurements from state estimation and streaming measurement data. Meanwhile, bad data identification and operation limit monitoring are also done during the state estimation procedure. The entire algorithm is real time and it iterates until no more measurements are available at the current time step.

It is important to notice that most of device models are nonlinear, which means the Jacobian matrix needs to be updated at each iteration. To increase the speed, the linear part of matrix H can be pre-calculated at the DDSE-T initialization procedure. The program will identify whether the device model is linear or nonlinear. If the model is linear, then the Jacobian matrix H will stay constant. Otherwise, the program will only update the nonlinear part of H to minimize the calculation. The sparsity-based state estimation algorithm mentioned previously is applied and only the non-zero data will contribute to the information matrix $H^T WH$ and the vector $H^T W\left(h(X^\upsilon) - Z\right)$.

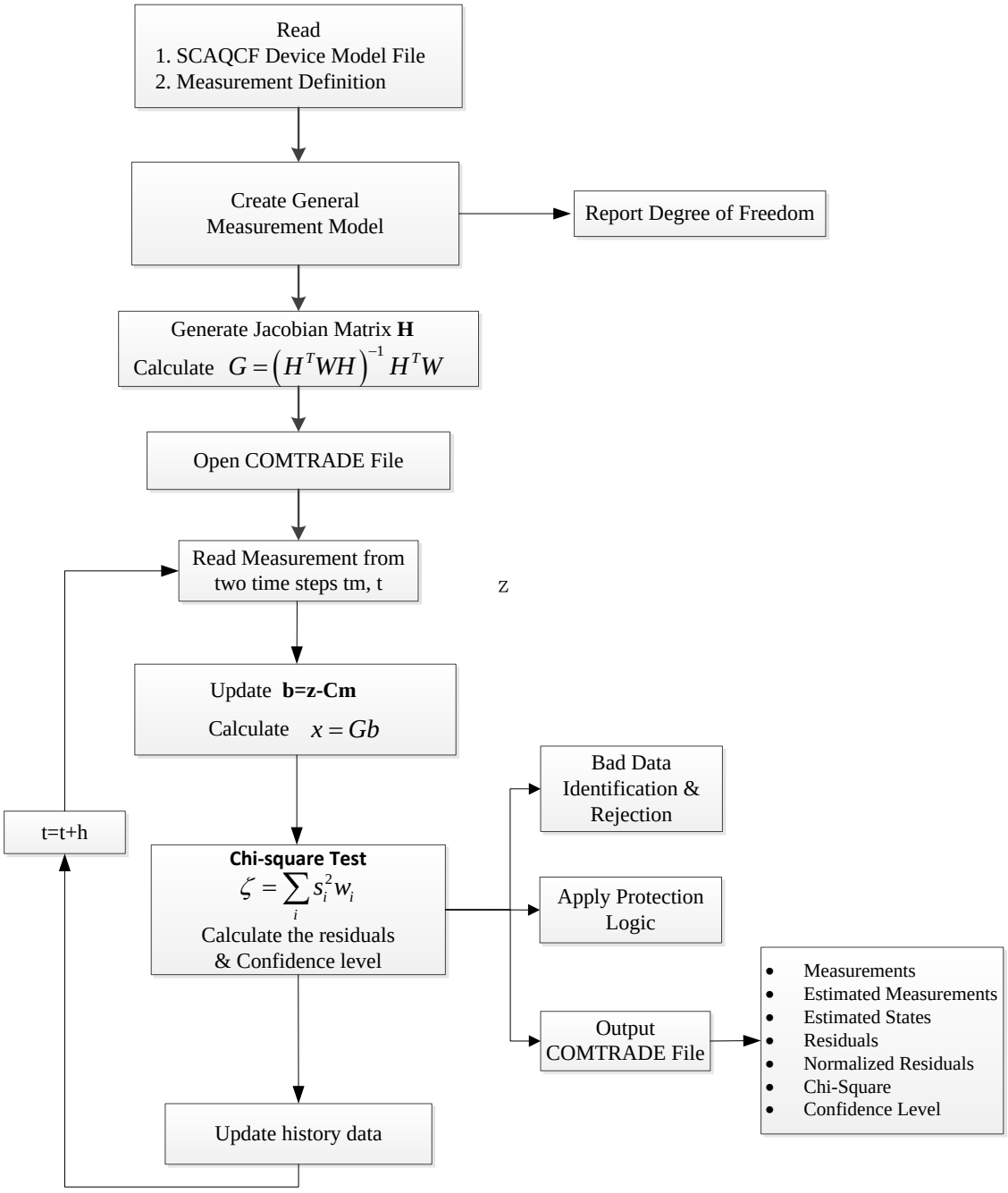

Figure 5.11. Flow chart of DDSE-T: linear case.

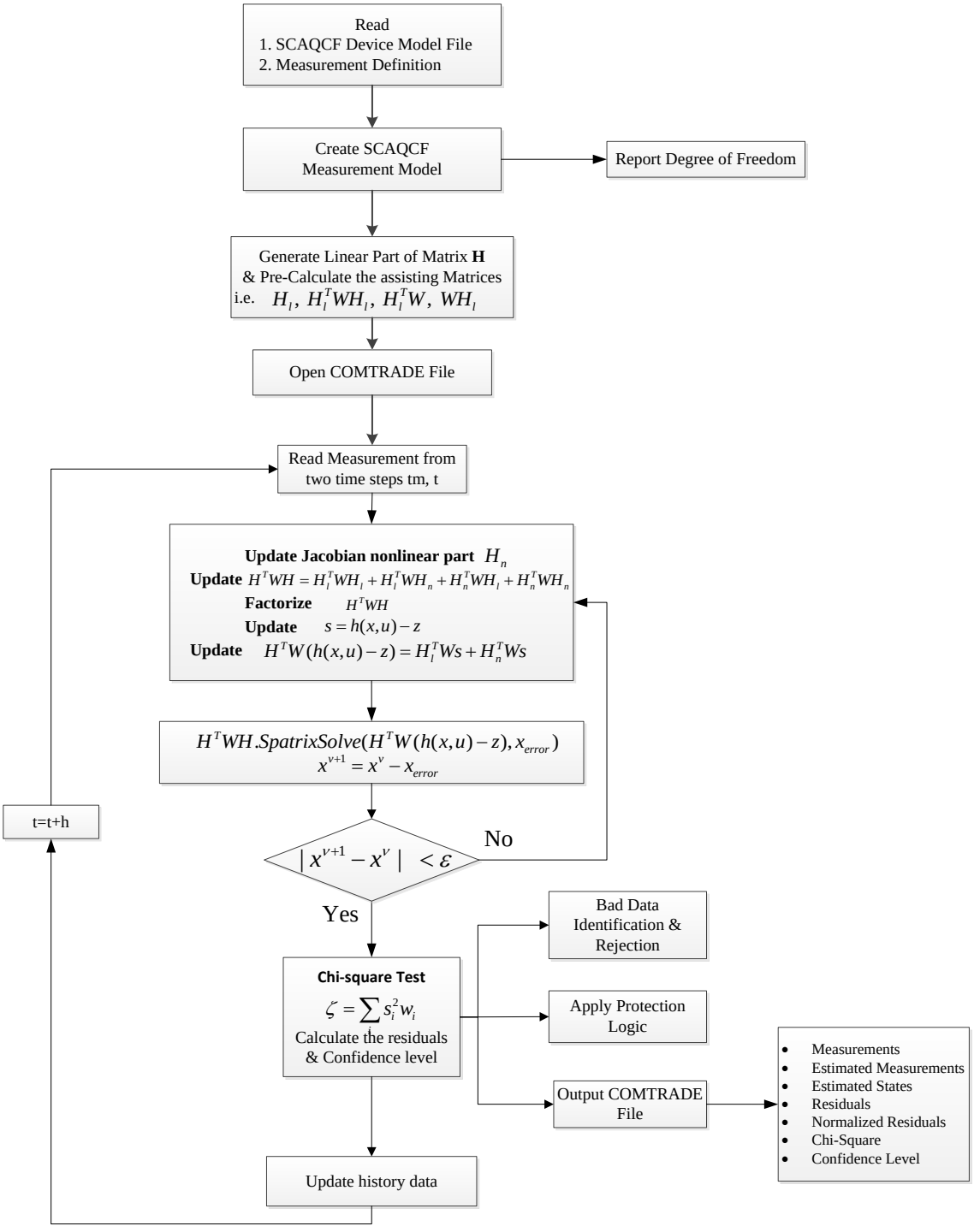

Figure 5.12. Flow chart of DDSE-T: nonlinear case.

5.9.2 Object-oriented Algorithm for DDSE-Q

Compared with the algorithms for relay level DDSE (DDSE-T), which is performed only for one device, the substation level DDSE (DDSE-Q) is performed for the entire substation. The substation model consists of many components in the substation and also the components connected with the substation. As a result, a topology and observability analysis is needed for the substation level DDSE before the DDSE is performed. The open and close activities of the breakers in the substation also contribute to the need of a topology analysis. The main purpose of the topology/obersvability analysis for the DDSE-Q is to find that based on the available measurements in the substation, which devices are observable and how these devices are connected with each other. This procedure takes account of the contributions from the pseudo measurements, virtual measurements, and derived measurements described in section 5.5, which can greatly increase the observability of the DDSE-Q. Figure 5.13 gives the flow chart for the procedure of the observability analysis for the DDSE-Q.

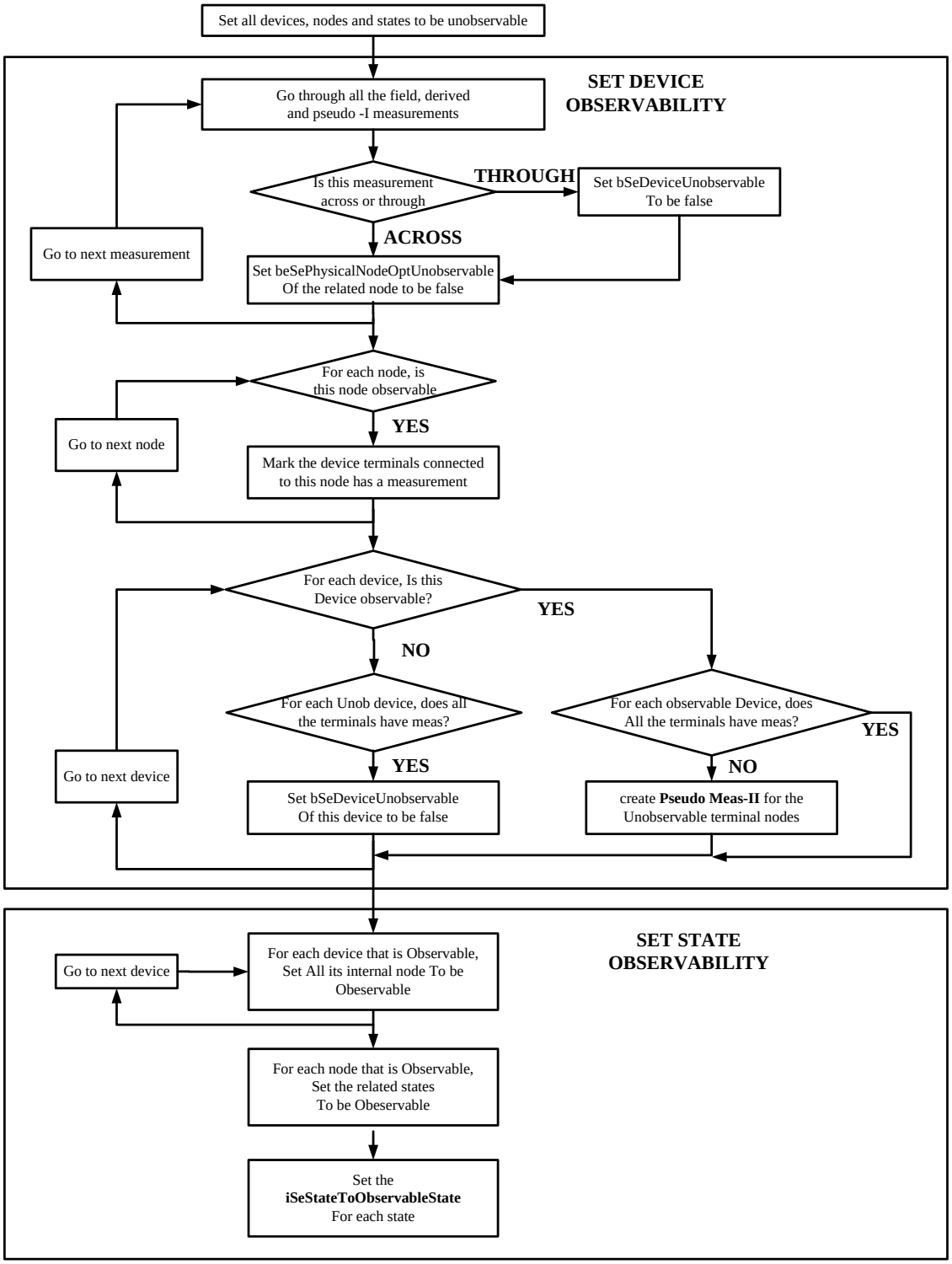

Figure 5.13. Observability analysis of substation level DDSE.

The block diagram describing the steps for the execution of the DDSE-Q is shown in Figure 5.14. Initially, the DDSE-Q identifies all the devices in the substation and all the devices (circuits/transmission lines) connected to the substation, and inserts the SCAQCF models of these devices into the device model data base of the SE. A network configuration analysis follows to analysis the network topology and define the system states.

After the SE initialization procedure, measurement reading starts. For each time step t, the measurement data are read in a streaming way (measurement by measurement) in real time, and based on the measurement type, the generalized measurement model is created for each measurement, as described in section 5.5. This procedure is repeated until all the measurements at a specific time instant t (all measurements with the same time stamp) are processed. Once the measurement reading for the time t is finished and all the measurement models are constructed, the sparse matrix based estimation procedure begins. After the estimation is completed, a Chi-Square test is performed to give the confidence level of the estimation procedure. If the confidence level shows that the performance of the estimation is good, the program updates the through variables and the states for the devices and also the results are reported. If the performance is not satisfying, a bad data identification and rejection procedure follows.

Details for processing the measurements are also shown in Figure 5.14. First the digital measurements related to the breaker and switch status are processed. If there is an indication of the breaker/switch status change, the network topology analysis will run again, the flag indicating the system configuration change will be set as true, the system states set will be updated, and the measurement database of the DDSE-Q will be cleared. The field analog and phasor measurements will be read and processed next. If the system

configuration change flag is true, new field measurements model will be created in the measurement database, otherwise only the values of the field measurements will be updated. Once the reading of the field measurements is finished, the DDSE-Q will create or update the derived measurements and pseudo measurements based on the field measurements and the system configuration flag. At this point, if the system configuration change flag is true, the states and device observability analysis will run to figure out which devices and states in the DDSE-Q database are not observable based on the available measurement set created previously. And if the system configuration change flag is false, which means there is no topology change in the system, the DDSE-Q will assume the observability of the states and devices keeping the same as the previous time step. Also the DDSE-Q adds all the virtual measurements for all the observable devices.

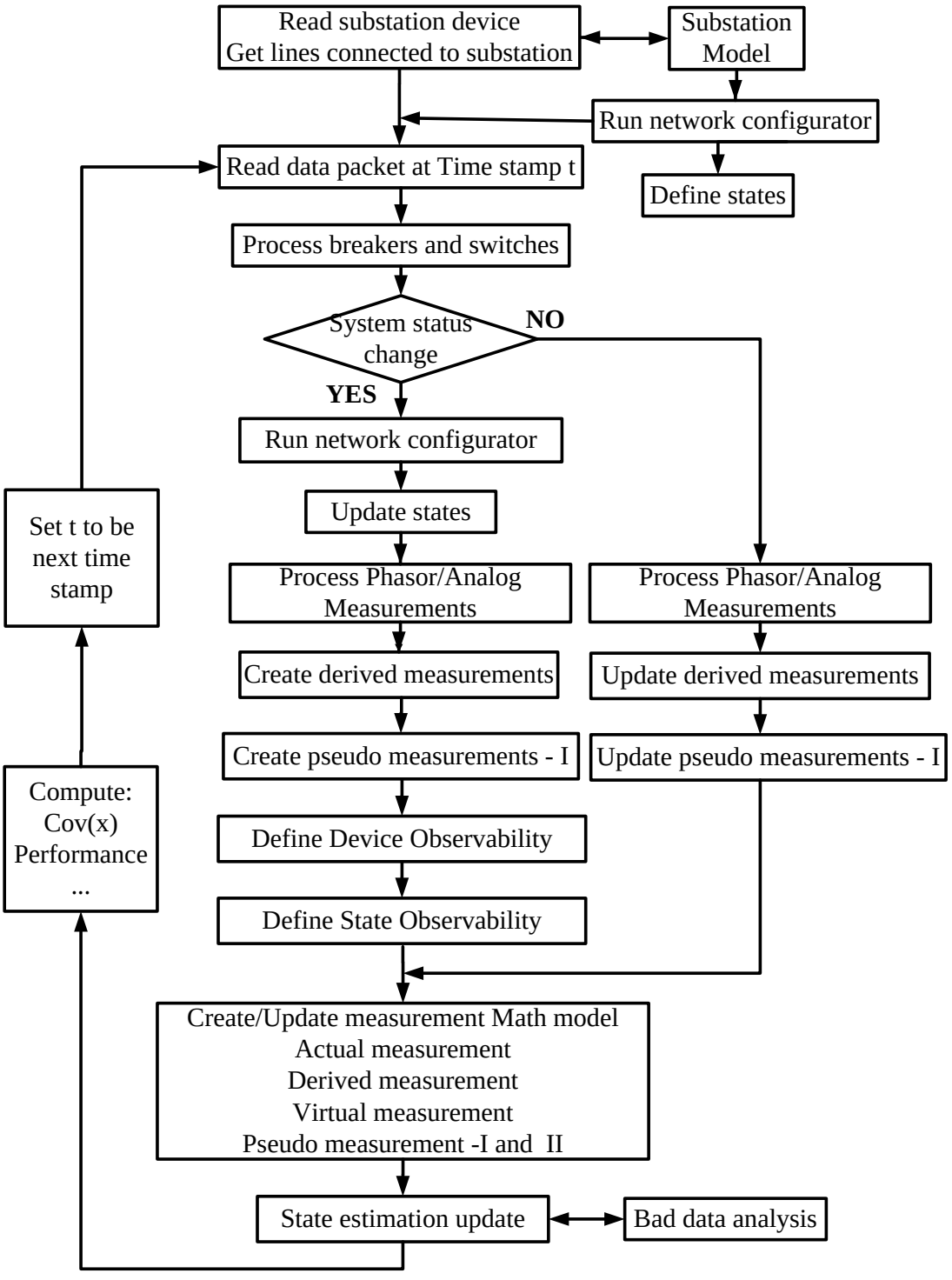

Figure 5.14. Flow chart of substation level DDSE.

5.10 Multi-Step State Estimation

The purpose of the multi-step state estimation is to provide a better filter for the noise and its influence on the state estimator and increase the accuracy of the state estimation results. It is applicable to both state estimators (DDSE-Q and DDSE-T). The end result is a state estimator combing several time step measurements with a higher accuracy.

There are some limitations for the implementation of the combination of single time step state estimations into multi-step state estimation. In order to illustrate these limitations, the general state estimation model is recalled. In general, both the DDSE-Q and the DDSE-T model can be cast in a standard form as follows:

$$\begin{bmatrix} Z_t \\ 0 \\ Z_{tm} \\ 0 \end{bmatrix} = Y_{eq,2m\times 2n} \cdot \begin{bmatrix} X_t \\ X_{tm} \end{bmatrix} + \left(\begin{bmatrix} X_t \\ X_{tm} \end{bmatrix} \cdot F_{eq} \cdot \begin{bmatrix} X_t & X_{tm} \end{bmatrix} \right) - \left(N_{eq,2m\times n} \cdot X_{t-h} + M_{eq,2m\times m} \cdot \begin{bmatrix} I_{t-h} \\ 0 \end{bmatrix} + K_{eq,2m\times n} \right) + \vec{\eta} \text{ , (5.39)}$$

where

Z_t: the measurements of the model.

I_{t-h}: the through variables of the model at the previous time step.

X_t: the states of the system.

Y_{eq}: matrix defining the linear part of the model.

F_{eq}: matrix defining the quadratic part of the model.

N_{eq}: constant matrix defining the contribution of the states of previous time steps.

M_{eq}: constant matrix defining the contribution of the through variables of previous time steps.

K_{eq}: vector defining the constant part of the model.

Note the difference of the notation Z_t and I_t, I_t is the through variables of the device model, which can be computed by the SCAQCF device model as follows:

$$\begin{bmatrix} i(t) \\ 0 \\ i(t_m) \\ 0 \end{bmatrix} = Y_{eq} \begin{bmatrix} v(t) \\ y(t) \\ v(t_m) \\ y(t_m) \end{bmatrix} + \begin{bmatrix} \begin{bmatrix} v^T(t) & y^T(t) & v^T(t_m) & y^T(t_m) \end{bmatrix} \cdot F_{eq} \cdot \begin{bmatrix} v(t) \\ y(t) \\ v(t_m) \\ y(t_m) \end{bmatrix} \end{bmatrix} - \begin{bmatrix} b_1(t-h) \\ b_2(t-h) \end{bmatrix}. \qquad (5.40)$$

The basic idea of the multi-step state estimation is to extend the single time step state estimation to several time steps, with the combination of the models of the single time step state estimation together. The main difference between the single and multi-step state estimation comes from the $N_{eq,2m\times n} \cdot X_{t-h}$ and $M_{eq,2m\times m} \cdot \begin{bmatrix} I_{t-h} \\ 0 \end{bmatrix}$ components, since for the single time step state estimation, the previous states X_{t-h} and through variables I_{t-h} are computable through the previous time step's state estimation results, while for the multi-step state estimation, some of the previous states X_{t-h} and through variables I_{t-h} are not computable through the previous time step' state estimation results. For the previous states X_{t-h}, it is easy to treat them as new unknown states while for the through variables I_{t-h} there is no such a good way to treat them as unknown states but by the same time still sustain the standard quadratic state estimation model.

For the reason described above, the discussion of the formulation for the multi-step state estimation assumes that both the single time step DDSE-Q and the DDSE-T model can be formed in a standard form as follows:

$$\begin{bmatrix} Z_t \\ 0 \\ Z_{tm} \\ 0 \end{bmatrix} = Y_{eq,2m\times 2n} \cdot \begin{bmatrix} X_t \\ X_{tm} \end{bmatrix} + \left(\begin{bmatrix} X_t \\ X_{tm} \end{bmatrix} \cdot F_{eq} \cdot \begin{bmatrix} X_t & X_{tm} \end{bmatrix} \right) - \left(N_{eq,2m\times n} \cdot X_{t-h} + K_{eq,2m\times n} \right) + \vec{\eta}\,, \quad (5.41)$$

where

Z_t: the measurements of the model.

X_t: the states of the system.

Y_{eq}: matrix defining the linear part of the model.

F_{eq}: matrix defining the quadratic part of the model.

N_{eq}: constant matrix defining the contribution of the states of previous time steps.

K_{eq}: vector defining the constant part of the model.

Considering the general case for the multi-step state estimation, assuming having k time step measurements and implementing a k-step state estimation, the following formula is given.

$$\begin{bmatrix} Z_{t1} \\ 0 \\ Z_{t1m} \\ 0 \\ Z_{t2} \\ 0 \\ Z_{t2m} \\ 0 \\ \vdots \\ Z_{tk} \\ 0 \\ Z_{tkm} \\ 0 \end{bmatrix} = \begin{bmatrix} Y_{eq,2m\times 2n} & 0_{2m\times 2n} & 0_{2m\times 2n} & 0_{2m\times 2n} \\ \begin{bmatrix} -N_{eq,2m\times n} & 0_{2m\times n} \end{bmatrix} & Y_{eq,2m\times 2n} & 0_{2m\times 2n} & 0_{2m\times 2n} \\ 0_{2m\times 2n} & \ddots & \ddots & 0_{2m\times 2n} \\ 0_{2m\times 2n} & 0_{2m\times 2n} & \begin{bmatrix} -N_{eq,2m\times n} & 0_{2m\times n} \end{bmatrix} & Y_{eq,2m\times 2n} \end{bmatrix} \cdot \begin{bmatrix} X_{t1} \\ X_{t1m} \\ X_{t2} \\ X_{t2m} \\ \vdots \\ X_{tk} \\ X_{tkm} \end{bmatrix}$$

$$+Feq(\begin{bmatrix} X_{t1} \\ X_{t1,m} \\ X_{t2} \\ X_{t2m} \\ \vdots \\ X_{tk} \\ X_{tkm} \end{bmatrix}) - \begin{bmatrix} K_{eq,2m\times n} + N_{eq,2m\times n} \cdot X_{t0} \\ K_{eq,2m\times n} \\ \vdots \\ K_{eq,2m\times n} \end{bmatrix} \quad , \qquad (5.42)$$

where the subscripts t_1, t_2, t_k denote the time step index for all the states and the measurements and $\left[X_{t1}, X_{t1m}, X_{t2}, X_{t2m}, \cdots X_{tk}, X_{tkm}\right]$ represents the states of the state estimation procedure.

Subsequently, the least square approach is applied to the above measurements and model.

5.11 DDSE-T Demonstration Results

In this section the results of the implementation of the DDSE-T on the physically based generator model is demonstrated. The test system that was used consists of a substation

with one generator unit connected to a step-up transformer, sending power through overhead transmission lines to the loads, as is illustrated in Figure 5.15.

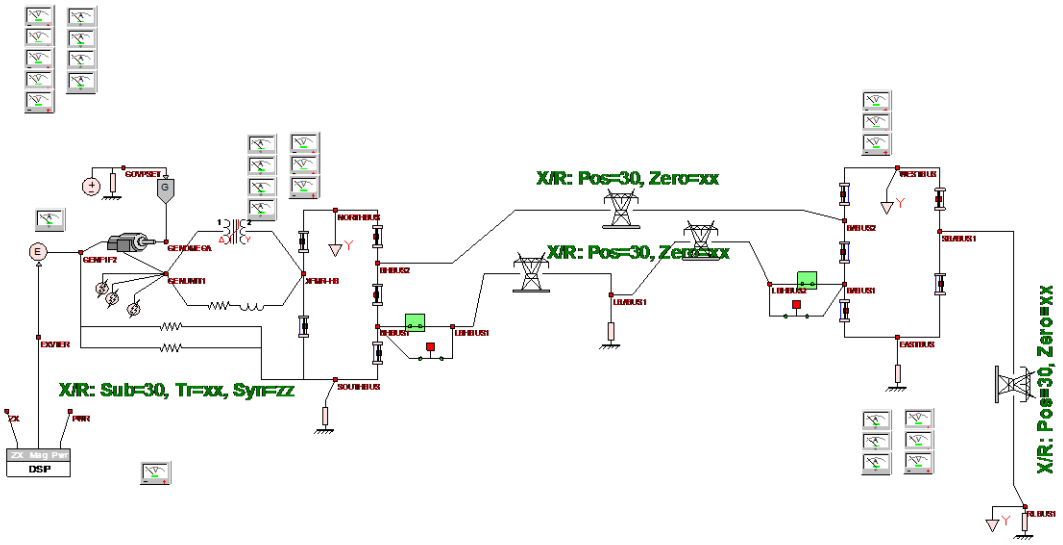

Figure 5.15. Test system for DDSE-T on the synchronous machine.

The parameters of the test system are given in Table 5.2. Figure 5.16 illustrates the physical parameters of the generator.

Table 5.2. Test system parameters.

Gen1	825MVA	18.0 kV
XFMR1	650MVA z=0.01 +j0.94 pu	18 kV/230kV
Transmission Line 1	z=1,47 + j20.21 ohms	230 kV
Transmission Line 2	z=2.70 + j28.01 ohms	230 kV
Transmission Line 3	z=0.79 + 11.52 ohms	230 kV
Load 1	300MW/90MVar	230 kV
Load 2	300MW/90MVar	230 kV

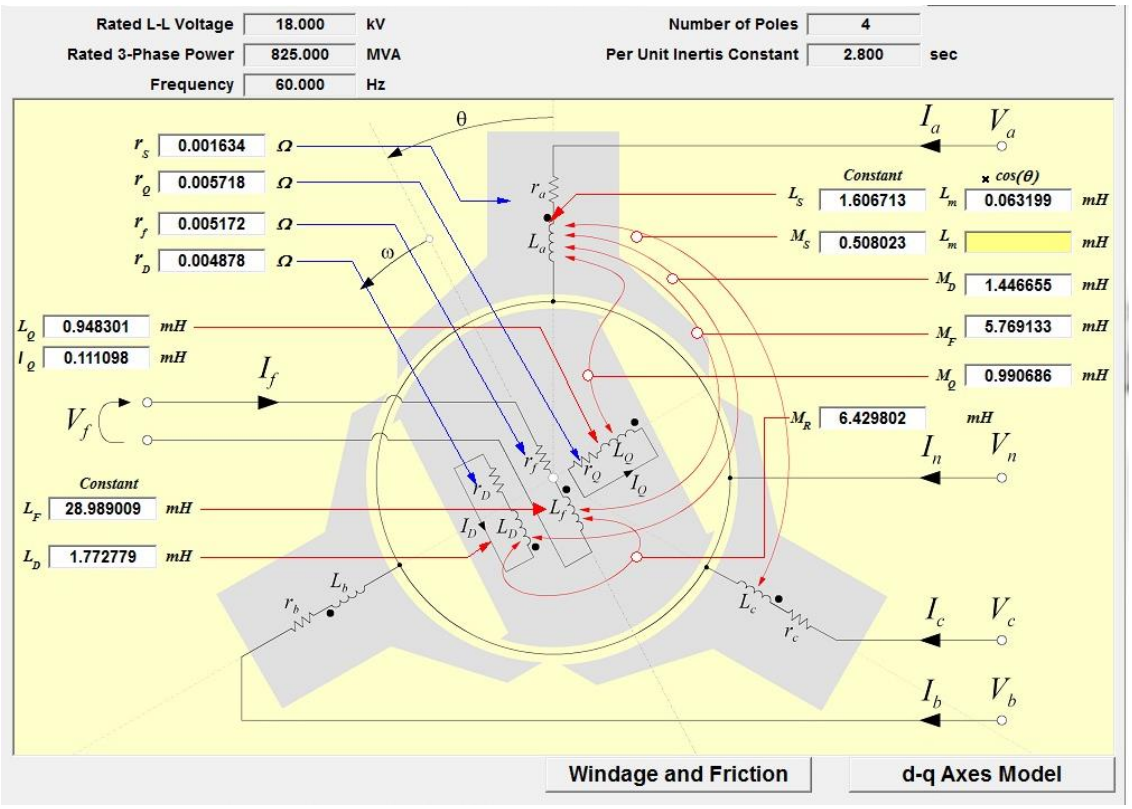

Figure 5.16. Generator physical parameters of the test system.

The test system was simulated for a total time of 15 seconds. Initially the system was simulated under normal operating conditions for 8 seconds in order to let the feedback integral control loop of the governor stabilize the mechanical speed of the generator to the nominal value (188 rad/s for a 4-pole generator). After the stabilization of the system, a three-phase line to ground fault was simulated at the terminals of the generator. The duration of the fault was 0.6 seconds. During the fault period, the mechanical speed of the generator increases and at the post fault period the integral control of the governor pulls the mechanical speed of the generator back to 188 rad/s as expected. Figure 5.17 shows the simulated measurements of the terminal voltages, terminal currents, and the mechanical speed of the generator.

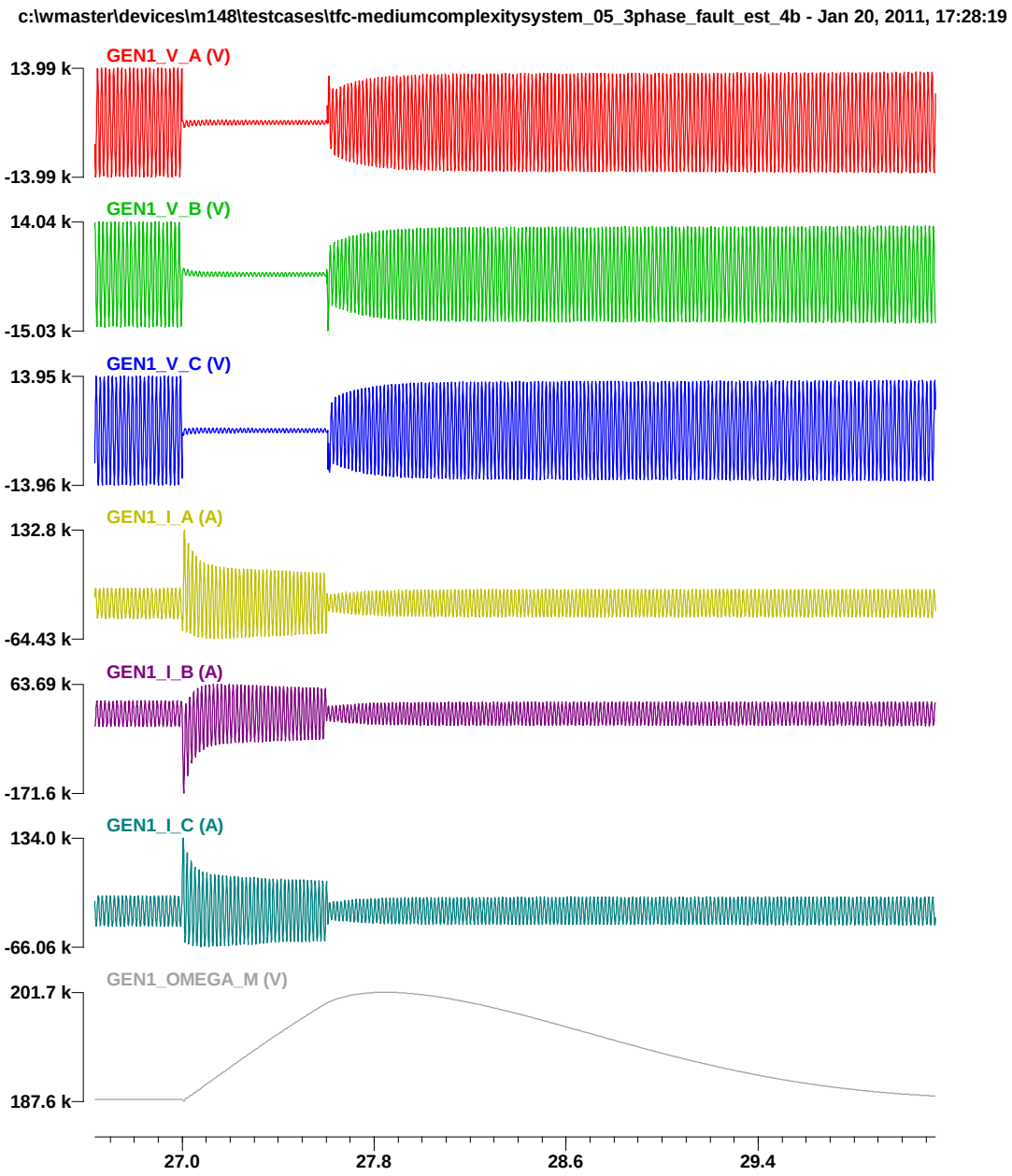

Figure 5.17. Simulated measurements of the generator

The next step was to apply the DDSE-T on the generator model as developed in Section 4.3. The measurements provided for the DDSE-T were the voltage and current waveforms at the terminals of the generator, as well as the mechanical speed of the

generator. These measurements are sufficient for the estimation of the entire state vector of the generator.

The DDSE-T results are compared with the simulation results. Figure 5.18 shows the terminal voltage of the generator at phase A, Figure 5.19 shows the terminal current of the generator at phase A, Figure 5.20 shows the electrical speed of the generator, and Figure 5.21 shows the torque angle of the generator as representative important quantities of the state vector. The red line represents the simulation results, while the blue dots illustrates the DDSE-T results.

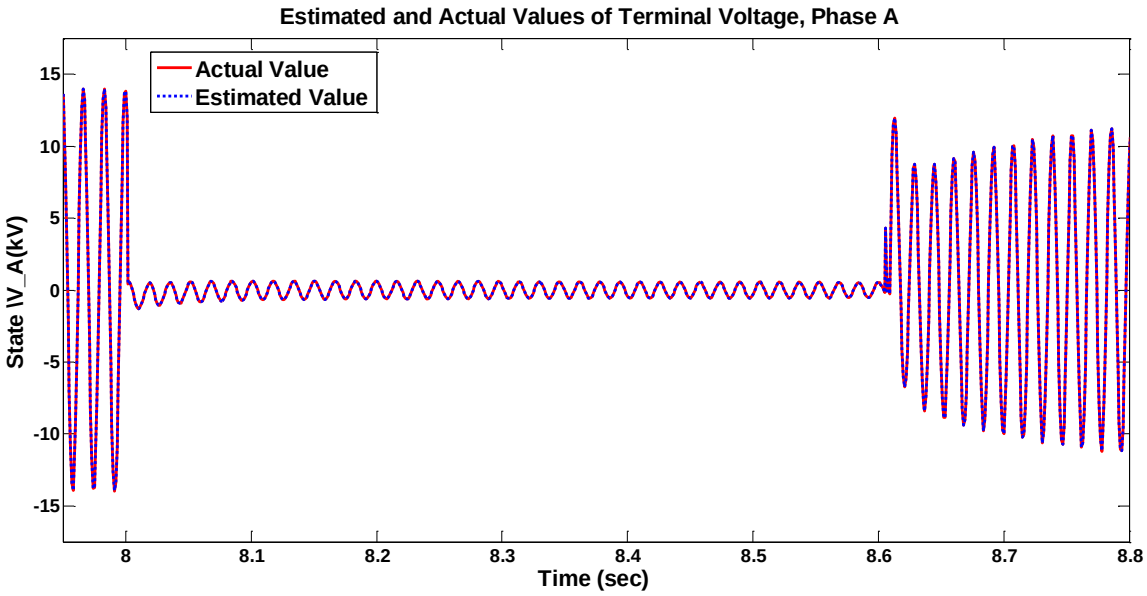

Figure 5.18. Terminal voltage, phase A, of the Generator

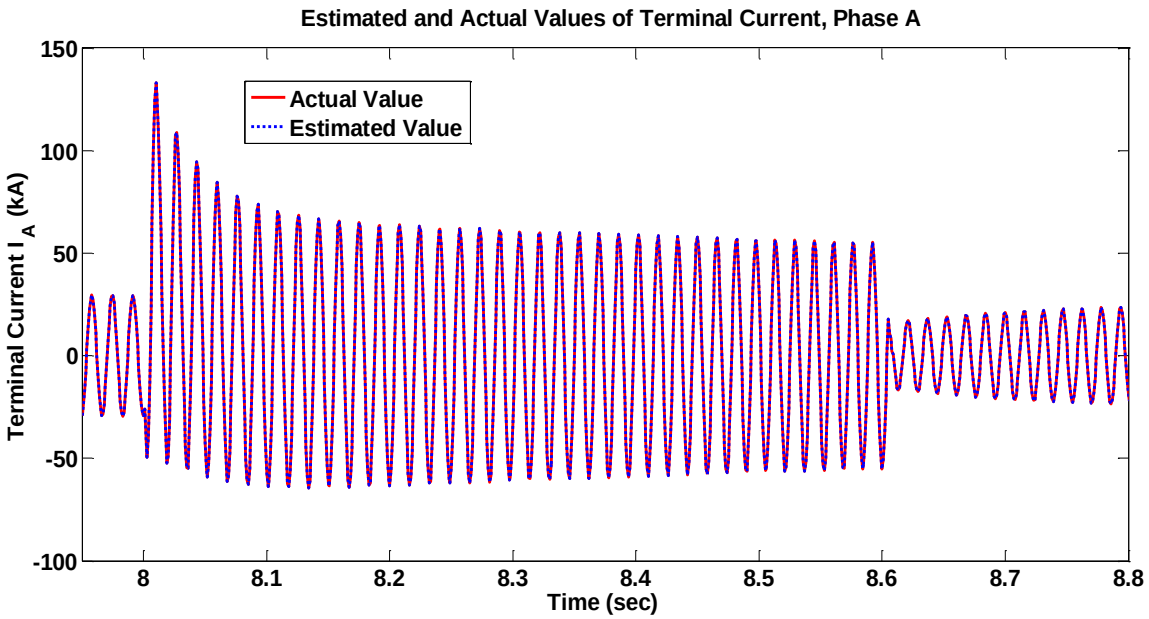

Figure 5.19. Terminal current, phase A, of the Generator

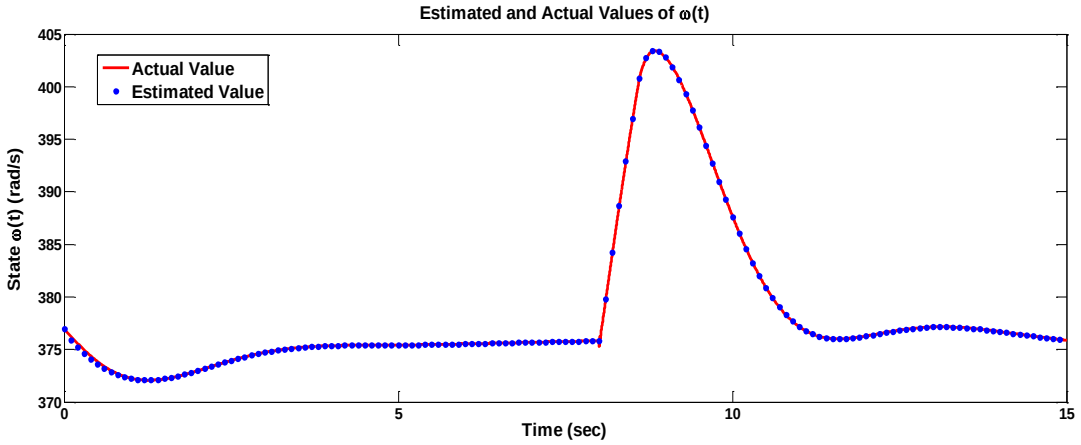

Figure 5.20. Electrical speed of the Generator

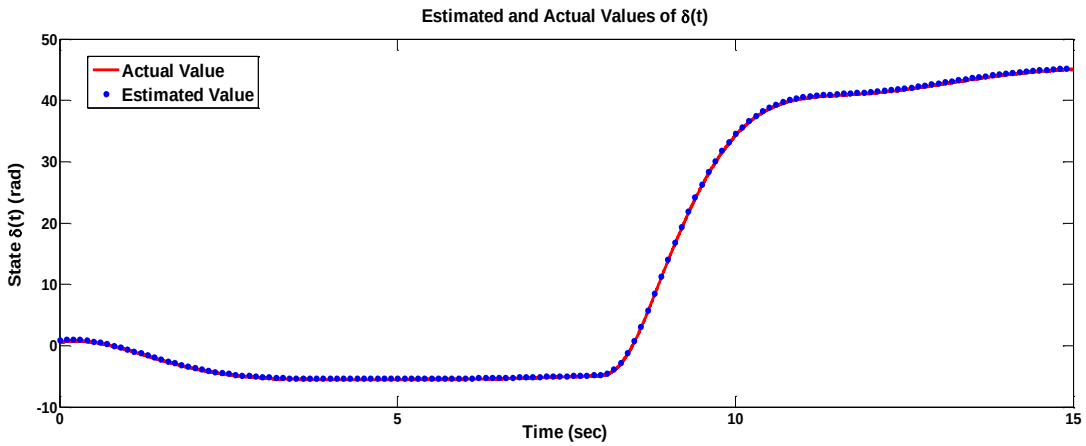

Figure 5.21. Machine torque angle of the Generator

The DDSE-T performed on the synchronous machine verifies the accuracy and the correctness of the physical parameter based generator model. The DDSE-T results indicate that the estimation is highly accurate both for steady state and transient conditions, and the electrical transients of the generator are captured by the DDSE-T.

5.12 DDSE-Q Demonstration Results

5.12.1 Measurement Model for the Synchronous Machine in DDSE-Q

Based on the SCAQCF synchronous machine model described in section 4.4, the measurement model for the synchronous machine is given here, which is used in the DDSE-Q. The available actual measurements for the synchronous machine are the three phase voltage and current phasors at the terminal of the generator, plus the real and reactive power of the generator. According to the PMUs functionality, the excitation field voltage and current of the generator can be classified as actual measurements or pseudo measurements. All the internal equations from the SCAQCF model in section 4.4.3 are

added into the measurement model as virtual measurements to achieve the observability of the generator model. As a summary, the following filter equations (5.43) are obtained as the measurement model for the synchronous machine for the DDSE-Q, and this measurement model is utilized in the next section for the DDSE-Q of the Gilboa-Blenheim substation of the New York Power Authority (NYPA).

$$
\begin{aligned}
& V_{gr}{}^{m}(t) = V_{gr}(t), \\
& V_{gi}{}^{m}(t) = V_{gi}(t), \\
& I_{gr}{}^{m}(t) = I_{dr}(t) + I_{qr}(t), \\
& I_{gi}{}^{m}(t) = I_{di}(t) + I_{qi}(t), \\
& I_{f}^{m}(t) = \frac{\sqrt{2}}{\omega \cdot M_{f}} \cdot E_{abs}(t), \\
& P^{m}(t) = V_{gr}(t) \cdot I_{dr}(t) + V_{gr}(t) \cdot I_{qr}(t) \\
& \qquad - V_{gi}(t) \cdot I_{di}(t) - V_{gi}(t) \cdot I_{qi}(t), \\
& Q^{m}(t) = V_{gr}(t) \cdot I_{di}(t) + V_{gr}(t) \cdot I_{qi}(t) \\
& \qquad + V_{gi}(t) \cdot I_{dr}(t) + V_{gi}(t) \cdot I_{qr}(t), \\
& 0 = E_{r}(t) - V_{gr}(t) + rI_{dr}(t) + rI_{qr}(t) - x_{d} I_{di}(t) - x_{q} I_{qi}(t) \\
& 0 = E_{i}(t) - V_{gi}(t) + rI_{di}(t) + rI_{qi}(t) + x_{d} I_{dr}(t) + x_{q} I_{qr}(t) \\
& 0 = E_{r}(t) \cdot s(t) - E_{i}(t) \cdot c(t) \\
& 0 = E_{r}(t) \cdot I_{dr}(t) + E_{i}(t) \cdot I_{di}(t) \\
& 0 = E_{i}(t) \cdot I_{qr}(t) - E_{r}(t) \cdot I_{qi}(t) \\
& 0 = z_{1}(t) \cdot \omega(t) - E_{r}(t) \\
& 0 = z_{2}(t) \cdot \omega(t) - E_{i}(t) \\
& 0 = E_{r}(t)^{2} + E_{i}(t)^{2} - E_{spec.} \\
& 0 = T_{e}(t) - 3 \cdot \left[z_{1}(t) \cdot \left(I_{dr}(t) + I_{qr}(t) \right) + z_{2}(t) \cdot \left(I_{di}(t) + I_{qi}(t) \right) \right]
\end{aligned}
\tag{5.43}
$$

$$0 = y_1(t) - c(t) \cdot \left(\omega(t) - \omega_0\right)$$

$$0 = y_2(t) + s(t) \cdot \left(\omega(t) - \omega_0\right)$$

$$0 = Q(t_m)$$

$$0 = \delta(t) - \delta(t-h) - \frac{h}{6}\omega(t) - \frac{2h}{3}\omega(t_m) - \frac{h}{6}\omega(t-h) + h \cdot \omega_0$$

$$0 = \delta(t_m) - \delta(t-h) + \frac{h}{24}\omega(t) - \frac{h}{3}\omega(t_m) - \frac{5h}{24}\omega(t-h) + \frac{h}{2} \cdot \omega_0$$

$$0 = J \cdot \omega(t) - J \cdot \omega(t-h) + \frac{h}{6}T_e(t) + \frac{2h}{3}T_e(t_m) + \frac{h}{6}T_e(t-h) - h \cdot T_m$$

$$0 = J \cdot \omega(t_m) - J \cdot \omega(t-h) - \frac{h}{24}T_e(t) + \frac{h}{3}T_e(t_m) + \frac{5h}{246}T_e(t-h) - \frac{h}{2} \cdot T_m$$

$$0 = s(t) - s(t-h) - \frac{h}{6}y_1(t) - \frac{2h}{3}y_1(t_m) - \frac{h}{6}y_1(t-h)$$

$$0 = s(t_m) - s(t-h) + \frac{h}{24}y_1(t) - \frac{h}{3}y_1(t_m) - \frac{5h}{24}y_1(t-h)$$

$$0 = c(t) - c(t-h) - \frac{h}{6}y_2(t) - \frac{2h}{3}y_2(t_m) - \frac{h}{6}y_2(t-h)$$

$$0 = c(t_m) - c(t-h) + \frac{h}{24}y_2(t) - \frac{h}{3}y_2(t_m) - \frac{5h}{24}y_2(t-h)$$

The first group of the filter equations (5.43) refers to the actual measurements. The second group refers to the algebraic (linear or quadratic) internal equations of the model that are introduced as virtual measurements. This set of equations (renamed as $Q(t)$) is also evaluated at the intermediate time t_m resulting in the set of equation $0 = Q(t_m)$ that are also introduced as virtual measurements. Finally, the last group refers to the integrated (using

quadratic integration) dynamic equations of the model which are also introduced as virtual measurements.

5.12.2 DDSE-Q Demonstration Results on NYPA System

The field demonstration results from the implementation of DDSE-Q on the Gilboa-Blenheim substation of the New York Power Authority (NYPA) are given in this section. NYPA's Blenheim-Gilboa electric power system is a special type of hydroelectric facility that is located at the base of Brown Mountain, Southwest of Albany. It has four 278 MVA generators (total of 1,112 MVA) which can generate more than one million kilowatts during peak demands and supply electricity to New York customers through the Fraser-Gilboa, the Gilboa-New Scotland, and the Gilboa-Leeds 345kV transmission lines. Figure 5.22 shows the single-line diagram of the Blenheim-Gilboa substation.

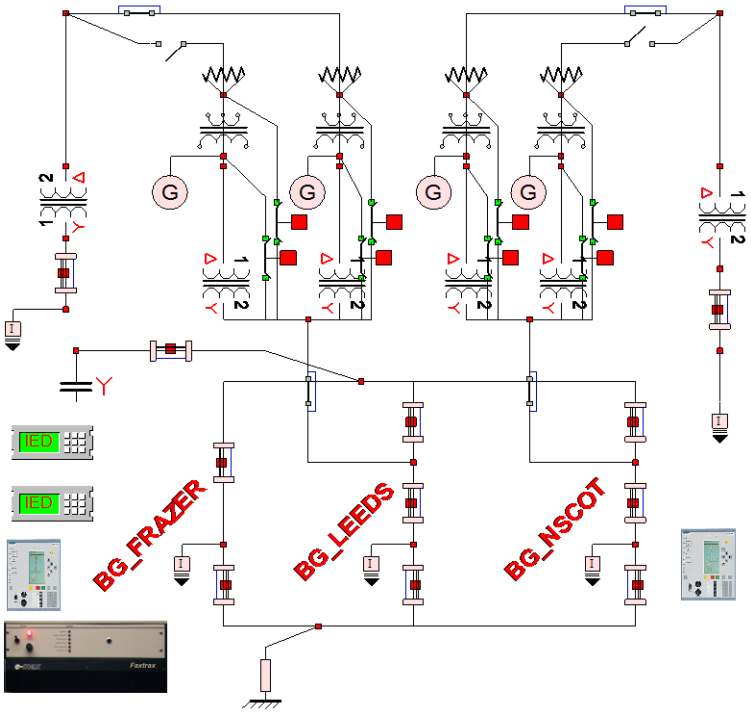

Figure 5.22. Single-line diagram of Blenheim-Gilboa including IEDs.

A breaker-oriented, three-phase, and physical model of the power plant was developed in the software WinIGS, based on the collected data from a field visit. The specific ratings of transmission lines and transmission tower types are built based on the given actual data. Multi-vendor numerical relays are installed at NYPA Blenheim-Gilboa plant, some of which support GPS-synchronized measurement. Figure 5.23 illustrates the system model of the Blenheim-Gilboa plant along with the numerical relays installed in WinIGS.

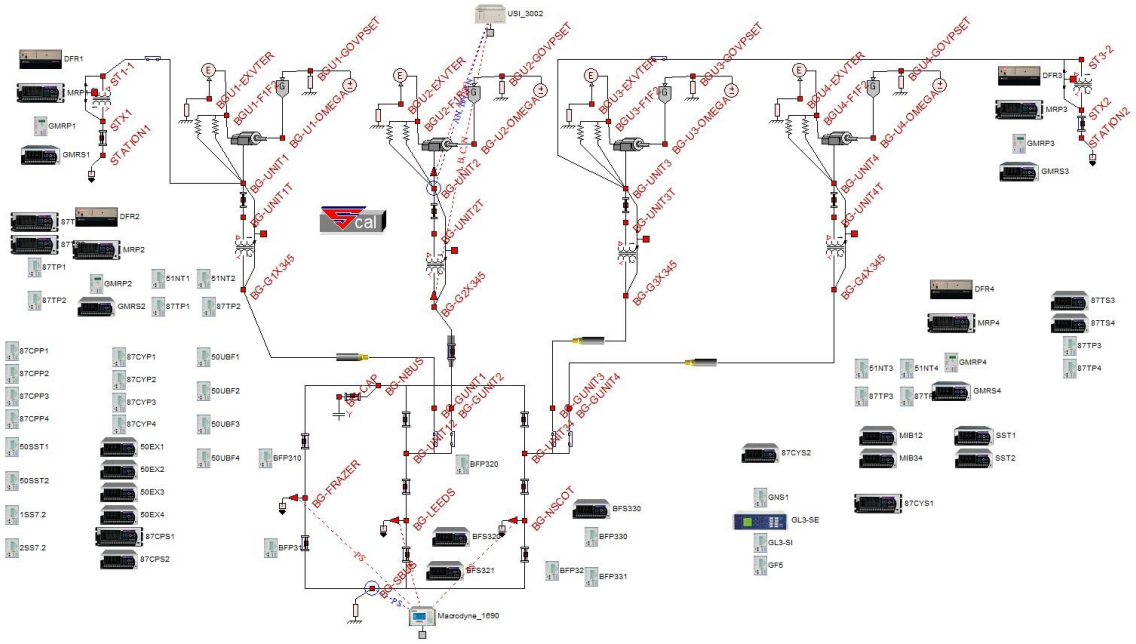

Figure 5.23. Blenheim-Gilboa plant built in WinIGS.

Measurement data, including the voltage and current phasors from the terminals of the generators, from high side of the four step-up transformers, and at the internal substation terminals of the three interconnection transmission lines that connect the Gilboa substation with the neighboring substations (Fraser, New Scotland and Leeds) were collected on March 14, 2013. The measurement data was fed into the DDSE to estimate the states inside

the substation, which include the voltage phasors of the substation buses and the speed, torque, and torque angle of the generator, as well as the voltage phasors at the other side of the interconnection transmission lines.

Figure 5.24 through Figure 5.29 show the comparison of voltage magnitudes and angles of the south bus in the Blenheim-Gilboa plant with the neighbor substations connected with the Gilboa plant through the 345 kV transmission lines, namely, the Leeds substation, the Norh Scotland substation, and the Frase substation. Note that there are slight differences for both the magnitude and the angle for the voltages at the south bus of the plant and the buses at the neighbor substations, which is due to the current flowing through the transmission lines.

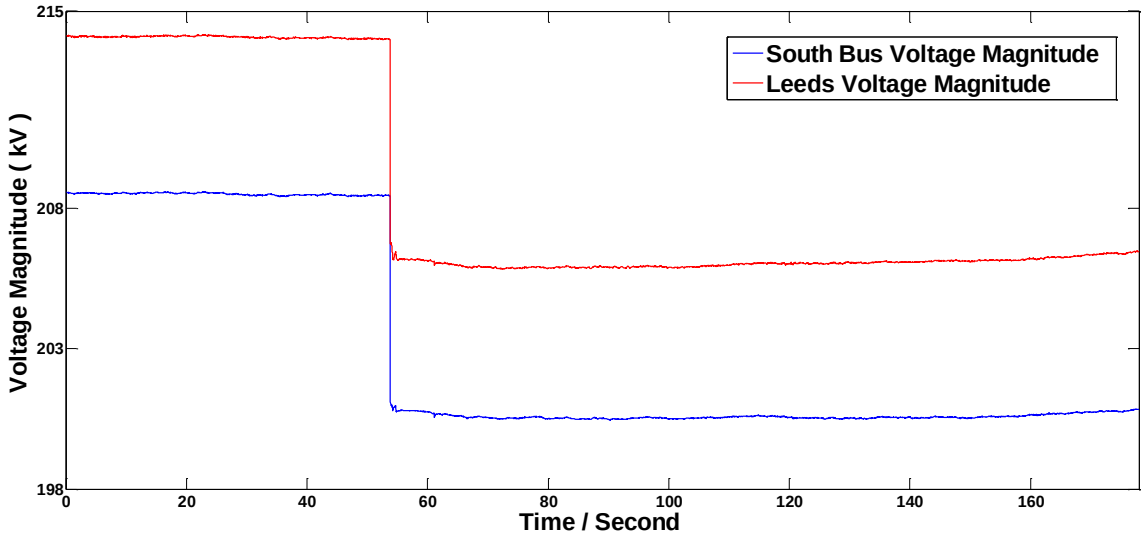

Figure 5.24. Estimated voltage magnitudes of south bus and Leeds.

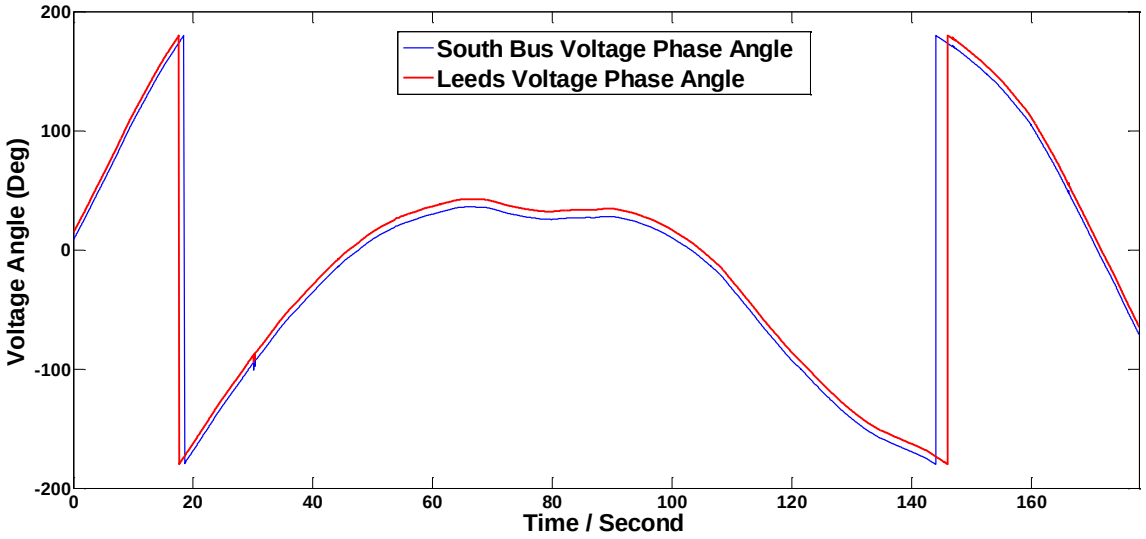

Figure 5.25. Estimated voltage phase angle of south bus and Leeds.

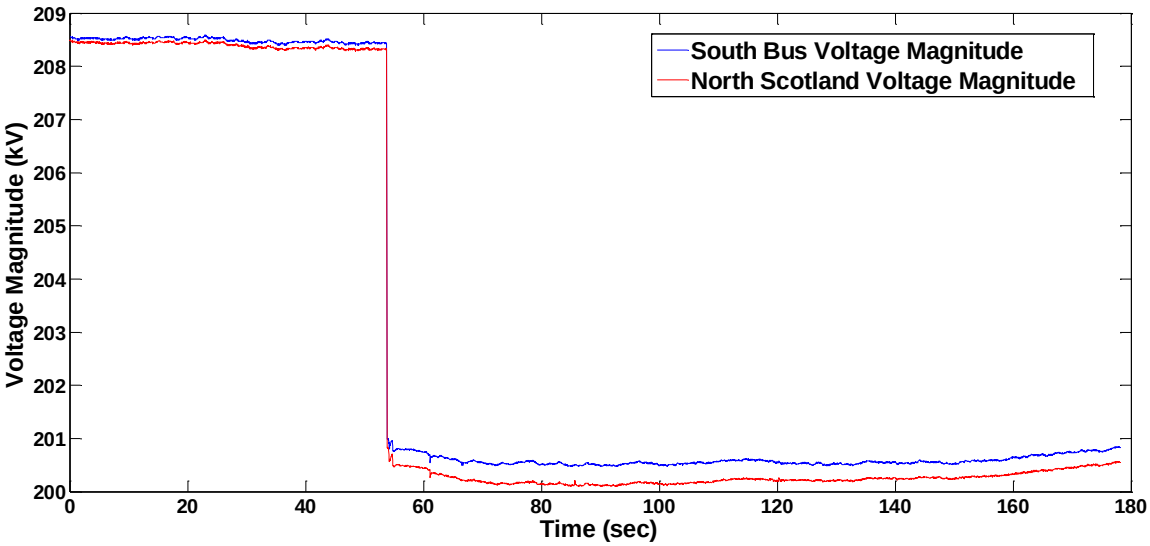

Figure 5.26. Estimated voltage magnitudes of south bus and North Scotland.

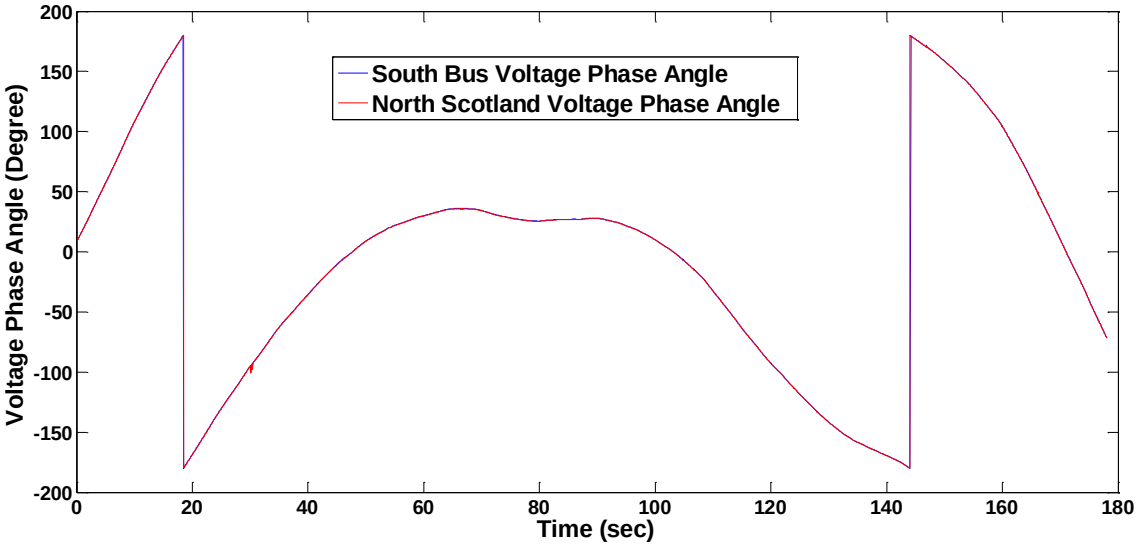

Figure 5.27. Estimated voltage phase angle of south bus and North Scotland.

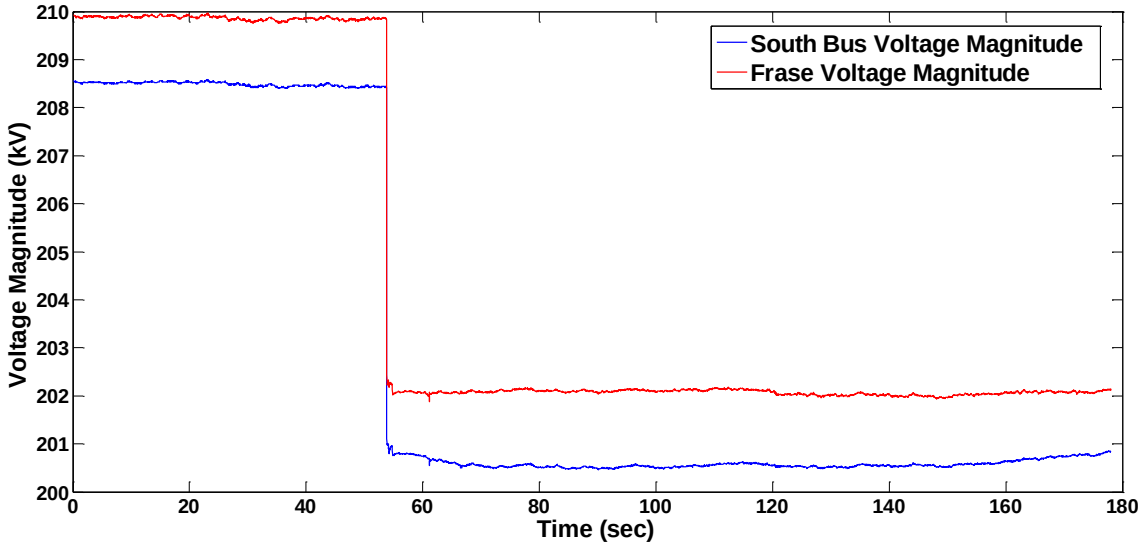

Figure 5.28. Estimated voltage magnitudes of south bus and Frase.

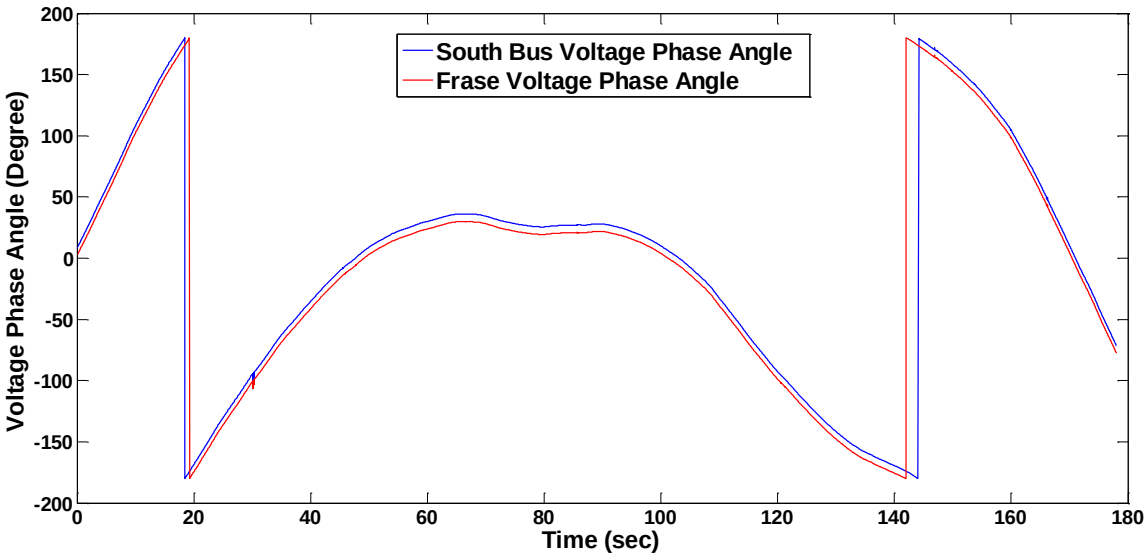

Figure 5.29. Estimated voltage phase angle of south bus and Frase.

Note that the generator units in the Blenheim-Gilboa plant are not always online. For the historical data, the DDSE captures the dynamic behavior of the generating unit #2 when it was connected to the grid. Figure 5.30 shows the estimated voltage magnitude of generator unit #2 and Figure 5.31 shows the comparison of the estimated voltage-phase angles of the south bus and the generator unit #2. Figure 5.32, Figure 5.33, and Figure 5.34 show the estimated electrical torque, the estimated torque angle and the estimated electrical speed of the generator, respectively. These figures clearly illustrate that the DDSE captures the ramping up and synchronization process of the generator. From Figure 5.30, it is clear that the generator begins to build up its terminal voltage to nominal value from 27.3 seconds to 45.3 seconds. From Figure 5.31, it is shown that after the fully building up of its voltage, the generator waits until its terminal voltage-phase angle becomes almost the same with the grid (at 54.2 seconds) and then the generator is connected to the grid (generator synchronization). Note that after the connection of the generator, there is still a

30 degree angle difference between the generator terminal voltage and the south bus voltage, and this is due to the delta-wye connection of the step-up transformer. From Figure 5.32, it is clear that after connecting to the grid at 54.2 seconds, the generator raises its output power, since the estimated electrical torque keeps increasing. Figure 5.33 and Figure 5.34 show the estimated torque angle and electrical speed of the generator, which indicates the generator is experiencing a slight oscillation when it goes online.

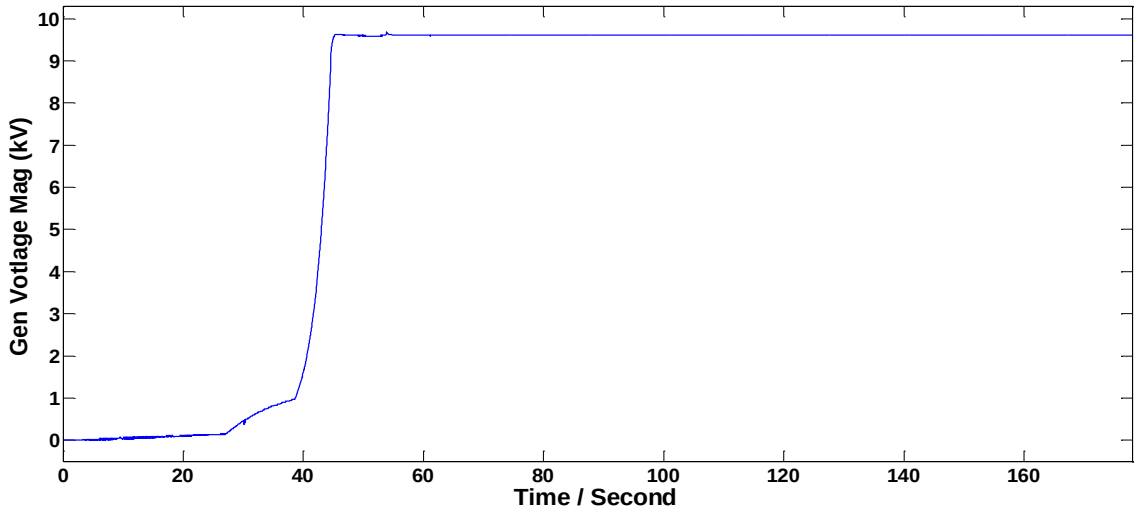

Figure 5.30. Estimated voltage magnitude of the generator.

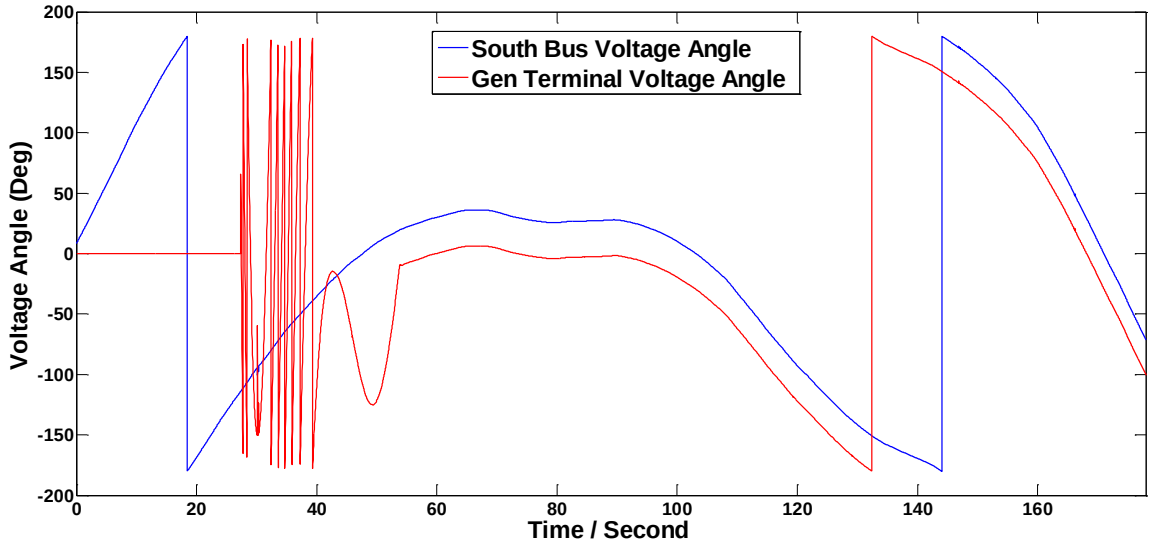

Figure 5.31. Comparison between estimated voltage angles.

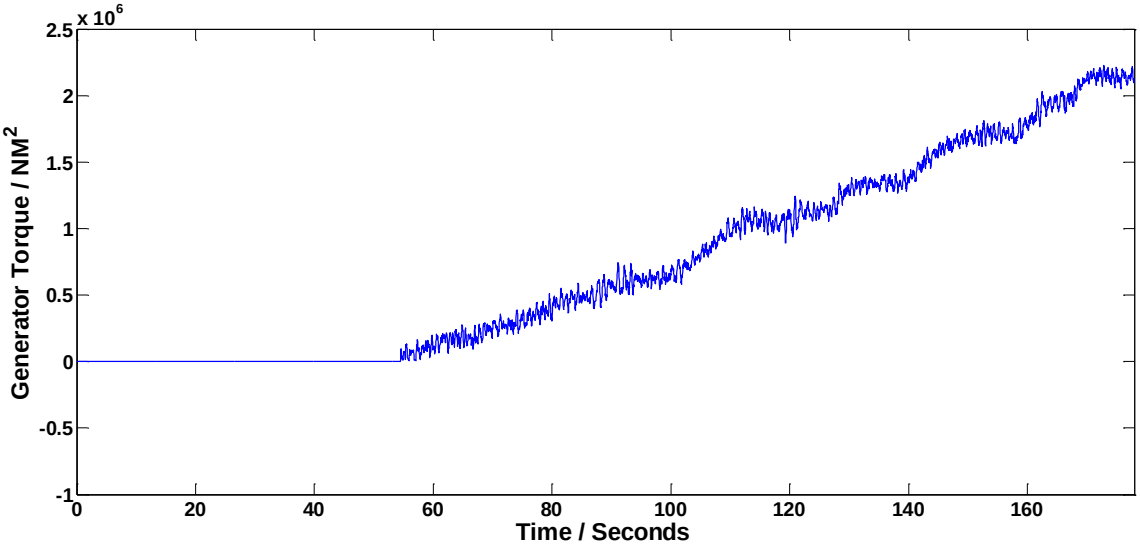

Figure 5.32. Estimated electrical torque of the generator.

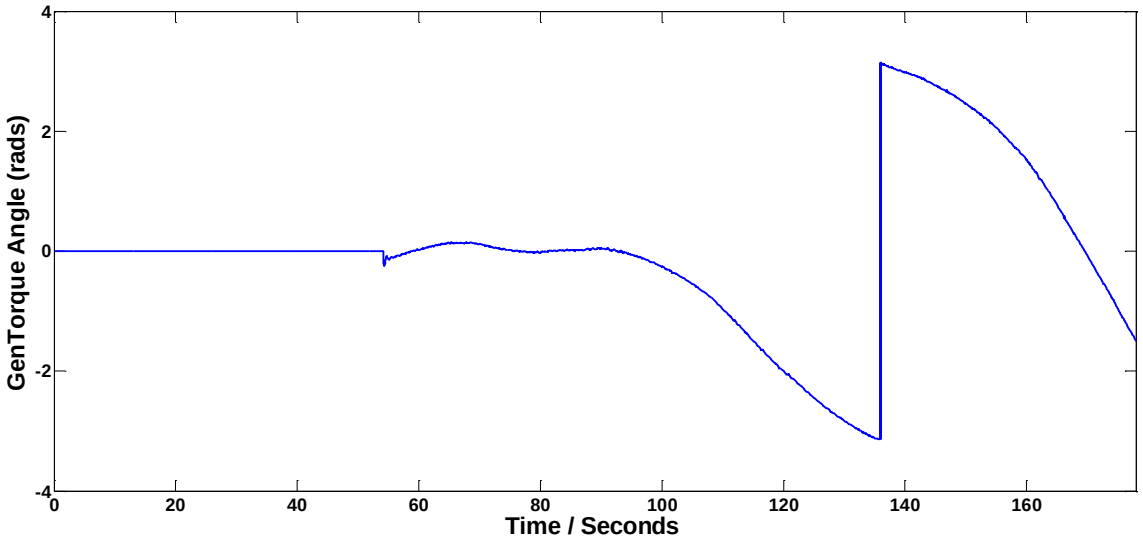

Figure 5.33. Estimated torque angle of the generator.

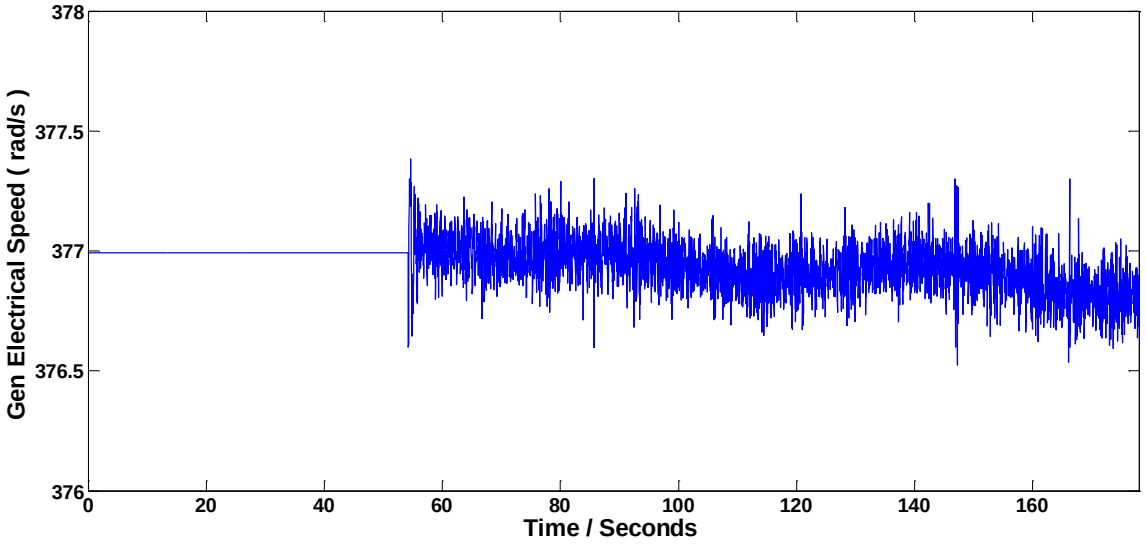

Figure 5.34. Estimated electrical speed of the generator.

5.13 Bad Data Identification and Topology Change Demonstration

Results

To validate the performance of the bad data detection, identification, and removal algorithm, numerical experiments were performed on the Gilboa-Blenheim substation. In particular, a measurement set was initially created with a bad datum which has a 15% error in the magnitude and 1.5^0 phase angle error in the voltage phasor measurement of phase A of bus BG-GA345. The Intelligent Electronic Device (IED) ID that generated the bad datum is 10. The algorithm, by performing the chi-square test detected the existence of bad data by indicating that the confidence level was 87.4% in this case. Note that a threshold of 90% has been set as the criterion of bad data existence. Representative results of the states of the substation are given in Table 5.3. Note that since Cartesian coordinates are used for the execution of the state estimation, the state for each phase has two parts, the

real and the imaginary component denoted with R and I respectively. Also note that apart from the state (voltage phasor) that is related to the erroneous measurement, the value of other states has been also affected.

Table 5.3. Single bad datum – state value comparison.

State Name (Bus Phase)	State Value (Simulation Result)	Estimated State Value
BG-GA345_A_R	198.75	195.05
BG-GA345_A_I	28.88	29.03
BG-GA345_B_R	-75.30	-75.30
BG-GA345_B_I	-185.33	-185.33
BG-GA345_C_R	-123.29	-123.28
BG-GA345_C_I	156.56	156.56
BG-Unit1_A_R	9.55	9.44
BG- Unit1_A_I	-2.71	-2.70
BG- Unit1_B_R	-7.13	-7.03
BG- Unit1_B_I	-6.90	-6.90
BG- Unit1_C_R	-2.37	-2.37
BG- Unit1_C_I	9.58	9.58

Representative results which compare the correct measurement values (simulation result) with the estimated measurement values are given in Table 5.4. Note that the estimated measurement value is computed given the state estimation results. As expected the largest residual appears for the erroneous measurement. However it is interesting to observe that a relatively large residual also appears for the same redundant measurement

(magnitude of the phase A, voltage phasor of bus BG-GA345) from another IED (IED 12) despite the fact that this measurement was accurate, as shown in the last two rows of Table 5.4.

The algorithm identified correctly the bad measurement based on its residual value and the measurement was removed by the measurement set. The chi-square test was repeated and demonstrated 100% confidence level.

Table 5.4. Single bad datum – measurement value comparison.

Voltage Phasor Measurement (Bus _Phase)	IED ID	Correct Meas. Value	Estimated Meas. Value	Residual
BG-GA345_A_R	10	198.75	195.05	23.05
BG-GA345_A_I	10	28.88	29.04	0.96
BG-GA345_B_R	10	-75.30	-75.30	0.006
BG-GA345_B_I	10	-185.33	-185.33	$7.7\ 10^{-5}$
BG-GA345_C_R	10	-123.29	-123.28	0.006
BG-GA345_C_I	10	156.56	156.56	$7.7\ 10^{-5}$
BG-GA345_A_R	12	198.75	195.05	3.7
BG-GA345_A_I	12	28.88	29.04	0.15

Another experiment was performed in which an IED of the system (IED ID: 25) malfunctions and reports zero values for all the measurements (three phase voltage phasors of bus STX1). The algorithm, by performing the chi-square test detected the existence of bad data by indicating the confidence level was 0.0% in this case. Representative results of

the states of the substation are given in Table 5.5. Note that apart from the state (voltage phasor) that is related to the erroneous measurement, the value of other states has been also affected.

Table 5.5. Multiple bad datum – state value comparison.

State Name (Bus Phase)	State Value (Simulation Result)	Estimated State Value
STX1_A_R	3.07	3.03
STX1_A_I	-3.16	-3.13
STX1_B_R	-4.26	-4.23
STX1_B_I	-1.08	-1.07
STX1_C_R	1.24	1.22
STX1_C_I	4.22	4.18
ST1_A_R	9.55	9.53
ST1_A_I	-2.71	-2.7
ST1_B_R	-7.13	-7.12
ST1_B_I	-6.90	-6.88
ST1_C_R	-2.37	-2.36
ST1_C_I	9.58	9.56

Representative results which compare the correct measurement values (simulation result) with the estimated measurement values are given in Table 5.6. As expected there is a relatively large residual for all three erroneous measurements. The measurements are removed sequentially and after the removal the chi-square test indicated 100% confidence level as expected. The residual for the same measurements (three phase voltage phasors of bus STX1) but from another IED which is working properly (IED ID: 22) and the estimated

measurements are also reported in Table 5.5. Note that in case of identifying that all measurements of a specific IED are erroneous for multiple time steps, an alarm is set, indicating that the functionality of this IED has to be checked.

Table 5.6. Multiple bad datum – measurment value comparison.

Voltage Phasor Measurement (Bus _Phase)	IED ID	Correct Meas. Value	Estimated Meas. Value	Residual
STX1_A_R	25	3.07	3.03	3.03
STX1_A_I	25	-3.16	-3.13	-3.13
STX1_B_R	25	-4.26	-4.23	-4.23
STX1_B_I	25	-1.08	-1.07	-1.07
STX1_C_R	25	1.24	1.22	1.22
STX1_C_I	25	4.22	4.18	4.18
STX1_A_R	22	3.07	3.03	0.04
STX1_A_I	22	-3.16	-3.12	0.04
STX1_B_R	22	-4.26	-4.23	0.03
STX1_B_I	22	-1.08	-1.07	0.01
STX1_C_R	22	1.24	1.22	0.02
STX1_C_I	22	4.22	4.18	0.04

In this section an example of a topology change in the test system and how this is identified in the state estimation procedure is also demonstrated. In particular, a fault was simulated in the test system that resulted in the operation of the two breakers that isolate the transmission line that is connected to the Leeds Substation. Given the three phases and breaker model that is used for the performance of the state estimation, the operation of the breakers was identified given the digital signals from the PMUs and the model of the

substation was updated accordingly. Figures 5.35 through Figure 5.36 illustrate representative results of the state estimation superimposed on the corresponding simulation results. In particular, the Phase A voltage magnitude and phase angle is shown for buses BG-Leeds and BG-Fraser. Note that the estimation results are highly accurate both for before and after the breaker operation.

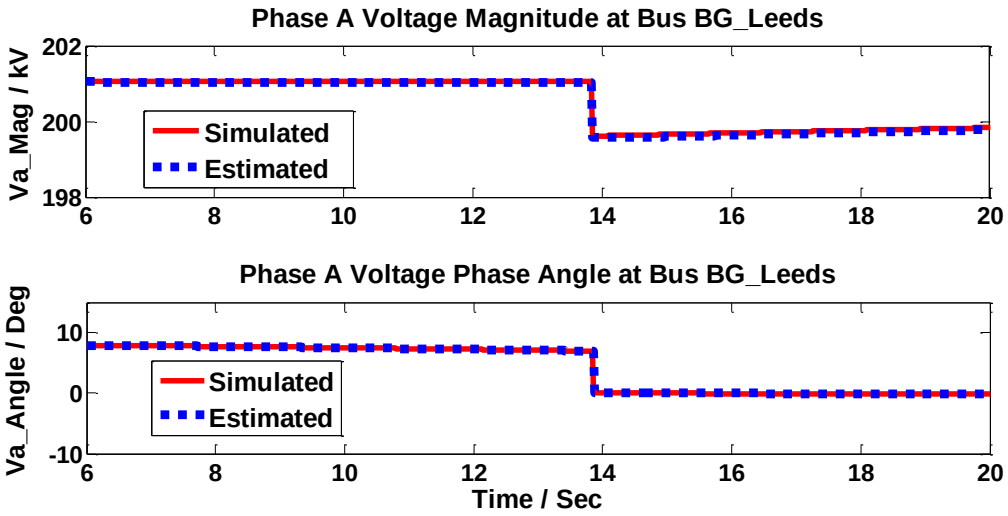

Figure 5.35. Voltage profile of phase A at BG-Leeds bus.

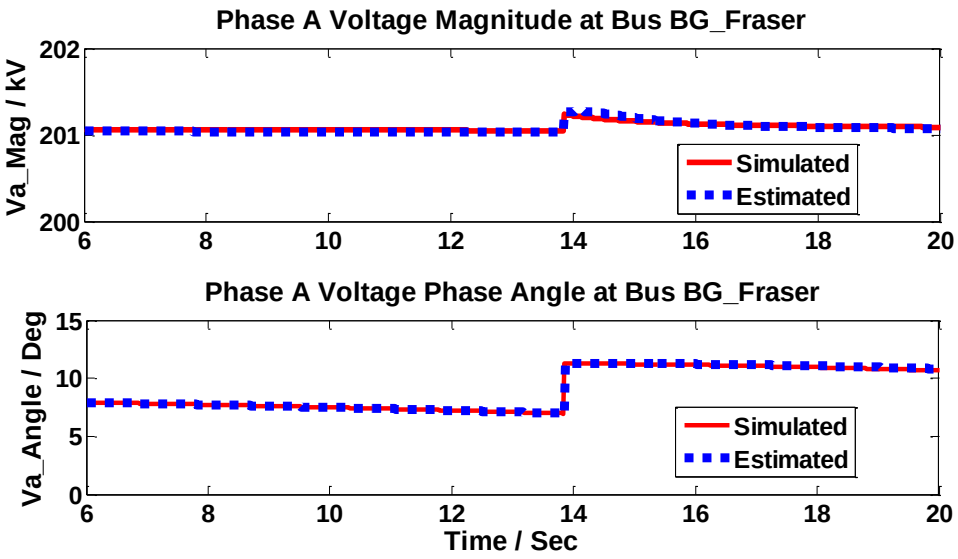

Figure 5.36. Voltage profile of phase A at BG-Fraser bus.

Note that in the pre-fault condition, the voltage value for both buses BG_Fraser and BG_Leeds is the same as expected since the breakers are closed. After the breaker operation though, these two buses are not electrically connected so in the post-fault period they have different voltage values.

5.14 Summary

The mathematical formulation, solution algorithm, and demonstration examples of the developed DDSE have been presented in this chapter. Emphasis is given on the object-oriented modeling approach of the DDSE. The distributed state estimator is enabled by synchrophasor technology. The proposed methodology eliminates the biases of traditional state estimators resulting from model biases as well as from imbalance biases because it uses a full model of the system and three phase measurements. The distributed state

estimator has been demonstrated with execution rates of 60 times per second for DDSE-Q and 2000 times per second for DDSE-T.

CHAPTER 6 MODEL VALIDATION – SYNCHRONOUS MACHINE PARAMETERS IDENTIFICATION

6.1 Overview

Modeling accuracy and fidelity are fundamental in the proposed design of the state estimator. For success the model must be high fidelity so that the component state estimator (DDSE-T) will reliably determine the operating status of the component.

For many power system components, high-fidelity models exist. For some new components such as inverter-interfaced power components, the modeling accuracy may not be as high as that of other components as a result of model parameter uncertainty. In both cases the DDSE can be utilized to fine tune the models and/or determine the parameters of the model with greater accuracy. The basic approach is to expand the DDSE to include some key parameters as unknown states. This is a procedure of parameters identification and model validation. Therefore the proposed overall approach can also provide better models with field-validated parameters compared with traditional approaches.

The proposed approach provides the possibility that a high-fidelity model can be used as the main depository of the component model (protective relay level). This data base of high-fidelity component models can provide appropriate models for other EMS applications, which achieves a seamless integration with these applications. For example, for EMS applications such as optimization of the system operation conditions, a positive-sequence model can be computed from the high-fidelity model and sent to the EMS data base. The object-oriented, unified, and seamless interoperable component model SCAQCF

syntax described in Chapter 4 is used to guarantee that the high-fidelity model can be seamlessly used across other EMS applications and across all relevant temporal and spatial scales. Figure 6.1 illustrates the basic idea that the high-fidelity component model verified by the DDSE can provide appropriate models for any other EMS application, through appropriate filters [99].

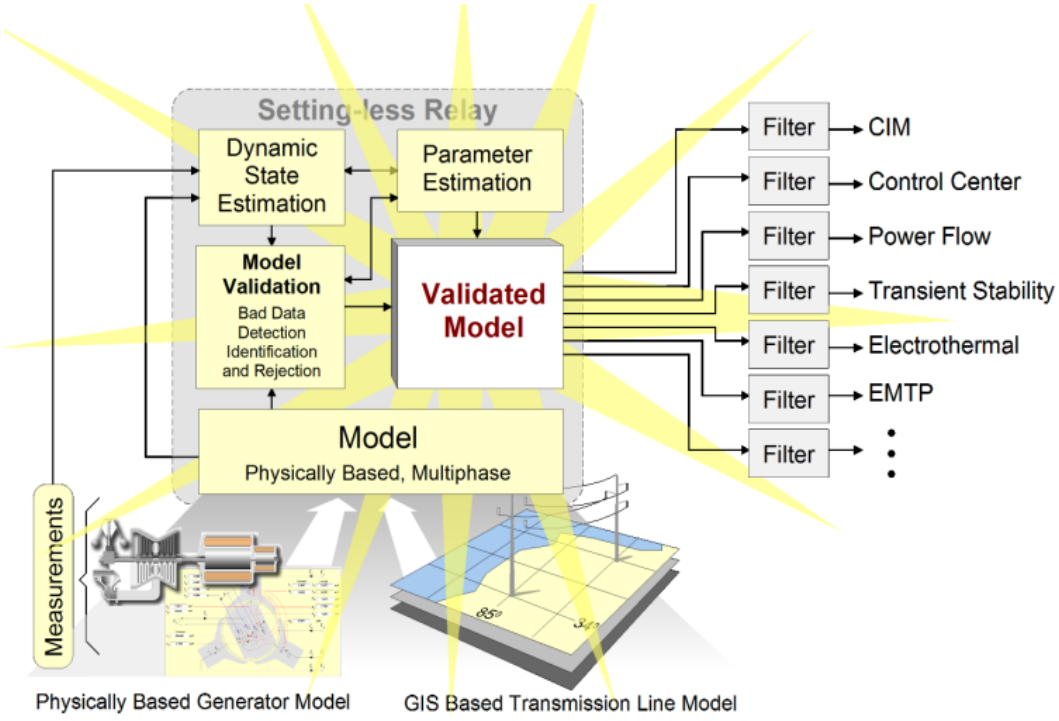

Figure 6.1. Illustration of the DDSE as the model gatekeeper [99].

Section 6.2 provides the mathematical formulation of the synchronous machine physical parameters identification problem, to illustrate the procedure of expanding the DDSE to include some key parameters as unknown states. Section 6.3 provides the demonstration results of the synchronous machine physical parameters identification.

6.2 Synchronous Machine Physical Parameters Identification

As proposed in Chapter 3, the DDSE can be augmented to include some key parameters of a component model as unknown states. Therefore, the DDSE can also provide a better model with field-validated parameters. Here an example of this kind of model parameters validation is provided. A physically-based synchronous-machine model expressed in terms of the self and mutual inductances of the generator windings as a function of the rotor position, is proposed for the purpose of synchronous-machine parameters identification. This model accounts for the different impedances along the two axes of the synchronous-machine as well as the generation of harmonics in the unit. Compared with the traditional parameters identification methods discussed in Section 2.5, the physical parameters based synchronous machine model used here has the following advantages: (1) there are no simplification assumptions for the proposed dynamic generator model, such as the park's transformation or dynamic order reduction, which is suitable for the situation of sudden application and removal of balanced and unbalanced loads, rectifier loads, and also symmetrical and asymmetrical faults; (2) the model is accurate for both round rotor machines and salient pole machines; (3) rotor angle and the physical parameters of the synchronous generator can be estimated together at the same time.

The model for the synchronous machine physical parameters identification is expressed with the following equations:

$$v_{abc}(t) = R_{abc} i_{abc}(t) + \frac{d\lambda_{abc}(t)}{dt}, \tag{6.1}$$

$$v_{fDQ}(t) = R_{fDQ} i_{fDQ}(t) + \frac{d\lambda_{fDQ}(t)}{dt}, \tag{6.2}$$

$$J\frac{d\omega_m(t)}{dt} = T_m(t) + T_e(t) + T_{wf}(t), \tag{6.3}$$

$$\frac{d\theta_m(t)}{dt} = \omega_m(t), \tag{6.4}$$

$$T_{wf}(t) = -\left(D_{fw} + D'_{fw}\cdot\omega_m(t) + D''_{fw}\cdot\omega_m(t)^2\right), \tag{6.5}$$

$$0 = T_e - \frac{1}{\sqrt{3}}\cdot n_p \cdot \begin{pmatrix} i_a(t)\lambda_b(t) - i_a(t)\lambda_c(t) + i_b(t)\lambda_c(t) \\ -i_b(t)\lambda_a(t) + i_c(t)\lambda_a(t) - i_c(t)\lambda_b(t) \end{pmatrix}, \tag{6.6}$$

$$\begin{bmatrix} \lambda_{abc}(t) \\ \lambda_{fDQ}(t) \end{bmatrix} = \begin{bmatrix} L_{ss}(\theta_m(t)) & L_{sr}(\theta_m(t)) \\ L_{rs}(\theta_m(t)) & L_{rr} \end{bmatrix} \begin{bmatrix} i_{abc}(t) \\ i_{fDQ}(t) \end{bmatrix}, \tag{6.7}$$

where $v_{abc}(t)$ and $i_{abc}(t)$ are the terminal voltages and currents, and $\boldsymbol{\lambda_{abc}(t)}$ are the flux linkage through the stator windings. Similarly, $v_{fDQ}(t)$ and $\boldsymbol{i_{fDQ}(t)}$ are the voltages and currents of the field terminal and the DQ-damper windings, and $\lambda_{fDQ}(t)$ are the flux linkage through field and DQ-damper windings. $\boldsymbol{T_m(t)}$, $\boldsymbol{T_e(t)}$, $T_{wf}(t)$, $\boldsymbol{\omega_m(t)}$, $\boldsymbol{\theta_m(t)}$ are mechanical torque, electrical torque, friction and wind-age torque, mechanical shaft speed, and rotor-angular position respectively. $L_{ss}(\theta(t))$, $L_{sr}(\theta(t))$, $L_{rs}(\theta(t))$ and $L_{rr}(\theta(t))$ are matrices of the self and mutual inductances of the stator and rotor windings, and they depend on the mechanical rotor-angular position. For example, the stator self-inductances, the stator mutual inductances, and the mutual inductances between the stator windings and the rotor windings have the following expressions:

$$\begin{aligned} L_{aa}(t) &= L_s + L_m\cos\left(2\theta(t)\right), \\ L_{ab}(t) &= -M_S - L_m\cos\left(2\theta(t) + \pi/3\right), \\ L_{af}(t) &= L_{fa}(t) = M_F\cos\theta(t). \end{aligned} \tag{6.8}$$

The detailed expressions of the physical self and mutual inductances for the other phases of the stator windings, the field winding, and the DQ-damping windings are discussed in Section 4.3. Table 6.1 lists the physical parameters of a synchronous machine that need to be estimated. These parameters appear in the equation set (6.7).

Table 6.1 Physical parameters required to be identified.

No.	Vari-able	Description	No.	Vari-able	Description
1	L_s	Stator self-inductance constant part, as a result of air-gap flux and armature leakage flux	6	M_S	Stator mutual inductance
2	L_m	Amplitude of Stator's self-inductance varying part as a result of rotor saliency	7	M_R	Field D-damper mutual inductance
3	L_f	Field self-inductance	8	M_F	Stator field mutual inductance
4	L_D	D-damper self-inductance	9	M_D	Stator D-damper mutual inductance
5	L_Q	Q-damper self-inductance	10	M_Q	Stator Q-damper mutual inductance

A quadratization procedure is used to convert the equation set from (6.1) to (6.7) to the quadratized model. Note that the generator parameters of Table 6.1 are considered as unknowns (states) that need to be estimated through the DDSE algorithm.

$$\tilde{v}^m_{abcf}(t) = v_{abcf}(t) + \eta, \tag{6.9}$$

$$\tilde{v}^m_{an\ bn\ cn\ fn}(t) = v_{an\ bn\ cn\ fn}(t) + \eta, \tag{6.10}$$

$$\tilde{i}^m_{abc}(t) = i_{aL\ bL\ cL}(t) + g_{as,bs,cs} \cdot (v_{abc}(t) - v_{an\ bn\ cn}(t)) + \eta, \tag{6.11}$$

$$\tilde{i}^m_{an\ bn\ cn}(t) = -i_{aL\ bL\ cL}(t) + g_{as,bs,cs} \cdot (v_{an\ bn\ cn}(t) - v_{abc}(t)) + \eta\ , \tag{6.12}$$

$$\tilde{i}^m_f(t) = i_{fL}(t) + g_{fs} \cdot (v_f(t) - v_{fn}(t)) + \eta, \tag{6.13}$$

$$\tilde{i}^m_{fn}(t) = -i_{fL}(t) + g_{fs} \cdot (v_{fn}(t) - v_f(t)) + \eta, \tag{6.14}$$

$$\tilde{T}_m^m(t) = T_{acc} - T_e(t) - T_{wf}(t) + \eta\,, \tag{6.15}$$

$$0 = v_{abc}(t) - v_{an\ bn\ cn}(t) - R_{abc} i_{aL\ bL\ cL}(t) + e_{abc}(t) + \eta\,, \tag{6.16}$$

$$0 = v_f(t) - R_f i_{fL}(t) - e_f(t) - v_{fn}(t) + \eta\,, \tag{6.17}$$

$$0 = R_{DQ} i_{DQ}(t) + e_{DQ}(t) + \eta\,, \tag{6.18}$$

$$0 = \frac{d\theta_m(t)}{dt} - \omega_m(t) + \eta\,, \tag{6.19}$$

$$0 = \theta(t) - \frac{p}{2}\theta_m(t) + \eta\,, \tag{6.20}$$

$$0 = \omega(t) - \frac{p}{2}\omega_m(t) + \eta\,, \tag{6.21}$$

$$0 = \theta(t) - \omega_s t - \delta(t) - \frac{\pi}{2} + \eta\,, \tag{6.22}$$

$$0 = T_{wf}(t) + \left(D_{fw} + D'_{fw} \cdot \omega_m(t) + D''_{fw} \cdot \omega_m(t)^2\right) + \eta\ , \tag{6.23}$$

$$0 = P_{em}(t) - e_{abc}(t)^T i_{aL\ bL\ cL}(t) - e_{fDQ}(t)^T i_{fL\ DQ}(t) + \eta\,, \tag{6.24}$$

$$0 = T_e - \frac{1}{\sqrt{3}} \cdot n_p \cdot \begin{pmatrix} i_{aL}(t)\lambda_b(t) - i_{aL}(t)\lambda_c(t) + i_{bL}(t)\lambda_c(t) \\ -i_{bL}(t)\lambda_a(t) + i_{cL}(t)\lambda_a(t) - i_{cL}(t)\lambda_b(t) \end{pmatrix}, \tag{6.25}$$

$$0 = \frac{d\lambda_{abc}(t)}{dt} - e_{abc}(t) + \eta\ , \tag{6.26}$$

$$0 = \frac{d\lambda_{fDQ}(t)}{dt} - e_{fDQ}(t) + \eta\,, \tag{6.27}$$

$$0 = \frac{d\omega_m(t)}{dt} - \frac{1}{J} T_{acc}(t) + \eta\,, \tag{6.28}$$

$$0 = \frac{dc(t)}{dt} - y_1(t) + \eta\,, \tag{6.29}$$

$$0 = \frac{ds(t)}{dt} - y_2(t) + \eta\,, \tag{6.30}$$

$$0 = y_1(t) + s(t)\cdot\omega(t) + \eta\,, \tag{6.31}$$

$$0 = y_2(t) - c(t)\cdot\omega(t) + \eta\ , \tag{6.32}$$

$$0 = c_2(t) - c^2(t) + s^2(t) + \eta\,, \tag{6.33}$$

$$0 = s_2(t) - 2c(t)s(t) + \eta\,, \tag{6.34}$$

$$0 = z_1 - L_m\cdot c_2(t) + \eta\,, \tag{6.35}$$

$$0 = z_2 - L_m\cdot s_2(t) + \eta\,, \tag{6.36}$$

$$0 = z_3 - M_F\cdot c(t) + \eta\,, \tag{6.37}$$

$$0 = z_4 - M_F\cdot s(t) + \eta\,, \tag{6.38}$$

$$0 = z_5 - M_D\cdot c(t) + \eta\,, \tag{6.39}$$

$$0 = z_6 - M_D\cdot s(t) + \eta\,, \tag{6.40}$$

$$0 = z_7 - M_Q\cdot c(t) + \eta\,, \tag{6.41}$$

$$0 = z_8 - M_Q\cdot s(t) + \eta\,, \tag{6.42}$$

$$0 = \begin{bmatrix}\lambda_{abc}(t)\\ \lambda_{fDQ}(t)\end{bmatrix} - A\cdot\begin{bmatrix}-i_{aL,bL,cL}(t)\\ i_{fL,D,Q}(t)\end{bmatrix} - B\cdot\begin{bmatrix}-i_{aL,bL,cL}(t)\\ i_{fL,D,Q}(t)\end{bmatrix}, \tag{6.43}$$

where

$$A = \begin{bmatrix}
z_1 & -\frac{1}{2}z_1 + \frac{\sqrt{3}}{2}z_2 & -\frac{1}{2}z_1 - \frac{\sqrt{3}}{2}z_2 & z_3 & z_5 & z_8\\
-\frac{1}{2}z_1 + \frac{\sqrt{3}}{2}z_2 & -\frac{1}{2}z_1 - \frac{\sqrt{3}}{2}z_2 & z_1 & -\frac{1}{2}z_3 + \frac{\sqrt{3}}{2}z_4 & -\frac{1}{2}z_5 + \frac{\sqrt{3}}{2}z_6 & -\frac{\sqrt{3}}{2}z_7 - \frac{1}{2}z_8\\
-\frac{1}{2}z_1 - \frac{\sqrt{3}}{2}z_2 & z_1 & -\frac{1}{2}z_1 + \frac{\sqrt{3}}{2}z_2 & -\frac{1}{2}z_3 - \frac{\sqrt{3}}{2}z_4 & -\frac{1}{2}z_5 - \frac{\sqrt{3}}{2}z_6 & \frac{\sqrt{3}}{2}z_7 - \frac{1}{2}z_8\\
z_3 & -\frac{1}{2}z_3 + \frac{\sqrt{3}}{2}z_4 & -\frac{1}{2}z_3 - \frac{\sqrt{3}}{2}z_4 & 0 & 0 & 0\\
z_5 & -\frac{1}{2}z_5 + \frac{\sqrt{3}}{2}z_6 & -\frac{1}{2}z_5 - \frac{\sqrt{3}}{2}z_6 & 0 & 0 & 0\\
z_8 & -\frac{\sqrt{3}}{2}z_7 - \frac{1}{2}z_8 & \frac{\sqrt{3}}{2}z_7 - \frac{1}{2}z_8 & 0 & 0 & 0
\end{bmatrix}, \tag{6.44}$$

$$B = \begin{bmatrix} L_s & -M_s & -M_s & 0 & 0 & 0 \\ -M_s & L_s & -M_s & 0 & 0 & 0 \\ -M_s & -M_s & L_s & 0 & 0 & 0 \\ 0 & 0 & 0 & L_f & M_R & 0 \\ 0 & 0 & 0 & M_R & L_D & 0 \\ 0 & 0 & 0 & 0 & 0 & L_Q \end{bmatrix}.$$

The external states, internal states and the actual measurements of the generator physical parameters identification problem are listed by Table 6.2, Table 6.3, and Table 6.4, respectively.

Table 6.2. External states of the generator parameters identification model.

Index	Variable	Description
0	$v_a(t)$	terminal voltage of stator phase A (kV)
1	$v_b(t)$	terminal voltage of stator phase B (kV)
2	$v_c(t)$	terminal voltage of stator phase C (kV)
3	$v_{an}(t)$	terminal voltage of stator phase A (kV)
4	$v_{bn}(t)$	terminal voltage of stator phase B (kV)
5	$v_{cn}(t)$	terminal voltage of stator phase C (kV)
6	$v_f(t)$	terminal voltage of rotor field winding (kV)
7	$v_{fn}(t)$	terminal voltage of rotor field winding neutral (kV)
8	$\omega_m(t)$	machine mechanical shaft speed (rad/s)

Table 6.3. Internal states of the generator parameters identification model.

Index	Variable	Description
9	$i_{aL}(t)$	current through the inductance of stator phase A (kA)
10	$i_{bL}(t)$	current through the inductance of stator phase B (kA)
11	$i_{cL}(t)$	current through the inductance of stator phase C (kA)
12	$i_{fL}(t)$	current through the inductance of field winding (kA)
13	$i_D(t)$	current through rotor d-axis damper-winding (kA)
14	$i_Q(t)$	current through rotor q-axis damper-winding (kA)

15	$\theta_m(t)$	rotor angular position w.r.t. a stationary reference axis (rad)
16	$\theta(t)$	electrical rotor position angle (rad)
17	$\omega(t)$	machine electrical shaft speed (rad/s)
18	$\delta(t)$	machine power angle (rad)
19	$T_{fw}(t)$	friction and windage torque (MNm)
20	$P_{em}(t)$	internal electrical power (MW)
21	$T_e(t)$	machine electrical torque (MNm)
22	$e_a(t)$	stator winding internal EMF, phase A (kV)
23	$e_b(t)$	stator winding internal EMF, phase B (kV)
24	$e_c(t)$	stator winding internal EMF, phase C (kV)
25	$e_f(t)$	field winding internal EMF (kV)
26	$e_D(t)$	D-damper winding internal EMF (kV)
27	$e_Q(t)$	Q-damper winding internal EMF (kV)
28	$\lambda_a(t)$	flux linkage through stator winding of phase A (kWb)
29	$\lambda_b(t)$	flux linkage through stator winding of phase B (kWb)
30	$\lambda_c(t)$	flux linkage through stator winding of phase C (kWb)
31	$\lambda_f(t)$	flux linkage through rotor field winding (kWb)
32	$\lambda_D(t)$	flux linkage through rotor d-axis damper-winding (kWb)
33	$\lambda_Q(t)$	flux linkage through rotor q-axis damper-winding (kWb)
34	$T_{acc}(t)$	machine accelerating torque (MNm)
35	$c(t)$	cos($\theta(t)$) [state 16]
36	$s(t)$	sin($\theta(t)$) [state 16]
37	$y_1(t)$	internal variable y1 (rad/s)
38	$y_2(t)$	internal variable y2 (rad/s)
39	$c_2(t)$	cos($2\theta(t)$) [state 16]
40	$s_2(t)$	sin($2\theta(t)$) [state 16]
41	$z_1(t)$	auxiliary state
42	$z_2(t)$	auxiliary state
43	$z_3(t)$	auxiliary state
44	$z_4(t)$	auxiliary state
45	$z_5(t)$	auxiliary state
46	$z_6(t)$	auxiliary state
47	$z_7(t)$	auxiliary state
48	$z_8(t)$	auxiliary state

49	$L_s(t)$	self-inductance
50	$L_m(t)$	mutual inductance
51	$L_f(t)$	field self-inductance
52	$L_D(t)$	D damper self-inductance
53	$L_Q(t)$	Q damper self-inductance
54	$M_S(t)$	Stator mutual inductance
55	$M_R(t)$	field D damper mutual inductance
56	$M_F(t)$	stator field mutual inductance
57	$M_D(t)$	stator D damper mutual inductance
58	$M_Q(t)$	stator Q damper mutual inductance

Table 6.4. Actual measurements for the generator parameters identification.

Index	Variable	Description
0	$v_a(t)$	terminal voltage of stator phase A (kV)
1	$v_b(t)$	terminal voltage of stator phase B (kV)
2	$v_c(t)$	terminal voltage of stator phase C (kV)
3	$v_f(t)$	terminal voltage of rotor field winding (kV)
4	$v_{fn}(t)$	terminal voltage of rotor field winding neutral (kV)
5	$i_a(t)$	current through stator winding of phase a
6	$i_b(t)$	current through stator winding of phase b
7	$i_c(t)$	current through stator winding of phase c
8	$i_{an}(t)$	current through stator winding of phase a
9	$i_{bn}(t)$	current through stator winding of phase b
10	$i_{cn}(t)$	current through stator winding of phase c
11	$i_f(t)$	current through rotor field winding
12	$i_{fn}(t)$	current through rotor field winding (neutral side)
13	$T_m(t)$	mechanical torque applied on the machine shaft (MNm)

After the quadratization, the quadratic integration method is applied to the quadratized model from equation (6.19) to (6.43) to convert the model to the standard SCAQCF syntax.

This procedure is the same as the procedure discussed in Section 4.3.3, and the details are not listed here.

These actual measurements together with the synchronous machine model which are treated as virtual measurements, contribute 40 measurements for the state estimator, while the state estimator has 44 states. Thus, given the measurements of one time step, the state estimator is not observable. The solution methodology for this un-observable problem is to apply a multi-step dynamic state estimation. The reason to implement this approach is that the dynamic state estimator runs at high rates and the physical parameters of the generator can be assumed to be constant within 2-3 consecutive time steps. For example, consider a two time step case where we will have 44+34=78 states (for the second time step the 10 physical parameters are considered the same as in the first time step) while we have 40*2=80 measurements, which will make the state estimator observable.

6.3 Synchronous Machine Parameters Identification – Numerical Results

A 4-pole synchronous machine of 825-MVA capacity with rated terminal voltage 18kV was used to validate the performance of the proposed methodology. The test system consists of one generator unit, connected to a step-up transformer, sending power through overhead transmission lines to the loads as is illustrated in Figure 6.2. Table 6.5 gives the parameters of the test system components and Table 6.6 presents the physical parameters of this generator and these parameters are from [88]. A three phase to ground fault is simulated at the terminals of the synchronous machine and Figure 6.3 illustrates the waveforms of the terminal voltages and currents of the phase A, B and C of stator windings

and field winding, along with the mechanical shaft speed, which were used as the actual measurements in the dynamic state estimation algorithm.

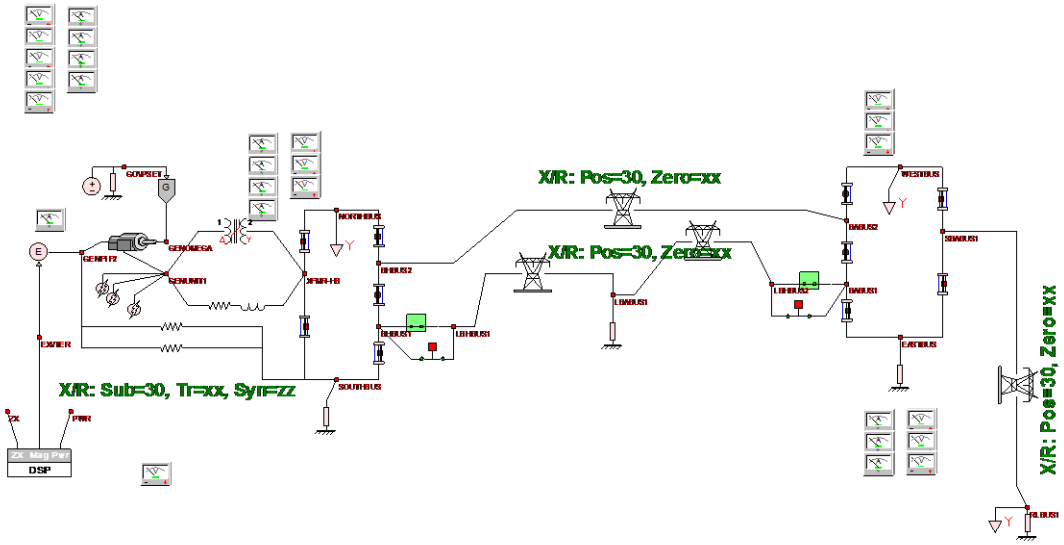

Figure 6.2. Test system for the generator parameters identification.

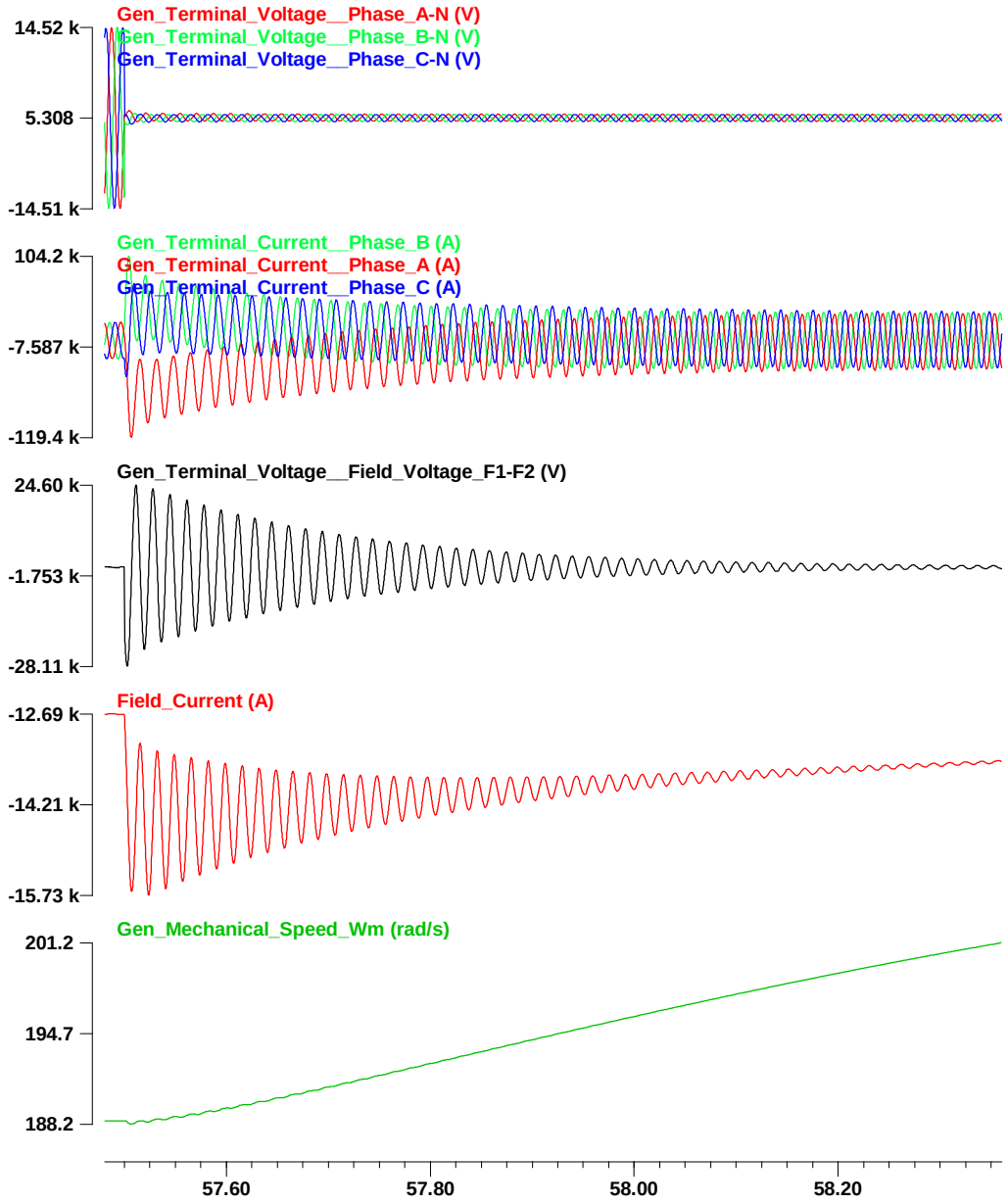

Figure 6.3. Actual measurement set for the generator parameter identification.

Table 6.5. Test system parameters for the generator parameters identification.

Gen1	825MVA	18.0 kV
XFMR1	650MVA z=0.08+j0.85 pu	18 kV/230kV
Transmission Line 1	z=1,47 + j20.21 ohms	230 kV
Transmission Line 2	z=2.70 + j28.01 ohms	230 kV
Transmission Line 3	z=0.79 + 11.52 ohms	230 kV
Load 1	600MW/90MVar	230 kV

Table 6.6 gives also the estimated values of the physical parameters of this synchronous machine and the errors between the actual and estimated values. Measurements from two consecutive time steps were used in this case. In Table 6.6 it is shown that the estimation errors for these physical parameters are below 5%, which verifies the effectiveness of the proposed methodology. Numerical experiments were performed using measurements from additional time steps, and the error of the estimated values was not affected.

Table 6.6. Physical parameters identification results.

Parameters	Actual Value (mH)	Estimated Value (mH)	Error
L_s	1.4376	1.4419	3.04%
L_m	0.0174	0.0175	4.70%
L_f	28.1109	28.9964	3.15%
L_D	1.7055	1.7651	3.49%
L_Q	1.0286	1.0126	-0.56%
M_S	0.6719	0.6743	3.60%
M_R	6.0204	6.2490	3.80%
M_F	5.4018	5.4163	2.70%

M_D	1.3545	1.3738	1.42%
M_Q	1.0564	1.0330	2.22%

6.4 Summary

This chapter has demonstrated that DDSE can be utilized to fine tune the models and/or determine the parameters of the model with greater accuracy by expanding the state estimator to include key model parameters as unknown states. The mathematical formulation of the synchronous machine physical parameters identification problem is presented to illustrate the parameters identification procedure. Demonstration results of the synchronous machine physical parameters identification are also provided in this chapter.

CHAPTER 7 SCAQCF-BASED OBJECT-ORIENTED OPF

7.1 Overview

The real-time component model computed from the results of the DDSE, and expressed in the SCAQCF syntax, is transmitted to the EMS control center to directly synthesize the real-time model of the system, which provides the real-time model of the entire power system across the spatial extent of the system. This model is of high fidelity and can be converted into other models of lower accuracy, such as models for load flow analysis.

The converted models can be seamlessly integrated with a variety of other applications of EMS. As an example, one of the important applications of the EMS, the optimization of grid operation conditions, is discussed here. The optimization of grid operation conditions can be formulated as an OPF problem with different objective functions and constraints. This chapter discusses the autonomous formulation of the OPF problem and its solution methodology by simply using the object-oriented SCAQCF component model.

Section 7.2 gives the detailed mathematical formulation of the OPF problem, with the emphasis on the autonomous formulation of the OPF with the help of the object-oriented SCAQCF component model. Section 7.3 proposes a robust and high efficient algorithm to solve the OPF problem. Section 7.4 discusses the object-oriented implementation of the proposed solution algorithm. Section 7.5 presents demonstration results of the proposed robust and high efficient OPF solution algorithm.

7.2 Autonomous Formulation of the OPF

Note that the SCAQCF model discussed in Section 4.2 includes the following four sets of data: (1) connectivity, (2) device model, (3) measurements, and (4) controls, and is organized into an object with specific structure. The autonomous formulation of the optimal power flow problem and its solution is discussed here by simply using the object-oriented SCAQCF component model.

The mathematical formulation of the optimal power flow problem is as follows:

$$\begin{aligned} &\min \quad f(\mathbf{x},\mathbf{u}) = \mu \sum \left(\left| \mathbf{I}_m \right| \right) + c(\mathbf{x},\mathbf{u}), \\ &s.t. \quad \mathbf{g}(\mathbf{x},\mathbf{u}) = 0, \\ &\mathbf{h}^{\min} \le \mathbf{h}(\mathbf{x},\mathbf{u}) \le \mathbf{h}^{\max}, \\ &\mathbf{u}^{\min} \le \mathbf{u} \le \mathbf{u}^{\max}, \end{aligned} \tag{7.1}$$

where $\mathbf{I}_m$ is the mismatch variable vector, $\mathbf{x}$ is the state variable vector, and $\mathbf{u}$ is the control variable vector. In the objective function f($\mathbf{x}$, $\mathbf{u}$), μ is the penalty factor and c($\mathbf{x}$, $\mathbf{u}$) is the cost function, which can be the total operational cost of the system.

$\mathbf{g}(\mathbf{x}, \mathbf{u}) = 0$ represents the power flow equations, and they are created by collecting the connectivity data of each component from the SCAQCF syntax, applying KCL at each node of the network, and adding the internal model equations of all components:

$$\mathbf{g}(\mathbf{x},\mathbf{u}) = \begin{cases} \sum_{j \in N(i)} I_{ji} = 0 \ \ for\ all\ the\ nodes \\ Internal\ equations\ of\ \ all\ devices \end{cases}, \tag{7.2}$$

where N(i) is the set of component connected to node i. In the equations above, all the currents are substituted with the appropriate equation from the component SCAQCF model yielding a set of equations in terms of the state and control variables only. This is a

synthesis procedure that combines the validated real-time model with high fidelity of all the components extracted from the DDSE.

$h_{min} \leqslant h(\mathbf{x}, \mathbf{u}) \leqslant h_{max}$ represents the operating constraints, which include the upper and lower bounds of the voltage magnitudes at each bus of the system and capacity constraints of transmission lines and transformers. For each node i of the system, the voltage constraints can be quadratized as:

$$\left(V_{mag}^{\min}\right)^2 \le V_{j,r}^2(t_k) + V_{j,i}^2(t_k) \le \left(V_{mag}^{\max}\right)^2, \; for \quad j = 1, 2, \cdots, N. \tag{7.3}$$

For each line or transformer in the system, the capacity constraint can be extracted from the SCAQCF component model as

$$\left(I_{mag}^{\min}\right)^2 \le \left\{ \begin{array}{l} \sum_i \sum_j Y_{eqx,i}^{2k} x_i x_j + \sum_i \sum_j Y_{eqx,i}^{2k+1} x_i x_j - \sum_i Y_{eqx,i}^{2k} B_{eq,2k} x_i \\ -\sum_i Y_{eqx,i}^{2k+1} B_{eq,2k+1} x_i + B_{eq,2k}^2 + B_{eq,2k+1}^2 \end{array} \right\} \le \left(I_{mag}^{\max}\right)^2, \tag{7.4}$$

where the subscript k represents the terminal k of the SCAQCF component model and $Y_{eq,x,i}^{2k}$ represents the i-th element of the 2k-th row of the matrix $Y_{eq,x}$ and so on.

The main advantage of the utilization of the proposed SCAQCF model is that it enables the automatic synthesis of the OPF problem as well as its solution. Any new component added to the system will be automatically accounted in the optimization as long as its model is presented in the SCAQCF syntax. Also note that by virtue of the quadratic structure of the SCAQCF model, all analytics of the optimization problem are in terms of quadratic equations.

7.3 Solution Algorithm

7.3.1 Introduction

The solution method for the OPF problem is based on interior point method and the flow chart of the algorithm is given in Figure 7.1. At the beginning the algorithm gives an artificial feasible arbitrary state ($\mathbf{x}^o$, $\mathbf{u}^o$, $\mathbf{I}_m{}^o$). The values of mismatch variables are obtained by substituting the values of the state and control variables into the power flow equations. After that the algorithm defines a reduced-size optimization problem through the following steps: first, substitute all mismatch variables by one control variable v; second, start with an empty initial operational constraint set and add constraints adaptively. Subsequently, the algorithm converts the OPF to a linearized optimization problem only with respect to the control variables using the co-state method [89]. The constraints contain operational constraints while the control variables are limited by their physical bounds. The algorithm then obtains the updated values of the control variables using interior point method and the updated values of the state variables by solving the power flow. If some modeled operation constraints are violated, the b vector will be updated in the linearized optimization problem and the previous solution is retrieved. If some other constraints are violated, the algorithm adds these constraints, retrieves the previous solution, and linearizes the new constraints. If mismatch variables are nonzero, the next iteration starts and variables may be reclassified.

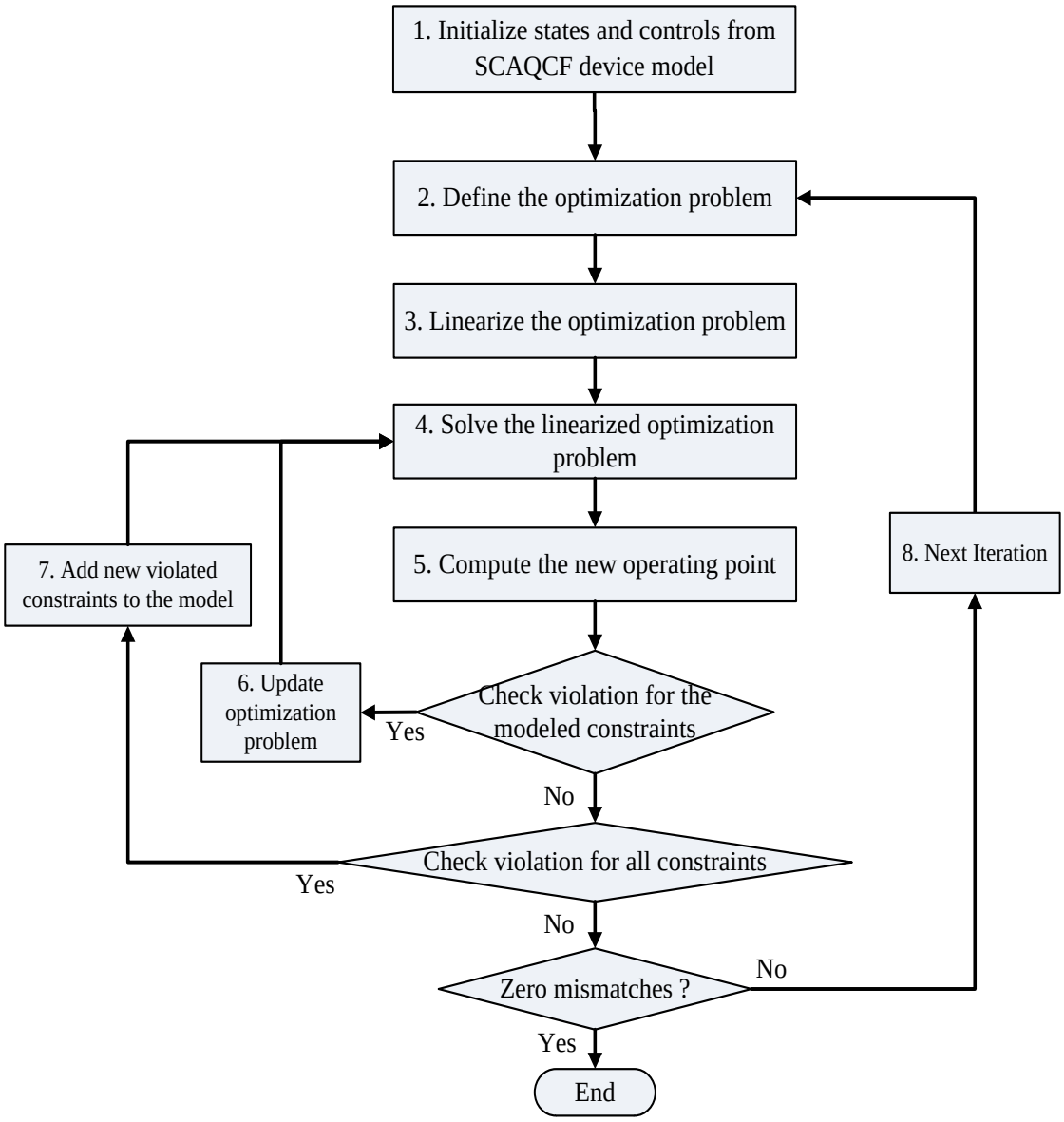

Figure 7.1. Flow chart of the proposed OPF solution algorithm.

The proposed algorithm for solving the OPF problem is robust and highly efficient. Robustness means the algorithm can provide a solution for any system. The algorithm starts from an infeasible optimal state and moves to the feasible region while maintaining optimality. System feasibility is maintained by introducing artificial mismatch current sources at each bus. At each iteration, the mismatches reduce while the optimization

method ensures the solution is optimal at each iteration. If the feasible solution is found, it is optimal; otherwise, the algorithm returns a suboptimal point, providing the best choice to solve system infeasibility by a set of remedial actions. High efficiency means fast convergence speed. First, the algorithm models OPF as a quadratic problem for fast convergence. Second, the algorithm reduces the size of the original optimization problem by two approaches: (1) identifying the active constraints and only adding the active constraint set to the optimization problem; (2) eliminating all the power flow equality constraints of the original optimization problem during the linearization procedure, since the linearization uses the co-state method [89] and the power flow equations are implicitly included in the linearization.

Section 7.3.2 to Section 7.3.7 give the details for each step of the proposed algorithm.

7.3.2 Initialization

The initialization procedure includes the following tasks: (1) classification of the state variables and control variables, (2) initialization of the values of the state variables and control variables, (3) computation of the mismatch variables $\mathbf{I}_m^o$, and (4) selection of the operation constraints.

The classification of control variables and state variables for each device is defined in the SCAQCF model. The system synthesizes the state variables and control variables by scanning each device in an autonomous manner, as discussed in Section 7.2. The initial values of state variables **x** and control variables **u** are also defined in the SCAQCF model. Note that based on these initial values, the system maybe infeasible, and mismatch values are calculated using power flow equations **g**(**x**, **u**) from the arbitrarily given states and

controls described above. The initial operational constraints include real and reactive power constraints of the slack bus generator.

7.3.3 Define the Reduced Optimization problem

To reduce the size of the problem, two methods are applied in this step: (1) mismatch variables are replaced by one control variable v, $\mathbf{I}_m = (1\text{-}v)\ \mathbf{I}_m^o$ ($v \in [0,1]$), where $\mathbf{I}_m^o$ represents the mismatch values in the current iteration, and (2) the high dimensional power flow equality constraints are eliminated at this step, since the co-state linearization methodology considers the power flow equations implicitly, which will be described in details in Section 7.3.4. It is emphasized here that the power flow conditions are actually sustained in the proposed algorithm, since once interior point method provides the updated values of the control variables, the system states will be solved through power flow equations based on the updated control variables, as Figure 7.1 illustrates.

Based on the above discussion, the reduced-size optimization problem derived from equation set (7.1) is as follows:

$$\begin{aligned} &\min\ f(\mathbf{x},\mathbf{u}) = \mu(1-v)\sum\left|\mathbf{I}_m^o\right| + c(\mathbf{x},\mathbf{u}), \\ &s.t. \\ &\quad \mathbf{h}^{\min} \le \mathbf{h}(\mathbf{x},\mathbf{u}) \le \mathbf{h}^{\max}, \\ &\quad \mathbf{u}^{\min} \le \mathbf{u} \le \mathbf{u}^{\max}, \end{aligned} \tag{7.5}$$

where $\mathbf{h}^{\min} \le \mathbf{h}(\mathbf{x}, \mathbf{u}) \le \mathbf{h}^{\max}$ is the operational constraint set in the current iteration.

7.3.4 Form the Linearized Optimization Problem

In this step, the algorithm eliminates state variables in the defined problem (7.5) and the problem is re-casted in terms of only control variables. This is achieved by linearization whereby all functions/quantities are expressed as linear combinations of control variables with co-state method [89]. Following subsections present formulas to linearize the objective function and operational constraints.

The linearized form of the cost function $f(\mathbf{x}, \mathbf{u})$ is

$$f(\mathbf{x},\mathbf{u}) = f(\mathbf{x}^o,\mathbf{u}^o) + \left.\frac{\partial f(\mathbf{x}^o,\mathbf{u}^o)}{\partial \mathbf{u}}\right|_{\mathbf{g}(\mathbf{x},\mathbf{u},v)=0} \cdot \Delta\mathbf{u} + o(\Delta\mathbf{u}), \tag{7.6}$$

where

$$\left.\frac{f(\mathbf{x}^o,\mathbf{u}^o)}{\partial \mathbf{u}}\right|_{\mathbf{g}(\mathbf{x},\mathbf{u},v)=0} = \frac{f(\mathbf{x}^o,\mathbf{u}^o)}{\partial \mathbf{u}} - \frac{f(\mathbf{x}^o,\mathbf{u}^o)}{\partial \mathbf{x}}\left(\frac{\partial \mathbf{g}(\mathbf{x}^o,\mathbf{u}^o)}{\partial \mathbf{x}}\right)^{-1}\frac{\partial \mathbf{g}(\mathbf{x}^o,\mathbf{u}^o)}{\partial \mathbf{u}}$$, and $\mathbf{g}(\mathbf{x},\mathbf{u},v) = 0$ is the set of power flow equations described by equation (7.2).

The linearized form of the operation constraints $h(\mathbf{x}, \mathbf{u})$ is

$$h(\mathbf{x},\mathbf{u}) = h(\mathbf{x}^o,\mathbf{u}^o) + \left.\frac{\partial h(\mathbf{x}^o,\mathbf{u}^o)}{\partial \mathbf{u}}\right|_{\mathbf{g}(\mathbf{x},\mathbf{u},v)=0} \cdot \Delta\mathbf{u} + \left.\frac{\partial h(\mathbf{x}^o,\mathbf{u}^o)}{\partial v}\right|_{\mathbf{g}(\mathbf{x},\mathbf{u},v)=0} \cdot v + o(\Delta\mathbf{u}) + o(v), \tag{7.7}$$

where

$$\left.\frac{\partial h(\mathbf{x}^o,\mathbf{u}^o)}{\partial \mathbf{u}}\right|_{\mathbf{g}(\mathbf{x},\mathbf{u},v)=0} = \frac{\partial h(\mathbf{x}^o,\mathbf{u}^o)}{\partial \mathbf{u}} - \frac{\partial h(\mathbf{x}^o,\mathbf{u}^o)}{\partial \mathbf{x}}\left(\frac{\partial \mathbf{g}(\mathbf{x}^o,\mathbf{u}^o,0)}{\partial \mathbf{x}}\right)^{-1}\frac{\partial \mathbf{g}(\mathbf{x}^o,\mathbf{u}^o,0)}{\partial \mathbf{u}}$$ and

$$\left.\frac{\partial h(\mathbf{x}^o,\mathbf{u}^o)}{\partial v}\right|_{\mathbf{g}(\mathbf{x},\mathbf{u},v)=0} = \frac{\partial h(\mathbf{x}^o,\mathbf{u}^o)}{\partial v} - \frac{\partial h(\mathbf{x}^o,\mathbf{u}^o)}{\partial \mathbf{x}}\left(\frac{\partial \mathbf{g}(\mathbf{x}^o,\mathbf{u}^o,0)}{\partial \mathbf{x}}\right)^{-1}\frac{\partial \mathbf{g}(\mathbf{x}^o,\mathbf{u}^o,0)}{\partial v}.$$

The linearized optimization problem is obtained via substituting these equations into the problem in equation set (7.5) and ignoring high order items:

$$\min\ \mu(1-v)\sum_{k=1}^{N}|\mathbf{I}_m^o| + c(\mathbf{x}^o,\mathbf{u}^o) + \left.\frac{\partial c(\mathbf{x}^o,\mathbf{u}^o)}{\partial \mathbf{u}}\right|_{\mathbf{g}(\mathbf{x},\mathbf{u},v)=0}\cdot\Delta\mathbf{u},$$

s.t.

$$\Delta\mathbf{h}^{\min} \le \left.\frac{\partial \mathbf{h}(\mathbf{x}^o,\mathbf{u}^o)}{\partial v}\right|_{\mathbf{g}(\mathbf{x},\mathbf{u},v)=0}\cdot v + \left.\frac{\partial \mathbf{h}(\mathbf{x}^o,\mathbf{u}^o)}{\partial \mathbf{u}}\right|_{\mathbf{g}(\mathbf{x},\mathbf{u},v)=0}\cdot\Delta\mathbf{u} \le \Delta\mathbf{h}^{\max}, \qquad (7.8)$$

$$\Delta\mathbf{u}^{\min} \le \Delta\mathbf{u} \le \Delta\mathbf{u}^{\max},$$

$$0 \le v \le v^{\max},$$

where $\Delta\mathbf{h}^{\min} = \mathbf{h}^{\min} - \mathbf{h}(\mathbf{x}^o, \mathbf{u}^o)$ and $\Delta\mathbf{h}^{\max} = \mathbf{h}^{\max} - \mathbf{h}(\mathbf{x}^o, \mathbf{u}^o)$ are the lower and upper bounds of operational constraints in the linearized problem.

7.3.5 Solve the System

This step includes two sub-steps (1) solving the linearized optimization problem defined by equation set (7.8), and (2) solving the power flow problem defined by equation set (7.2).

The solution of the linearized optimization problem is obtained by interior point method, which is a standard algorithm for the linear optimization problem. The solution of the linearized optimization problem gives v and $\Delta\mathbf{u}$. Based on the obtained mismatch variable and control variables v and $\Delta\mathbf{u}$, the control variables and mismatch variables can be computed as

$$\mathbf{u} = \mathbf{u}^o + \Delta\mathbf{u},$$

$$\mathbf{I}_m = (1\text{-}v)\mathbf{I}_m^o, \qquad (7.9)$$

$$\Delta\mathbf{I}_m = -v\mathbf{I}_m^o.$$

Once the updated values of the control variables and mismatch variables are obtained via equation set (7.9), the state variables **x** can be obtained by applying the Newton-

Raphson method on the power flow equations (7.2), assuming the control variables have the fixed values defined by the equation set (7.9).

7.3.6 Check the Violations of the Constraints

Modeled constraints defined in the equation set (7.5) are checked at the new operation point based on the updated values of the state variables and control variables obtained by applying the methodology described in Section 7.3.5. Some modeled operational constraints may be out of their bounds, as a results of the linearization error, especially for those constraints reaching upper or lower bounds in the linearized optimization problem. These violations are small, since linearization errors are limited in a small region.

If any modeled constraint is not satisfied, its corresponding constant item ***b*** in the linearized optimization problem will be updated, the previous solution will be retrieved, and the updated linearized optimization problem and the power flow problem will be resolved again.

The new value of *b* for an upper bound constraint is [89]

$$\begin{cases} \Delta h^{\max}, & \text{if } h(\mathbf{x},\mathbf{u}) \le h^{\max} \text{ is not violated}; \\ \Delta h^{\max} - [h(\mathbf{x},\mathbf{u}) - h^{\max}] & \\ -\left\{ \Delta h^{\max} - \sum_{u_i \in \mathbf{u}} \left[\Delta u_i \left(\left. \frac{\partial \mathbf{h}(\mathbf{x}^o,\mathbf{u}^o)}{\partial \mathbf{u}} \right|_{\mathbf{g}(\mathbf{x},\mathbf{u},v)=0} \right) \right] - v \cdot \left. \frac{\partial \mathbf{h}(\mathbf{x}^o,\mathbf{u}^o)}{\partial v} \right|_{\mathbf{g}(\mathbf{x},\mathbf{u},v)=0} \right\}. & \\ \text{if } h(\mathbf{x},\mathbf{u}) \le h^{\max} \text{ is violated}. \end{cases} \tag{7.10}$$

The new value of *b* for a lower bound constraint is [89]

$$
\begin{cases}
\Delta h^{\min}, & \text{if } h^{\min} \le h(\mathbf{x},\mathbf{u}) \text{ is not violated};\\
\Delta h^{\min} + [h^{\min} - h(\mathbf{x},\mathbf{u})] & \\
+\left\{ \Delta h^{\min} - \sum_{u_i \in \mathbf{u}} \left[\Delta u_i \left(\left. \frac{\partial \mathbf{h}(\mathbf{x}^o,\mathbf{u}^o)}{\partial \mathbf{u}} \right|_{\mathbf{g}(\mathbf{x},\mathbf{u},v)=0} \right) \right] - v \cdot \left. \frac{\partial \mathbf{h}(\mathbf{x}^o,\mathbf{u}^o)}{\partial v} \right|_{\mathbf{g}(\mathbf{x},\mathbf{u},v)=0} \right\}. & \\
\qquad\qquad \text{if } h^{\min} \le h(\mathbf{x},\mathbf{u}) \text{ is violated}.
\end{cases}
\tag{7.11}
$$

Once the modeled constraints defined in the equation set (7.5) are all satisfied, the algorithm will check the un-modeled constraints that are not defined in the equation set (7.5) but are included in the equation set (7.1). Since the linearized problem does not include all operational constraints, the power flow solution may not satisfy some un-modeled operational constraints. If these violated un-modeled constraints exist, the algorithm adds these violated constraints to the equation set (7.5), retrieves the previous operating point ($\mathbf{x}^o$, $\mathbf{u}^o$, $\mathbf{I}_m{}^o$), linearizes the new constraints, and solves the updated linearized optimization problem and power flow problem.

7.3.7 Procedure for the Next Iteration

At the end of the current iteration, all the constraints are satisfied and the algorithm will check the values of the mismatch values. If all mismatches of the vector $\mathbf{I}_m$ are zero, the optimal solution is found; otherwise, the algorithm stores the current operating point and process to the next iteration.

Power flow may fail to converge after one iteration time or give a solution with very large violations at some state variables, while the system has a valid power flow solution indeed. This usually occurs when the moving ranges of control variables are too large. Using smaller range can avoid this circumstance, but will reduce the converge speed of the

algorithm. Sometimes reclassifying state and control variables is another option to solve these power flow violations.

If the reactive power output of a generator at a PV bus is far out of its bound, the algorithm will change the bus type to PQ mode. That is, Q_g becomes a control variable and V_{mag} becomes a state variable. On the other hand, if the voltage magnitude at a PQ bus is far out of its bound, the algorithm will change the bus type to PV mode. That is, V_{mag} becomes a control variable and Q_g becomes a state variable.

7.4 Object-oriented Implementation

It is emphasized that the object-oriented SCAQCF component model enables the solution for the OPF problem, autonomously, regardless of different types and features of the components in the system. Here one specific computational task of the OPF is presented as an example: the task of linearization of the OPF problem. First both the objective function and the constraints of the OPF problem can be expressed in the following generic quadratic form (these equations are provided by the SCAQCF):

$$J(\mathbf{x},\mathbf{u}) = A_J \cdot \mathbf{x} + \mathbf{x}^T \cdot B_J \cdot \mathbf{x} + D_J \cdot \mathbf{u} + \mathbf{u}^T \cdot E_J \cdot \mathbf{u} + \mathbf{x}^T \cdot F_J \cdot \mathbf{u} + c, \tag{7.12}$$

where A_J, B_J, D_J, E_J, and F_J represent the linear part of state, quadratic part of state, linear part of control variable, quadratic part of control variable, and quadratic part of state and control variable, respectively. The co-state method is used here to eliminate the state variables for both the objective function and the constraints, and to re-cast the optimization problem, which is expressed only in terms of control variables linearly [89]. The formula to compute the coefficients of all control variables is as follows:

$$\frac{dJ(\mathbf{x}^o,\mathbf{u}^o)}{d\mathbf{u}} = \frac{\partial J(\mathbf{x}^o,\mathbf{u}^o)}{\partial \mathbf{u}} - \hat{\mathbf{x}}^T \frac{\partial \mathbf{g}(\mathbf{x}^o,\mathbf{u}^o)}{\partial \mathbf{u}},$$
$$\text{where} \quad \hat{\mathbf{x}}^T = \frac{\partial J_k(\mathbf{x}^o,\mathbf{u}^o)}{\partial \mathbf{x}} \left(\frac{\partial \mathbf{g}(\mathbf{x}^o,\mathbf{u}^o)}{\partial \mathbf{x}} \right)^{-1}. \tag{7.13}$$

Based on the SCAQCF model and the form of the object function and constraint, each term in equation set (7.13) is automatically computed as follows:

$$\begin{aligned}
\frac{\partial \mathbf{g}(\mathbf{x}^o,\mathbf{u}^o)}{\partial \mathbf{u}} &= Y_{equ} + \left\{\mathbf{u}^{o,T} F_{equ,i}\right\} + \left\{\left(F_{equ,i}\mathbf{u}^o\right)^T\right\} + \left\{\mathbf{x}^{o,T} F_{eqxu,i}\right\}, \\
\frac{\partial J(\mathbf{x}^o,\mathbf{u}^o)}{\partial \mathbf{x}} &= A_J + \mathbf{x}^{o,T} \cdot B_J + \left(B_J \cdot \mathbf{x}^o\right)^T + \left(F_J \cdot \mathbf{u}^o\right)^T, \\
\frac{\partial J(\mathbf{x}^o,\mathbf{u}^o)}{\partial \mathbf{u}} &= D_J + \mathbf{u}^{o,T} \cdot E_J + \left(E_J \cdot \mathbf{u}^o\right)^T + \mathbf{x}^{o,T} \cdot F_J, \\
\frac{\partial \mathbf{g}(\mathbf{x}^o,\mathbf{u}^o)}{\partial \mathbf{x}} &= Y_{eqx} + \left\{\mathbf{x}^{o,T} F_{eqx,i}\right\} + \left\{\left(F_{eqx,i}\mathbf{x}^o\right)^T\right\} + \left\{\left(F_{eqxu,i}\mathbf{u}^o\right)^T\right\}.
\end{aligned} \tag{7.14}$$

7.5 OPF Demonstrative Results

7.5.1 Three-Bus Test Case

In this section, the proposed OPF algorithm is demonstrated on a three-bus system of three generating units, three step-up transformers, one tap-change transformer and three overhead transmission lines as illustrated in Figure 7.2. The objective function is the total operational cost of generators, and the operational constraints include the voltage magnitude limitations and the capacity limitations of generators, transmission lines, and transformers. The generator operational cost is expressed as $f(P_k)=a_{kj} + b_{k,j}P_{k,} + c_{k,j}P_{k,}^2$ where P_k is the active power of the kth generator and a, b, c are the coefficients from reference [92]. The parameters of the generators are given in Table 7.1, and the parameters of other components are given in Table 7.2.

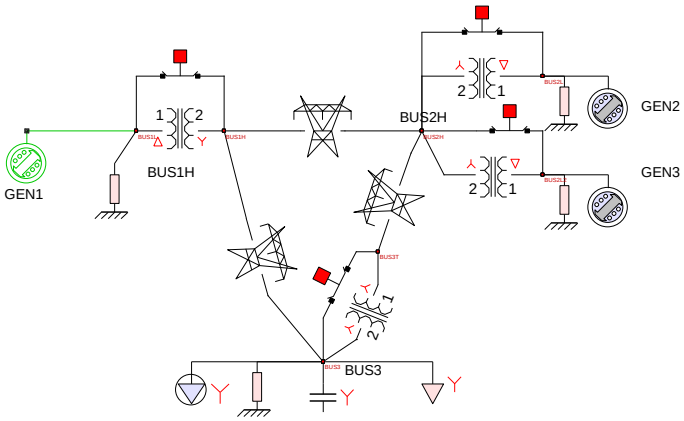

Figure 7.2. Single-line diagram of three-bus system.

Table 7.1. Generator parameters of test system.

	Mode	**a**	**b**	**c**	**Pmax (MW)**	**Pmin (MW)**	**Qmax (MVA)**	**Qmin (MVA)**
Unit #1	SLACK	102	12	0.01	150	11	75	-50
Unit #2	PQ	95	13	0.01	75	8	35	-25
Unit #3	PV	180	12	0.01	150	15	70	-40

Table 7.2. Other test system parameters.

Step-up XFMR	150MVA	z=0.001+j0.1 pu	18 kV/115kV
Tap XFMR	150MVA	z=0.001+j0.1 pu	115 kV/115kV
Transmission Line 1		z=0.074+0.578 pu	115 kV
Transmission Line 1		z=0.094+0.743 pu	115 kV
Transmission Line 3		z=0.059+0.463 pu	115 kV
Load - Constant Power		S=2+j0.58pu	115 kV
Load – Constant Impedance		S=0.2+j0.1 pu	115 kV
Common S_{base}=100 MVA			

At the beginning, the total mismatch of the power conservation equations is 87.67. The proposed algorithm uses four iterations to reduce the total mismatch to zero and reaches the optimal solution. Table 7.3 lists the total operational cost of three generators, the total mismatch, and the values of the control variables of the generators and the tap-changeable transformer at each iteration.

Table 7.3. Details of the OPF at each iteration.

Iter #	Operation Cost	Mis-match	Control Variables
1	3618.43	65.752	Slack Gen: V=0.9589 pu; XFMR tap ratio =1.04; PV Gen: P= 50.29 MW, V=1.03 pu ; PQ Gen: P= 75 MW, Q=21.79 MW.
2	3552.58	43.833	Slack Gen: V=1.0418 pu; XFMR tap ratio =0.98; PV Gen: P= 15 MW, V=0.95 pu ; PQ Gen: P= 75 MW, Q=21.60 MW.
3	3554.62	21.917	Slack Gen: V=1.048 pu; XFMR tap ratio =1.0; PV Gen: P= 15 MW, V=0.97 pu ; PQ Gen: P= 75 MW, Q=35 MW.
4	3470.58	0.0	Slack Gen: V=1.049 pu; XFMR tap ratio =1.01; PV Gen: P= 15 MW, V=0.98 pu ; PQ Gen: P= 75 MW, Q=35 MW.

7.5.2 RTS-79 System Test Case

The RTS-79 system is originally from the paper [90] and also the zone 1 in the paper [91] shown in Figure 7.3. This system has 24 buses and 2 voltage levels, 138kV and 230kV connected through tap-control transformers.

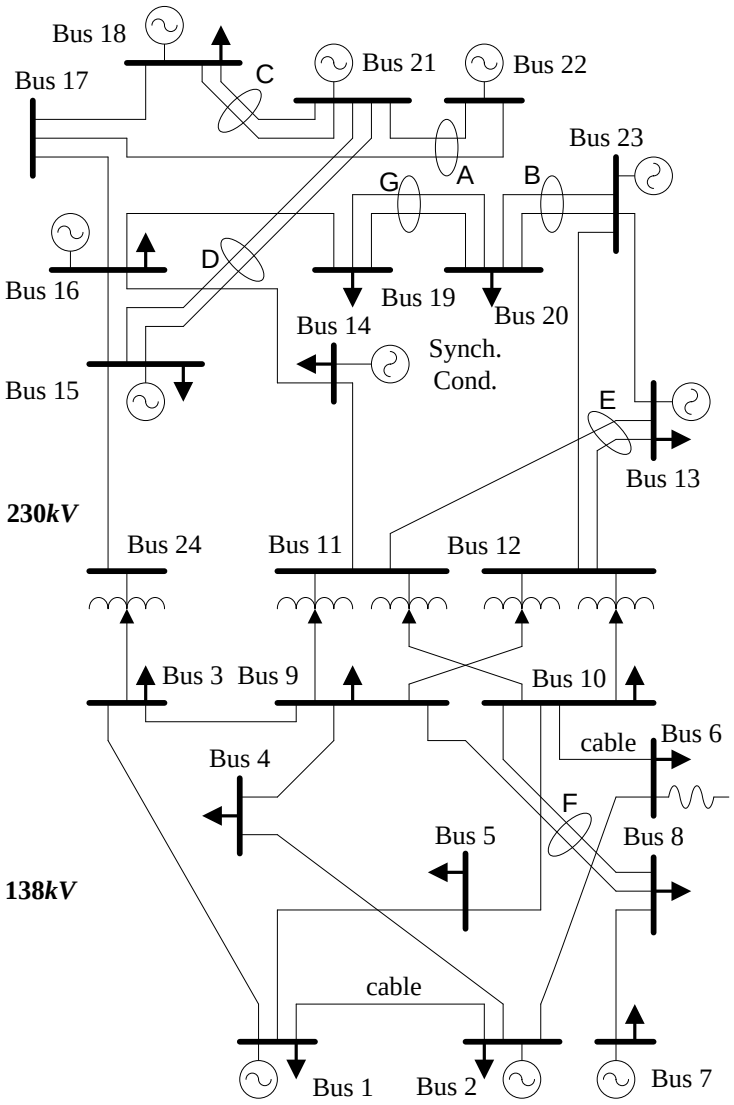

Figure 7.3. Single-line diagram of IEEE RTS-79 system.

Paper [92] gives the modified version of the IEEE RTS-79 system in a three-phase, breaker-oriented, and substation represented manner. Since the OPF methodology proposed in the dissertation handles with three-phase generator model and transformer model, the dissertation chooses the three-phase RTS-79 system described in paper [92] as the test system. Figure 7.4 gives the single-line diagram of this three-phase, breaker-oriented RTS-79 system. The generator parameters are obtained from Table 3 in [92]. The transmission line parameters are obtained from Table 4 in [92].

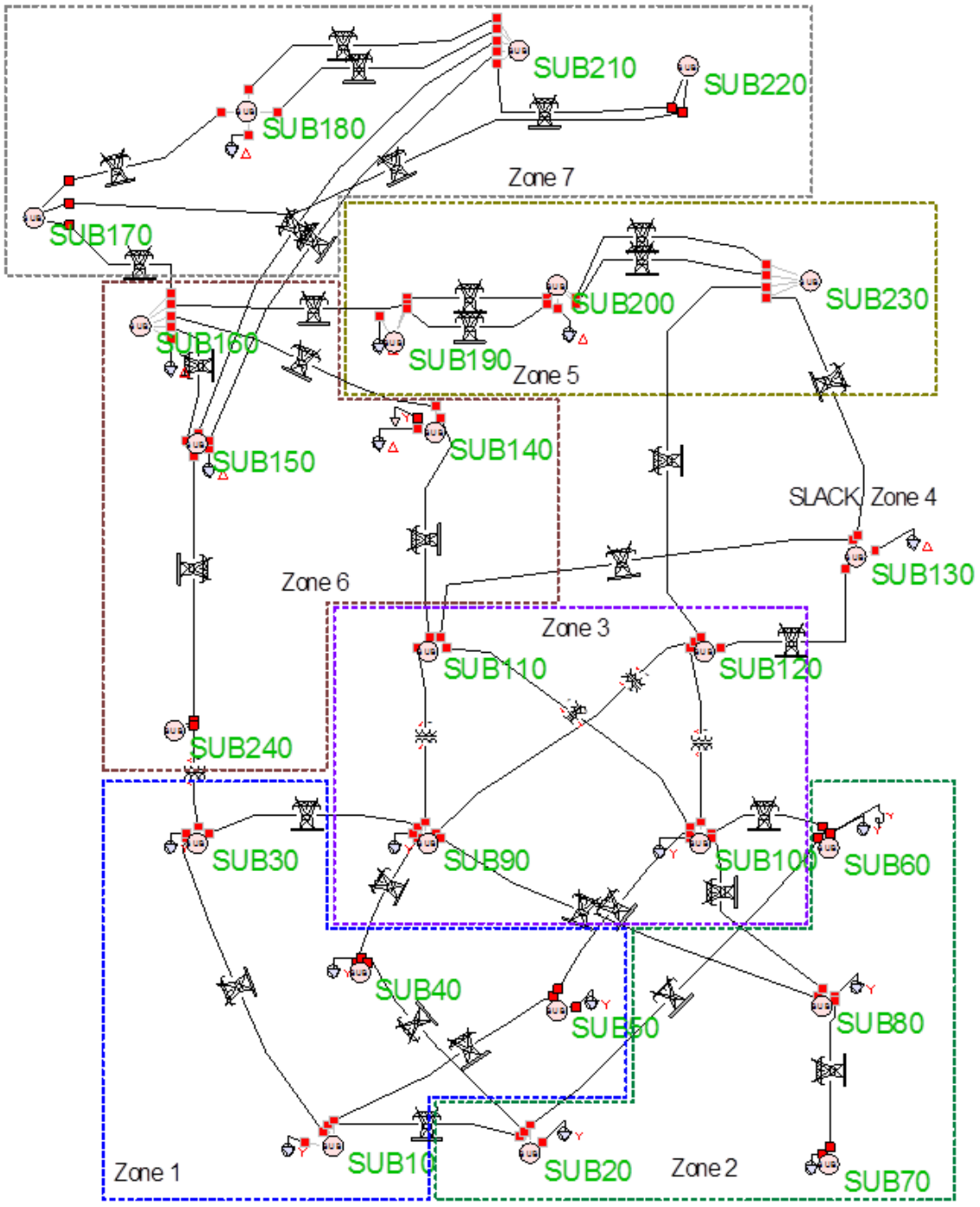

Figure 7.4. Single-line diagram of three-phase RTS-79 system.

The OPF algorithm successfully reduces the mismatch variables of the three-phase RTS-79 system to zero in 5 iterations. The penalty factor μ is set to 10^7. Bus voltages are limited between 0.95*pu* and 1.05*pu*. Figure 7.5 shows the sum of the absolute values of the mismatches of each power flow equations, $\sum \left| \mathbf{I}_m^o \right|$, in the equation set (7.2). From Figure 7.5, it is shown that the mismatches are reduced adaptively at each iteration. Figure 7.6 shows the generation cost of the system at each iteration.

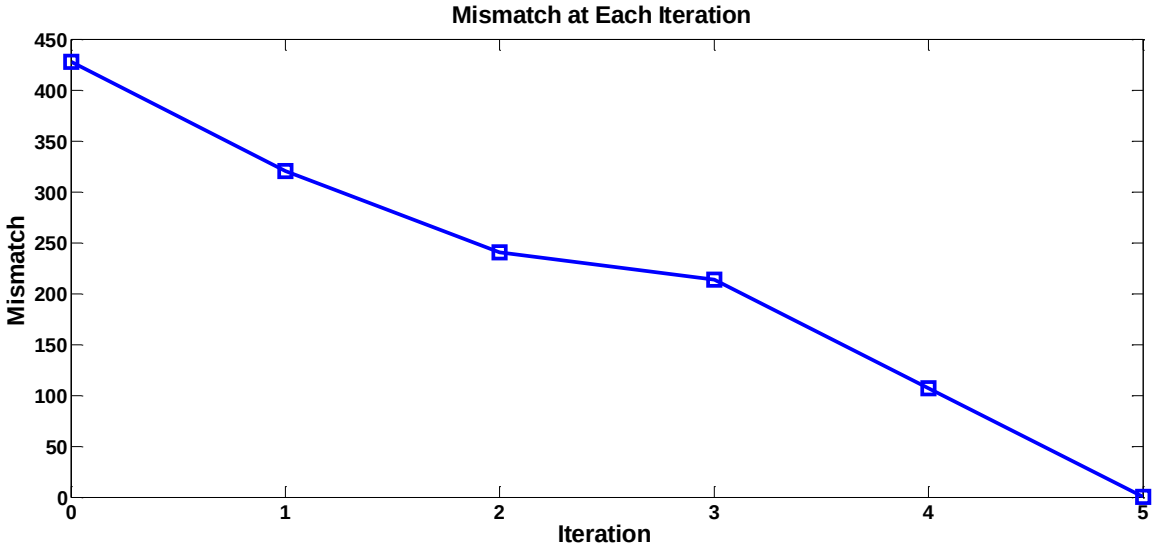

Figure 7.5. Mismatch at each iteration for the RTS-79 system.

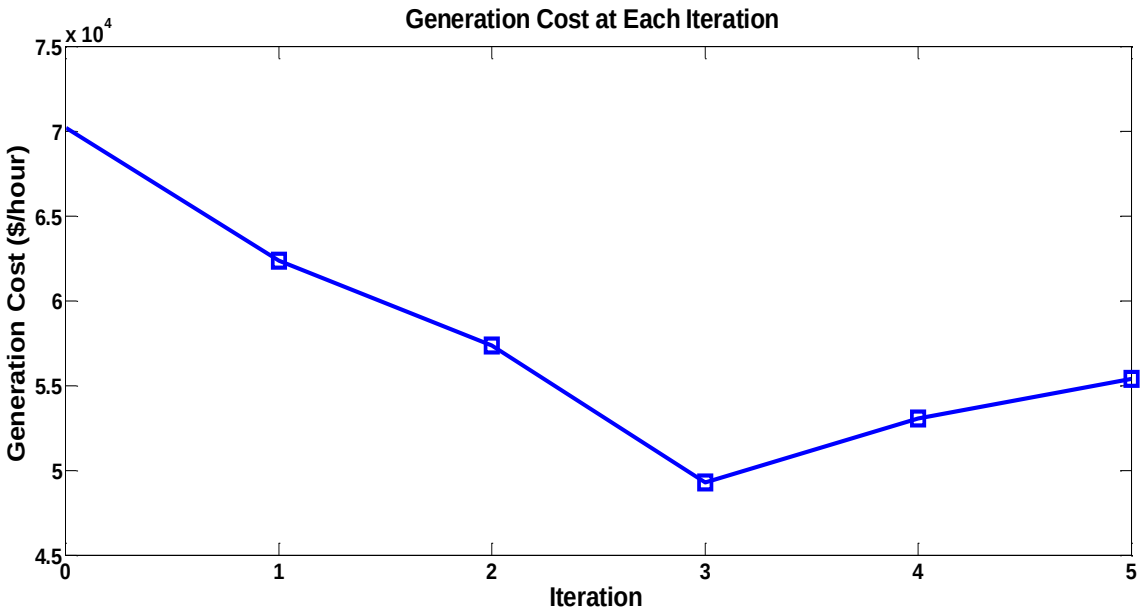

Figure 7.6. Generation cost at each iteration for the RTS-79 system.

The three-phase RTS-79 system has 33 transmission lines, 33 generators, 33 step up transformers for the generators, and four 138 kV to 230 kV transformers. The total number of effective nodes in the system is 266, and the total number of current conservation equations (power flow equations) of the system is 441. For a traditional OPF problem, if the OPF problem includes all the power flow constraints, voltage magnitude constraints at each node, and the operation constraints for all the power components (the capacity constraints (thermal constraints) for the transmission lines and transformers, the real power and reactive power constraints for the slack bus generator, the reactive power constraints for the PV mode generator, and the real power constraints for the PQ mode generator), the total number of the constraints for the OPF problem is 881. Table 7.4 lists the active constraints added into the LP problem at each iteration for the proposed OPF algorithm implemented in the three-phase RTS-79 system. The numbers of active constraints modeled and added at each iteration are 25, 8, 1, 8, and 0, respectively. Compared with the

traditional OPF problem formulation, the proposed algorithm reduced the constraints in the LP problem by 96% in average, which raises the computation efficiency for the solution of the LP problem, since the dimension of the LP problem is reduced dramatically. This validates the proposed algorithm has a high efficiency.

Table 7.4. Active constraints at each iteration.

#	**Operation Constraints**
1	Slack bus generator P constraint; Slack bus generator Q constraint; Voltage Mag at node BUS10-1_B; Voltage Mag at node BUS130-G2_B Voltage Mag at node BUS220_A; Voltage Mag at node BUS220_B Voltage Mag at node BUS220_C; Voltage Mag at node BUS70-G1_B Voltage Mag at node BUS70_A; Voltage Mag at node BUS70_B Voltage Mag at node BUS70_C; Voltage Mag at node BUS80_A Voltage Mag at node BUS80_B; Voltage Mag at node BUS80_C Voltage Mag at node BUS230_A; Voltage Mag at node BUS130-G2_A Voltage Mag at node BUS190_ A; Voltage Mag at node BUS190_B Voltage Mag at node BUS200_A; Voltage Mag at node BUS200_B Voltage Mag at node BUS200_C; Voltage Mag at node BUS200_A Voltage Mag at node BUS230_B; Voltage Mag at node BUS230_C Voltage Mag at node BUS180_C
2	Voltage Mag at node BUS110_A; Voltage Mag at node BUS110_C Voltage Mag at node BUS110_B; Voltage Mag at node BUS50_B Voltage Mag at node BUS100_A; Voltage Mag at node BUS100_C Voltage Mag at node BUS50_A; Voltage Mag at node BUS50_C
3	Generator at BUS180_G Q constraint
4	Generator at BUS160_G Q constraint; Generator at BUS150_G Q constraint Voltage Mag at node BUS160_A; Voltage Mag at node BUS160_B Voltage Mag at node BUS160_C; Voltage Mag at node BUS140_A

	Voltage Mag at node BUS140_B; Voltage Mag at node BUS140_C
5	0

Table 7.5 through Table 7.9 list the values of some of the key control variables of the system at each iteration, provided by the LP solution.

Table 7.5. Control variables at the first iteration.

Control Variable	Value (p.u.)	Lower Bound (p.u.)	Upper Bound (p.u.)
Mismatch Control v	0.250000	0.000000	0.250000
P of Generator at Bus 230	0.516895	0.100000	1.000000
V of Generator at Bus 230	1.016933	0.950000	1.050000
P of Generator at Bus 160	0.851612	0.296703	1.000000
V of Generator at Bus 160	0.950021	0.950000	1.050000
P of Generator at Bus 180	0.999943	0.100000	1.000000
V of Generator at Bus 180	0.961947	0.950000	1.050000
P of Generator at Bus 210	0.999989	0.100000	1.000000
V of Generator at Bus 210	0.950007	0.950000	1.050000
P of Generator at Bus 220	0.280151	0.100000	1.000000

V of Generator at Bus 220	1.006281	0.950000	1.050000
P of Generator at Bus 150	0.109143	0.109091	1.000000
V of Generator at Bus 150	1.000130	0.950000	1.050000
V of Generator at Bus 130	1.046074	0.950000	1.050000
P of Generator at Bus 10	0.999765	0.080000	1.000000
V of Generator at Bus 10	0.983012	0.950000	1.050000
P of Generator at Bus 20	0.108121	0.108108	1.000000
V of Generator at Bus 20	0.950600	0.950000	1.050000
P of Generator at Bus 70	0.221568	0.075000	1.000000
V of Generator at Bus 70	0.950022	0.950000	1.050000

Table 7.6. Control variables at the second iteration.

Control Variable	Value (p.u.)	Lower Bound (p.u.)	Upper Bound (p.u.)
Mismatch Control v	0.250000	0.000000	0.333333
P of Generator at Bus 230	0.205583	0.100000	1.000000
V of Generator at Bus 230	0.954580	0.950000	1.050000

P of Generator at Bus 160	0.851612	0.296703	1.000000
V of Generator at Bus 160	0.951213	0.950000	1.050000
P of Generator at Bus 180	0.999897	0.100000	1.000000
V of Generator at Bus 180	1.049967	0.950000	1.050000
P of Generator at Bus 210	0.950000	0.100000	1.000000
V of Generator at Bus 210	0.950007	0.950000	1.050000
P of Generator at Bus 220	0.280151	0.100000	1.000000
V of Generator at Bus 220	0.953209	0.950000	1.050000
P of Generator at Bus 150	0.209133	0.109091	1.000000
V of Generator at Bus 150	0.952371	0.950000	1.050000
V of Generator at Bus 130	0.972631	0.950000	1.050000
P of Generator at Bus 10	0.984539	0.080000	1.000000
V of Generator at Bus 10	0.993012	0.950000	1.050000
P of Generator at Bus 20	0.108108	0.108108	1.000000
V of Generator at Bus 20	1.050000	0.950000	1.050000
P of Generator at Bus 70	0.812038	0.075000	1.000000

V of Generator at Bus 70	1.047829	0.950000	1.050000

Table 7.7. Control variables at the third iteration.

Control Variable	Value (p.u.)	Lower Bound (p.u.)	Upper Bound (p.u.)
Mismatch Control v	0.333333	0.000000	0.333333
P of Generator at Bus 230	0.216743	0.100000	1.000000
V of Generator at Bus 230	0.954501	0.950000	1.050000
P of Generator at Bus 160	0.851648	0.296703	1.000000
V of Generator at Bus 160	0.958945	0.950000	1.050000
P of Generator at Bus 180	0.999879	0.100000	1.000000
V of Generator at Bus 180	0.990631	0.950000	1.050000
P of Generator at Bus 210	0.999989	0.100000	1.000000
V of Generator at Bus 210	0.950007	0.950000	1.050000
P of Generator at Bus 220	0.180151	0.100000	1.000000
V of Generator at Bus 220	0.953151	0.950000	1.050000
P of Generator at Bus 150	0.109091	0.109091	1.000000

V of Generator at Bus 150	0.952443	0.950000	1.050000
V of Generator at Bus 130	0.975957	0.950000	1.050000
P of Generator at Bus 10	1.000000	0.080000	1.000000
V of Generator at Bus 10	0.950000	0.950000	1.050000
P of Generator at Bus 20	0.108108	0.108108	1.000000
V of Generator at Bus 20	1.050000	0.950000	1.050000
P of Generator at Bus 70	0.790153	0.075000	1.000000
V of Generator at Bus 70	1.043561	0.950000	1.050000

Table 7.8. Control variables at the fourth iteration.

Control Variable	Value (p.u.)	Lower Bound (p.u.)	Upper Bound (p.u.)
Mismatch Control v	0.500000	0.000000	0.500000
P of Generator at Bus 230	0.287650	0.100000	1.000000
V of Generator at Bus 230	0.951829	0.950000	1.050000
P of Generator at Bus 160	0.851648	0.296703	1.000000
V of Generator at Bus 160	1.005022	0.950000	1.050000

P of Generator at Bus 180	1.000000	0.100000	1.000000
V of Generator at Bus 180	1.017651	0.950000	1.050000
P of Generator at Bus 210	1.000000	0.100000	1.000000
V of Generator at Bus 210	0.992774	0.950000	1.050000
P of Generator at Bus 220	0.370151	0.100000	1.000000
V of Generator at Bus 220	0.951422	0.950000	1.050000
P of Generator at Bus 150	0.109091	0.109091	1.000000
V of Generator at Bus 150	1.033624	0.950000	1.050000
V of Generator at Bus 130	0.974351	0.950000	1.050000
P of Generator at Bus 10	1.000000	0.080000	1.000000
V of Generator at Bus 10	1.050000	0.950000	1.050000
P of Generator at Bus 20	0.108108	0.108108	1.000000
V of Generator at Bus 20	1.050000	0.950000	1.050000
P of Generator at Bus 70	0.874474	0.075000	1.000000
V of Generator at Bus 70	1.047405	0.950000	1.050000

Table 7.9. Control variables at the fifth iteration.

Control Variable	Value (p.u.)	Lower Bound (p.u.)	Upper Bound (p.u.)
Mismatch Control v	1.000000	0.000000	1.000000
P of Generator at Bus 230	0.100235	0.100000	1.000000
V of Generator at Bus 230	1.040765	0.950000	1.050000
P of Generator at Bus 160	0.851627	0.296703	1.000000
V of Generator at Bus 160	1.027116	0.950000	1.050000
P of Generator at Bus 180	0.999939	0.100000	1.000000
V of Generator at Bus 180	1.032585	0.950000	1.050000
P of Generator at Bus 210	0.999989	0.100000	1.000000
V of Generator at Bus 210	1.018077	0.950000	1.050000
P of Generator at Bus 220	0.100129	0.100000	1.000000
V of Generator at Bus 220	0.951013	0.950000	1.050000
P of Generator at Bus 150	0.798645	0.109091	1.000000
V of Generator at Bus 150	1.048702	0.950000	1.050000
V of Generator at Bus 130	0.953654	0.950000	1.050000
P of Generator at Bus 10	0.999980	0.080000	1.000000

V of Generator at Bus 10	1.049968	0.950000	1.050000
P of Generator at Bus 20	0.108624	0.108108	1.000000
V of Generator at Bus 20	1.049973	0.950000	1.050000
P of Generator at Bus 70	0.918317	0.075000	1.000000
V of Generator at Bus 70	1.047544	0.950000	1.050000

7.6 Summary

This chapter presented a highly-efficient and robust OPF algorithm. The algorithm is based on the object-oriented SCAQCF component model which enables the autonomous formulation and solution of the OPF problem.

Robustness means the algorithm can provide a solution for any problem – if a solution exists, it is the optimal, and if a solution does not exist, it will provide the closest possible solution. This algorithm starts from an infeasible optimal stage and moves to the feasible region while maintaining optimality. System infeasibility is described in terms of artificial mismatch current sources at each bus. These mismatches are reduced iteratively while the method ensures the solution is optimal at each iteration. When the mismatches are reduced to zero, the feasible solution is found, and it is optimal; otherwise, the algorithm returns a suboptimal point, providing the best choice for the condition by translating the mismatches into a set of remedial actions.

High efficiency means a less runtime compared with traditional solution methods for the OPF problem. First, the algorithm models the OPF problem as a quadratic problem for

fast convergence. In other words, the formulated optimization problem is a quadratic optimization problem. Second, the algorithm identifies the active constraints gradually and adds them to the modeled constraint set if needed. For example, operational constraints are added when they are violated in the previous iteration, and mismatch variables are represented by one control variable. These features of the algorithm ensure that at each iteration, the dimensionality of the problem is the smallest possible for the specific power system.

CHAPTER 8 CONCLUSION AND FUTURE WORK DIRECTION

8.1 Conclusion

The main contributions of this dissertation include: (1) an infrastructure of data acquisition systems that provide the necessary information for an automated EMS system enabling autonomous distributed state estimation, model validation, simplified protection, and seamless integration of other EMS applications, (2) an object-oriented, interoperable, and unified component model that can be seamlessly integrated with a variety of applications of the EMS, (3) a distributed dynamic state estimator (DDSE) that can be performed at the substation level using existing data acquisition systems and the object-oriented, interoperable, and unified component model, (4) a physically-based synchronous machine model, which is expressed in terms of the actual self and mutual inductances of the synchronous machine windings as a function of rotor position, for the purpose of synchronous machine parameters identification, and (5) a robust and highly efficient algorithm for the optimal power flow (OPF) problem, one of the most important applications of the EMS, based on the validated states and models of the power system provided by the DDSE.

In particular, it has been proposed and implemented a distributed and seamless infrastructure of data acquisition systems that provided the necessary information for an automated and interoperable EMS system. At the lower level (relay level), a dynamic state estimation is performed for each single component in the substation separately. The distributed dynamic state estimation provides the real-time dynamic model of the

component as well as the real-time operating conditions. By using GPS synchronized measurements, the real-time model is time tagged with GPS accuracy. Next, the real-time model of substation is autonomously created by combining the real-time models of all the components in the substation and interconnecting lines of the same time tag. This process is referred as the substation level state estimation. The substation state model is send to the control center where the real-time model of the entire system is also autonomously created by combining the real-time model of all substations of the same time tag. The system-wide real-time model can be utilized by any EMS application seamlessly.

To guarantee that the system-wide real-time model can be used across all the EMS applications and across all relevant temporal and spatial scales, an object-oriented, unified, and seamless interoperable component model syntax is proposed and referred as the state and control algebraic quadratic companion form (SCAQCF). This can be viewed as an advanced common information model. Applications can directly access and use this model without any filters or interfaces (seamless). To illustrate the implementation of this methodology, examples of the derivation of the SCAQCF model for the synchronous machine in the full-time domain and the phasor domain are presented in the dissertation respectively.

The DDSE plays an essential role in the proposed modern EMS architecture. The DDSE is performed for each single component in the substation by utilizing only local measurements available from PMUs, relays, and FDRs in the substation only, thus avoiding all issues associated with transmission of data and associated time latencies. This approach enables very fast DDSE update rate. Two formulations of the proposed DDSE are presented. The first one, referred to as DDSE-Q, is used to capture with high fidelity the

electromechanical dynamics of the system. The second one, referred to as DDSE-T, is used to capture both electromechanical and electrical transients. The approach utilizes the SCAQCF model of the components, in order to implement the DDSE algorithm in an object-oriented manner and improve the convergence of the algorithm. Moreover, the SCAQCF model is a three-phase, asymmetric and breaker oriented power system model in order to account for system imbalances, asymmetries and topology changes. The object-oriented formulation of the DDSE is emphasized which is one of the key characteristics in the implementation of the DDSE towards its very fast execution rates. Demonstration results for the DDSE-T, DDSE-Q, and the bad data identification are given to illustrate the effectiveness of the proposed DDSE methodology.

Modeling accuracy and fidelity are fundamental in this DDSE approach. For many power system components, high-fidelity models exist. For some new components such as inverter-interfaced power components, the modeling accuracy may not be as high as that of other components. In both cases the DDSE can be utilized to fine tune the models and/or determine the parameters of the model with great accuracy. The basic approach is to expand the dynamic state estimator to include some key parameters as unknown states to be estimated. Therefore the proposed modern EMS architecture can also provide better models with field-validated parameters compared with traditional approaches. The dissertation provides an example of this kind of model parameters identification for a synchronous machine.

The field-validated real-time model of the system with SCAQCF syntax can be seamlessly integrated with a variety of other applications of EMS. One of the important applications of the EMS, the optimization of grid operation conditions, is discussed in the

dissertation. The optimization of grid operation conditions can be formulated as an OPF problem with different objective functions and constraints. The dissertation presented the autonomous formulation of the OPF problem and its solution methodology by simply integrating the object-oriented SCAQCF component model. The solution methodology is robust and highly efficient with the help of a number of innovations that control the size of the optimization problem and using sparsity methods. Demonstration results for different test systems are given in the dissertation to validate the robustness and high efficiency of the proposed method.

8.2 Future Work Directions

The relay level DDSE (DDSE-T) provides a novel dynamic state estimation based protection scheme. The basic idea is to continuously implement the DDSE-T using a detailed SCAQCF model of a single component (protection zone) under normal operation conditions. By checking the confidence level of the DDSE-T, which reflects how well the measurements fit with the component model under normal operation conditions, whether the component under monitoring suffers from internal fault can be determined. If the confidence level is high, the component is under normal operation, while if the confidence level is low, the component is under abnormal operations (fault curers inside the component). The advantage of this dynamic state estimation based protection scheme is that there is no need to know the information for the rest of the system, and no coordination of the settings of the relays is required. The dynamic state estimation based protection can be further developed to address many more power system issues. The ability of the dynamic state estimation to validate the model of the protection zone as well as the ability to be

extended into parameter state estimation opens up the possibility of using the relays as the gatekeeper of the models of the various components of the system, validating the models continuously and adjusting the model parameters as necessary. Then the relay can provide the validated models to other entities in the operation of the power system for any application that requires validated models.

The demonstrated methods in this thesis can be pivotal for the integration of renewable sources (wind, solar etc.) and of storage devices into the grid. This integration will increase the complexity of the system but on the same time allows for the implementation of control and optimization schemes that can coordinate the operation of the non-dispatchable units with the bulk power system with the objective being the maximization of the utilization of the available resources but on the same time improve the operation and reliability of the system. Maximum utilization of these resources requires fast and accurate monitoring and control for the purpose of continuous coordination and optimization of the system. Towards this goal, the SCAQCF based OPF can be extended to include the models of the renewables, and will enable new approaches for control, operation and protection of systems with high penetration of renewables.

The proposed EMS infrastructure in the dissertation could enable a cyber-physical modeling and simulation approach for situational awareness of the power system. This approach can be achieved by detecting adversarial data and commands at the protective relay level via context-based authentication procedures: (1) capture commands, (2) determine the effect of the captured commands on power system using real-time model and faster than real-time simulation, and (3) authenticate or block the commands based on the faster than real-time simulation results. While the context-based authentication approach

is not new, the work presented in this thesis will make the authentication procedure very fast, which is a key requirement for the success of context-based authentication approach. The detailed real-time model provided by the proposed EMS infrastructure in the thesis enables the fast evaluation of future system operating conditions and contingencies as will be affected by the execution of a command through simulation of the system. Because of the distributed nature of the methodologies proposed in this thesis, this simulation will be performed faster than real time and the effect of the command will be known in a very short time. Any adverse effects will be quantified and this can form the basis for authentication or blocking of the command. The critical issue is the ability to perform this analysis in a short time so that the delay of the execution of the command will not generate any concerns. This simulation integrates the distributed state estimator with intrusion detection and validation of control commands to assess the impact of potentially maliciously altered commands on the system. Because this kind of simulation is performed at the substation level (distributed) using high end computers, it can be performed "faster than real time" to identify possible future vulnerabilities before they occur. Intrusion sensors can be placed at the station and process buses in the substation to intercept command messages and analyze the effect of these commands on the performance of the system.

PUBLICATIONS

1. A. P. Meliopoulos, G. Cokkinides, R. Huang, E. Farantatos, S. Choi, Y. Lee and X. Yu, "Smart Grid Technologies for Automomous Operation and Control", *IEEE Trans. Smart Grid*, Vol. 2, No. 1, 2011.

2. A. P. Meliopoulos, E. Polymeneas, Z. Tan, R. Huang, and D. Zhao, " Advanced Distribution Management System ", *IEEE Trans. Smart Grid*, Vol. 4, No. 4, 2013.

3. A. P. Meliopoulos, R. Huang, G. Cokkinides, "Distributed State Estimation Based Energy Management System ", *IEEE Trans. Smart Grid* (under second round review).

4. A. P. Meliopoulos, R. Huang, G. Cokkinides, "Distribution System Distributed Dynamic State Estimator ", *IEEE Trans. Smart Grid* (under second round review).

5. E. Farantatos, R. Huang, A. P. Meliopoulos, G. Cokkinides, "A Transient Stability Monitoring Scheme Enabled by a Distributed Dynamic State Estimator ", *IEEE Trans. Power System* (under second round review).

6. E. Farantatos, R. Huang, A. P. Meliopoulos, G. Cokkinides, "A Predictive Generator Out-of-Step Protection Scheme Enabled by a Distributed Dynamic State Estimator ", *IEEE Trans. Power System* (under second round review).

7. R. Huang, E. Farantatos, G. Cokkinides, and A. P. Meliopoulos, "Substation Based Dynamic State Estimator - Numerical Experiments", *Proceedings of the IEEE-PES 2010 T&D Conference*, New Orleans, LA, April 19-22, 2010

8. A.P Meliopoulos, G. Cokkinides, R. Huang, E. Farantatos, S. Choi, Y. Lee , "Wide Area Dynamic Monitoring and Stability Controls," in *Proc. IREP Symposium 2010, Bulk Power System Dynamics and Control VIII*, Buzios, Brazil, Aug. 2010.

9. R. Huang, E. Farantatos, G. Cokkinides, and A. P. Meliopoulos, " Object-Oriented 3-Phase Distributed Dynamic State Estimator", *Proceedings of the IEEE-PES 2011 General Meeting*, Detroit, MI, July 24-28, 2011.

10. E. Farantatos, R. Huang, G. Cokkinides, and A. P. Meliopoulos, "A Predictive Out-of-Step Protection Scheme based on PMU enabled Dynamic State Estimation," *Proceedings of the IEEE-PES 2011 General Meeting*, Detroit, MI, July 24-28, 2011.

11. E. Farantatos, R. Huang, G. Cokkinides and A. P. Meliopoulos, "Implementation of a 3-Phase State Estimation Tool Suitable for Advanced Distribution Management Systems," *Proceedings of the IEEE 2011 Power Systems Conference & Exposition*, Phoenix, AZ, Mar. 2011.

12. A. P Meliopoulos, G. Cokkinides, R. Huang, E. Farantatos, S. Choi, Y. Lee, and X. Yu, "Smart Grid Infrastructure for Distribution Systems and Applications," in *Proc. 44th Annual Hawaii Int. Conf. System Sciences (HICSS)*, Koloa, Kauai, Hawaii, Jan. 2011.

13. A. P. Meliopoulos, G. Cokkinides, S.Choi, E. Farantatos, R. Huang and Y. Lee, "Symbolic integration and autonomous state estimation: Building blocks for an intelligent power grid", *in Proc. 16th International Conference on Intelligent System Applications to Power Systems (ISAP)*, Hersonissos, Crete, Greece, Sept. 25-28, 2011

14. R. Huang, E. Farantatos, G. Cokkinides, and A. P. Meliopoulos, "Impact of Non-Dispatchable Renewables and Generator Cycling and Control via a Hierarchical Control Scheme", *Proceedings of the IEEE T&D Conference*, Orlando, FL, May, 2012.

15. R. Huang, E. Farantatos, G. Cokkinides, and A. P. Meliopoulos, "Advanced Disturbance Recording and Playback enabled by a Distributed Dynamic State Estimation Including Bad Data Detection and Topology Change Identification", *Proceedings of the IEEE-PES 2012 General Meeting*, San Diego, CA, July 23-27, 2012.

16. A. P. Meliopoulos, E. Farantatos, R. Huang, Y. Cho, E. Polymeneas, Z. Tan and G. Cokkinides, "Methodology for Monitoring, Control and Operation of Power Systems with Wind Farms", *Proceedings of the IEEE-PES 2012 General Meeting*, San Diego, CA, July 23-27, 2012.

17. A. P Meliopoulos, G. Cokkinides, R. Huang, and E. Farantatos, “Integrated Smart Grid Hierarchical Control”, *in Proc. 45th Annual Hawaii International Conference on System Sciences (HICSS)*, Grand Wailea, Maui, Hawaii, Jan. 4-7, 2012

18. F. Cai, E. Farantatos, R. Huang, A.P. Meliopoulos, J. Papapolymerou, “Self-powered Smart Meter with Synchronized Data”, *in Proc. 2012 IEEE Radio and Wireless Week*, Santa Clara, CA, Jan. 15-18, 2012

19. R. Huang, E. Polymeneas, G. Cokkinides, and A. P. Meliopoulos, “Autonomous Optimal Power Flow via Object Orientation”, *Proceedings of the 17th Interbnational Conference on Intelligent System Applications to Power Systems (ISAP)*, pp 1-7, Tokyo Japan, July 1-4, 2013.

20. R. Huang, E. Farantatos, G. Cokkinides and A. P. Meliopoulos, "Physical Parameters Identification of Synchronous Generators by a Dynamic State Estimator", *Proceedings of the IEEE-PES 2013 General Meeting*, Vancouver, CN, July, 2013

21. E. Farantatos, R. Huang, G. Cokkinides and A. P. Meliopoulos, " A Novel Scheme for Real-Time Power System Dynamic Equivalencing With Respect to the System Center of Oscillations Provided by a PMU-Based Dynamic State Estimator ", *Proceedings of the IEEE-PES 2013 General Meeting*, Vancouver, CN, July, 2013

22. A. P. Meliopoulos, G. J. Cokkinides, S. Grijalva, R. Huang, E. Polymeneas, Paul Myrda, and Mel Gehrs, “Integration & Automation: From Protection to Advanced Energy Management Systems”, *Proceedings of the 2013 IREP Symposium on Bulk Power System Dynamics and Control*, Rethymnon, Greece, Aug. 25-30, 2013.

23. A. P. Meliopoulos, R. Huang, E. Polymeneas, and Paul Myrda, “Grid Modernization: Seamless Integration of Protection, Optimization & Control”, *in Proc. 47th Annual Hawaii International Conference on System Sciences (HICSS)*, Hawaii, HI, Jan. 6-9, 2014.

APPENDICES

Appendix A: Quadratic Integration

Quadratic integration method is a numerical integration method that assumes that time domain functions vary quadratically within the integration time step. This assumption is illustrated in Figure A.1. Note that the three points, $x(t-h)$, x_m and $x(t)$ fully define the quadratic function in the interval $[t-h, t]$. The method is an implicit numerical integration method (it can be easily observed that it makes use of information at the unknown point $x(t)$) and therefore demonstrates the desired advanced numerical stability properties compared to explicit methods.

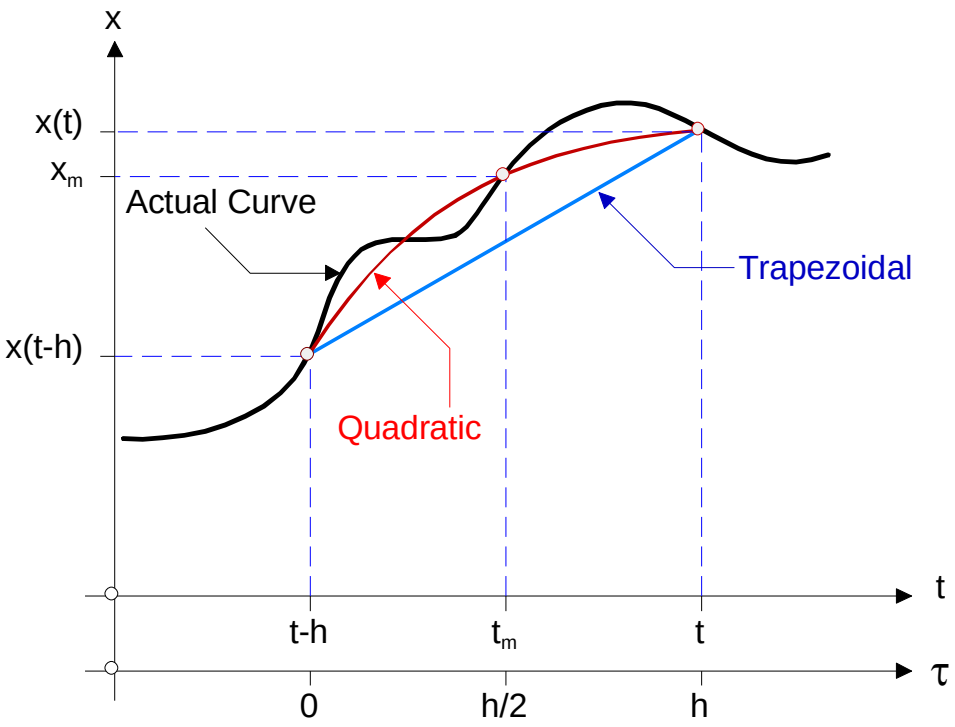

FigureA.1. The quadratic integration method.

The general integration results are listed as follows,

Integration over time interval $[t-h, t_m]$:

$$\int_{t-h}^{t_m} x(\tau)d\tau = \frac{5h}{24}x(t-h) + \frac{h}{3}x_m - \frac{h}{24}x(t)$$

(A.1)

Integration over time interval $[t-h, t]$:

$$\int_{t-h}^{t} x(\tau)d\tau = \frac{h}{6}x(t-h) + \frac{2h}{3}x_m + \frac{h}{6}x(t) \qquad \text{(A.2)}$$

Integration over time interval $t_m, t]$:

$$\int_{t_m}^{t} x(\tau)d\tau = -\frac{h}{24}x(t-h) + \frac{h}{3}x_m + \frac{5h}{24}x(t) \qquad \text{(A.3)}$$

Appendix B: Generator Model with SCAQCF Syntax for OPF

B.1 Generators – PQ Mode– Compact Form

The PQ control mode forces the real and reactive power output of the generator to the user specified values P and Q. The model equations are as follows:

$$\tilde{I}_a = (g + jb)(\tilde{V}_a - \tilde{V}_n - \tilde{E}_a), \tag{B.1}$$

$$\tilde{I}_b = (g + jb)(\tilde{V}_b - \tilde{V}_n - \tilde{E}_b), \tag{B.2}$$

$$\tilde{I}_c = (g + jb)(\tilde{V}_c - \tilde{V}_n - \tilde{E}_c), \tag{B.3}$$

$$\tilde{I}_n = (g + jb)(-\tilde{V}_a - \tilde{V}_b - \tilde{V}_c + 3\tilde{V}_n), \tag{B.4}$$

$$\mathrm{Re}\left\{\tilde{V}_a\tilde{I}_a^* + \tilde{V}_b\tilde{I}_b^* + \tilde{V}_c\tilde{I}_c^*\right\} = -P_{sg}\ , \tag{B.5}$$

$$\mathrm{Im}\left\{\tilde{V}_a\tilde{I}_a^* + \tilde{V}_b\tilde{I}_b^* + \tilde{V}_c\tilde{I}_c^*\right\} = -Q_{sg}\ . \tag{B.6}$$

The operation constraints are:

$$\begin{aligned} &P_{sg}^2 + Q_{sg}^2 \le S_{\max} \\ &P_{\min} \le P_{sg} \le P_{\max} \\ &Q_{\min} \le Q_{sg} \le Q_{\max} \end{aligned} \tag{B.7}$$

where

$$g = -\frac{R}{R^2 + \omega^2 L^2},\ b = -\frac{\omega L}{R^2 + \omega^2 L^2},$$

and

$$\tilde{E}_a = Ee^{j\delta},\ \tilde{E}_b = Ee^{j(\delta - \frac{2\pi}{3})},\ \text{and}\ \tilde{E}_c = Ee^{j(\delta - \frac{4\pi}{3})}.$$

B.2 Generators – PQ Mode–Quadratized Form

State Variables: $\mathbf{x} = \left[V_{ar},\ V_{ai},\ V_{br},\ V_{bi},\ V_{cr},\ V_{ci},\ V_{nr},\ V_{ni},\ E_r,\ E_i \right]$

Control Variables: $\mathbf{u} = \left[P_{sg},\ Q_{sg} \right]$

$$I_{ar} = gV_{ar} - bV_{ai} - gV_{nr} + bV_{ni} - gE_r + bE_i \tag{B.8}$$

$$I_{ai} = bV_{ar} + gV_{ai} - gV_{ni} - bV_{nr} - gE_i - bE_r \tag{B.9}$$

$$I_{br} = gV_{br} - bV_{bi} - gV_{nr} + bV_{ni} + \left(\frac{1}{2}g - \frac{\sqrt{3}}{2}b \right) E_r + \left(-\frac{\sqrt{3}}{2}g - \frac{1}{2}b \right) E_i \tag{B.10}$$

$$I_{bi} = bV_{br} + gV_{bi} - bV_{nr} - gV_{ni} + \left(\frac{\sqrt{3}}{2}g + \frac{1}{2}b \right) E_r + \left(\frac{1}{2}g - \frac{\sqrt{3}}{2}b \right) E_i \tag{B.11}$$

$$I_{cr} = gV_{cr} - bV_{ci} - gV_{nr} + bV_{ni} + \left(\frac{1}{2}g + \frac{\sqrt{3}}{2}b \right) E_r + \left(\frac{\sqrt{3}}{2}g - \frac{1}{2}b \right) E_i \tag{B.12}$$

$$I_{ci} = bV_{cr} + gV_{ci} - bV_{nr} - gV_{ni} + \left(-\frac{\sqrt{3}}{2}g + \frac{1}{2}b \right) E_r + \left(\frac{1}{2}g + \frac{\sqrt{3}}{2}b \right) E_i \tag{B.13}$$

$$I_{nr} = -gV_{ar} + bV_{ai} - gV_{br} + bV_{bi} - gV_{cr} + bV_{ci} + 3gV_{nr} - 3bV_{ni} \tag{B.14}$$

$$I_{nr} = -bV_{ar} - gV_{ai} - bV_{br} - gV_{bi} - bV_{cr} - gV_{ci} + 3bV_{nr} + 3gV_{ni} \tag{B.15}$$

$$
\begin{aligned}
0 = {} & gV_{ar}{}^2 - gV_{ar}V_{nr} + bV_{ar}V_{ni} - gV_{ar}E_r + bV_{ar}E_i \\
& + gV_{ai}{}^2 - bV_{ai}V_{nr} - gV_{ai}V_{ni} - bV_{ai}E_r - gV_{ai}E_i \\
& + gV_{br}{}^2 - gV_{br}V_{nr} + bV_{br}V_{ni} + \left(\frac{1}{2}g - \frac{\sqrt{3}}{2}b\right)V_{br}E_r + \left(-\frac{\sqrt{3}}{2}g - \frac{1}{2}b\right)V_{br}E_i \\
& + gV_{bi}{}^2 - bV_{bi}V_{nr} - gV_{bi}V_{ni} + \left(\frac{\sqrt{3}}{2}g + \frac{1}{2}b\right)V_{bi}E_r + \left(\frac{1}{2}g - \frac{\sqrt{3}}{2}b\right)V_{bi}E_i \\
& + gV_{cr}{}^2 - gV_{cr}V_{nr} + bV_{cr}V_{ni} + \left(\frac{1}{2}g + \frac{\sqrt{3}}{2}b\right)V_{cr}E_r + \left(\frac{\sqrt{3}}{2}g - \frac{1}{2}b\right)V_{cr}E_i \\
& + gV_{ci}{}^2 - bV_{ci}V_{nr} - gV_{ci}V_{ni} + \left(\frac{1}{2}b - \frac{\sqrt{3}}{2}g\right)V_{ci}E_r + \left(\frac{1}{2}g + \frac{\sqrt{3}}{2}b\right)V_{ci}E_i + \{P_{sg}\}
\end{aligned}
$$

(B.16)

$$
\begin{aligned}
0 = {} & -bV_{ar}{}^2 + gV_{ar}V_{ni} + bV_{ar}V_{nr} + gV_{ar}E_i + bV_{ar}E_r \\
& - bV_{ai}{}^2 - gV_{ai}V_{nr} + bV_{ai}V_{ni} - gV_{ai}E_r + bV_{ai}E_i \\
& - bV_{br}{}^2 + bV_{br}V_{nr} + gV_{br}V_{ni} + \left(-\frac{\sqrt{3}}{2}g - \frac{1}{2}b\right)V_{br}E_r + \left(-\frac{1}{2}g + \frac{\sqrt{3}}{2}b\right)V_{br}E_i \\
& - bV_{bi}{}^2 - gV_{bi}V_{nr} + bV_{bi}V_{ni} + \left(\frac{1}{2}g - \frac{\sqrt{3}}{2}b\right)V_{bi}E_r + \left(-\frac{\sqrt{3}}{2}g - \frac{1}{2}b\right)V_{bi}E_i \\
& - bV_{cr}{}^2 + bV_{cr}V_{nr} + gV_{cr}V_{ni} + \left(\frac{\sqrt{3}}{2}g - \frac{1}{2}b\right)V_{cr}E_r + \left(-\frac{1}{2}g - \frac{\sqrt{3}}{2}b\right)V_{cr}E_i \\
& - bV_{ci}{}^2 - gV_{ci}V_{nr} + bV_{ci}V_{ni} + \left(\frac{1}{2}g + \frac{\sqrt{3}}{2}b\right)V_{ci}E_r + \left(\frac{\sqrt{3}}{2}g - \frac{1}{2}b\right)V_{ci}E_i + \{Q_{sg}\}
\end{aligned}
$$

(B.17)

$$
\begin{aligned}
& \left\{P_{sg}^2 + Q_{sg}^2\right\} \le S_{\max} \\
& P_{\min} \le \{P_{sg}\} \le P_{\max} \\
& Q_{\min} \le \{Q_{sg}\} \le Q_{\max}
\end{aligned}
$$

(B.18)

B.3 Generators – PV Mode – Compact Form

The PV control mode forces the real power output to the user specified value of P, and the line to line voltage (phases A, B) to the user specified value . The model equations are as follows:

$$\tilde{I}_a = (g + jb)(\tilde{V}_a - \tilde{V}_n - \tilde{E}_a), \quad \text{(B.19)}$$

$$\tilde{I}_b = (g + jb)(\tilde{V}_b - \tilde{V}_n - \tilde{E}_b), \quad \text{(B.20)}$$

$$\tilde{I}_c = (g + jb)(\tilde{V}_c - \tilde{V}_n - \tilde{E}_c), \quad \text{(B.21)}$$

$$\tilde{I}_n = (g + jb)(-\tilde{V}_a - \tilde{V}_b - \tilde{V}_c + 3\tilde{V}_n), \quad \text{(B.22)}$$

$$\mathrm{Re}\left\{\tilde{V}_a \tilde{I}_a^* + \tilde{V}_b \tilde{I}_b^* + \tilde{V}_c \tilde{I}_c^*\right\} = -P_{sg}, \quad \text{(B.23)}$$

$$\left|\tilde{V}_a - \tilde{V}_b\right| = V_{sg}. \quad \text{(B.24)}$$

The operation constraints are

$$P_{\min} \le P_{sg} \le P_{\max}$$
$$V_{\min} \le V_{sg} \le V_{\max} \quad \text{(B.25)}$$

Where $g = -\dfrac{R}{R^2 + \omega^2 L^2}$, $b = -\dfrac{\omega L}{R^2 + \omega^2 L^2}$,

and $\tilde{E}_a = Ee^{j\delta}$, $\tilde{E}_b = Ee^{j(\delta - \frac{2\pi}{3})}$, $\tilde{E}_c = Ee^{j(\delta - \frac{4\pi}{3})}$.

B.4 Generators – PV Mode – Quadratized Form

State Variables: $\mathbf{x} = \left[V_{ar},\ V_{ai},\ V_{br},\ V_{bi},\ V_{cr},\ V_{ci},\ V_{nr},\ V_{ni},\ E_r,\ E_i\right]$

Control Variables: $\mathbf{u} = \left[P_{sg},\ V_{sg} \right]$

$$I_{ar} = gV_{ar} - bV_{ai} - gV_{nr} + bV_{ni} - gE_r + bE_i \tag{B.26}$$

$$I_{ai} = bV_{ar} + gV_{ai} - gV_{ni} - bV_{nr} - gE_i - bE_r \tag{B.27}$$

$$I_{br} = gV_{br} - bV_{bi} - gV_{nr} + bV_{ni} + \left(\frac{1}{2}g - \frac{\sqrt{3}}{2}b \right) E_r + \left(-\frac{\sqrt{3}}{2}g - \frac{1}{2}b \right) E_i \tag{B.28}$$

$$I_{bi} = bV_{br} + gV_{bi} - bV_{nr} - gV_{ni} + \left(\frac{\sqrt{3}}{2}g + \frac{1}{2}b \right) E_r + \left(\frac{1}{2}g - \frac{\sqrt{3}}{2}b \right) E_i \tag{B.29}$$

$$I_{cr} = gV_{cr} - bV_{ci} - gV_{nr} + bV_{ni} + \left(\frac{1}{2}g + \frac{\sqrt{3}}{2}b \right) E_r + \left(\frac{\sqrt{3}}{2}g - \frac{1}{2}b \right) E_i \tag{B.30}$$

$$I_{ci} = bV_{cr} + gV_{ci} - bV_{nr} - gV_{ni} + \left(-\frac{\sqrt{3}}{2}g + \frac{1}{2}b \right) E_r + \left(\frac{1}{2}g + \frac{\sqrt{3}}{2}b \right) E_i \tag{B.31}$$

$$I_{nr} = -gV_{ar} + bV_{ai} - gV_{br} + bV_{bi} - gV_{cr} + bV_{ci} + 3gV_{nr} - 3bV_{ni} \tag{B.32}$$

$$I_{nr} = -bV_{ar} - gV_{ai} - bV_{br} - gV_{bi} - bV_{cr} - gV_{ci} + 3bV_{nr} + 3gV_{ni} \tag{B.33}$$

$$\begin{aligned}
0 = {} & gV_{ar}^{\,2} - gV_{ar}V_{nr} + bV_{ar}V_{ni} - gV_{ar}E_r + bV_{ar}E_i \\
& + gV_{ai}^{\,2} - bV_{ai}V_{nr} - gV_{ai}V_{ni} - bV_{ai}E_r - gV_{ai}E_i \\
& + gV_{br}^{\,2} - gV_{br}V_{nr} + bV_{br}V_{ni} + \left(\frac{1}{2}g - \frac{\sqrt{3}}{2}b \right) V_{br}E_r + \left(-\frac{\sqrt{3}}{2}g - \frac{1}{2}b \right) V_{br}E_i \\
& + gV_{bi}^{\,2} - bV_{bi}V_{nr} - gV_{bi}V_{ni} + \left(\frac{\sqrt{3}}{2}g + \frac{1}{2}b \right) V_{bi}E_r + \left(\frac{1}{2}g - \frac{\sqrt{3}}{2}b \right) V_{bi}E_i \\
& + gV_{cr}^{\,2} - gV_{cr}V_{nr} + bV_{cr}V_{ni} + \left(\frac{1}{2}g + \frac{\sqrt{3}}{2}b \right) V_{cr}E_r + \left(\frac{\sqrt{3}}{2}g - \frac{1}{2}b \right) V_{cr}E_i \\
& + gV_{ci}^{\,2} - bV_{ci}V_{nr} - gV_{ci}V_{ni} + \left(\frac{1}{2}b - \frac{\sqrt{3}}{2}g \right) V_{ci}E_r + \left(\frac{1}{2}g + \frac{\sqrt{3}}{2}b \right) V_{ci}E_i + \left\{ P_{sg} \right\}
\end{aligned} \tag{B.34}$$

$$0 = V_{ar}{}^2 + V_{ai}{}^2 + V_{br}{}^2 + V_{bi}{}^2 - 2V_{ar}V_{br} - 2V_{ai}V_{bi} - \left\{V_{sg}{}^2\right\} \tag{B.35}$$

$$\begin{aligned} P_{\min} &\le \left\{P_{sg}\right\} \le P_{\max} \\ V_{\min} &\le \left\{V_{sg}\right\} \le V_{\max} \end{aligned} \tag{B.36}$$

B.5 Generators –Slack Mode– Compact Form

The slack bus control mode forces the internal source phase angle to zero, and the line to line voltage (phases A, B) to the user specified value. The model equations are as follows:

$$\tilde{I}_a = (g + jb)(\tilde{V}_a - \tilde{V}_n - \tilde{E}_a), \tag{B.37}$$

$$\tilde{I}_b = (g + jb)(\tilde{V}_b - \tilde{V}_n - \tilde{E}_b), \tag{B.38}$$

$$\tilde{I}_c = (g + jb)(\tilde{V}_c - \tilde{V}_n - \tilde{E}_c), \tag{B.39}$$

$$\tilde{I}_n = (g + jb)(-\tilde{V}_a - \tilde{V}_b - \tilde{V}_c + 3\tilde{V}_n), \tag{B.40}$$

$$\delta = 0.0 \tag{B.41}.$$

$$\left|\tilde{V}_a - \tilde{V}_b\right| = V_{sg} \tag{B.42}$$

The operation constraints are

$$V_{\min} \le V_{sg} \le V_{\max} \quad , \tag{B.43}$$

where $g = -\dfrac{R}{R^2 + \omega^2 L^2}$, $b = -\dfrac{\omega L}{R^2 + \omega^2 L^2}$,

and $\tilde{E}_a = Ee^{j\delta}$, $\tilde{E}_b = Ee^{j(\delta - \frac{2\pi}{3})}$, $\tilde{E}_c = Ee^{j(\delta - \frac{4\pi}{3})}$.

B.6 Generators – Slack Mode – Quadratized Form

State Variables: $\mathbf{x} = \left[V_{ar},\ V_{ai},\ V_{br},\ V_{bi},\ V_{cr},\ V_{ci},\ V_{nr},\ V_{ni},\ E_r,\ E_i \right]$

Control Variables: $\mathbf{u} = \left[V_{sg} \right]$

$$I_{ar} = gV_{ar} - bV_{ai} - gV_{nr} + bV_{ni} - gE_r + bE_i \tag{B.44}$$

$$I_{ai} = bV_{ar} + gV_{ai} - gV_{ni} - bV_{nr} - gE_i - bE_r \tag{B.45}$$

$$I_{br} = gV_{br} - bV_{bi} - gV_{nr} + bV_{ni} + \left(\frac{1}{2}g - \frac{\sqrt{3}}{2}b \right) E_r + \left(-\frac{\sqrt{3}}{2}g - \frac{1}{2}b \right) E_i \tag{B.46}$$

$$I_{bi} = bV_{br} + gV_{bi} - bV_{nr} - gV_{ni} + \left(\frac{\sqrt{3}}{2}g + \frac{1}{2}b \right) E_r + \left(\frac{1}{2}g - \frac{\sqrt{3}}{2}b \right) E_i \tag{B.47}$$

$$I_{cr} = gV_{cr} - bV_{ci} - gV_{nr} + bV_{ni} + \left(\frac{1}{2}g + \frac{\sqrt{3}}{2}b \right) E_r + \left(\frac{\sqrt{3}}{2}g - \frac{1}{2}b \right) E_i \tag{B.48}$$

$$I_{ci} = bV_{cr} + gV_{ci} - bV_{nr} - gV_{ni} + \left(-\frac{\sqrt{3}}{2}g + \frac{1}{2}b \right) E_r + \left(\frac{1}{2}g + \frac{\sqrt{3}}{2}b \right) E_i \tag{B.49}$$

$$I_{nr} = -gV_{ar} + bV_{ai} - gV_{br} + bV_{bi} - gV_{cr} + bV_{ci} + 3gV_{nr} - 3bV_{ni} \tag{B.50}$$

$$I_{nr} = -bV_{ar} - gV_{ai} - bV_{br} - gV_{bi} - bV_{cr} - gV_{ci} + 3bV_{nr} + 3gV_{ni} \tag{B.51}$$

$$0 = E_i \tag{B.52}$$

$$0 = V_{ar}{}^2 + V_{ai}{}^2 + V_{br}{}^2 + V_{bi}{}^2 - 2V_{ar}V_{br} - 2V_{ai}V_{bi} - \left\{ V_{sg}{}^2 \right\} \tag{B.53}$$

$$V_{\min} \le \left\{ V_{sg} \right\} \le V_{\max} \tag{B.54}$$

Appendix C: Transformer Model with SCAQCF Syntax for OPF

C.1 Single Phase Transformers – Compact Form

This section describes the model of the single-phase two-winding transformer. Three of these models can be connected into the four subcases of Y-Y, Y-Δ, Δ-Y, and Δ-Δ connected three-phase transformers.

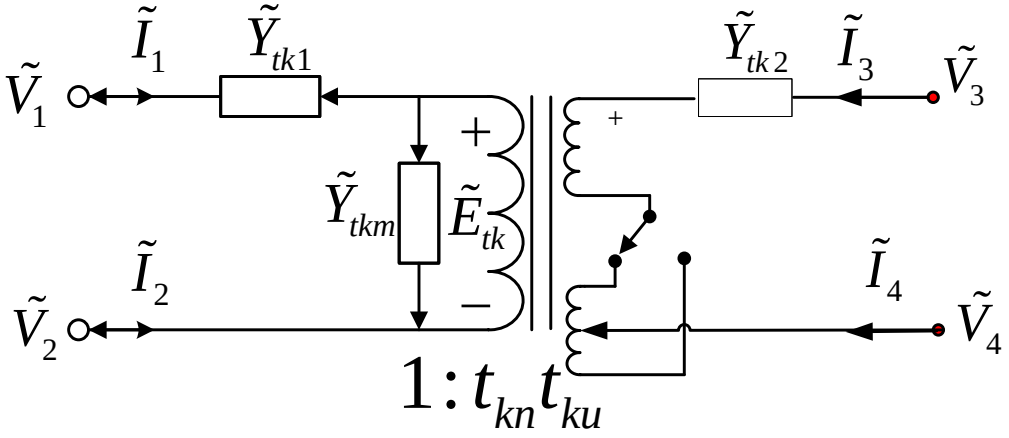

FigureC.2. The single-phase transformer model.

Figure A.1 illustrates the physical model of the single-phase variable-tap transformer. In Figure A.1, the turn ratio *t* consists of two parts. One is the nominal transformation ratio t_{kn} and the other is the per-unit tap selection t_{ku}. The overall turn ratio is $t = t_{ku} t_{kn}$. And the admittance Y_1 and Y_2 of the transformer are expressed as follows:

$$\tilde{Y}_{tk1} = 2\tilde{Y}_{tk} t_{kn}^2 = \frac{1}{r_1 + j\omega L_1}, \qquad \text{(C.1)}$$

$$\tilde{Y}_{tk2} = \frac{2\tilde{Y}_{tk}}{1 + abs(1 - t_{ku})} = \frac{1}{r_2 + j\omega L_2}, \tag{C.2}$$

where Y_{tk} is the nominal admittance of the transformer referred to the secondary side. Y_{tkm} is the magnetizing admittance referred to the primary side. The model assumes that the leakage impedance is proportional to the number of turns.

The single-phase model is based on the equivalent circuit illustrated in Figure C.1. According to Kirchhoff's laws, the single-phase transformer equations are

$$\tilde{I}_1 = \tilde{Y}_{tk1}\left(\tilde{V}_1 - \tilde{V}_2 - \tilde{E}_{tk}\right) \tag{C.3}$$

$$\tilde{I}_2 = -\tilde{Y}_{tk1}\left(\tilde{V}_1 - \tilde{V}_2 - \tilde{E}_{tk}\right) \tag{C.4}$$

$$\tilde{I}_3 = \tilde{Y}_{tk2}\left(\tilde{V}_3 - \tilde{V}_4 - t_{kn}t_{ku}\tilde{E}_{tk}\right) \tag{C.5}$$

$$\tilde{I}_4 = -\tilde{Y}_{tk2}\left(\tilde{V}_3 - \tilde{V}_4 - t_{kn}t_{ku}\tilde{E}_{tk}\right) \tag{C.6}$$

$$0 = -\tilde{Y}_{tk1}\left(\tilde{V}_1 - \tilde{V}_2 - \tilde{E}_{tk}\right) - t_{kn}t_{ku}\tilde{Y}_{tk2}\left(\tilde{V}_3 - \tilde{V}_4 - t_{kn}t_{ku}\tilde{E}_{tk}\right) + \tilde{Y}_{tkm}\tilde{E}_{tk} \tag{C.7}$$

$$0.9 \le t_{ku} \le 1.1 \tag{C.8}$$

where $\tilde{Y}_{tk} = g_{tk} + jb_{tk}$ is the nominal admittance of the transformer referred to the secondary side. $\tilde{Y}_{tkm} = g_{tkm} + jb_{tkm}$ is the magnetizing admittance referred to the primary side. The model assumes that the leakage impedance is proportional to the number of turns. And the turn ratio t_k consists of two parts. One is the nominal transformation ratio t_{kn} and the other is the per-unit tap selection t_{ku}. The overall turn ratio $t_k = t_{kn}t_{ku}$.

C.2 Single Phase Transformers–Quadratized Form

Two state variables $u_{tk1} = \sqrt{(1-t_{ku})^2}$ and $u_{tk2} = \dfrac{1}{1+u_{tk1}}$ are introduced to eliminate the absolute function in the denominator in $\tilde{Y}_{tk2}$. Other two state variables $u_{tk3} = u_{tk2}t_{ku}$ and $u_{tk4} = u_{tk3}t_{ku}$ are introduced to reduce the order of the equations. Substituting them into (C.3) to (C.8) and separating equations into real and imaginary parts, we have the quadratized equations describing the single-phase transformer:

State Variables: $\mathbf{x} = [V_{1r}, V_{1i}, V_{2r}, V_{2i}, V_{3r}, V_{3i}, V_{4r}, V_{4i}, E_{tk1r}, E_{tk1i}, u_{tk1}, u_{tk2}, u_{tk3}, u_{tk4}, u_{tk5}]$

Control Variables: $\mathbf{u} = [t_{ku}]$

$$I_{1r} = 2t_{kn}^2 g_{tk}(V_{1r} - V_{2r} - E_{tkr}) - 2t_{kn}^2 b_{tk}(V_{1i} - V_{2i} - E_{tki}), \tag{C.9}$$

$$I_{1i} = 2t_{kn}^2 g_{tk}(V_{1i} - V_{2i} - E_{tki}) + 2t_{kn}^2 b_{tk}(V_{1r} - V_{2r} - E_{tkr}), \tag{C.10}$$

$$I_{3r} = 2u_{tk2} g_{tk}(V_{3r} - V_{4r}) - 2u_{tk2} b_{tk}(V_{3i} - V_{4i}) - 2g_{tk} t_{kn} u_{tk3} E_{tkr} + 2b_{tk} t_{kn} u_{tk3} E_{tki}, \tag{C.11}$$

$$I_{3i} = 2u_{tk2} g_{tk}(V_{3i} - V_{4i}) + 2u_{tk2} b_{tk}(V_{3r} - V_{4r}) - 2g_{tk} t_{kn} u_{tk3} E_{tki} - 2b_{tk} t_{kn} u_{tk3} E_{tkr}, \tag{C.12}$$

$$\begin{aligned} 0 = {} & 2t_{kn}^2 g_{tk}(V_{1i} - V_{2i}) + 2t_{kn}^2 b_{tk}(V_{1r} - V_{2r}) \\ & + 2t_{kn} g_{tk} u_{tk3}(V_{3i} - V_{4i}) + 2t_{kn} b_{tk} u_{tk3}(V_{3r} - V_{4r}) \\ & - (2t_{kn}^2 g_{tk} + 2t_{kn}^2 g_{tk} u_{tk4} + g_{tmk}) E_{tki} - (2t_{kn}^2 b_{tk} + 2t_{kn}^2 b_{tk} u_{tk4} + b_{tmk}) E_{tkr} \end{aligned}, \tag{C.13}$$

$$\begin{aligned} 0 = {} & 2t_{kn}^2 g_{tk}(V_{1r} - V_{2r}) - 2t_{kn}^2 b_{tk}(V_{1i} - V_{2i}) \\ & + 2t_{kn} g_{tk} u_{tk3}(V_{3r} - V_{4r}) - 2t_{kn} b_{tk} u_{tk3}(V_{3i} - V_{4i}) \\ & - (2t_{kn}^2 g_{tk} + 2t_{kn}^2 g_{tk} u_{tk4} + g_{tmk}) E_{tkr} + (2t_{kn}^2 b_{tk} + 2t_{kn}^2 b_{tk} u_{tk4} + b_{tmk}) E_{tki} \end{aligned}, \tag{C.14}$$

$$0 = u_{tk1}^2 + \{2t_{ku} - t_{ku}^2\} - 1, \tag{C.15}$$

$$0 = u_{tk2} + u_{tk1} u_{tk2} - 1, \tag{C.16}$$

$$0 = u_{tk2}u_{tk5} - u_{tk3}, \tag{C.17}$$

$$0 = u_{tk3}u_{tk5} - u_{tk4}, \tag{C.18}$$

$$0 = u_{tk5} - \{t_{ku}\} \tag{C.19}$$

$$0.9 \le \{t_{ku}\} \le 1.1 \tag{C.20}$$

REFERENCE

[1] A. Monticelli, *State estimation in electric power systems: a generalized approach*, Kluwer Academic Publishers, Boston, 1999.

[2] A. Abur and A. Gómez Expósito, *Power system state estimation: theory and implementation*, Marcel Dekker, New York, 2004.

[3] A. P. Meliopoulos and G. Stefopoulos, "Characterization of state estimation biases," *Probability in the Engineering and Informational Sciences, Cambridge University Press*, vol. 20, pp. 157-174, 2006.

[4] F. Wu, K. Moslehi and A. Bose, "Power System Control Centers: Past, Present and Future," *Proceedings of the IEEE*, vol. 93, No. 11, pp. 1890-1908, Nov. 2005.

[5] J. Giri, M. Parashar, J. Trehern and V. Madani, "The situation room," *IEEE Power and Energy Magazine*, vol.10, No.5, pp.58-69, Sept. 2012.

[6] F. C. Schweppe and J. Wildes, "Power system static-state estimation, Part I: Exact Model" *IEEE Trans. Power App. Syst.*, vol. PAS-89, no.1, pp.120-125, Jan. 1970.

[7] F. C. Schweppe and D. B. Rom, "Power system static-state estimation, Part II: Approximate Model" *IEEE Trans. Power App. Syst.*, vol. PAS-89, no.1, pp.125-130, Jan. 1970.

[8] F. C. Schweppe, "Power system static-state estimation, Part III: Implementation" *IEEE Trans. Power App. Syst.*, vol. PAS-89, no.1, pp.130-135, Jan. 1970.

[9] K. A. Clements, O. J. Denison, and R. J. Ringlee, "The effects of measurement non-simultaneity, bias, and parameter uncertainty on power system state estimation," in *Proceedings of the 1973 PICA Conference*, pp. 327-331, Jun. 1973.

[10] M. C. de Almeida, E. N. Asada, A. V. Garcia, "Effects of load imbalance and system asymmetry on three-phase state estimation," in *Proceedings IEEE Power Engineering Society 2006 General Meeting*, Jun. 2006.

[11] A. P. Meliopoulos, F. Zhang, and S. Zelingher, "Power System Harmonic State Estimation," *IEEE Trans. Power Systems*, vol. 9, no. 3, pp. 1701-1709, Jul. 1994.

[12] A. G. Phadke, J. S. Thorp, and K. J. Karimi, "State estimation with phasor measurements," *IEEE Trans. Power Systems*, vol. PWRS-1, no.1, pp. 233-241, Feb. 1986.

[13] A. P. Meliopoulos, "State Estimation for Mega RTOs," in *Proceedings of the 2002 IEEE PES Winter Meeting*, New York, NY, Jan. 2002.

[14] B. Fardanesh, S. Zelingher, A. P. Meliopoulos, G. Cokkinides, and J. Ingleson, "Multifunctional Synchronized Measurement Network", *IEEE Computer Applications in Power*, vol. 11, no. 1, pp. 26-30, Jan. 1998.

[15] J. S. Thorp, A. G. Phadke, K. J. Karimi, "Real time voltage-phasor measurement for static state estimation," *IEEE Trans. Power App. Syst.*, vol. PAS-104, No 11, pp. 3098-3106, Nov. 1985.

[16] S. Chakrabarti, E. Kyriakides, T. Bi, D. Cai, V. Terzija, "Measurements get together", *IEEE Power and Energy Magazine*, vol. 7, no. 1, pp. 41-49, Jan. 2009.

[17] A. P. Meliopoulos, G. J. Cokkinides, and G. K. Stefopoulos, "Numerical experiments for three-phase state estimation performance and evaluation," *in Proceedings of IEEE Power Tech Conference*, pp.1-7, St. Petersburg, Russia, Jun. 2005.

[18] IEEE Standard for Synchrophasors for Power Systems, Std C37.118-2005, IEEE Power Engineering Society.

[19] M. Adamiak, W. Premerlani, B. Kasztenny, "Synchrophasors: Definition, Measurement and Application," *GE Multilin Publications*, pp. 1-13.

[20] J. Zhu, Ali Abur, M. Rice, G. T. Heydt, and A. P. Meliopoulos, "Enhanced state estimators," *Final project report for PSERC project S-22*, Nov. 2006.

[21] S. Chakrabarti, E. Kyriakides, G. Valverde, V. Terzija, "State estimation including synchronized measurements," *in Proceedings of the IEEE Power Tech Conference*, Bucharest, Jul. 2009.

[22] T. Yang, H. Sun, A. Bose, "A Transition to a Two-Level Linear State Estimator—Part I: Architecture," *IEEE Trans. Power Systems*, vol. 26, no.1, pp. 46-53, Feb. 2011.

[23] T. Yang, H. Sun, A. Bose, "A Transition to a Two-Level Linear State Estimator—Part II: Algorithm," *IEEE Trans. Power Systems*, vol. 26, no.1, pp. 54-62, Feb. 2011.

[24] T. Van Cutsem, M. Ribbens-Pavella, "Critical survey of hierarchical methods for state estimation of electric power systems," *IEEE Trans. Power App. Syst.*, vol. PAS-102, no. 10, pp. 3415-3424, Oct. 1983.

[25] D. M. Falcao, F. F. Wu, and L. Murphy, "Parallel and distributed state estimation," *IEEE Trans. Power Systems*, vol. 10, no 2, pp. 724-730, May 1995.

[26] Zhao Liang and A. Abur, "Multi area state estimation using synchronized phasor measurements," *IEEE Trans. Power Systems*, vol. 20, no 2, pp. 611-617, May 2005.

[27] Y. Li, X. Zhou, and J. Zhou, "A new algorithm for distributed power system state estimation based on PMUs," in *Proc. 2006 International Conference on Power System Technology (PowerCon 2006)*, Oct. 2006.

[28] A. P. S. Meliopoulos, G. J. Cokkinides, F. Galvan, B. Fardanesh, and P. Myrda, "Delivering accurate and timely data to all," *IEEE Power and Energy Magazine*, vol. 5, no. 3, pp. 74-86, 2007.

[29] R. Ebrahimian and R. Baldick, "State estimation distributed processing [for power systems]," *IEEE Trans. Power Systems*, vol. 15, no. 4, pp. 1240-1246, Nov. 2000.

[30] A. P. Meliopoulos, G. J. Cokkinides, F. Galvan, B. Fardanesh, and P. Myrda, "Advances in the SuperCalibrator Concept – Practical Implementations," *in Proceedings of the 40st Annual Hawaii Int. Conf. System Sciences (HICSS)*, Waikoloa, Big Island, HI, USA, Jan. 2007.

[31] A. P. Meliopoulos, G. J. Cokkinides, Clinton Hedrington, and Terry L. Conrad, "The SuperCalibrator – A Fully Distributed State Estimator," *in Proceedings of the IEEE-PES General Meeting*, Minneapolis, MN, Jul. 2010.

[32] S. Mohagheghi, R. H. Alaileh, G. J. Cokkinides, and A. P. Meliopoulos, "Distributed state estimation based on the SuperCalibrator concept – Laboratory Implementation," *in Proceedings of the IREP 2007 Symposium on Bulk Power System Dynamics and Control*, Charleston, SC, Aug. 2007.

[33] A. P. Meliopoulos, G. J. Cokkinides, F. Galvan, and B. Fardanesh, "Distributed state estimator – Advances and demonstration," *in Proceedings of the 41st Annual Hawaii Int. Conf. System Sciences (HICSS)*, Kona, HI, Jan. 2008.

[34] A. S. Debs and R. E. Larson, "A dynamic estimator for tracking the state of a power system," *presented at the IEEE Winter Power Meeting*, New York, NY, Jan. 1970.

[35] I. M. Ferreira and F. P. Barbosa, "An algorithm for dynamic state estimation and bad data analysis using a square root filtering technique," *IEEE Athens PowerTech Conf.*, Athens, Greece, Sept. 1993.

[36] K-R Shih and S.-J. Huang, "Application of a robust algorithm or dynamic state estimation of a power system," *IEEE Trans. Power Systems*, Vol. 17, no.1, pp. 141-147, Feb. 2002.

[37] G. Durgaprasad and S. S. Thakur, "Robust dynamic state estimation of power systems based on M-estimation and realistic modeling of system dynamics," *IEEE Trans. Power Systems*, Vol. 13, no.4, pp. 1331-1336, Nov. 1998.

[38] H. Zhenyu, K. Schneider, J. Nieplocha, "Feasibility studies of applying Kalman Filter techniques to power system dynamic state estimation", *in Proceedings of the International Power Engineering Conference, IPEC*, Charleston, SC, Aug. 2007.

[39] A.K. Sinha, L.K. Mondal, "Dynamic state estimator using ANN based bus load prediction," *IEEE Trans. Power Systems*, Vol. 14, no.4, pp. 1219-1225, Nov. 1999.

[40] A. M. Sasson, F. Viloria, and F. Aboytes, "Optimal load flow solution using the hessian matrix," *IEEE Transactions on Apparatus and Power Systems*, Vol. 92, no. 1, pp. 31-41, Jan. 1973.

[41] G. F. Reid and L. Hasdorff, "Economic dispatch using quadratic programming," *IEEE Trans. on Apparatus and Power Systems*, Vol. 92, Issue: 6, pp. 2015-2023, Nov. 1973.

[42] R. Billinton and S. S. Sachdeva, "Optimal real and operation in a hydro-thermal system," *IEEE Trans. on Apparatus and Power Systems*, vol. 91, no. 4, pp. 1405-1411, July. 1972.

[43] R. R. Shoults and D. T. Sun, "Optimal power flow based on P-Q decomposition," *IEEE Trans. on Apparatus and Power Systems*, vol. 101, no. 2, pp. 397-405, Feb. 1982.

[44] R. A. Ponrajah and F. D. Galiana, "The minimum cost optimal power flow problem solved via the restart homotopy continuation method," *IEEE Trans. Power Systems*, vol. 4, no. 1, pp. 139-148, Feb. 1989.

[45] C. J. Rehn, J. A. Bubenko and D. Sjelvgven, "Voltage optimization using augmented Lagrangian functions and quasi-Newton techniques," *IEEE Trans. Power Systems*, vol. 4, no. 4, pp. 1470-1483, Dec. 1989.

[46] M. A. El-Kady, B. D. Bell, V. F. Carvalho, R. C. Burdhett, H. H. Happ, and D. R. Vierath, "Assessment of real-time optimal voltage control," *IEEE Trans. Power Systems*, vol. 1, no. 2, pp. 99-107, May 1986.

[47] A. J. Monticelli, M. V. P. Pereira, and S. Granville, "Security-constrained optimal power flow with post-contingency corrective rescheduling," *IEEE Trans. Power Systems*, vol. 2, no. 1, pp. 175-182, Feb. 1987.

[48] J. Martinez-Crespo, J. Usaola, and J. L. Fernandez, "Optimal security-constrained power scheduling by Benders decomposition," *Electric Power Systems Research*, vol. 77, no. 7, pp. 739-753, May 2007.

[49] C. W. Sanders and C. A. Monroe, "An algorithm for real-time security constrained dispatch," *IEEE Trans. Power Systems*, vol. 2, no. 4, pp. 175-182, Nov. 1987.

[50] J. Carpentier, "Contribution to the economic dispatch problem," *Bull. Soc. France Elect*, vol. 8, pp. 431-437, Aug. 1962.

[51] O. Alsac, J. Bright, M. Prais, and B. Stott, "Further developments in LP-based optimal power flow," *IEEE Trans. Power Systems*, vol. 5, no. 3, pp. 697-711, Aug. 1990.

[52] B. Stott and E. Hobson, "Power system security control calculations using linear programming," *IEEE Trans. Power Apparatus and Systems*, vol. 97, no. 5, pp. 1713-1731, Oct. 1978.

[53] B. Stott and J. L. Marinho, "Linear programming for power system network security applications," *IEEE Trans. Apparatus and Power Systems*, vol. 98, no. 3, pp. 837-848, May 1979.

[54] M. Santos-Neito and V. H. Quintana, "Linear Reactive Power Studies for Longitudinal Power Systems," in *Proceedings of 9th Power Systems Computation Conference*, pp. 783-787, Jan. 1987.

[55] R. Mota-Palomino and V. H. Quintana, "Sparse reactive power scheduling by a penalty-function - linear programming technique," *IEEE Trans. Power Systems*, vol. 1, no. 3, pp. 31-39, Aug. 1986.

[56] S. A. Farghal, M. A. Tantawy, M. S. Abou-Hussein, S. A. Hassan, and A. A. Abou-Slela, "A fast technique for power system security assessment using sensitivity parameters of linear programming," *IEEE Trans. Apparatus and Power Systems*, vol. 103, no. 5, pp. 946-953, May 1984.

[57] Y. C. Wu, A. S. Debs, and R. E. Marsten, "A direct nonlinear predictor–corrector primal-dual interior point algorithm for optimal power flows," *IEEE Trans. Power Systems*, vol. 9, no. 2, pp. 876-883, May 1994.

[58] S. Granville, "Optimal reactive dispatch through interior point methods," *IEEE Trans. Power Systems*, vol. 9, no. 1, pp. 136-142, Feb. 1994.

[59] G. L. Torres and V. H. Quintana, "An interior-point method for nonlinear optimal power flow using rectangular coordinates," *IEEE Trans. Power Systems*, vol. 13, no. 4, pp. 1211-1218, Nov. 1998.

[60] G. D. Irisarri, X. Wang, J. Tong, and S.Mokhtari, "Maximum loadability of power systems using interior point nonlinear optimization method," *IEEE Trans. Power Systems*, vol. 12, no. 1, pp. 162-172, Aug. 1997.

[61] D. I. Sun, B. Ashley, B. Brewer, A. Hughes, and W. F. Tinney, "Optimal power flow by Newton approach," *IEEE Trans. Power Apparatus and Systems*, vol. 103, no. 10, pp. 2864-2880, Oct. 1984.

[62] A. M. Sasson, "Nonlinear programming solutions for load-flow, minimum-loss, and economic dispatching problems," *IEEE Trans. Power Apparatus and Systems*, vol. 88, no. 4, pp. 399-409, Apr. 1969.

[63] L. S. Vargas, V. H. Quintana, A. Vannelli, "A tutorial description of an interior point method and its application to security-constrained economic dispatch," *IEEE Trans. Power Systems*, vol. 8, no. 3, pp. 1315-1324, Aug. 1993.

[64] R.A Jabr, A.H. Coonick, and B.J. Cory, "A primal-dual interior point method for optimal power flow dispatching," *IEEE Trans. Power Systems*, vol. 17, no. 3, pp. 654-662, Aug. 2002.

[65] R. A. Jabr, "Optimal power flow using an extended conic quadratic formulation," *IEEE Trans. Power Systems*, vol. 3, no. 23, pp. 1000-1008, Aug. 2008.

[66] H. R. Cai, C. Y. Chung, and K. P. Wong, "Application of differential evolution algorithm for transient stability constrained optimal power flow," *IEEE Trans. Power Systems*, vol. 23, no. 2, pp. 719-728, May 1998.

[67] P. E. O. Yumbla, J. M. Ramirez, and C. A. C. Coello, "Optimal power flow subject to security constraints solved with a particle swarm optimizer," *IEEE Trans. Power Systems*, vol. 23, no. 1, pp. 33-40, Feb. 2008.

[68] M. M. El Metwally, A. A. El Emary, F. M. El Bendary, and M. I. Mosaad, "Optimal power flow using evolutionary programming techniques," *in Proceedings of the 2th International Middle-East Power System Conference*, Mar. 2008.

[69] D. W. Wells, "Method for economic secure loading of a power system," in *Proceedings of the Institution of Electrical Engineers*, vol. 115, no. 8, pp. 1190-1194, Aug. 1968.

[70] C. M. Shen and M. A. Laughton, "Power system load scheduling with security constraints using dual linear programming," in *Proceedings of the Institution of Electrical Engineers*, vol. 117, no. 11, pp. 2117-2127, Nov. 1970.

[71] K. A. Clements, P. W. Davis, K. D. Frey, S. A. Hassan, and A. A. Abou-Slela, "An interior point algorithm for weighted least absolute value power system state estimation," in *Proceedings of IEEE/PES 1991 Winter Meeting*.

[72] H. W. Dommel and W. F. Tinney, "Optimal power flow solutions," *IEEE Trans. Power Apparatus and Systems*, vol. 87, no. 10, pp. 1866-1876, Oct. 1968.

[73] G. Tognola and R. Bacher, "Unlimited point algorithm for OPF problems," *IEEE Trans. Power Systems*, vol. 14, no. 3, pp. 1046-1054, Aug. 1999.

[74] S. Granville and F. R. de M. Alves, "Active-reactive coupling in optimal reactive dispatch, a solution via Karush-Kuhn-Tucker optimality conditions," *IEEE Trans. Power Systems*, vol. 9, no. 4, pp. 1774-1779, Nov. 1994.

[75] G. D. Irisarri, X. Wang, J. Tong, and S.Mokhtari, "Maximum loadability of power systems using interior point nonlinear optimization method," *IEEE Trans. Power Systems*, vol. 12, no. 1, pp. 162-172, Aug. 1997.

[76] G. L. Torres and V. H. Quintana, "On a nonlinear multiple-centrality-corrections interior-point method for optimal power flow," *IEEE Trans. Power Systems*, vol. 16, no. 2, pp. 222-228, May 2001.

[77] A. M. Sasson, C. Trevino, and F. Aboytes, “Improved Newton's load flow through a minimization technique,” *IEEE Trans. Apparatus and Power Systems*, vol. 90, no. 5, pp. 1974-1981, Sept. 1971.

[78] A. G. Bakirtzis, P. N. Biskas, C. E. Zoumas, and V. Petridis, “Optimal power flow by enhanced genetic algorithm,” *IEEE Trans. Power Systems*, vol. 17, no. 2, pp. 229-236, May 2002.

[79] J. Kennedy and R. Eberhart, “Particle swarm optimization,” in *Proceedings of IEEE International Conference on Neural Networks*, vol. 4, pp. 1942-1948, Dec. 1995.

[80] M. A. Abido, “Optimal power flow using particle swarm optimization,” in *Proceedings of the International Journal of Electrical Power and Energy Systems*, vol. 24, no. 7, pp. 563-571, Oct. 2002.

[81] B. Zhao, C. X. Guo, and Y. J. Cao, “Improved particle swarm optimization algorithm for OPF problem,” in *Proceedings of the IEEE PES Power Systems Conference and Exposition*, vol. 1, pp. 233-238, Oct. 2004.

[82] J. G. Vlachogiannis and K. Y. Lee, “A comparative study on particle swarm optimization for optimal steady-state performance of power systems,” *IEEE Trans. Power Systems*, vol. 21, no. 4, pp. 1718-1728, Nov. 2006.

[83] J. G. Vlachogiannis and K. Y. Lee, “Coordinated aggregation particle swarm optimization applied in reactive power and voltage control,” in *Proceedings of the IEEE Power Engineering Society General Meeting*, Jun. 2006.

[84] A. P. Meliopoulos, G. J. Cokkinides, and G. Stefopoulos, "Quadratic Integration Method," in *Proceedings of the International Power System Transients Conference*, Montreal, Jun. 2005.

[85] A. P. Meliopoulos, G. J. Cokkinides, and G. K. Stefopoulos, "Symbolic integration of dynamical systems by collocation methods," in *Proceedings of the IEEE PES Power Systems Conference and Exposition*, Oct. 2006,

[86] M. A. Pai, *Power Systems Stability*, North Holland Publishing Co., New York, 1981.

[87] P. Kundur, *Power System Stability and Control*, McGraw-Hill, New York, 1994.

[88] P. M. Anderson, A. A. Fouad, *Power System Control and Stability*, IEEE Press, 2003.

[89] Ye Tao, *Optimal Power Flow via Quadratic Modeling*, Ph.D. Thesis, Georgia Institute of Technology, 2011.

[90] P.M. Subcommittee, “IEEE reliability test system,” IEEE Transactions on Apparatus and Power Systems, Vol. 98, Issue: 6, Nov. 1979, pp. 2047-2054.

[91] P.M. Subcommittee, "IEEE reliability test system - 1996," IEEE Transactions on Power Systems, Vol. 14, No. 3, Aug. 1999, pp. 1010-1020.

[92] Q. B. Dam, A. P. Meliopoulos, G. T. Heydt, and A. Bose, "A breaker-oriented, three-phase IEEE 24-substation test system," *IEEE Trans. Power Systems*, vol. 25, no.1, pp. 59-67, Feb. 2010.

[93] IEEE Standard 115-1995: "Test procedures for synchronous machines. Part I: Acceptance and performance testing, Part II: Test procedures and parameter determination for dynamic analysis."

[94] Z. Zhengming, Z. Fungshi, J.Gao, and L. Xu, "A dynamic on-line parameter identification and full-scale system experimental verification for large synchronous machines," *IEEE Trans. Energy Convers*., vol. 10, no. 3, pp. 392–398, Sept. 1995.

[95] H. J. Vermeulen, J.M. Strauss, and V. Shikoana, "Online estimation of synchronous generator parameters using PRBS perturbations," *IEEE Trans. Power System*, vol. 17, no. 3, pp. 694–700, Aug. 2002.

[96] E. Kyriakides, G. T. Heydt, and V. Vittal, "On-line parameter estimation of round rotor synchronous generators including magnetic saturation," *IEEE Trans. Energy Convers.*, vol. 20, no. 3, pp. 529–537, Sept. 2005.

[97] E. Ghahremani, M. Karrari, and O.P.Malik, "Synchronous generator third-order model parameter estimation using online experimental data," *IET Gener. Transm. Distrib.*, vol. 2, no. 5, pp. 708–709, 2008.

[98] G. Valverde, E. Kyriakides, G. T. Heydt, and V. Terzija, "Nonlinear Estimation of Synchronous Machine Parameters Using Operating Data," *IEEE Trans. Energy Convers.*, vol. 26, no. 3, pp. 831–839, Sep. 2011.

[99] A. P. Meliopoulos, G. J. Cokkinides, S. Grijalva, R. Huang, E. Polymeneas, Paul Myrda, and Mel Gehrs, "Integration & Automation: From Protection to Advanced Energy Management Systems", *Proceedings of the 2013 IREP Symposium on Bulk Power System Dynamics and Control*, pp 1-13, Rethymnon, Greece, Aug. 25-30, 2013.

[100] A. P. Meliopoulos, G. J. Cokkinides, R. Huang, E. Polymeneas, and Paul Myrda, "Grid Modernization: Seamless Integration of Protection, Optimization & Control", *Proceedings of the of the 47st Annual Hawaii International Conference on System Sciences*, Hawaii, HI, Jan. 6-9, 2014.

[101] Evangelos Farantatos, *A Predictive Out-of-Step Protection Scheme Based on PMU Enabled Distributed Dynamic State Estimation*, Ph.D. Thesis, Georgia Institute of Technology, 2012.